EJA

European Journal of Anatomy

Volume 28 - Number 3 May 2024

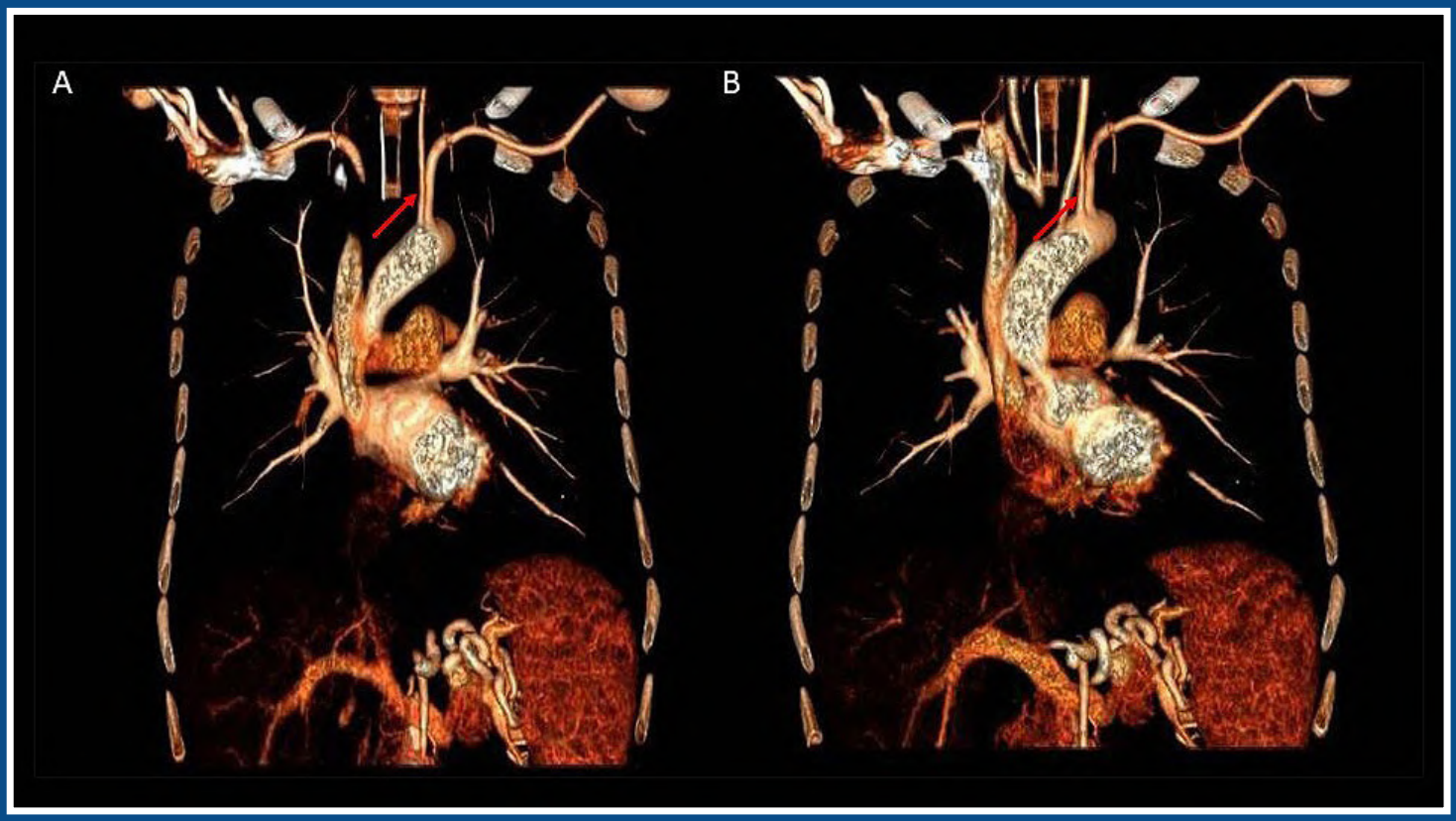

Indexed in:

CLARIVATE
- JCR:2020
- Q4 (21/23)
- I.F. J.C.I.: 0.19

DIALNET

EMBASE / Excerpta Medica

SCOPUS
- SJCR: 2020
- Q4 (31/39)
- I.F.: 0.162

Emerging Sources Citation Index

LATINDEX. Catálogo v1.0 (2002-2017)

Official Journal of the Spanish Society of Anatomy

Published by: **LOKI & DIMAS**

www.eurjanat.com

EJA
European Journal of Anatomy
Volume 28 - Number 3 May 2024

ORIGINAL ARTICLES

CASE REPORTS

REVIEW

Anatomic study of flexor carpi ulnaris and brachioradialis muscles and their implication in reconstructive surgeries

Sushma S. Mandala, Prameela M Dass, Mangala M. Pai, Rajanigandha Vadgaonkar, Rajalakshmi Rai, Murlimanju B.V., Lakshmisha Rao

Department of Anatomy, Kasturba Medical College, Mangalore, Manipal Academy of Higher Education, Manipal, Karnataka, India

SUMMARY

Management of soft tissue loss around the posterior aspect of the elbow region is most challenging for clinicians, as it may require reconstructive methods for the better healing of wounds. One of the options for reconstructive surgery is local muscle rotational flaps by the flexor carpi ulnaris (FCU) and brachioradialis (BR). This study aimed to explore the morphometry and vascular anatomy of FCU and BR. Thirty formalin-embalmed cadaveric upper extremities (16 right and 14 left) were utilized for this study. The average length of the FCU muscle belly was 28.96 ±2.16 cm within a range of 24.3 to 32.5 cm, and the average length of the tendon was 10.05 ± 2.2 cm, with a range of 6.9 to 14.3 cm. The number of vascular pedicles for FCU was one in 5, two in 21, and three and four in 2 specimens respectively. All the pedicles arose from the ulnar artery. The average length of the BR muscle was 28.2 ±3.58 cm, with a range of 22.8 to 36.8 cm, and the average length of its tendon was 8.2 cm, with a range of 5.7 to 13.5 cm. In 90% of specimens, BR had only one vascular pedicle and in 10% there were two pedicles. These pedicles arose from the radial recurrent artery and the radial artery. Detailed morphometric and topographic anatomy of the vascular pedicles of FCU and BR are provided in this study, which can be considered the morphological database for the South Indian population.

Key words: Elbow – Musculocutaneous flap – Morphometry – Tendon transfer – Ulnar artery

INTRODUCTION

The posterior aspect of the elbow region is prone to soft tissue loss. Tissue loss is usually due to injury, wound infection, burns, tumor excision, etc. (Ooi et al., 2016). Management of tissue loss around the posterior elbow region is more challenging for the clinicians, especially if infections, exposure of bones or nerves complicate it. This may require reconstructive methods for the better healing of wounds (Sharpe et al., 2014). Improper correction of the tissue loss may restrict the function of elbow movement and impair the function of the upper limb (Kelly et al., 2015).

Corresponding author:
Dr Prameela M Dass, MD. Department of Anatomy, Kasturba Medical College, Mangalore, Manipal Academy of Higher Education, Manipal, 576 104, India. E-mail: prameela.md@manipal.edu

Submitted: June 16, 2023. **Accepted:** September 19, 2023

https://doi.org/10.52083/LEXE5555

There are several choices available for coverage of soft tissue loss around the elbow. Local muscle rotational flaps by flexor carpi ulnaris (FCU) and brachioradialis (BR) are one such option for tissue reconstruction (Sharpe et al., 2014). A distal FCU flap is useful in the correction of defects around the wrist and hand areas, including the lower part of the forearm (Yang et al., 2019). A few studies have recently showed that FCU flap was used to improve vascular supply and soft tissue coverage at non-union sites (Meals, 1989). The use of FCU as transplant material for loss or paralysis of extensor carpi radialis longus and brevis muscle was reported by several authors (Green et al., 1962; Wenner et al., 1988). Zambelli et al. (2019) have used BR muscle flap for soft tissue repair at the posterior elbow region with good results. BR can be used as graft material in patients with lower brachial plexus injury (C7-T1), causing paralysis of the flexor muscles of the forearm (Shrikanth et al., 2018). FCU is the superficial muscle of the forearm present on the medial aspect (Strandring, 2008). Its origin is from the humerus and ulna and a tendinous arch connecting them. It takes origin in the medial epicondyle of the humerus, the medial margin of the olecranon process and the upper part of subcutaneous posterior border of the ulna. It gets inserts into the pisiform bone mainly, through the pisohamate and pisometacarpal ligament to the hamate and fifth metacarpal bone. Its actions are flexion at the wrist and adduction of the hand. The BR is the superficial muscle along the lateral aspect of the forearm, and it forms the lateral boundary of the cubital fossa. It arises from the lateral intermuscular septa and the upper part of the lateral supracondylar ridge of the humerus and gets inserted into the radius proximal to its styloid process. It is a flexor of the elbow in the mid-prone position. It is supplied by the radial or radial recurrent artery.

Several studies have described the morphometry and vascular pedicles of FCU with variable results (Sharpe et al., 2014; Payne et al., 2011; Wysocki, 2008). Reports on the morphometry of BR (Hospatna et al., 2020; Rohrich et al., 1995) and the vascular anatomy of BR (Rohrich et al., 1995; Sanger et al., 1994; Gilbert et al., 1980; Shen et al., 2008) are available in different studies. Data related to the morphometry and vascular anatomy of FCU and BR in the Indian population are rarely available in the literature.

The objective of the present research is to explore the morphometry and vascular anatomy of both the FCU and BR in a South Indian population.

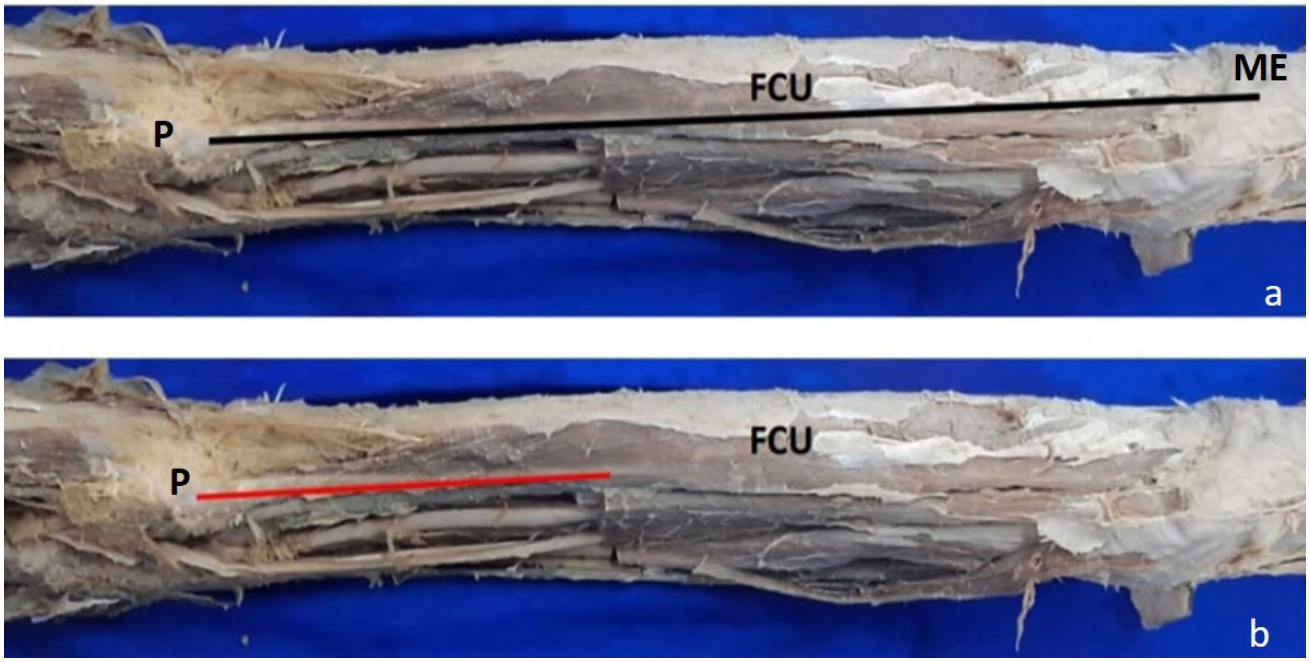

Fig. 1.- Dissected upper limb specimen depicting measurement of length of Flexor carpi ulnaris (FCU). **a)** Black line represents the length of the FCU from the medial epicondyle (ME) to the pisiform bone (P). **b)** Red line represents the length of the tendon from the musculocutaneous junction until the insertion on pisiform bone.

MATERIALS AND METHODS

Thirty formalin embalmed cadaveric upper extremities (16 right and 14 left sides) were utilized for this study. Approval from Institutional Ethics Committee, Kasturba Medical College, Mangalore was obtained for this study. The skin of the forearm was incised and the superficial and deep fascia were reflected. The forearm region was meticulously dissected to look for the FCU and BR muscles. FCU was reflected medially, and BR was reflected laterally to observe the pattern of its blood supply. The following parameters were measured using a measuring tape and a digital Vernier caliper (Aerospace Digital Vernier Caliper, 6"- 150 mm, China. Resolution: 0.01 mm):

1. Length of the FCU muscle was measured from the medial epicondyle of the humerus to the pisiform bone (Fig. 1).
2. Length of the FCU tendon from the myotendinous junction until the insertion in the pisiform bone (Fig. 1b).
3. The total number of proximal vascular pedicles of FCU and the source of origin of these vessels.
4. Distance of the vascular pedicles of FCU from the tip of the medial epicondyle of humerus.
5. Distance of the distal vascular pedicle of FCU from the ulnar styloid process.
6. Length of BR from its origin from the lateral supracondylar ridge to its insertion above the radial styloid process (Fig. 2).
7. The total number of vascular pedicles of BR and the source of origin of these vessels.
8. Distance of the vascular pedicle of BR from tip of lateral epicondyle (LE) of the humerus and the tip of the olecranon process (OP) of the ulna.

RESULTS

Flexor carpi ulnaris

The average length of FCU was 28.9 6 ± 2.16 cm with a range of 24.3 to 32.5 cm. The average length of its tendon was 10.05 ± 2.2 cm, with a range of 6.9 to 14.3 cm (Table 1). The number of vascular pedicles for FCU was one in 5, two in 21, and three and four in 2 specimens respectively (Fig. 3 a, b, c). All the pedicles of FCU arose from the ulnar artery. The distance of the vascular pedicles of FCU from medial epicondyle and the distal-most pedicle from the ulnar styloid process is depicted in Table 1.

Brachioradialis

The average length of the BR muscle was 28.2 ± 3.58 cm with a range of 22.8 cm to 36.8 cm. The average length of the BR tendon was 8.2 cm with the range of 5.7 cm to 13.5 cm. In the majority of specimens, 27 (90%), BR had only one vascular pedicle. However, in three specimens there were two pedicles (10%). In 17 specimens (56.66%) the arterial pedicles arose from the radial recurrent artery (RRA), whereas in 13 specimens (43.33%) they arose from the radial artery (RA) (Fig. 4a and 4b).

Fig. 2.- Dissected upper limb depicting measurement of length of brachioradialis (BR). The black line represents the length of the brachioradialis muscle from the lateral supracondylar ridge to its insertion above the radial styloid process, and the red line represents the length of the tendon from the musculotendinous junction to its insertion.

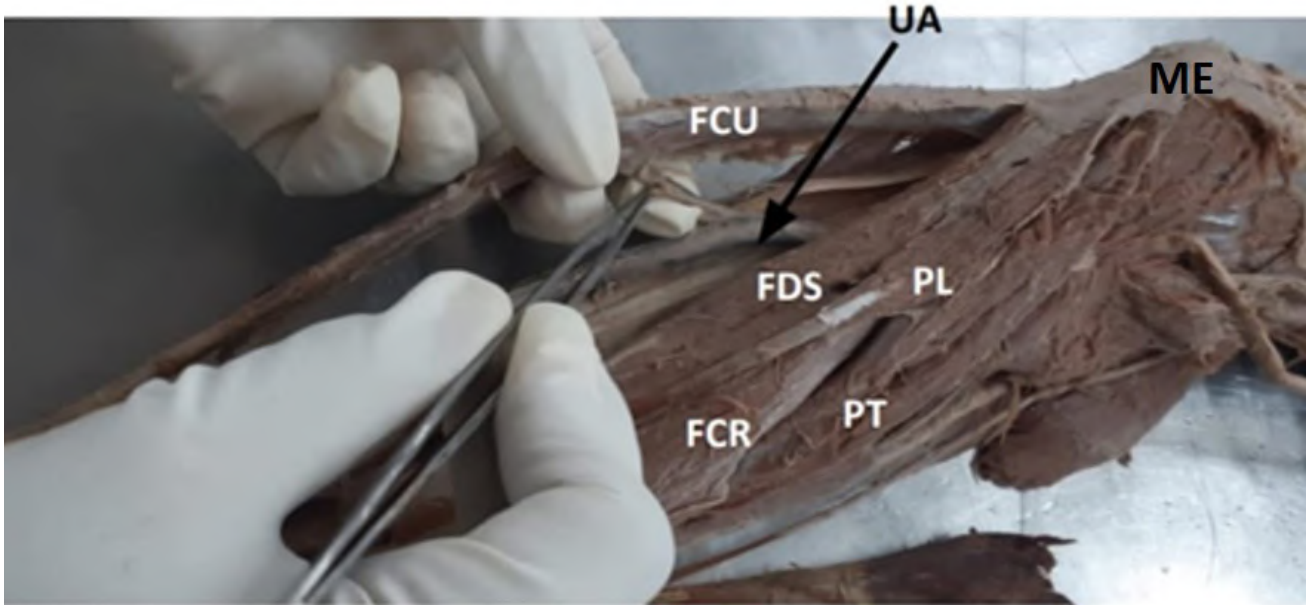

Fig. 3a.- Left upper limb showing flexor carpi ulnaris with one proximal vascular pedicle (black arrow) arising from ulnar artery. FCU- Flexor carpi ulnaris, UA- Ulnar artery, FDS- Flexor digitorum superficialis, FCR- Flexor carpi radialis, PL- Palmaris longus, PT- Pronator teres, ME- medial epicondyle.

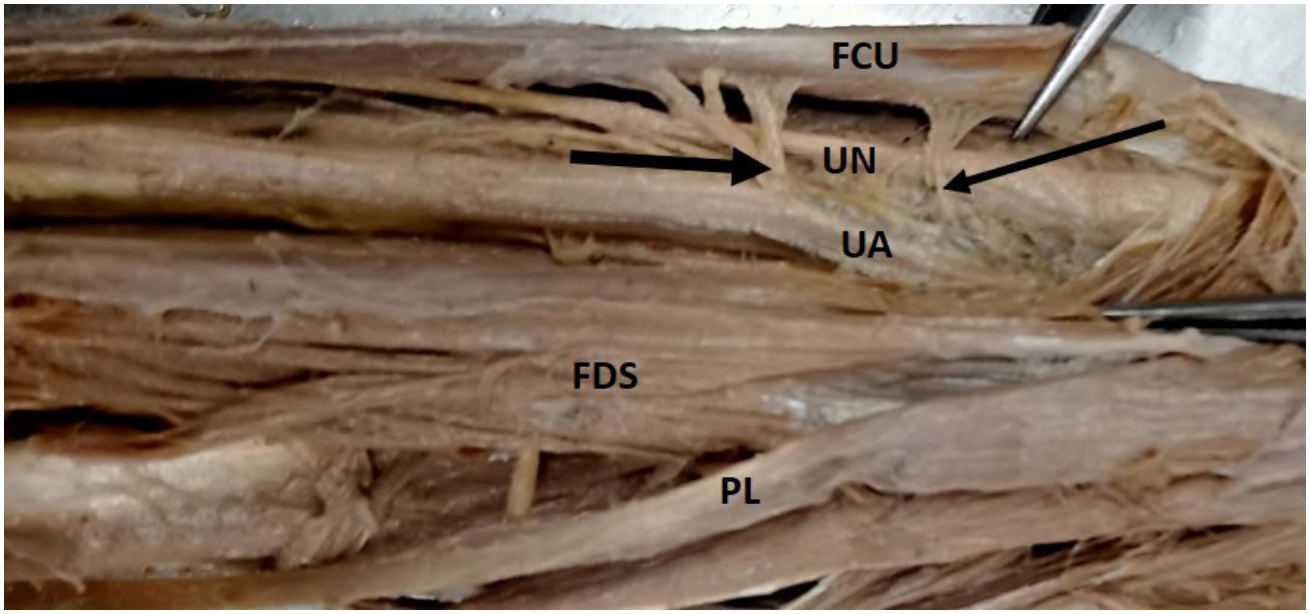

Fig. 3b.- Flexor carpi ulnaris with two proximal vascular pedicles indicated by black arrows. FCU- Flexor carpi ulnaris, UN- Ulnar nerve, UA- Ulnar artery, FDS- Flexor digitorum superficialis, PL- Palmaris longus.

Table 1. Morphometric data and vascular pedicles of Flexor carpi ulnaris. ME: Medial epicondyle.

Parameters	Min	Max	Mean	SD
Length of FCU (cm)	24.3	32.5	28.96	2.16
Length of FCU tendon (cm)	6.9	14.3	10.05	2.2
Distance of first vascular pedicle from ME (cm)	5.2	14.5	9.74	2.34
Distance of second vascular pedicle from ME (cm)	9.6	22.9	13.45	3.06
Distance of third vascular pedicle from ME (cm)	12.6	21.7	16.87	4.41
Distance of fourth vascular pedicle from ME (cm)	23	23	23.3	0.21
Distance of distal most vascular pedicle from the ulnar styloid process (cm)	3.7	18.6	11.91	5.13

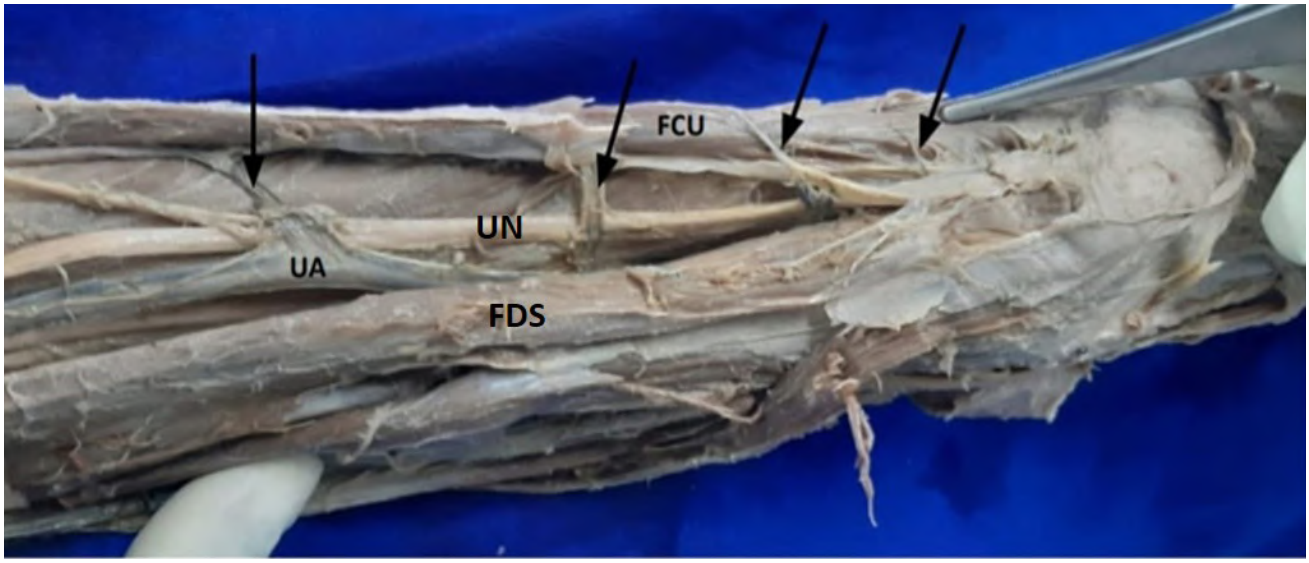

Fig. 3c.- Left upper limb showing flexor carpi ulnaris with four proximal vascular pedicles indicated by black arrows. FCU- Flexor carpi ulnaris, UN- Ulnar nerve, UA- Ulnar artery, FDS- Flexor digitorum superficialis.

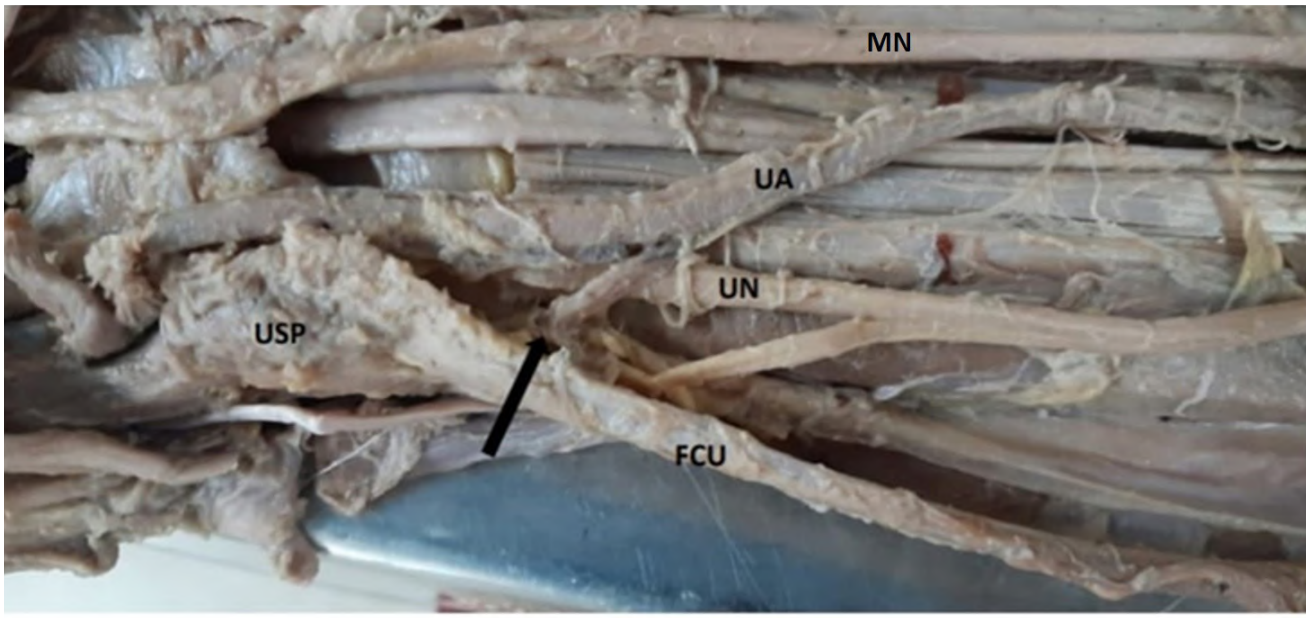

Fig. 3d.- Dissected lower part of front of forearm showing distal vascular pedicle of Flexor carpi ulnaris arising from the ulnar artery (arrow). FCU- Flexor carpi ulnaris, UN- Ulnar nerve, UA- Ulnar artery, MN- Median nerve, ME- medial epicondyle, USP- ulnar styloid process.

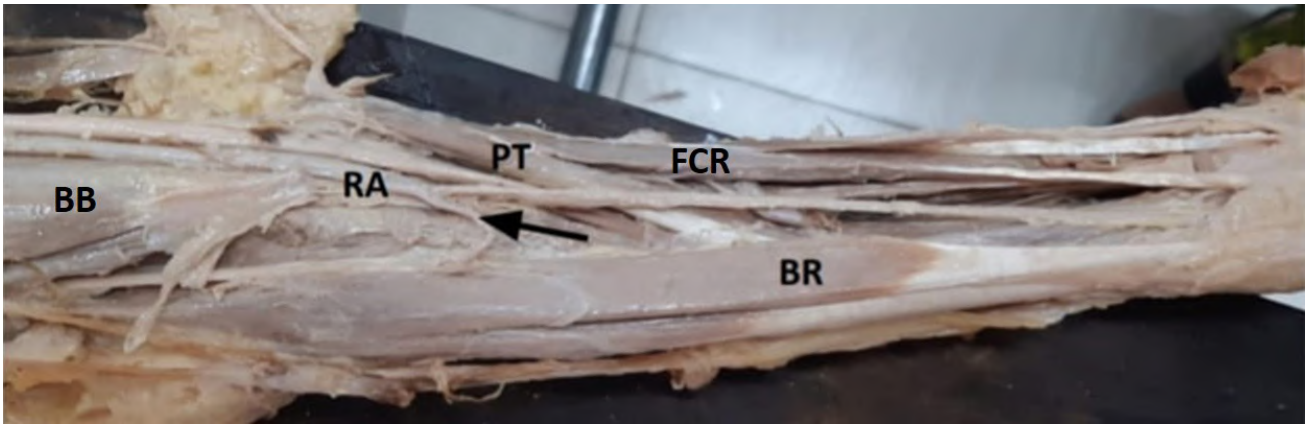

Fig. 4a.- Dissected right upper limb showing brachioradialis with vascular pedicle (black arrow) arising from radial artery. BR- Brachioradialis, RA- Radial artery, PT- Pronator teres, BB- Biceps brachii muscle, FCR- Flexor carpi radialis.

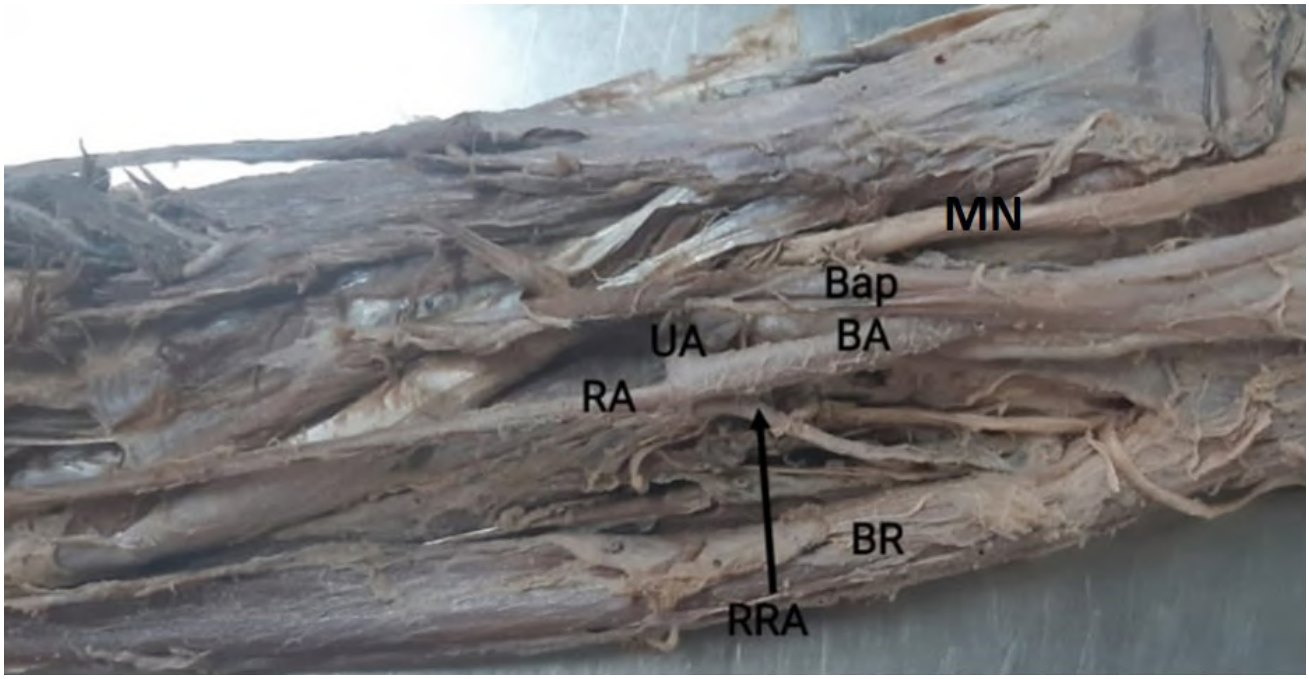

Fig. 4b.- Brachioradialis with vascular pedicle arising from radial recurrent artery (arrow). BR- Brachioradialis, RA- Radial artery, RRA- Radial recurrent artery, BA- Brachial artery, UA- Ulnar artery, Bap- Bicipital aponeurosis, MN- Median nerve.

The average distance of the vascular pedicle of BR from the LE was 6.56 cm with a range of 4 cm to 13 cm, and from the OP was 8.84 cm with a range of 6.2 cm to 14.5 cm.

DISCUSSION

The option available for the corrections of soft tissue loss around the elbow region include local and axial fascio-cutaneous flaps, distant pedicle flap, local muscle flaps by using anconeus, BR and FCU, or distant muscle flaps by using latissimus dorsi, etc. (Sharpe et al., 2014). Results of the previous studies have shown significant benefits in using FCU flap for soft tissue reconstruction around the proximal forearm, elbow and distal arm region (Sharpe et al., 2014; Payne et al., 2011).

The average length of the FCU muscle and its tendons were 28.96 ± 2.16 cm and 10.05 ± 2.2 cm respectively in our study. Sharpe et al. (2014) measured the length of FCU from the medial epicondyle to the pisiform bone, and found its average length as 28.3 cm with a range from 25.2 cm and 32.6 cm. Payne et al. (2011) reported the average length of FCU from the olecranon process to the pisiform bone as 27.4 cm. Wysocki et al. (2008) measured the FCU length from the olecranon process to the ulnar styloid process and reported it as 26.6 cm. These findings correspond to our study. The knowledge of the morphometry of FCU is important because it can be transplanted to improve the wrist function in patients suffering from cerebral palsy. The FCU can be transplanted to the extensor carpi radialis longus and the extensor carpi brevis to improve the hand function (Green et al., 1962; Wenner et al., 1988).

In our study, the average number of vascular pedicles was 2.3 with the range of 1 to 4 and all the pedicles were arising from ulnar artery. The average distance of the first, second, third and fourth vascular pedicles from the medial epicondyle was 9.74 cm, 13.45 cm, 16.87 cm and 23.3 cm, respectively. This finding is different from the study by Sharpe et al. (2014). They have reported that the average number of vascular pedicles of FCU is 3.8, with a range from 2 to 7 and all the pedicles were arising from the ulnar artery. The distance of seven vascular pedicles were 5.6 cm, 8.2 cm, 12.2 cm, 14.6 cm, 20.1 cm, 21.3 cm and 27.5 cm from the medial epicondyle. The average distance of the proximal pedicle from OP was 5.9 cm and 5.0 cm by Payne et al. (2011) and Wysocki et al. (2008), respectively. Shen et al. (2008) in their anatomical study reported that the ulnar artery provided vascular pedicle in 86% and ulnar recurrent artery in 14% of specimens. Andre et al. (2014) reported harvesting FCU musculocutaneous flap is rel-

atively a faster and reliable procedure for tissue loss around the olecranon process, as the proximal pedicle is more constant in position (6 cm from OP), and it does not require microsurgery, because the pedicle can be easily visible. Anatomical knowledge of FCU like the long length of the muscle belly, its rich vascularity and its vicinity to the elbow region, confirms that it is the best suitable graft material for soft tissue loss.

In the present study, the average distance of the distal capsular pedicle from the ulnar styloid process was 11.91 cm with the range between 3.7 cm to 18.6 cm. The distal vascular pedicle is the least reported in the literature. Yang et al. (2019) studied the distance of the distal vascular pedicle from the ulnar styloid process and reported that the average distance was 3 cm, with a range of 2.6 to 3.5 cm. They used a distal FCU flap for the treatment of median nerve neuroma with carpal tunnel syndrome in a patient following a previous median nerve injury repair. Complete recovery from symptoms of carpal tunnel syndrome like cessation of pain and tingling sensation were achieved in the patient within 4 weeks of treatment. They concluded that the distal FCU flap can also be utilized for the soft tissue reconstruction of the distal forearm, wrist and hand region.

The average length of the BR muscle in our study was 28.2 cm and its tendon was 8.2 cm. In a study by Hospatna et al. (2020), the average length of the muscle belly and tendon of the BR were 21.22 cm and 12.7 cm respectively. Rohrich et al. (1995) reported the mean length of the BR tendon as 6.9 cm. BR can be used as a graft material in cases of lower part of brachial plexus injury (C7-T1), causing paralysis of flexor muscles of the forearm, as BR is commonly spared in these injuries because of its innervation by C5, C6 (Srikanth et al., 2018). BR can also be used as graft for flexor pollicis longus to improve lateral pinch in tetraplegic patients (Waters et al., 1985).

Rohrich et al. (1995) found vascular pedicle to BR arising from RRA in 58%, BA in 24% and RA in 17% of the study sample. Sanger et al. (1994) reported the vascular pedicles from RA in 39.4%, RRA in 33.3% and BA in 27.3%. The report from Shen et al. (2008) stated that the pedicles wearosere arising from RA in 38%, RRA in 33.3% and BA in 27.3% of cases. Gilbert et al. (1980) found pedicles from RRA (10%), RA (78%) and BA (12%). In our study, we found that the arterial pedicles of the BR from RRA in 56.66% and RA in 43.33% (Fig. 4) of cases. We did not find vascular pedicles from BA. The comparison of the vascular pedicle to BR between our study and others in depicted in the Fig. 5.

Average distance of the vascular pedicle of from LE was 6.4 cm in our study with the range of 4 cm to 13 cm. The average distance of the pedicle from

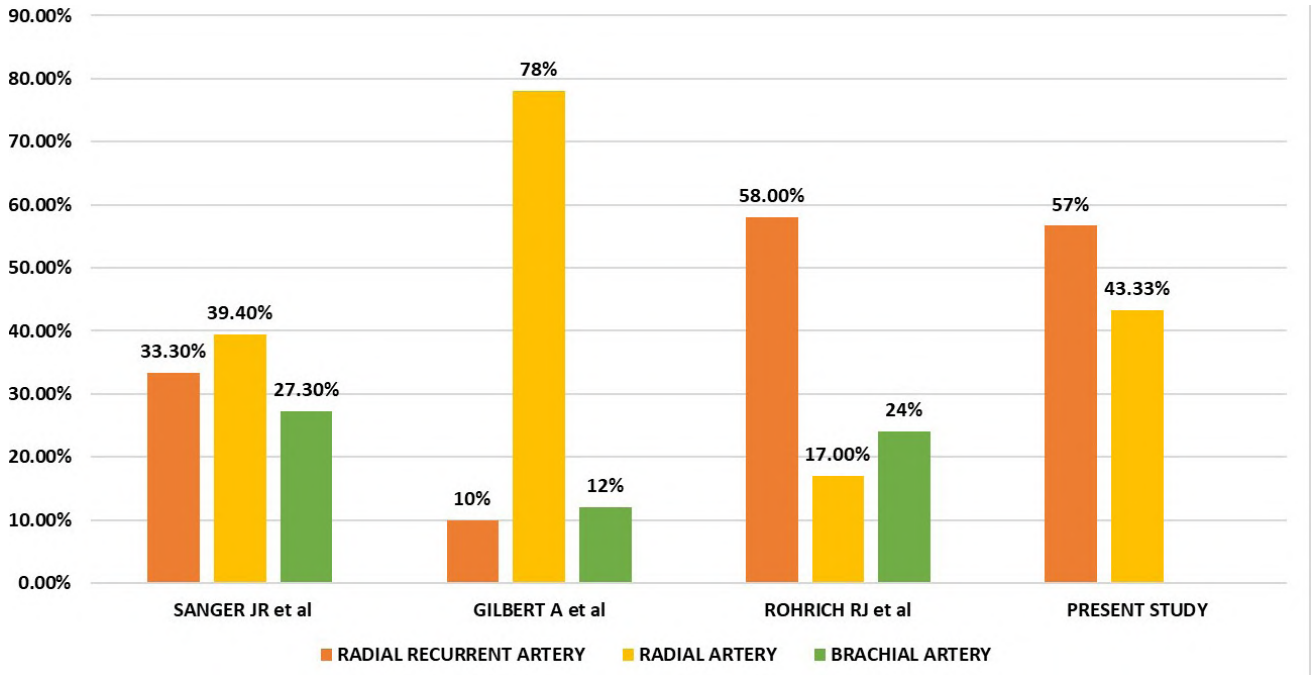

Fig. 5.- Comparison data of origin of vascular pedicles of brachioradialis.

OP was 8.84 cm with the range of 6.2 cm to 14.5 cm. Sanger et al. (1994) reported that the proximal perforator of the BR was at the middle third of the muscle in a majority of the specimens. However, in literature review we did not find the distance of the vascular pedicles from any bony landmarks. Therefore, result of this study may benefit the clinicians and researchers to know the level of vascular pedicle from the LE and OP and where to pivot the flap. Zampeli et al. (2019) have used BR muscle flap for soft tissue defect around elbow due to arthroplasty, postoperative infection or neuropathic arthropathy causing elbow arthrodesis. They have reported that all their patients had viable and functional soft tissue coverage after flap surgery.

Increase in the knowledge of the anatomy of the muscle, its blood supply, and level of perforators is important in plastic and reconstructive surgeries. Muscle flaps by anconeus, BR and FCU are the preferred choice for significant defects in the posterior elbow region, especially when it is associated with infection, because they provide bulkier tissue than the other type of flap (Patel et al., 2013).

We have presented the comprehensive data of the morphometry and vascular anatomy of FCU and BR in a South Indian population. We have also provided the data related to the level of vascular pedicles of BR, which is scarcely available in the literature. However, the age and gender differences of these morphometric data were not determined in this study. These are the limitations of this research.

CONCLUSION

The present study reports the morphometric and vascular anatomy of FCU and BR. The detailed data about the topographic anatomy of the vascular pedicle are provided, which can be considered the morphological database for the South Indian population. These data are beneficial to the surgeons for tendon transplants and muscle flap surgery to cover the soft tissue loss around the elbow and wrist region.

ACKNOWLEDGEMENTS

The authors sincerely thank those who donated their bodies to science so that anatomical research and teaching could be performed. Results from such research can potentially increase scientific knowledge and can improve patient care. Therefore, these donors and their families deserve our highest respect.

REFERENCES

ANDRE A, BONNEVIALLE N, GROLLEAU JL, MANSAT P (2014) Soft-tissue coverage of olecranon with musculocutaneous flexor carpi ulnaris flap. *Orthop Traumatol Surg Res*, 100(8): 963-966.

GILBERT A, RESTREPO J (1980) Le long supinateur: anatomie et utilisation comme lambeau de rotation musculaire [The brachioradial muscle: anatomy and use as a muscular rotation flap]. *Ann Chirurgie Plastique*, 25(1): 72-75.

GREEN WT, BANKS HH (1962) Flexor carpi ulnaris transplant and its use in cerebral palsy. *J Bone Joint Surg Am*, 44-A: 1343-1430.

HOSAPATNA M, SOUZA AD, RAO M, HARI ANKOLEKAR V (2020) Morphology and innervation of brachioradialis and flexor carpi radialis and their utility in tendon transfer surgeries: A cadaveric study. *Morphologie: Bull l'Assoc Anat*, 104(345): 91-96.

KELLY BP, CHUNG KC (2015) Soft-tissue coverage for elbow trauma. *Hand Clinics*, 31(4): 693-703.

MEALS RA (1989) The use of a flexor carpi ulnaris muscle flap in the treatment of an infected non-union of the proximal ulna. A case report. *Clin Orthop Relat Res*, (240):168-172.

OOI A, NG J, CHUI C, GOH T, TAN BK (2016) Maximizing outcomes while minimizing morbidity: an illustrated case review of elbow soft tissue reconstruction. *Plast Surg Int*, 2016: 2841816.

PATEL KM, HIGGINS JP (2013) Posterior elbow wounds: soft tissue coverage options and techniques. *Orthop Clin North Am*, 44(3): 409-417.

PAYNE DE, KAUFMAN AM, WYSOCKI RW, RICHARD MJ, RUCH DS, LEVERSEDGE FJ (2011) Vascular perfusion of a flexor carpi ulnaris muscle turnover pedicle flap for posterior elbow soft tissue reconstruction: a cadaveric study. *J Hand Surg Am*, 36(2): 246-251.

ROHRICH RJ, INGRAM AE JR (1995) Brachioradialis muscle flap: clinical anatomy and use in soft-tissue reconstruction of the elbow. *Ann Plast Surg*, 35(1): 70-76.

SANGER JR, YE Z, YOUSIF NJ, MATLOUB HS (1994) The brachioradialis forearm flap: anatomy and clinical application. *Plast Reconstr Surg*, 94(5): 667-674.

SHARPE F, BARRY P, LIN SD, STEVANOVIC M (2014) Anatomic study of the flexor carpi ulnaris muscle and its application to soft tissue coverage of the elbow with clinical correlation. *J Shoulder Elbow Surg*, 23(1): 82-90.

SHEN S, PANG J, SENEVIRATNE S, ASHTON MW, CORLETT RJ, TAYLOR GI (2008) A comparative anatomical study of brachioradialis and flexor carpi ulnaris muscles: implications for total tongue reconstruction. *Plast Reconstr Surg*, 121(3): 816-829.

SRIKANTH R, RAYIDI KR, KAKUMANU S (2018) Brachioradialis to flexor digitorum profundus tendon transfer to restore finger flexion. *Indian J Plast Surg*, 51(2): 123-130.

STANDRING S (2008) Gray's Anatomy. The Anatomical Basis of Clinical Practice. 40th ed. Churchill-Livingstone, London, pp 847-849.

WATERS R, MOORE KR, GRABOFF SR, PARIS K (1985) Brachioradialis to flexor pollicis longus tendon transfer for active lateral pinch in the tetraplegic. *J Hand Surg Am*, 10(3): 385-391.

WENNER SM, JOHNSON KA (1988) Transfer of the flexor carpi ulnaris to the radial wrist extensors in cerebral palsy. *J Hand Surg Am*, 13(2): 231-233.

WYSOCKI RW, GRAY RL, FERNANDEZ JJ, COHEN MS (2008) Posterior elbow coverage using whole and split flexor carpi ulnaris flaps: a cadaveric study. *J Hand Surg Am*, 33(10): 1807-1812.

YANG K, RIVEDAL D, BOEHM L, YAN JG, SANGER J, MATLOUB H (2019) Distally based pedicled flexor carpi ulnaris muscle flap: an anatomical study and clinical application. *Hand (NY)*, 14(1): 121-126.

ZAMPELI F, SPYRIDONOS S, FANDRIDIS E (2019) Brachioradialis muscle flap for posterior elbow defects: a simple and effective solution for the upper limb surgeon. *J Shoulder Elbow Surg*, 28(8): 1476-1483.

The possible protective role of vitamin C on rat parotid gland exposed to mobile phone radiation

Zainab Altaib[1], W.S. Sabbah[2], Ashraf Albrakati[3], Ali Abdelhady[4,5], Abeer Mostafa[6]

[1] Department of Histology and Cell Biology, Faculty of Medicine, Helwan University, Helwan, Egypt

[2] Department of Anatomy, Faculty of Medicine for Girls, Al Azhar University, Cairo, Egypt

[3] Department of Human Anatomy, College of Medicine, Taif University, Taif, Saudi Arabia

[4] MBBCh, School of Medicine, Ain shams University

[5] Department of Surgery, School of Medicine, Tulane University, New Orleans, Louisiana 70112, USA

[6] Department of Medical Biochemistry and Molecular Biology, Faculty of Medicine, Cairo University, Cairo, Egypt

SUMMARY

The widespread use of cell phones recently has raised interest in studying the safety of exposure to their electromagnetic waves. This study aimed to evaluate the possible protective role of vitamin C (Vit. C) against the pathological effects produced by the relatively long duration of third-generation mobile phone radiation exposure in the parotid gland of male white albino rats. Also, to detect the expected recovery after 4 weeks of withdrawal by immunohistochemical, histopathological, and biomolecular studies. Forty male adult white albino rats were used in this study, equally divided into 4 groups of 10 rats in each group: Group I served as the sham control group; Group II was exposed to radiation by phone generator (2100 MHz) for 3 hours/day for 5 days/week for 6 weeks; and Group III was exposed to phone radiation similar to Group II and supplemented with Vit. C at a dose of 40 mg/kg for 5 days per week for 6 weeks. Group IV (withdrawal) was exposed to radiation as Group II, then left without intervention for 4 weeks. Histological and immunohistochemical, and the biochemical evaluation of oxidative stress within parotid tissue (malonaldehyde (MDA), superoxide dismutase (SOD), salivary total protein, and amylase activity). qRT-PCR for TGF, MMP2, NFKB, and TNF gene expression was performed in this study. Histological examination of the parotid gland in group II showed many histological changes, such as degenerative changes in the duct system, epithelial lining of the acini, interstitial space which different collagen fibers and polysaccharides, blood capillaries, and nuclei. Also, alpha smooth muscle actin (α-SMA) and Ki-67 were aggravated. The statistical analysis showed that treating rats with vitamin C improved the parotid glands' ability to secrete amylase activity and total protein. It also fixed the antioxidant. Inflammatory cytokines TNF, NFKB, and fibrotic marker TGF and MMP2 gene expression were significantly upregulated in the exposed group,

Corresponding author:
Abeer Mostafa. Department of Medical Biochemistry and Molecular Biology, Faculty of Medicine, Cairo University, Cairo, Egypt. E-mail: abeer.mostafa@kasralainy.edu.eg / dr_abeer.mostafa@cu.edu.eg / Dr_abeer.mostafa@yahoo.com

Submitted: May 14, 2023. **Accepted:** September 26, 2023

https://doi.org/10.52083/GGDJ8047

which was restored nearly to the control group after Vit C supplementation. Long-term exposure to mobile radiation affected the secretory function and the histological structure of the parotid tissues. Vitamin C supplementation ameliorated these pathological effects.

Key words: Mobile phone radiation – MDA – SOD – Vitamin C – α-SMA

INTRODUCTION

In recent times, non-ionizing radiation, particularly microwave radiation emitted by mobile phones, has become ubiquitous, with almost the entire global population utilizing these devices (Rosado et al., 2014). The potential health impacts of mobile phone radiation had been the previously studied with relevant positive association. The International Agency for Research on Cancer (IARC) has classified the electromagnetic fields (EMF) generated by mobile phones as potentially carcinogenic, emphasizing the importance of ongoing public health surveillance. Over the last two decades, several studies had been developed on the effects of mobile phone radiation on head and neck cancers, with the parotid gland being identified as particularly vulnerable due to its proximity to mobile phone usage. The widespread adoption of 3G mobile technology has raised concerns about both the thermal and non-thermal effects of electromagnetic radiation. There is growing apprehension regarding the mechanisms by which mobile phones may exert their adverse effects, including the potential for inducing oxidative stress and disrupting antioxidant defense systems. Saliva, a critical component in maintaining oral health, is produced predominantly by the major salivary glands, with the parotid gland contributing significantly. Disruptions in salivary gland function can lead to xerostomia, a condition with challenging side effects, highlighting the urgency for effective protective measures against mobile phone radiation. This study aims to explore the protective effects of Vitamin C on the parotid glands of male Albino rats exposed to 3G mobile phone radiation, assessing both the immediate and long-term recovery potential through histopathological, immunohistochemical, and biomolecular analyses.

MATERIALS AND METHODS

Used drug

Effervescent Vit C (vitacid C) tablets were purchased from Chemical Industries Development Company, Giza, Egypt. Each tablet contains 1000 mg of Vit C.

Animals

The study included 40 healthy adult male white albino rats had 3-4 months age, weighing 200-230 gm obtained from the animal house of Faculty of Medicine Helwan University and handled according to the guidelines after the approval of the Research Ethics Committee (REC) for human and animal research with approval number (REC-FM-HU-38-2023) from the animal house-Faculty of Medicine Helwan University. The animals were maintained at 50-70% humidity, temperature of 22 ± 2°C and with a 12 h light/dark cycle. All efforts were done to reduce animals' suffering. Sample size was calculated using the G power software. Based on Rosado et al. (2014), we found that ten rats per group were an appropriate sample size for the study, with total sample size 40 rats (four groups). α error probability = 0.05, power = 80% and, effect size = 0.56, after acclimatization, rats were randomly divided equally into 4 groups (10 rats for each group):

- Group I (Sham control): rats were given 0.5 ml of distilled water once /day/orally for 5 days/ week for 6 weeks.
- Group II (irradiated group): rats were exposed to mobile phone generator radiation 2100 MHz EMF 3hrs/day (between 10 am and 1 pm) for 5 consecutive days /week for 6 weeks.
- Group III:(irradiated + vitamin C group): rats were given 40mg/kg Vit C orally, one hour before exposure to irradiation as in group II (Jelodar et al., 2013).
- Group IV: (irradiated + withdrawal group): rats were exposed to irradiation as in group II, then left for withdrawal without intervention for further4 weeks.

Exposure system and application of electromagnetic field

Animals were exposed to 2100 MHz radiofrequency radiation emitted by an electromagnetic field generator (Trannsteltrafo. LTS 602) simulating a 3G mobile phone for 3hrs/day (between 10 am and 1 pm) for 5 consecutive days /week for 6weeks. A specially designated exposure system of electromagnetic field (EMF) was used with dipole exposure antenna and round plastic tube cage (Holiday Industries Inc., UK) (El-Bediwi et al., 2011). The animals were sacrificed by cervical dislocation (El-Akabawy et al., 2015) at the end of the experiment, right parotid glands of all rats were carefully dissected and divided into two parts. One part was used for histological evaluation, and the other is for biomolecular analysis.

Biomolecular analysis

Estimation of oxidative markers MDA and antioxidant marker SOD

Parotid tissue Malondialdehyde (MDA) was assessed by ELISA technique according to kit instruction: MYBio source, USA. Cat # MBS2605193 Parotid tissue superoxide dismutase (SOD) was assessed by ELISA technique according to kit instruction: MYBio source, USA. Cat # MBS036924.

Collection and preparation of saliva

Whole saliva was collected after 10-hrs fasting according to a standardized method. Using 0.1 ml/kg Hypnorm IM (Janssen Pharmaceutical, Beerse, Belgium) The animals were anaesthetized. Saliva secretion was stimulated by injection of a combination of 2.5 mg/kg body weight of isoproterenol (Sigma Chemical Co., St. Louis, MO) and 2.5 mg/kg body weight of pilocarpine (Sigma Chemical Co., St. Louis, MO) subcutaneously. To prevent the contamination from tears and nasal secretion, the rats were put with their mouth placed over a plastic cup; also to ensure a constant body temperature for 3-5 minutes during saliva collection, the rats were placed under electric lamps. The collected saliva samples were centrifuged for 10 minutes at 3000 rpm; the biochemical parameters of the supernatants were analyzed (Johansson et al., 1989).

Estimation of salivary amylase activity

Salivary amylase activity was assessed by ELISA technique according to kit instruction: MYBio source, USA. Cat # MBS8806064.

Estimation of salivary total protein

Salivary total protein was assessed by ELISA technique according to kit instruction: MYBio source, USA. Cat # MBS3808613.

Quantitative RT-PCR for studied genes

Parotid tissues from all groups were homogenized for total RNA extraction in 300 µl of lysis buffer according to kit instruction Gene JET Kit (Thermo Fisher Scientific Inc., Germany, #K0732). 5 µl from the total RNA were used for qRT-PCR using the Step-one instrument (Applied Biosystems, U.S.A.) according to kit instructions (SensiFASTTM SYBR R Hi-ROX) (catalog number PI-50217 V). Thermal cycles were as follows: 15min for 45°C for one cycle for cDNA synthesis, 10 min at 95°C for reverse transcriptase enzyme inactivation, followed by 40 cycles for amplification. Each cycle was continued for: 10 s at 95°C, 30 s at 60°C, and 30 s at 72°C. The expression of studied genes was normalized to GAPDH and analyzed by ΔΔ ct method.

Primer sequences for TGF gene:

forward, 5′-CCCAGCATCTGCAAAGCTC3′

reverse, 5′GTCAATGTACAGCTGCCGCA3′

MMP2gene

Forward, 5′GTCTTCCCCTTCACTTTTCTG3′

reverse, 5′CGGAA GTTCTTGGTGTAGGTG3′

NFKB gene

forward, 5′AATTGCCCCGGCAT3′

reverse, 5′TCCCGTAACCGCGTA3

TNF gene

forward, 5′CTCTTCTGCCTGCTGCACTTTG3′

reverse, 5′ATGGGCTACAGGCTTGTCACTC3′

GAPDH gene

forward, 5′CATGTTCGTCATGGGGTGAACCA3′

reverse, 5′AGTGATGGCATGGACTGTGGTCAT-3′

Histological study

The right parotid salivary glands of all rats were dissected and were fixed in neutral buffered 10% formalin, dehydrated, embedded in paraffin, sections of 5 µm-thick were cut, stained with H&E to analyze the histological structure, Masson's trichrome stain was done to assess collagen fiber content. The presence of glycoprotein at the basement membrane was detected by Periodic acid Schiff (PAS) staining histochemical study (Suvarna et al., 2013).

Immunohistochemical study

In this study using immunohistochemistry for alpha smooth muscle actin (αSMA) helped identify the myoepithelial cells (MECs) during their differentiation **(**Suvarna et al., 2013), and Ki- 67 immune staining was used to detect the cellular proliferation (Maher et al., 2020).

Immunostaining for α-SMA

It was performed on deparaffinized, rehydrated, sections of 5-µm-thick were blocked with 1.5% normal goat serum in PBS. The sections were incubated with 6 ml prediluted primary (1ry) mouse monoclonal antiα-SMA antibody (Ab) (ab5694) (Dako Corporation, Glostrup, Denmark) for 45 minutes at room temperature, then incubated with a second-stage biotinylated antibody for 1 h, at room temperature (biotin conjugated goat anti-rabbit IgG, 1:200,). The reaction products were visualized after rinsing in PBS by immersing the section into the chromogen diaminobenzidine. Finally, counterstaining of the sections was done with Mayer's hematoxylin, dehydrated, and mounted. The positive cells for α-SMA showed brown cytoplasmic reaction. The negative control was processed in the same way, but omitting the step of 1ry Ab (Suvarna et al., 2013).

Immunostaining for Ki-67

5-µm paraffin sections were used for immunohistochemical detection of Ki-67 antigen using a rabbit monoclonal antibody. Hydration, and blocking of endogenous peroxidase was done after standard deparaffinization, sections were processed in a microwave oven twice (5 min each) at high power. Followed by a standard streptavidin-biotin peroxidase technique to detect the antigen. Sections were incubated at room temperature with anti-Ki-67 (dilution 1:40, DAKO, USA) for 30 min diaminobenzidine (Sigma Fast DAB). Mayer's haematoxylin solution was used for counterstaining. The same streptavidin–biotin technique was used in tissue sections, where 1% BSA in PBS replaced the primary antibody for negative control. The nuclear (nucleoplasmic) staining for Ki-67 was considered positive (Maher et al., 2020).

Morphometric study

Using Leica Quin 500LTD (Cambridge, UK) computer assisted image analysis system. The count of vesicular nuclei was performed in H&E-stained sections. The area percentage of collagen fibers stained with Masson trichrome and PAS positive staining of basement membrane was measured using binary mode.

The area percentage of α-SMA +ve MECs and that of Ki-67 positive nuclei were performed using interactive measurements menu (The Ki-67-positive nuclei were counted through a minimum of 200 cells per field in five different fields at ×400 magnification). The Ki-67 labeling index (Ki-67 LI) is the number (%) of positive cells (Luo et al., 2005; Hashemipour et al., 2014). The measurements were done in 10 high power fields.

Statistical analysis

Statistical analysis of the studied parameters was performed by using SPSS program (version 25; SPSS Inc., Chicago, Illinois, USA). Values were expressed as means ± SD and compared using ANOVA test. $P < 0.05$ was considered statistically significant (Emsley et al., 2010).

RESULTS

General observations

No rat deaths were observed during the experiment. The electromagnetic fields were well tolerated by the animals throughout the study.

Histological results

Haematoxylin.and.Eosin.stain

G*roup I (sham control group)*: The sections of parotid glands of the control group using the light

microscope showed the normal architecture. It is formed of stroma, which consists of the connective tissue capsule and the septa extending from capsule and dividing the glands into lobules. The parenchyma between the septa consists of groups of pure serous acini, and were lined by pyramidal cells having rounded central vesicular nuclei and basal basophilic cytoplasm. The duct portion, consisting of striated, interlobular and intra-lobular ducts, were easily detected. There was a network of capillaries in between the acini and in a connective tissue septum (Fig. 1A).

G*roup II* showed widened connective tissue septa between some lobules and homogenous acidophilic material in others; besides, disorganized acini in some areas could be observed. Some acinar cells showed dark nuclei and others showed cytoplasmic vacuoles. Inter-lobular septa contain dense connective tissue fibers with cellular infiltration between the lobules and around a dilated duct. Dilated and congested blood vessels were seen. There was also loss of the architecture of multiple lobules (Fig. 1B).

G*roup III (irradiated + Vit C)* showed the capsule, septa between the lobules. Also, an inter-lobular duct in a connective tissue septum and intra-lobular ducts in between the acini apparently normal serous acini, intra-lobular duct, interlobular ducts and non-congested blood vessel in a slightly thickened connective tissue septum containing homogeneous material (Fig. 1C).

G*roup IV (irradiated + Withdrew)*: Apart from the presence of few vacuolations, few pyknotic nuclei, and slightly congested blood vessels, it showed apparently normal histological features (Fig. 1D).

Masson's Trichrome Stain

Group I (sham control group): few blue collagen fibers in the capsule, fibers in the septa between the lobes and the lobules and around the interlobular ducts and blood vessels were detected (Fig. 2A).

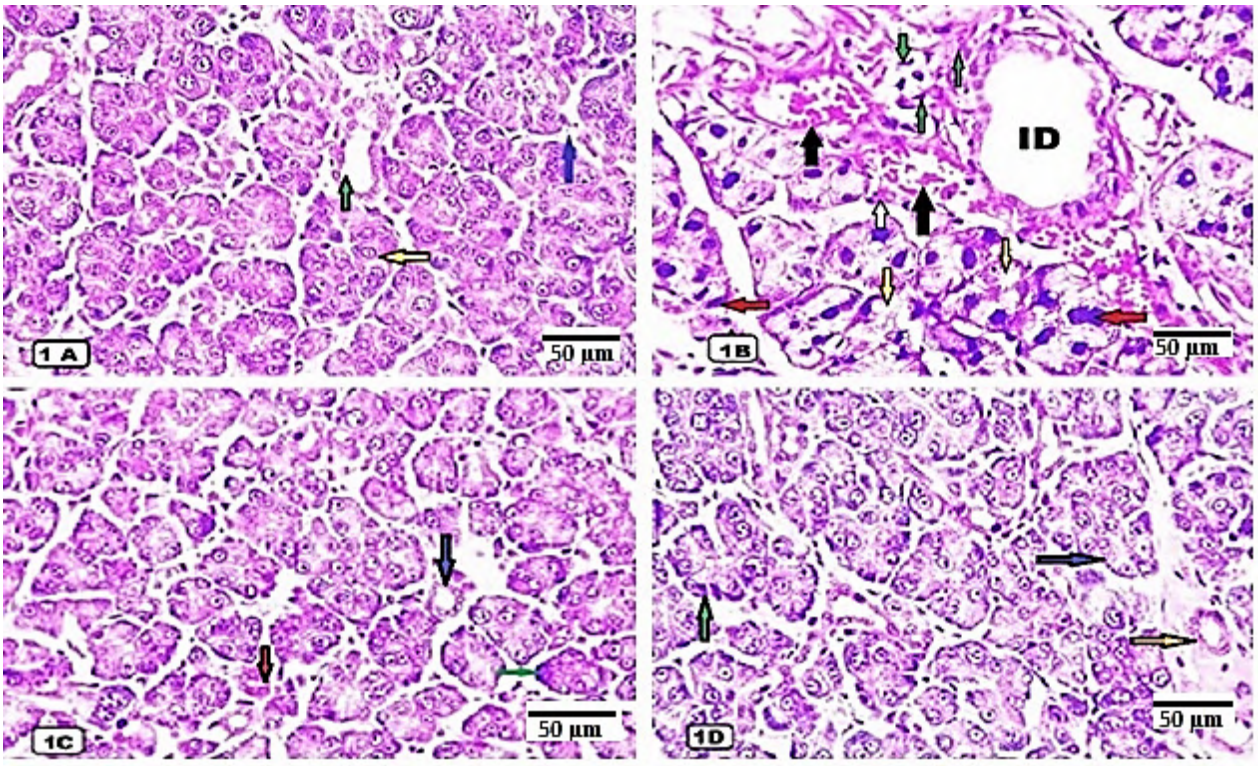

Fig. 1.- H&E-stained parotid gland sections of all groups. x 400. Scale bars = 50 µm. (**1A**): Group I (sham control) showing rounded serous acini (yellow arrow) with narrow lumen. They have basal vesicular nuclei and basal basophilia. Note normal appearance of intralobular ducts (green arrow) and thin septa (blue arrow). (**1B**): group II (Radiation) showing irregular acini with ill-defined outline and darkly stained nuclei (red arrows) and cytoplasmic vacuoles (yellow arrows) and homogenous acidophilic material (white arrows). Cellular infiltration (green arrow) inside thick connective tissue septa and around a dilated interlobular duct (ID) with dilated congested blood vessels (black arrows). (**1C**): group III (Radiation +Vit C) showing acini and interlobular ducts nearly as control group (blue arrow) with few dark stained nuclei (green arrow), septa are also seen showed nearly normal blood vessels (red arrows). (**1D**): Group IV (Radiation + Withdrawal) showing nearly as control in acini (blue arrow) and intralobular ducts (yellow arrow) but few of dark stained nuclei and some vacuoles in few acini could be detected (green arrow).

G*roup II (irradiated)*: Multiple blue collagen fibers in the capsule, excessive collagen fibers in interlobular septa, around interlobular ducts in addition to blood vessels were detected (Fig. 2B).

G*roup III (irradiated+ Vit C)*: Sections clarified that the low amount of collagen fibers appeared in between the lobes and lobules and around ducts and blood vessels (Fig. 2C).

G*roup IV (irradiated +Withdrew)*: sections clarified that a moderate amount of collagen fibers (more than in Group III) appeared in between the lobes and lobules and around ducts and blood vessels (Fig. 2D).

PAS reaction

Group I (sham control group) showed obvious positive (a magenta color) PAS reaction in the basement membrane of the acini (Fig. 3A).

G*roup II (irradiated)*: The basement membrane of some acini showed moderate positive PAS reaction and absent in others (Fig. 3B).

G*roup III (irradiated + Vit C)* showed obvious positive PAS reaction in the basement membrane of the acini (Fig. 3C).

G*roup IV (irradiated + Withdrew)* showed obvious positive PAS reaction in the basement membrane of the acini nearly as in Group III (Fig. 3D).

Immunohistochemistry

Alpha smooth muscle actin (α-SMA)

Group I (sham control group): Immunoreaction to α-SMA showed brown cytoplasm in multiple MECs at the periphery of the acini and intra-lobular ducts. Mild positive reaction is also seen in the lining of blood vessels (Fig. 4A).

G*roup II (irradiated group)*: Section showed an increase in α-SMA immunoreaction at the interlobular ducts and periphery of the acini (Fig. 4B).

G*roup III (irradiated + Vit C group)*: Immunoreaction to α-SMA Sections showed α-SMA immunoreaction in multiple MECs at the periphery of

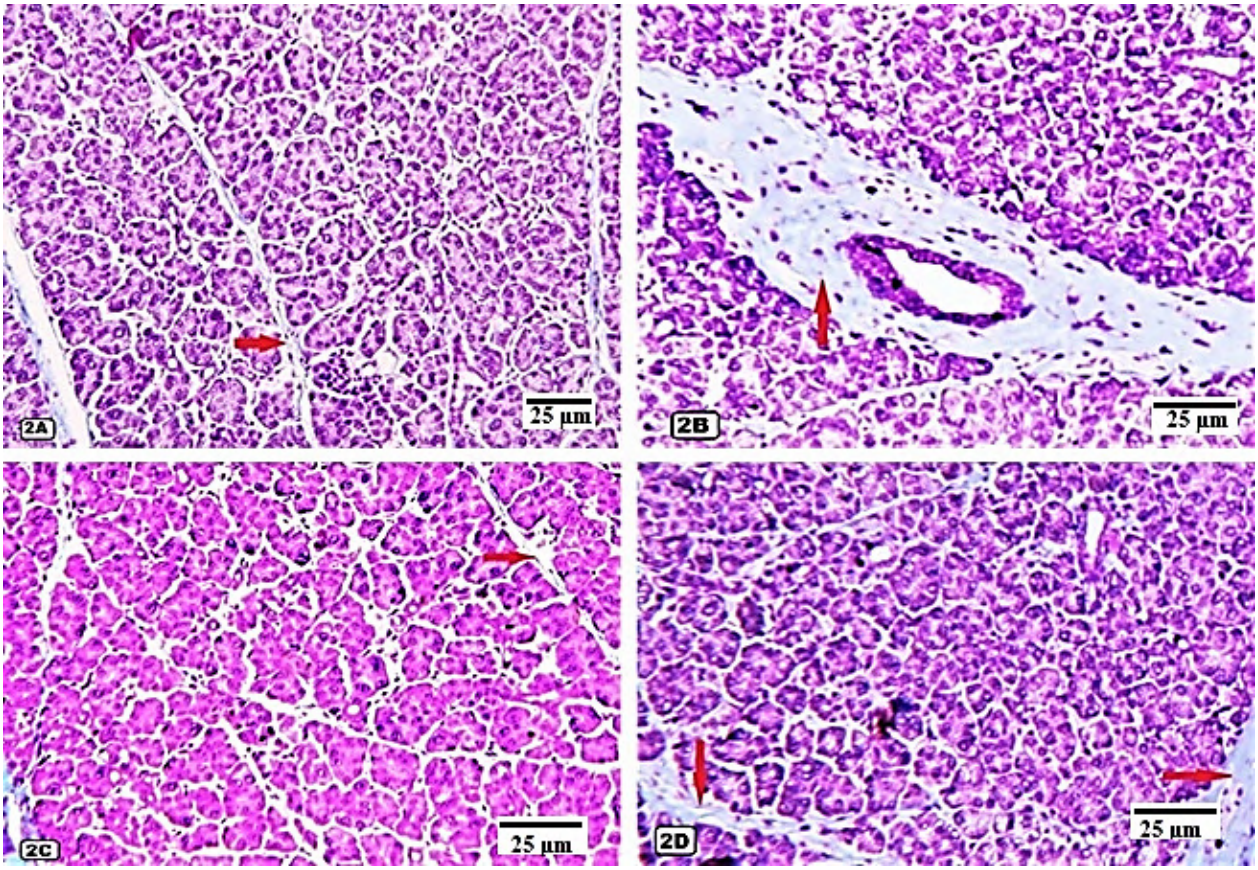

Fig. 2.- Masson's trichrome stain for all groups. ×200. Scale bars = 25 µm. **(2A)**: Section of the parotid gland of a sham control rat showing few blue stained collagen fibers (red arrow) in the connective tissue septa between the lobules. **(2B)**: Section from Group II showing extensive blue collagen surrounding lobules, interlobular ducts, and blood vessels. (red arrow). **(2C)**: Section from Group III showing few blue collagen fibres in inter and intra lobular septa (red arrow). **(2D)**: Section from Group IV showing moderate amount of blue collagen fibres in inter and intra lobular septa (red arrows).

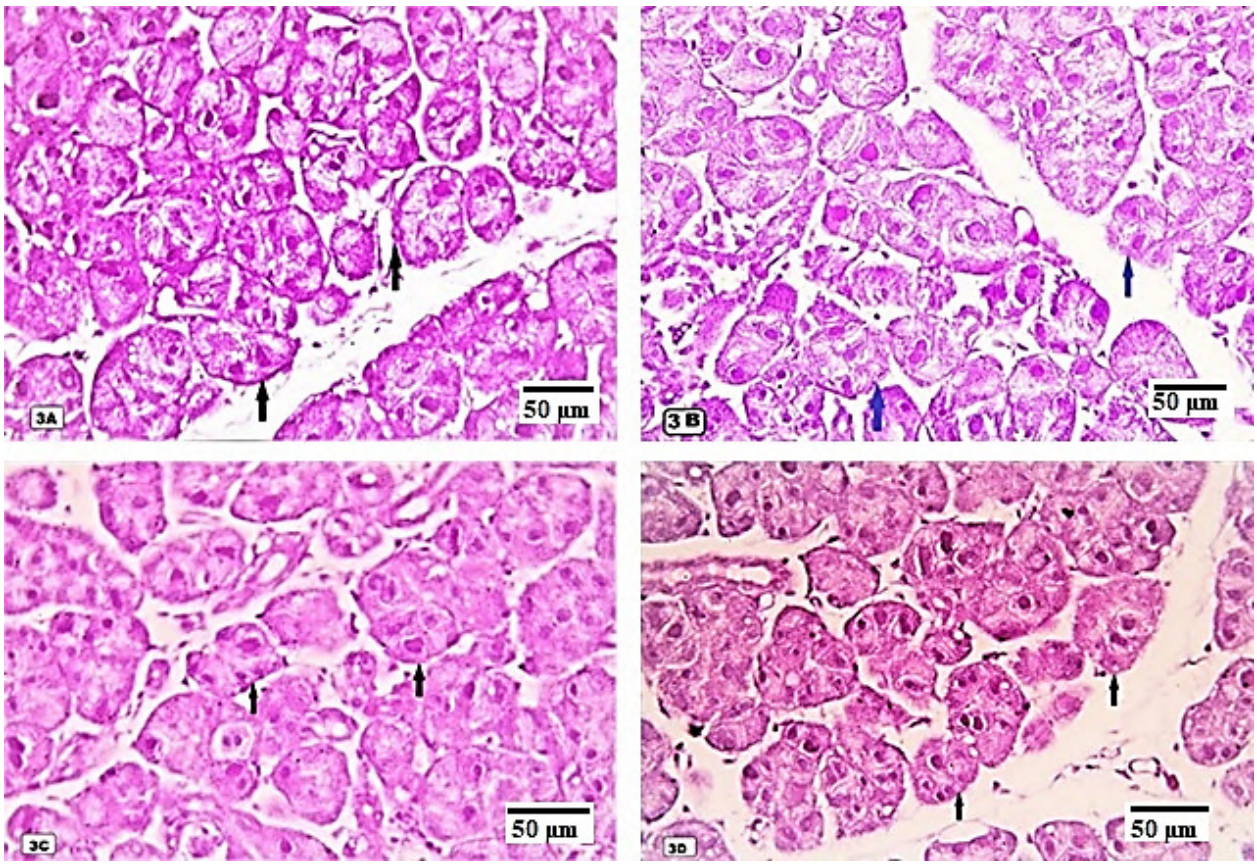

Fig. 3.- PAS reaction of all groups. ×400. Scale bars = 50 µm. **(3A)**: Section of the parotid gland of a control rat showing obvious positive PAS reaction in the basement membrane of the acini (black arrows). **(3B)**: Section of the parotid gland of irradiated group showing mild PAS reaction in the basement membrane of acini (blue arrows). **(3C)**: Section of the parotid gland of a rat in irradiated and with vit. C showing strong positive PAS reaction in basement membrane of almost acini (black arrows). **(3D)**: Section of the parotid gland of a rat in operated and withdrawal group showing moderate PAS reaction in basement membrane of almost acini (black arrows).

the acini and intra-lobular ducts more or less as control (Fig. 4C).

G*roup IV (irradiated +Withdrew group)*: Sections showed α-SMA immunoreaction in multiple MECs at the periphery of the acini and intra-lobular ducts more or less as control and less than Group II (Fig. 4D).

(Ki-67)

Group I (sham control group): Immunoreaction to Ki-67 showed positive immune reaction in very few nuclei (nucleoplasm) of acinar cells and the cells lining an intra-lobular duct (Fig. 5A).

G*roup II (irradiated group)*: Immunohistochemical examination showed of Ki- 67 slightly increased in positive reaction nuclei of the lining cells of acini and some cells lining an interlobular duct (Fig. 5B).

G*roup III (irradiated + Vit C group)*: Immunoreaction to Ki-67 in few nuclei of acinar cells nearly as control group (Fig. 5C).

G*roup IV (irradiated + Withdrew group)*: Immunoreaction to Ki-67 in few nuclei of acinar cells more or less as in Group II (Fig. 5D).

Morphometric analysis

The statistical analysis between the studied groups revealed that there was a significant increase in the mean number of vesicular nuclei ($P < 0.05$) in the sham control group (I) when compared with exposure group (II). But no significant differences ($P > 0.05$) were found when group III and group IV were compared, or when the last two groups compared with sham control group (Table 1). No significant increase ($P > 0.05$) in the mean area % of collagen fibers stained by Masson's trichrome were found when compared between sham control group and group III or group IV. But a significant increase ($P < 0.05$) in the mean area % of collagen fibers stained by Masson's trichrome of exposure group II was found when compared with shame control group (Table 1). No significant difference was found ($P > 0.05$)

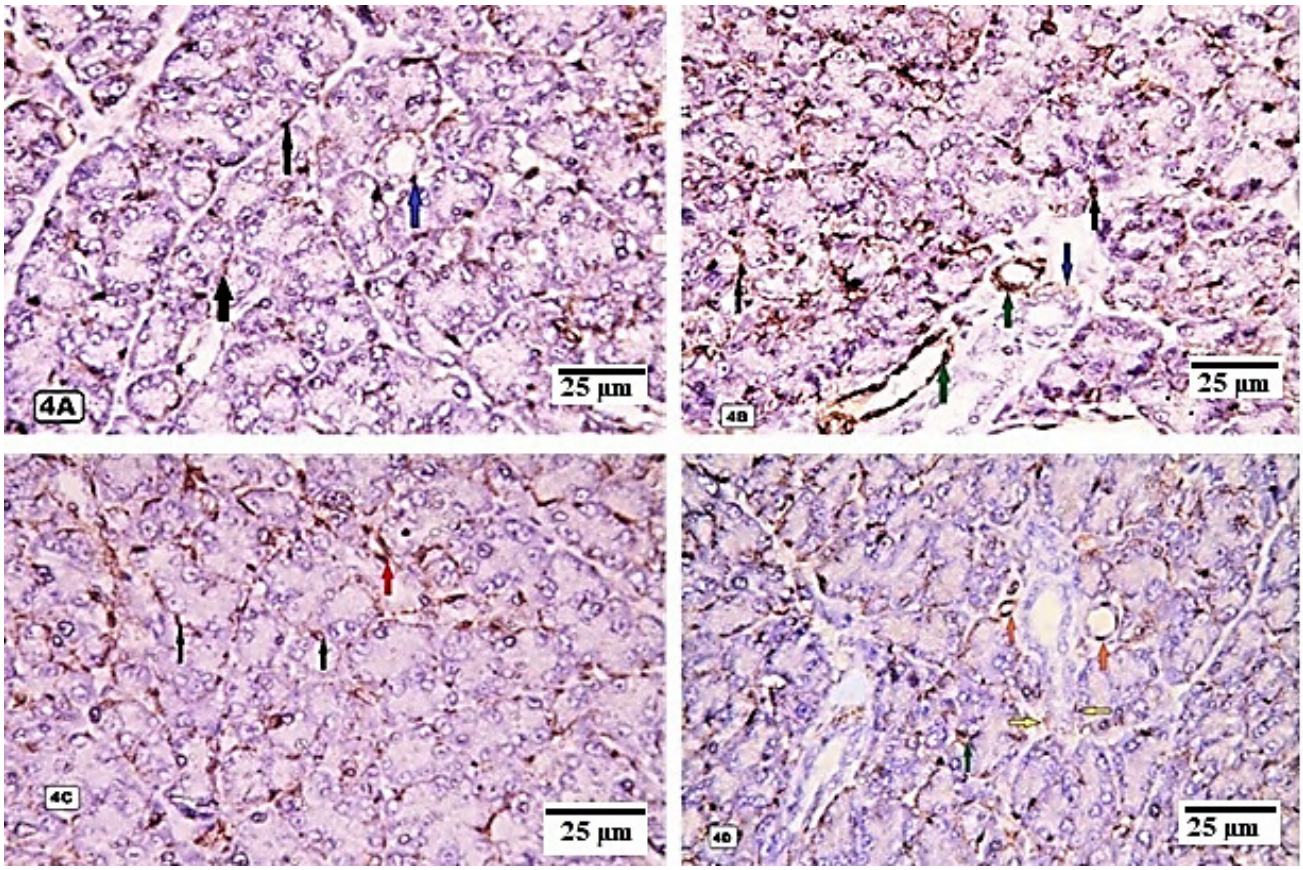

Fig. 4.- α-SMS immunoreaction of all groups. ×200. Scale bars = 25 µm. **(4A)**: Section of the parotid gland of a control rat showing a moderate α-SMA immunoreaction in multiple MECs at the periphery of the acini (black arrows) and intralobular ducts (blue arrow). **(4B)**: Section of the parotid gland of a rat in irradiated group showing an apparent increase in immune reaction for α-SMA in MECs at the periphery of the acini (black arrows), interlobular ducts (blue arrow) and in the lining of two blood vessels (green arrow) is also seen. **(4C)**: Section of the parotid gland of a rat in irradiated and with vit. C group showing a moderate α smooth muscle actin immunoreaction at the periphery of the acini (black arrows) intralobular ducts (red arrow), nearly as a control group. **(4D)**: Section of the parotid gland of a rat in irradiated and then withdrawal group showing α-SMA immunoreaction in multiple MECs at the periphery of the acini (green arrows) and intralobular ducts (yellow arrow) and in the lining of blood vessels (red arrows) less more than control group but less than irradiated group.

in the mean area % of PAS reaction in group III compared with sham control Groups I, and IV. But a significant decrease (P <0.05) in the mean area % of PAS reaction in Exposure group II was found when compared with sham control group I (Table 1). A significant increase (P <0.05) in the mean number of positive α-SMA in cytoplasm of MECs and mean number of positive Ki- 67 nuclei expression in exposure group II was found compared with sham control group. But no significant differences (P >0.05) were found when compared between group III and group IV or when the last two groups were compared with sham control group (Table 1).

Table 1. Mean count of vesicular nuclei, mean area percentage of Masson trichrome stained collagen fibers and PAS +ve staining, area percentage of α-SMA +ve MECs and Ki67 + in all studied groups.

	Group I (sham control)	**Group II (irradiated)**	**Group III (irradiated+ vit C)**	**Group IV (irradiated + withdrew)**
Count of vesicular nuclei	11.5 ± 1.3	6.1 ± 0.5*	10.7 ± 1.4 #	9.6± 1.2#
Collagen fibers	2.9 ± 0.5	7.8± 1.1*	3.4± 0.3 #	3.9±0.6 #
PAS +ve staining	4.1± 0.3	2. 6 ± 0.4*	3.8 ± 0.6#	3.2 ± 0.5#
SMA+ve MECs	2.47± 0.2	4.96 ± 0.7*	2.27± 0.3 #	2.52±0.2 #
Ki-67 +ve nuclei	0.35 ±0.04	0.95±0.20*	0.31 ±0.04#	0.38±0.05#

*significant <0.05

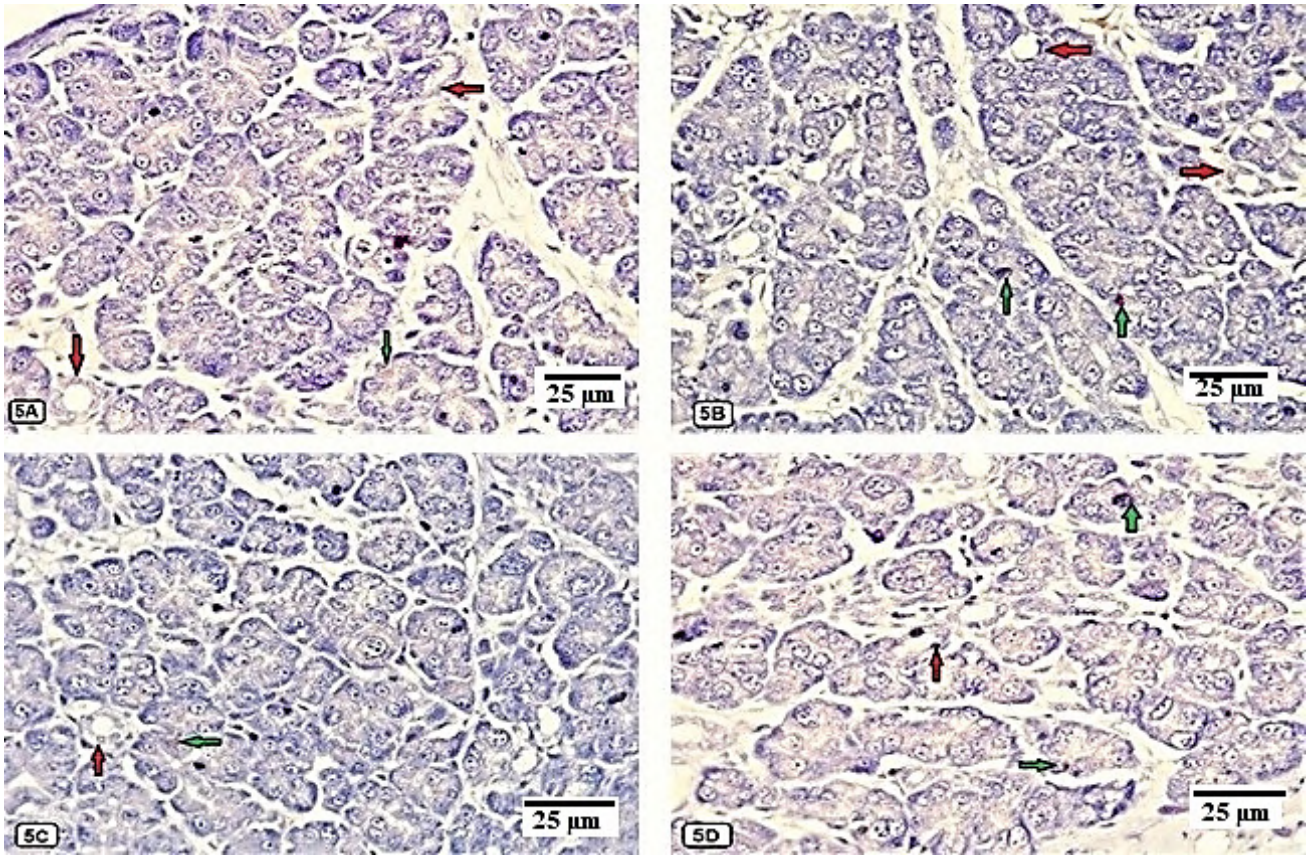

Fig. 5.- Ki-67 immunoreaction of all groups. x 200. Scale bars = 25 µm. **(5A)**: Section of the parotid gland of a rat of control group showing weak +ve Ki-67 immunoreaction in few nuclei of acinar cells (green arrow) but -ve reaction in the cells lining in an interlobar duct (red arrow). **(5B)**: Section of the parotid gland of group II (irradiated) rat showing moderate +ve Ki-67 immunoreactivity in nuclei of some cells of acini (green arrows) and also +ve in some nuclei of duct cells (red arrows). **(5C)**: Section of the parotid gland of a rat in Group III showing nearly to the control group in a few weak +ve Ki-67 immunoreaction in few nuclei of acinar cells (green arrow) but -ve reaction in the cells lining in an interlobar duct (red arrow). **(5D)**: Section of the parotid gland of rats in Group IV showing Ki- 67 immunoreaction in few nuclei (green arrow) of acinar cells.

Biomolecular analysis

Salivary amylase and total protein

There was a significant reduction in the secretory activity of the parotid gland (P <0.05) regarding the values of total protein and amylase activity in exposure group II compared with sham control groups I. But both Vit C administration and radiation withdrawal significantly (p<0.05) retain the secretory activity. No significant differences (P >0.05) between group I, III and group IV were found (Table 2).

Parotid tissue MDA and SOD

Exposure to mobile phone radiation significantly (p<0.05) increase the oxidative stress within the parotid tissue denoted by increase MDA levels and decrease SOD levels while Vit C administration

Table 2. Mean value of total protein (µg/ml), mean value of amylase activity (ng /ml), mean value of MDA (moL/mg tissue) and SOD (U/ml) in all studied groups.

	Group I (sham control)	Group II (irradiated)	Group III (irradiated + vit C)	Group IV (irradiated+ withdrew)
Total protein	83.7±3.8	60.9±3.6 *	78.6±9.8#	71.7±9.8#
Amylase activity	220.1±9.9	165.9±7.2 *	209.2±9.1#	198.7±8.8#
MDA	4.8± 0.3	9.9± 1.2 *	5.2±0.5#	5.9±0.6#
SOD	29.8± 5.57	12.65± 1.45 *	22.5±5.07#	23.3±3.22#

*significant P <0.05 compared to control
#significant P <0.05 compared to irradiated group

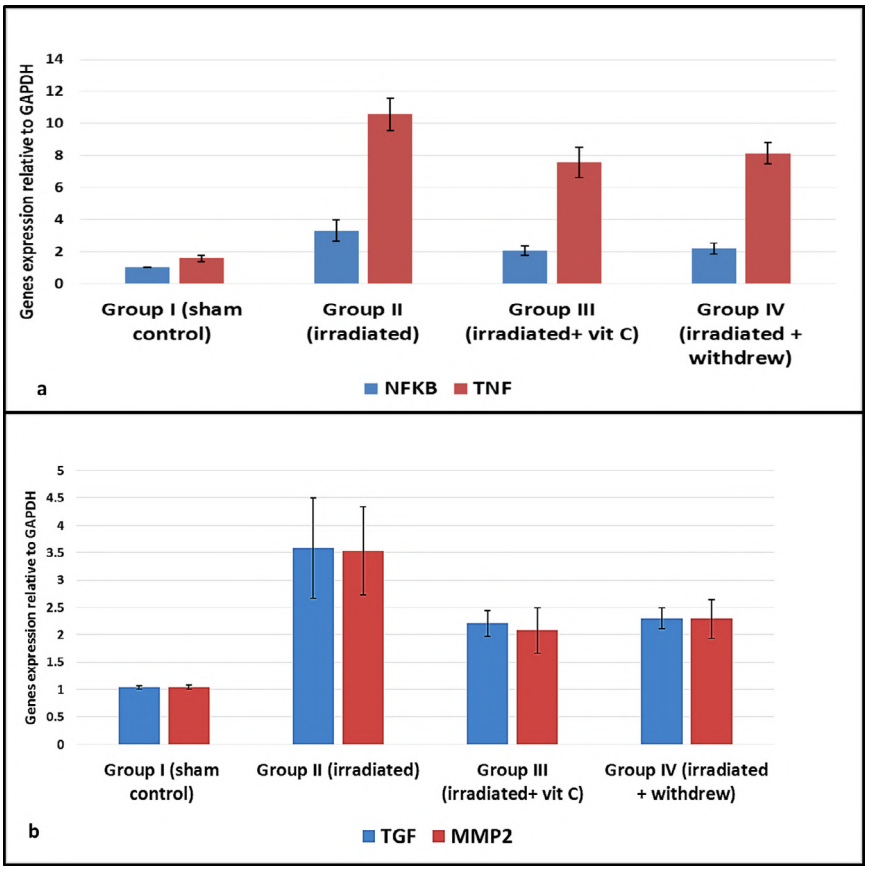

Fig. 6.- a: Inflammatory cytokines NFKB, TNF, **b:** fibrotic genes TGF, MMP2 expressions with the highest expression in irradiated group and significant reduction in their expression with Vit. C administration also after withdrawal from radiation exposure.

and radiation withdrawal significantly ($p<0.05$) restore the antioxidant/oxidant capacity through increase SOD and decrease MDA. No significant differences ($P >0.05$) between group, III and group IV (Table 2) were found.

PCR results

Mobile phone radiation exposure significantly ($p<0.05$) up-regulates the expression of inflammatory cytokines NF KB, TNF and the fibrotic markers TGF, MMP2 within the parotid tissue while Vit C administration and radiation withdrawal significantly ($p<0.05$) decrease their expression. No significant differences ($P >0.05$) between group, III and group IV were found (Fig. 6).

DISCUSSION

In the past two decades, a continuous accumulation of knowledge about the possible health risks from exposure to the electromagnetic fields radiated from phones has been observed (Helal and Abdelrahman, 2012), raising concerns about their long-term effect on the parotid salivary gland (Ghadhban and Mhaibes, 2018).

The parotid gland is the largest salivary gland and, together with the submandibular salivary gland, produces the majority of saliva volume. The anatomical site of the parotid gland makes it more sensitive to EMR than the submandibular gland (Zhang et al., 2020a). The parotid gland is composed mainly of serous cells. Thus, injury to the parotid gland is the main cause of xerostomia (Altayeb, 2018). This is the main reason for this study's choice of the parotid gland. In this study, the parotid glands of rats that were exposed to 2100 MHz radiofrequency radiation from a generator that looked like a 3G cell phone changed a lot histologically compared to rats that were put in a sham control group. The changes were observed in the connective tissue, epithelial cells, and interstitial spaces. Mononuclear cell infiltration, dilated, congested blood vessels, dark stained nuclei, and vacuoles in the cytoplasm of acinar cells were observed, and this coincides with previous studies reporting that exposure to EMR from a mobile phone of the third generation, with a frequency of

2100 MHz, results in changes in the histological structure of parotid gland in rats (Maher et al., 2020). Other research confirmed that EMR had non-thermal effects that led to more oxidative stress in the tissue that was exposed to it (Imam et al., 2021). Another study suggested that exposure to such EMR leads to an increase in the level of free radicals (Carvalho Siqueira et al., 2016). According to additional studies (Aydogan et al., 2015), oxidative stress and several pathophysiological changes after irradiation cause damage to the parotid glands. ROS play a crucial role in signal transduction, regulating cellular functions like cell death and growth (Kivrak et al., 2017). Excessive ROS production attenuates the cells' antioxidant capacity, creating a state of oxidative stress and leading to severe cellular damage (Dasdag et al., 2016). A previous study reported that ROS levels sharply increased in salivary glands after EMR (Aydogan et al., 2015).

In the present study, the connective tissue stroma of the parotid glands of radiation showed dense interlobular and moderate intralobular fibrosis, characterized by a significant increase in the mean area percentage of collagen fibers. These findings were in accordance with the authors (Maher et al., 2020), who reported that fibrosis is common in advanced EMR injuries. Radiation can cause oxidative stress, which can strengthen the inflammatory response and cause more inflammatory cytokines to be made (Siqueira et al., 2016). The current study showed cellular infiltration and congested blood vessels in some areas in parotid sections that could be part of the inflammatory response. MDA is a byproduct of polyunsaturated fatty acid oxidation, and is a marker of oxidative stress-mediated lipid peroxidation (Gaweł et al., 2004). In the current study, there is a significant increase in tissue MDA and a decrease in SOD levels in the radiation-exposed group compared to a control group, with a significant reduction in its level after Vit C supplementation. It has been reported that vitamins E and C have antiapoptotic activity through the reduction of MDA and restoration of SOD in many organs. (Younus, 2018). Previous studies suggested that SOD partially protects against injuries produced by head-and-neck irradiation (Nagler et al., 2000). Cell phone radiation exposure increases the concentration of peroxynitrite, and superoxide that destroy DNA, proteins, and lipids and consequently result in apoptosis and necrosis (Aydogan et al., 2015). Our study showed a significant decrease in the mean area per cent of PAS-positive material in irradiated rats compared to the control group due to the depletion of basement membrane at some injured areas in response to the toxic effects of EMR, as explained before. This was preserved as nearly in groups III and IV as in the control group. The latter was the role of vitamin C in cell protection from breakthrough inflammation. These findings agreed with those of other studies (Anan et al., 2021).

Saliva is an underused diagnostic tool, but in the last three decades it has gained much attention, as it is easy and non-invasive in its collection (Kaufmann and Lamster, 2002). We found a significant decrease in total protein and amylase activity in the saliva of the exposed group compared to the control group, while there was a significant increase in their levels in the Vit-C-supplemented group. Goldwein and Aframian (2010) reported that microwave radiation exposure decreases salivary protein secretion as a result of continuous and cumulative glandular damage. More studies reported that higher salivary levels of amylase, LDH and MDA were detected in high mobile users than low mobile users. (Shivashankara et al., 2015).

In recent years, plant-derived antioxidants have received increased attention due to their potent antitoxic effect, low toxicity, and lower cost (Liu et al., 2021). Previous studies reported that patients' saliva with prolonged phone exposure has decreased flow rate, pH, buffer capacity, and total protein (Hashemipour et al., 2014; Madhukar et al., 2019). In this study, the MECs demonstrated by immunohistochemistry for αSMA revealed a highly significant increase in α-SMA immunoreactivity around acini and intra-lobular ducts in the irradiated group. The MECs undergo proliferative and morphological changes during the atrophy and regeneration of acinar cells, with subsequent increases in size and number. In stressful conditions, it seems that gland function recovery requires increasing the surviving cells' secretory

capacity. More MECs need to squeeze the accumulated secretion (Altayeb, 2018).

In the present study, an increase in Ki-67 immuno-reaction in the parotids of rats Exposed to EMR was in accordance with a previous study that reported that exposure to EMF radiation from many sources, like cell phones, has a proliferative effect on salivary acini, and revealed that the increase in Ki-67 expression was directly related to the severity of the EMF exposure. Also, several previous studied reported the relation between benign and malignant tumor and long-term exposure of phone radiation (Hantke et al., 2002).

In this study, Ki-67 immunoreaction appeared nearly as a control in GIII, in which rats took Vit C. Previous studies explained that Vit C could restore normal cell proliferation of the salivary gland (Maher et al., 2020). Several studies over the past decade have reported that increasing usage of mobile phones could have possible carcinogenic effects as a result of exposure to radiofrequency (Choi et al., 2020).

Vitamin C is a powerful antioxidant that helps to reduce oxidative stress molecules in the body, such as MDA; vitamin C acts as a redox buffer that could reduce and neutralize reactive oxygen species. Various studies explained that electromagnetic waves emitted from mobile phones (900MHz) affect cell proliferation and apoptosis through the induction of ROS. ROS are scavenged by SOD, glutathione peroxidase, and catalase (Ashor et al., 2014; Ahmad et al., 2016).

Ki-67 is a human nuclear protein important for cell proliferation (Scholzen and Gerdes, 2000). The results of the current study indicate an increase in immune expression of Ki67 protein in glandular tissue cells. This indicates an increased ability of these cells for mitotic division in response to oxidative stress damage.

Transforming growth factor-β (TGF-β) is a multifunctional cytokine that influences salivary gland homeostasis and development. TGF-β induces the ECM deposition by inducing the biosynthesis of fibronectin and collagens (Leask and Abraham, 2004) in addition to protease inhibitors. Moreover, TGF-β1 enhances epithelial-mesenchymal transition with increased formation of myofibroblasts. Salivary gland tissue damage from inflammation or radiation exposure could result in reparative TGFβ-induced ECM production (Zavadil and Böttinger., 2005). In the current study, there is significant upregulation in TGF gene expression in parotid tissue of the exposed group compared to a control group, with a significant reduction in its expression after Vit C supplementation. This is in agreement with a previous study, which reported that irradiation of the submandibular salivary gland causes a significant decrease in salivary secretion and amylase activity, but the elevation of MDA with an increase in collagen deposition and TGF expression (Xu et al., 2016). Further studies reported that treating diabetic rats with vitamin C prevents the increase in TGF in glomerular and cortical tissues (Craven et al., 1997).

TGF-β-signaling has a crucial role in fibrosis, including salivary gland fibrosis. Previous studies mentioned that TGF-β/BMP-signaling molecules could be a promising anti-fibrotic drug target (Zhang et al., 2020b). A previous study reported 10-fold increase in salivary TGF-β protein expression in patients with radiation-induced salivary dysfunction (Hakim et al., 2011, Spiegelberg et al., 2014). Another study revealed that TGF-β1 expression increased after irradiation in an experimental mouse model and then decreased after hyperbaric oxygen therapy (Hoesel and Schmid, 2013).

NF-κB is a central factor in cell differentiation, proliferation, inflammation, stress response, and cell death. NF-κB is activated by many stimuli and a network of signaling pathways, which influence each other (Freudlsperger et al., 2013). TGF-β activates NF-κB signaling involving TAK1 and IKK kinases leading to IκBα phosphorylation, nuclear translocation of NF-κB and activation of NF-κB downstream targets (Kim et al., 2016). In the parotid tissue of the exposed group, NF-κB and TNF gene expression were significantly higher than in the control group. However, these genes were significantly lower in expression after vitamin-C supplementation. Our results are in accordance with Matsuno et al. (2002), who reported a significant increase in the expression of inflammatory cytokines NF-κB, IκB-α, and fibrotic marker TGF-β1 in salivary gland exposed to radiation in experimental rats.

Tumor necrosis factor-α (TNF-α) is a pro-inflammatory cytokine that is found to be increased in numerous autoimmune or inflammatory diseases (Sullivan et al., 2005). A previous study reported that TNF-α up-regulates TGF-β1 expression in primary mouse lung fibroblasts (Han et al., 2001). It has been reported that TNF-alpha stimulates activation of proMMP2 in human skin through NF-kB (Brew and Nagase, 2010). Matrix metalloproteinases (MMPs) are a group of enzymes that play an important role in the turnover of ECM in normal and pathological processes. Herein we found significant up-regulation of MMP2 in the exposed group, which retains to nearly normal in Vit C supplemented group, which is in accordance with Brew and Nagase (2010), who reported that Vit C and E were shown to reduce MMP expression and activity in human dermal fibroblasts after UVA irradiation.

CONCLUSION

Radiofrequency emitted from mobile phones has harmful effects on different organs and tissues. Exposure to these waves affects the secretory function of the parotid gland due to oxidative stress and the release of inflammatory cytokines with subsequent fibrosis. In addition to accelerated cellular proliferation to replace the damaged tissues, the currently used drugs have many intolerable side effects, so we urgently need to discover a safe method of protection against phone exposure side effects. Vitamin C is a powerful antioxidant that helps in prophylactic protection against these harmful effects by ameliorating oxidative stress.

Recommendation: The study recommended the need for more work on changing the behaviors that constitute a danger to users of mobile phones, and more research must be done to adopt preventive measures, such as the reduction and rationalization of direct exposure to mobile use. Long-term experimental and clinical studies are needed to clarify the effect of radiofrequency radiation emitted from 3G mobile phones on parotid tissue.

REFERENCES

AHMAD AG, KOBRA S, DARYOUSH MN (2016) Protective effects of vitamin E consumption against 3MT electromagnetic field effects on oxidative parameters in substantia nigra in rats. *Basic Clin Neurosci*, 7(4): 315-322.

ALTAYEB ZM (2018) Possible protective role of green tea extract on male rat parotid gland in high fat diet induced obesity (histological study). *J Med Histol*, 2(1): 69-80.

ANAN H, GAWISH M, AMER M, IBRAHIM N (2021) Effects of low magnetic irradiation on morphology and ultrastructure of parotid glands in rats and amelioration by vitamin E. *J Cytol Histol*, 3: 139-142.

ASHOR AW, LARA J, MATHERS JC, SIERVO M (2014) Effect of vitamin C on endothelial function in health and disease: a systematic review and meta-analysis of randomised controlled trials. *Atherosclerosis*, 235(1): 9-20.

AYDOGAN F, UNLU I, AYDIN E, YUMUSAK N, DEVRIM E, SAMIM EE, OZGUR E, UNSAL V, TOMRUK A, OZTURK GG, SEYHAN N (2015) The effect of 2100 MHz radiofrequency radiation of a 3G mobile phone on the parotid gland of rats. *Am J Otolaryngol*, 36: 39-46.

BREW K, NAGASE H (2010) The tissue inhibitors of metalloproteinases (TIMPs): An ancient family with structural and functional diversity. *Biochim Biophys Acta*, 1803(1): 55-71.

CARVALHO SIQUEIRA E, ALVIM DE SOUZA FT, FERREIRA E, PEDRA SOUZA R, COSTA MACEDO S, FRIEDMAN E, VINICIUS GOMEZ M, CAVALIÉRI GOMES C, SANTIAGO GOMEZ R (2016) Cell phone use is associated with an inflammatory cytokine profile of parotid gland saliva. *J Oral Pathol Med*, 45: 682-686.

CHOI YJ, MOSKOWITZ JM, MYUNG SK, LEE YR, HONG YC (2020) Cellular phone use and risk of tumors: systematic review and meta-analysis. *Int J Environ Res Public Health*, 17(21): 8079.

CRAVEN PA, DERUBERTIS FR, KAGAN VE, MELHEM M, STUDER RK (1997) Effects of supplementation with vitamin C or E on albuminuria, glomerular TGF-beta, and glomerular size in diabetes. *J Am Soc Nephrol*, 8(9): 1405-1414.

DASDAG S, AKDAG MZ (2016) The link between radiofrequencies emitted from wireless technologies and oxidative stress. *J Chem Neuroanat*, 75: 85-93.

EL-AKABAWY G, EL-KHOLY W (2014) Neuroprotective effect of ginger in the brain of streprozotocin-induced diabetic rats. *Ann Anat*, 169: 119-128.

EL-BEDIWI A, ATTALL F, SAAD EM, EID F (2011) Effects of electromagnetic radiation produced by mobile phone on some visceral organs of rat. *J Med Sci*, 11: 256-260.

EMSLEY R, DUNN G, WHITE I (2010) Mediation and moderation of treatment effects in randomized controlled trials of complex interventions. *Stat Methods Med Res*, 19(3): 237-270.

FREUDLSPERGER C, BIAN Y, CONTAG WISE S, BURNETT J, COUPAR J, YANG X, CHEN Z, VAN WAES C (2013) TGF-β and NF-κB signal pathway cross-talk is mediated through TAK1 and SMAD7 in a subset of head and neck cancers. Oncogene, 32(12): 1549-1559.

GHADHBAN R, MHAIBES A (2018) Study effect electromagnetic field and mobile phone radiation on some hematological, biochemical and hormonal parameters in female rats. *Basrah J Vet Res*, 17: 155-164.

GOLDWEIN O, AFRAMIAN DJ (2010) The influence of handheld mobile phones on human parotid gland secretion. *Oral Dis*, 16(2): 146-150.

HAKIM SG, RIBBAT J, BERNDT A, RICHTER P, KOSMEHL H, BENEDEK GA, JACOBSEN HC, TRENKLE T, SIEG P, RADES D (2011) Expression of Wnt-1, TGF-β and related cell-cell adhesion components following radiotherapy in salivary glands of patients with manifested radiogenic xerostomia. *Radiother Oncol*, 101(1): 93-99.

HAN YP, TUAN TL, WU H, HUGHES M, GARNER WL (2001) TNF-alpha stimulates activation of pro-MMP2 in human skin through NF-(kappa)B mediated induction of MT1-MMP. *J Cell Sci*, 114(Pt 1): 131-139.

HANTKE B, LAHMANN C, VENZKE K, FISCHER T, KOCOUREK A, WINDSOR LJ, BERGEMANN J, STÄB F, TSCHESCHE H (2002) Influence of flavonoids and vitamins on the MMP- and TIMP-expression of human dermal fibroblasts after UVA irradiation. *Photochem Photobiol Sci*, 1(10): 826-833.

HASHEMIPOUR M, YARBAKHT M, GHOLAMHOSSEINIAN A, FAMORI H (2014) Effect of mobile phone use on salivary concentrations of protein, amylase, lipase, immunoglobulin A, lysozyme, lactoferrin, peroxidase and C-reactive protein of the parotid gland. *J Laryngol Otol*, 128(5): 454-462.

HELAL M, ABDELRAHMAN M (2012) Ki-67 expression on major salivary gland exposed to mobile cell phone radiation. *EDJ*, 58(3).

HOESEL B, SCHMID JA (2013) The complexity of NF-κB signaling in inflammation and cancer. *Mol Cancer,* 12: 86.

IMAM HASAN, TANJINA AMIN, RAFIQUL ALAM, MOHAMMAD RAFIQUL ISLAM (2021) Hematobiochemical and histopathological alterations of kidney and testis due to exposure of 4G cell phone radiation in mice. *Saudi J Biol Sci*, 28(5): 2933-2942.

JELODAR G, NAZIFI S, AKBARI A (2013) The prophylactic effect of vitamin C on induced oxidative stress in rat testis following exposure to radio frequency wave generated by a BTS antenna model. *Electromagn Biol Med*, 32(3): 409-416.

JOHANSSON I, LINDER J, BRATT P (1989) Comparison of saliva secretion rate and composition in the rat using a pentobarbital or a neuroleptanalgesic type of anaesthesia. *Caries Res*, 3: 75-77.

KAUFMANN E, LAMSTER IB (2002) The diagnostic applications of saliva, a review. *Crit Rev Oral Biol Med*, 13: 197-212.

KIM JH, KIM KM, JUNG MH, JUNG JH, KANG KM, JEONG BK, KIM JP, PARK JJ, WOO SH (2016) Hoon protective effects of alpha lipoic acid on radiation-induced salivary gland injury in rats. *Oncotarget*, 7(20): 29143-29153.

KIVRAK EG, YURT KK, KAPLAN AA, ALKAN I, ALTUN G (2017) Effects of electromagnetic fields exposure on the antioxidant defense system. *J Microsc Ultrastruct*, 5: 167-176.

LEASK A, ABRAHAM DJ (2004) TGF-beta signaling and the fibrotic response. *FASEB J,* 18: 816-827.

LIU Z, DONG L, ZHENG Z, LIU S, GONG S, MENG L, XIN Y, JIANG X (2021) Mechanism, prevention, and treatment of radiation-induced salivary gland injury related to oxidative stress. *Antioxidants (Basel)*, 10(11): 1666.

LUO. S, TAN. W, DENG W, ZHUANG S, LUO J (2005) Expression of albumin, IGF1, IGFBP-3 in tumor tissues and adjacent non-tumor tissues of hepatocellular carcinoma patients with cirrhosis. *World J Gastroenterol*, 11: 4272-4276.

MADHUKAR VASHISTHA, RITESH KATIYAR, PRIYADERSHINI RANGARI (2019) The influence of cell phone radiation on saliva: an observational study. *Int J Med Sci Diagn Res*, 3(7): 22-27.

MAHER AL-ASSAF, CHARIF BARAKAT, MAJID G.A. ABO FAKHER, ADNAN ALMALKI, MOURAD A. ABO FAKHER (2020) Effects of mobile phone radiation on parotid gland: immunohistochemical study. *J Stoma*, 73(3): 112-117.

MATSUNO H, YUDOH K, KATAYAMA R, NAKAZAWA F, UZUKI M, SAWAI T, YONEZAWA T, SAEKI Y, PANAYI GS, PITZALIS C, KIMURA T (2002) The role of TNF-alpha in the pathogenesis of inflammation and joint destruction in rheumatoid arthritis (RA): a study using a human RA/SCID mouse chimera. *Rheumatology (Oxford)*, 41(3): 329-337.

NAGLER RM, REZNICK AZ, SLAVIN S, NAGLER A (2000) Partial protection of rat parotid glands from irradiation-induced hyposalivation by manganese superoxide dismutase. *Arch Oral Biol*, 45(9): 741-747.

ROSADO MM, NASTA F, PRISCO MG, LOVISOLO GA, MARINO C, PIOLI C (2014) Effects of GSM▁modulated 900 MHz radiofrequency electromagnetic fields on the hematopoietic potential of mouse bone marrow cells. *Bioelectromagnetics*, 35: 559-567.

SCHOLZEN T, GERDES J (2000) The Ki-67 protein: from the known and the unknown. *J Cell Physiol*, 182(3): 311-322.

SHIVASHANKARA AR, JOY J, SUNITHA V, RAI MP, RAO S, NAMBRANATHAYIL S, BALIGA MS (2015) Effect of cell phone use on salivary total protein, enzymes and oxidative stress markers in young adults: a pilot study. *J Clin Diagn Res*, 9(2): BC19-22.

SIQUEIRA EC, DE SOUZA FTA, FERREIRA E, SOUZA RP, COSTA MACEDO S, FRIEDMAN E, GOMEZ MV, CAVALIERI GOMES V, GOMEZ RS (2016) Cell phone use is associated with an inflammatory cytokine profile of parotid gland saliva. *J Oral Pathol Med*, 45: 682-686.

SPIEGELBERG L, SWAGEMAKERS SMA, VAN IJCKEN WFJ, OOLE E, WOLVIUS EB, ESSERS J, BRAKS JAM (2014) Gene expression analysis reveals inhibition of radiation-induced TGF beta-signaling by hyperbaric oxygen therapy in mouse salivary glands. *Mol Med*, 20: 257-269.

SULLIVAN DE, FERRIS M, POCIASK D, BRODY AR (2005) Tumor necrosis factor-alpha induces transforming growth factor-beta1 expression in lung fibroblasts through the extracellular signal-regulated kinase pathway. *Am J Respir Cell Mol Biol*, 32(4): 342-349.

SUVARNA SK, LAYTON C, BANCROFT JD (Eds.) (2013) Bancroft's *Theory and Practice of Histological Techniques*. 7th ed., ch10. Churchill Livingstone, Philadelphia, pp 172-186, 382-434, 493, and 239-270.

XU L, YANG X, CHEN J, GE X, QIN Q, ZHU H, ZHANG C, SUN X (2016) Simvastatin attenuates radiation-induced salivary gland dysfunction in mice. *Drug Des Devel Ther,* 10: 2271-2278.

YOUNUS H (2018) Therapeutic potentials of superoxide dismutase. *Int J Health Sci*, 12(3): 88-93.

ZAVADIL J, BÖTTINGER EP (2005) TGF-beta and epithelial-to-mesenchymal transitions. *Oncogene,* 24: 5764-5774.

ZHANG T, LIU C, MA S, GAO Y, WANG R (2020a) Protective effect and mechanism of action of rosmarinic acid on radiation-induced parotid gland injury in rats. *Dose Response*, 18(1): 1559325820907782.

ZHANG X, YUN JS, HAN D, YOOK JI, KIM HS, CHO ES (2020b) TGF-β pathway in salivary gland fibrosis. *Int J Mol Sci*, 21(23): 9138.

Transpalpebral transorbital endoscopic lateral approach to the middle cranial fossa: anatomical study in cadaver

Juan R. Gras-Cabrerizo[1,2], María Martel-Martin[2,3], Maria Casasayas-Plass[1,2], Juan C. Villatoro-Sologaistoa[2,4], Ainhoa García-Lliberós[5], Humbert Massegur-Solench[1], Francisco Reina[6], Fernando Muñoz-Hernández[7]

[1] Department of Otolaryngology/Head and Neck Surgery, Hospital de la Santa Creu i Sant Pau, Universitat Autònoma de Barcelona, Spain

[2] Department of Otolaryngology/Head and Neck Surgery, Corachán Clinic, Spain

[3] Department of Otolaryngology/Head and Neck Surgery, Hospital del Mar, Universitat Autònoma de Barcelona, Spain

[4] Department of Otolaryngology/Head and Neck Surgery Hospital General de Catalunya, Universitat Internacional de Catalunya, Spain

[5] Department of Otolaryngology/Head and Neck Surgery Hospital Universitario de Valencia, Spain

[6] Department of Ciencias Médicas (Grupo de Investigación en Anatomía Clínica, Embriología y Neurociencia NEOMA) Universitat de Girona, Spain

[7] Department of Neurosurgery, Hospital de la Santa Creu i Sant Pau, Universitat Autònoma de Barcelona and Corachán Clinic, Spain

SUMMARY

Transorbital expanded endoscopic approaches allow different areas of the skull base to be approached. The aim of our study is to analyse the main anatomical bone and neurovascular structures of the middle cranial fossa by means of a transpalpebral transorbital lateral endoscopic approach (TTLEA). An anatomical study was performed on 12 orbital cavities corresponding to 6 cadaver heads. All specimens were previously injected with colored latex through both carotid systems.

The mean distance from the orbital rim to the zygomatic-facial foramen and to the zygomatic-temporal foramen was 11 mm and 16 mm respectively. In all cases the meningo-orbital foramen was found at a mean distance from the orbital rim of 34 mm. The superior orbital fissure (SOF) was located posterior to the meningo-orbital foramen at 39 mm. The foramen rotundum and foramen ovale were located separated from each other by 10 mm on average. Anterior to the foramen ovale a bony prominence was observed in all cases. In 11 cases (92%) the entrance of the accessory meningeal artery into the foramen ovale was evident and in one case an accessory foramen was observed. The middle meningeal artery was located in all dissections within the foramen spinosum. The TTLEA offers a wide and direct exposure of the middle cranial fossa. It should be considered as an alternative to transcranial approaches in certain lesions invading the lateral region of the middle cranial fossa, the lateral wall of the cavernous sinus or the infratemporal fossa.

Corresponding author:
Juan Ramón Gras-Cabrerizo. C/ Mas Casanovas 90, 08041 Barcelona, Spain. Phone: 34-93-5565679. E-mail: jgras@santpau.cat

Submitted: July 17, 2023. **Accepted:** November 11, 2023

https://doi.org/10.52083/HNNK7711

Key words: Endoscopic – Transpalpebral – Meningoorbital – Foramen rotundum – Foramen spinosum – Middle meningeal artery

INTRODUCTION

In recent years, endonasal endoscopic approaches have exponentially expanded their indications, reaching territories usually treated by other specialties. Expanded transnasal approaches have made it possible to approach different areas of both the skull base and the orbital cavity. The main limitation they present is being able to reach certain lateral areas without having to cross vital neurovascular structures. In order to access these anatomical territories with the minimum possible morbidity, the alternative is to use the orbital cavity as a corridor. Historically, in the late 19th century, the first surgical approaches to the orbit were used in the treatment of thyroid orbitopathy (Alper, 1995), and in the early 20th century, lateral (frontotemporal) approaches were described to treat orbital tumours (Dandy, 1941). With technological advances and improvements in radiological studies, these lateral approaches evolved, with increasingly smaller craniotomies being performed. In 1971 Donald Wilson first used the surgical term keyhole or microcraniotomy (Wilson, 1971). The use of the endoscope as a support instrument had a decisive influence on the development of this concept, with the supraorbital keyhole becoming particularly popular in the 1990s (Ramos-Zúñiga, 1999; Eroglu et al., 2019). Moe et al. (2010) and Rivkin et al. (2013) described a series of transorbital endoscopic approaches preserving the orbital rim to treat different pathologies, which he called TONES (transorbital neuroendoscopic surgery). In recent years, several anatomical studies have been published that have made it possible to systematise these endoscopically assisted approaches (Koppe et al., 2013; Dallan et al., 2017, 2018; Di Somma et al., 2018).

The aim of our study is to analyse the main anatomical bone and neurovascular structures of the middle cranial fossa (MCF) using an endoscopic lateral transorbital transpalpebral endoscopic approach.

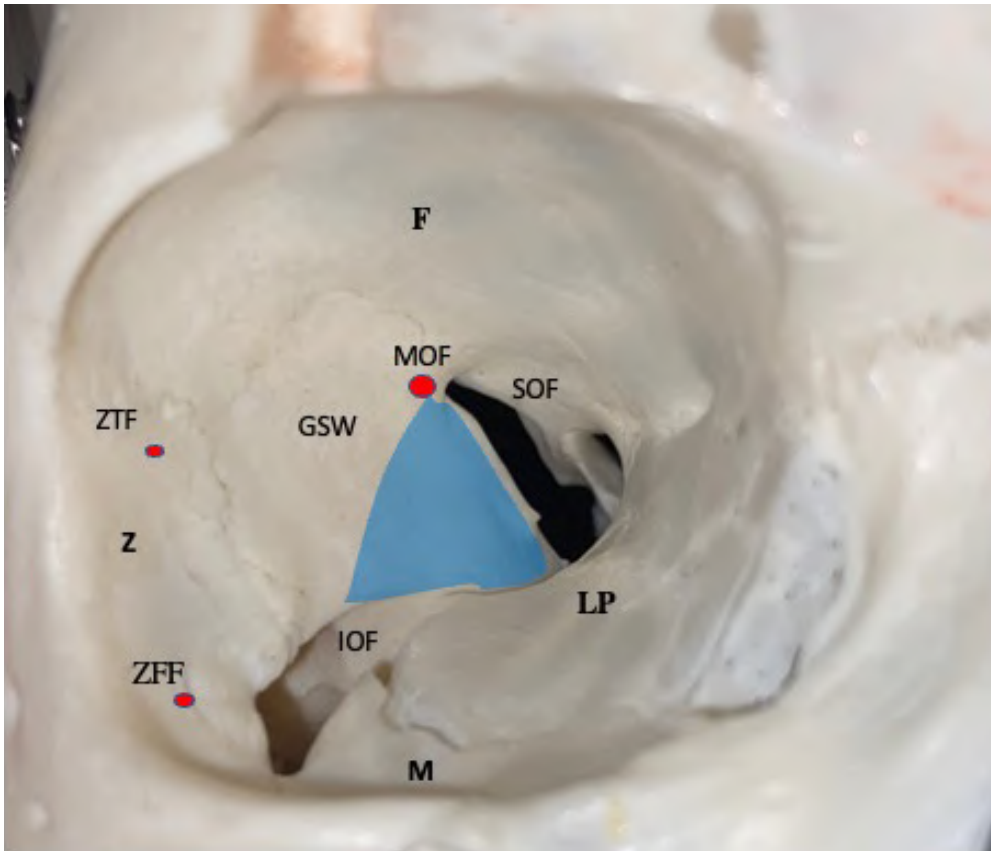

Fig. 1.- Right orbital cavity. In blue access area middle cranial fossa. Z: zygomatic bone; GSW: greater sphenoid wing; M: maxillary bone; SOF: superior orbital fissure; IOF: inferior orbital fissure; ZFF: zygomatic facial foramen; ZTF: zygomatic temporal foramen; MOF: meningo-orbital foramen; LP: lamina papyracea; F: frontal bone.

MATERIALS AND METHODS

An anatomical study was carried out on 12 orbital cavities corresponding to 6 cadaver heads prepared and preserved the modified Larsen's solution. All specimens were obtained from the body donation programme of the University of Girona, which is regulated according to the ethical and legal laws of our country. All specimens were previously injected with colored latex through both carotid systems. A graduated malleable hysterometer and a rigid precision ruler were used for the different measurements.

Surgical technique. An incision was made in the superior palpebral fold approximately 10 mm from the palpebral margin, dissecting from superficial to deep the skin and the orbicularis oculi muscle in its pretarsal, preseptal and orbital portions. Superficial to the orbicularis oculi muscle, the lateral orbital rim was approached and a deep subperiosteal dissection was performed, displacing the orbital contents medially, thus locating the superior orbital fissure (SOF) and the inferior orbital fissure (IOF). During this dissection of the lateral wall, the zygomatic-facial foramen, the zygomatic-temporal foramen superiorly and the meningo-orbital foramen in depth were identified. The distance of these orifices from the orbital margin was calculated from the frontozygomatic suture (Fig. 1). The orbital lateral wall was then drilled until the temporalis muscle fascia was exposed, and the greater wing of the sphenoid was drilled between the SOF and the IOF until the dura mater of the temporal lobe was exposed (Fig. 2). With a blunt instrument, the floor of the MCF was dissected, displacing the temporal lobe superiorly, identifying from medial to lateral, the foramen rotundum with the maxillary nerve (V2), the foramen ovale with the mandibular nerve (V3) and the accessory meningeal artery (AMA) and finally the foramen spinosum with the middle meningeal artery (MMA) (Figs. 3 and 4).

The distance between the foramen ovale and the foramen rotundum was measured from the posterior margin of the foramen ovale to the anterior margin of the foramen rotundum. Finally, along the lateral margin of the SOF we identified the

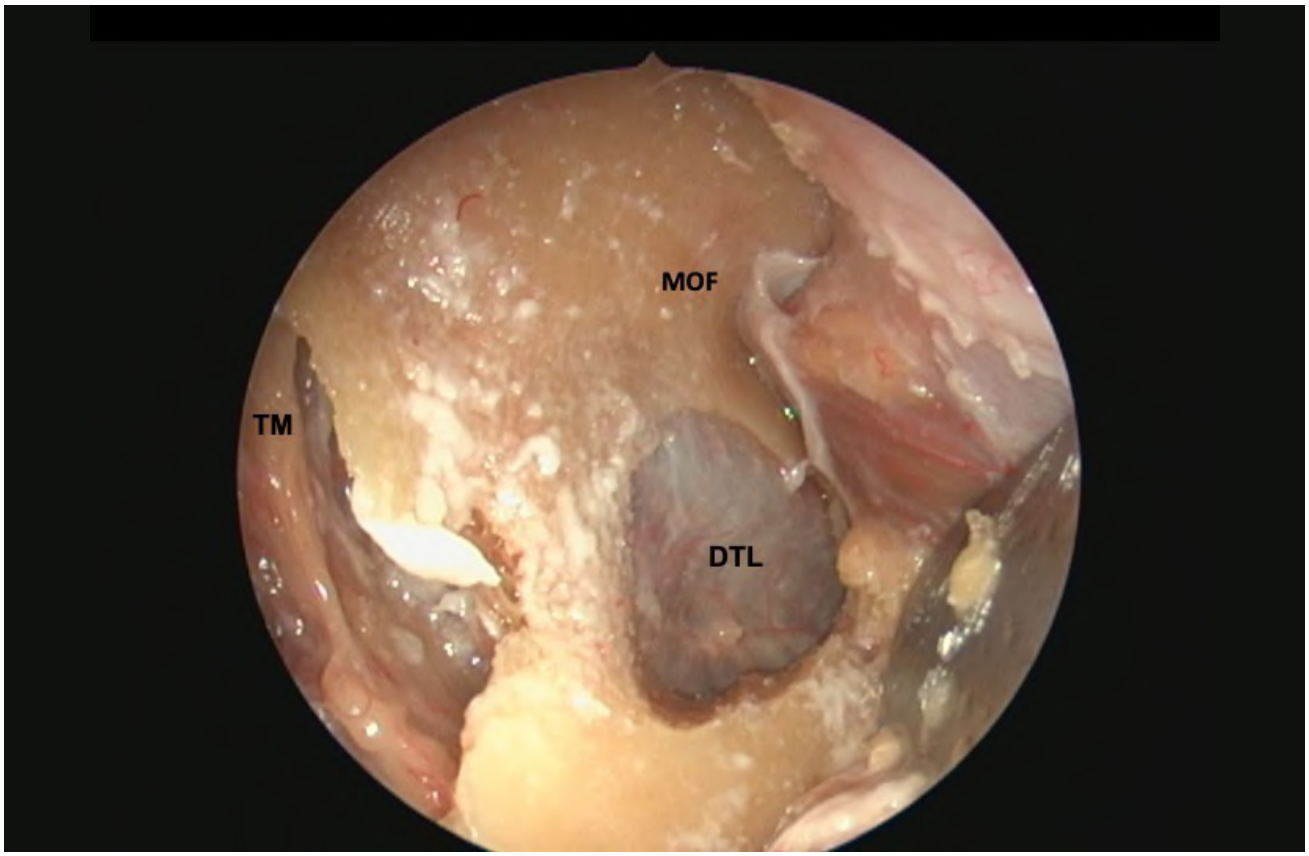

Fig. 2.- Right orbital cavity after drilling the lateral wall (zygomatic) and greater wing of sphenoid. TM: temporalis muscle; DTL: dura mater of temporal lobe; MOF: meningo-orbital foramen.

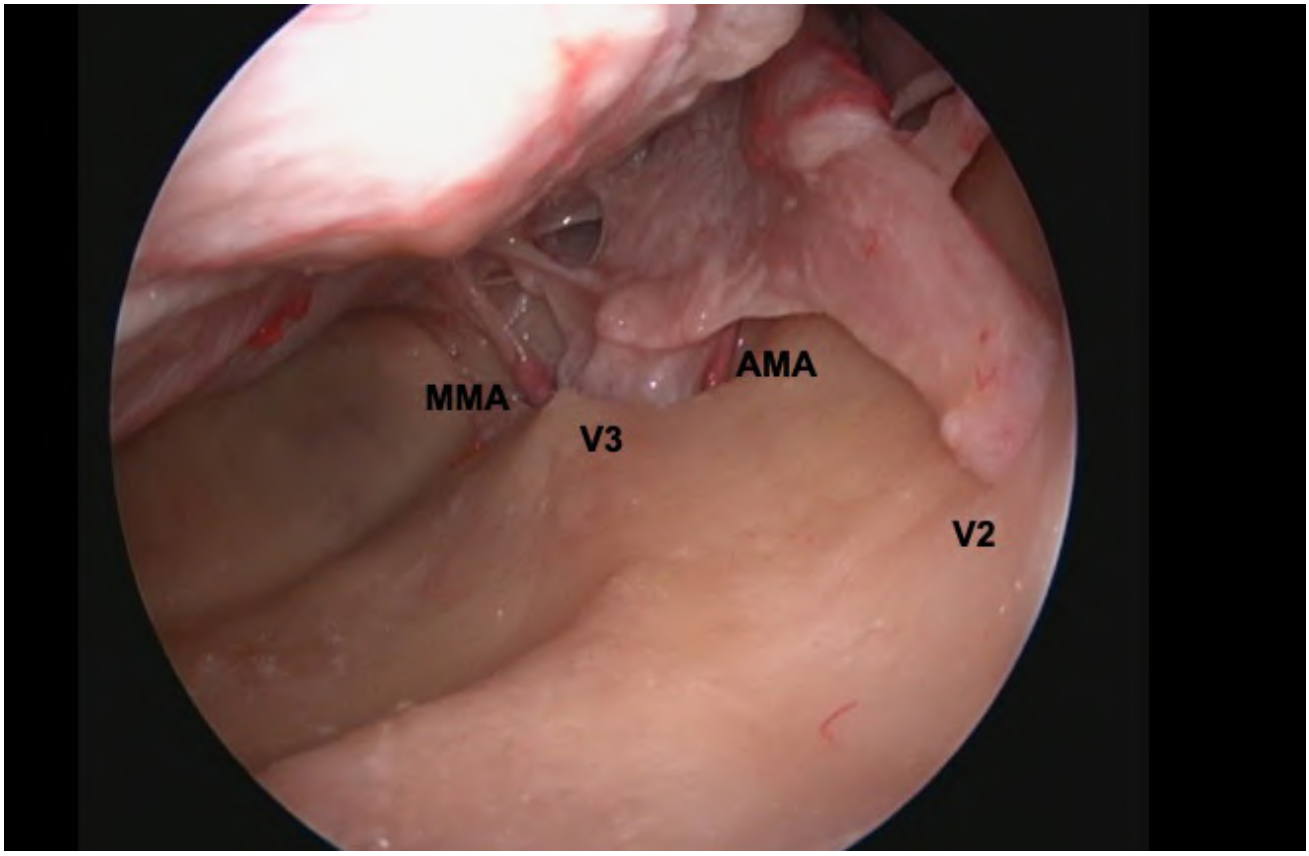

Fig. 3.- Floor of the right middle cranial fossa after subperiosteal elevation of the temporal lobe. V2: maxillary nerve; V3: mandibular nerve; AMA: accessory meningeal artery; MMA: middle meningeal artery.

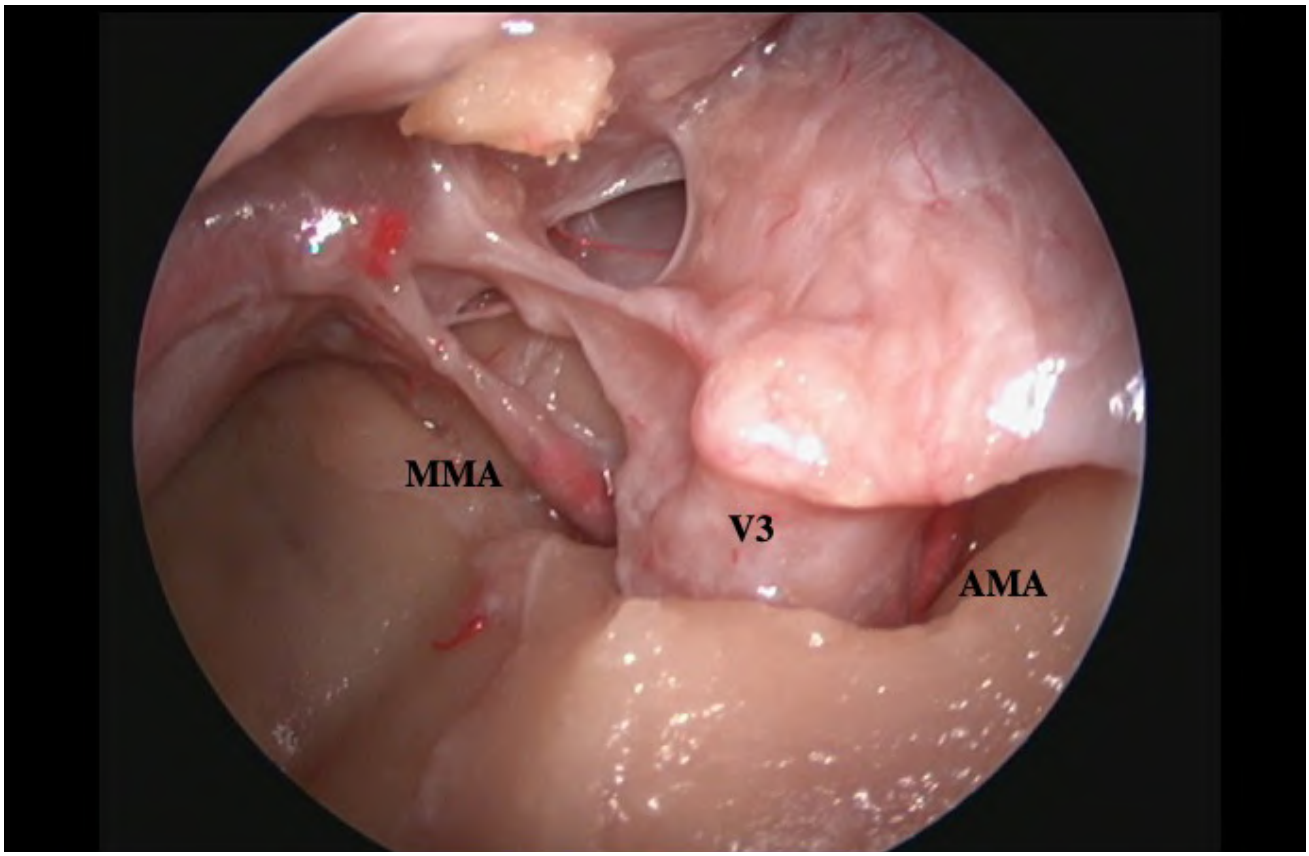

Fig. 4.- Floor of the right middle cranial fossa after subperiosteal temporal lobe elevation (deeper than Fig. 3). V3: mandibular nerve; AMA: accessory meningeal artery; AMM: middle meningeal artery.

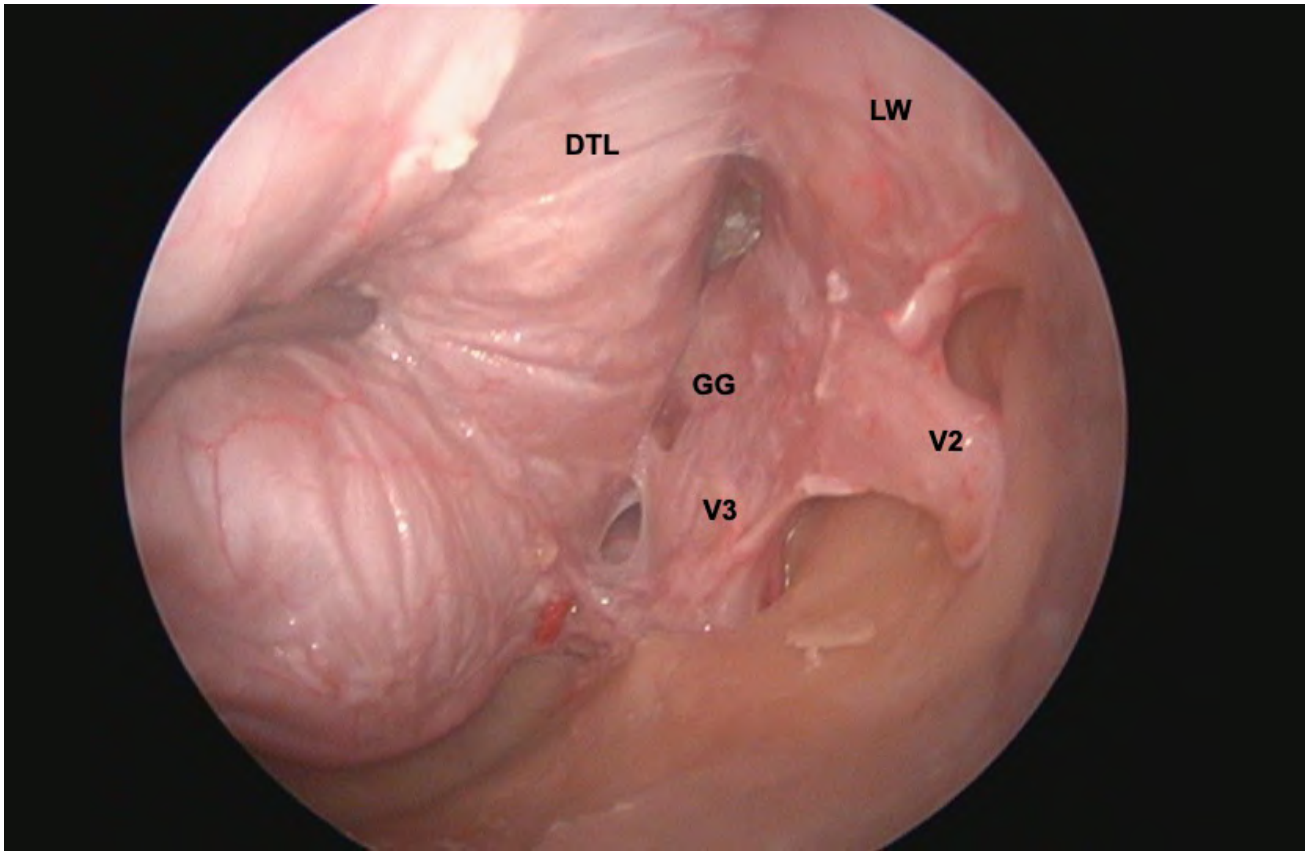

Fig. 5.- Approach to the lateral wall of the right cavernous sinus. DTL: dura mater of the temporal lobe; LW: lateral wall of the cavernous sinus; V2: maxillary nerve; V3: mandibular nerve; GG: Gasser ganglion.

meningo-orbital band, a structure that represents the fold between the periorbita and the dura mater of the temporal lobe. This reference allowed us to dissect the double layer that forms the lateral wall of the cavernous sinus (Fig. 5).

RESULTS

Dissection of the MCF. The mean distance from the zygomatico-facial foramen to the orbital rim was 11 mm (range: 10-20 mm) and 16 mm from the zygomatico-temporal foramen (range: 10-22 mm). In 100% of cases (12/12) the meningo-orbital foramen was found at a mean distance from the orbital rim of 34 mm (range 32-40 mm). The SOF was located posterior to the meningo-orbital foramen at a mean distance of 39 mm (range: 35-43 mm) from the orbital rim.

In all cases the foramen rotundum and foramen ovale were located separated from each other by 10 mm (range: 8-14 mm). In all dissections a bony prominence was located in front of the foramen ovale (Fig. 6).

In 11 cases (92%) the entrance of the AMA was evident within the foramen ovale anterior and/or medial to mandibular nerve (V3). In only one case an accessory foramen (Vesalius) was observed. The MMA was located in all dissections within the foramen spinosum.

Lateral wall dissection of the cavernous sinus. During dissection of the lateral wall of the cavernous sinus it was possible to identify the meningo-orbital band in all cases, as well as to locate the oculomotor nerves (III-IV) and the ophthalmic nerve (V1) in the internal (periosteal) layer (Fig. 7).

DISCUSSION

Endoscopic approaches using the orbit as a corridor are one of the most attractive new techniques in recent years. These approaches can be classified into orbital endoscopic, transorbital endoscopic and neuroendoscopic transorbital approaches (TONES) (Balakrishnan and Moe, 2011). The term TONES describes four access corridors, medial (precaruncular), lateral, inferior, and su-

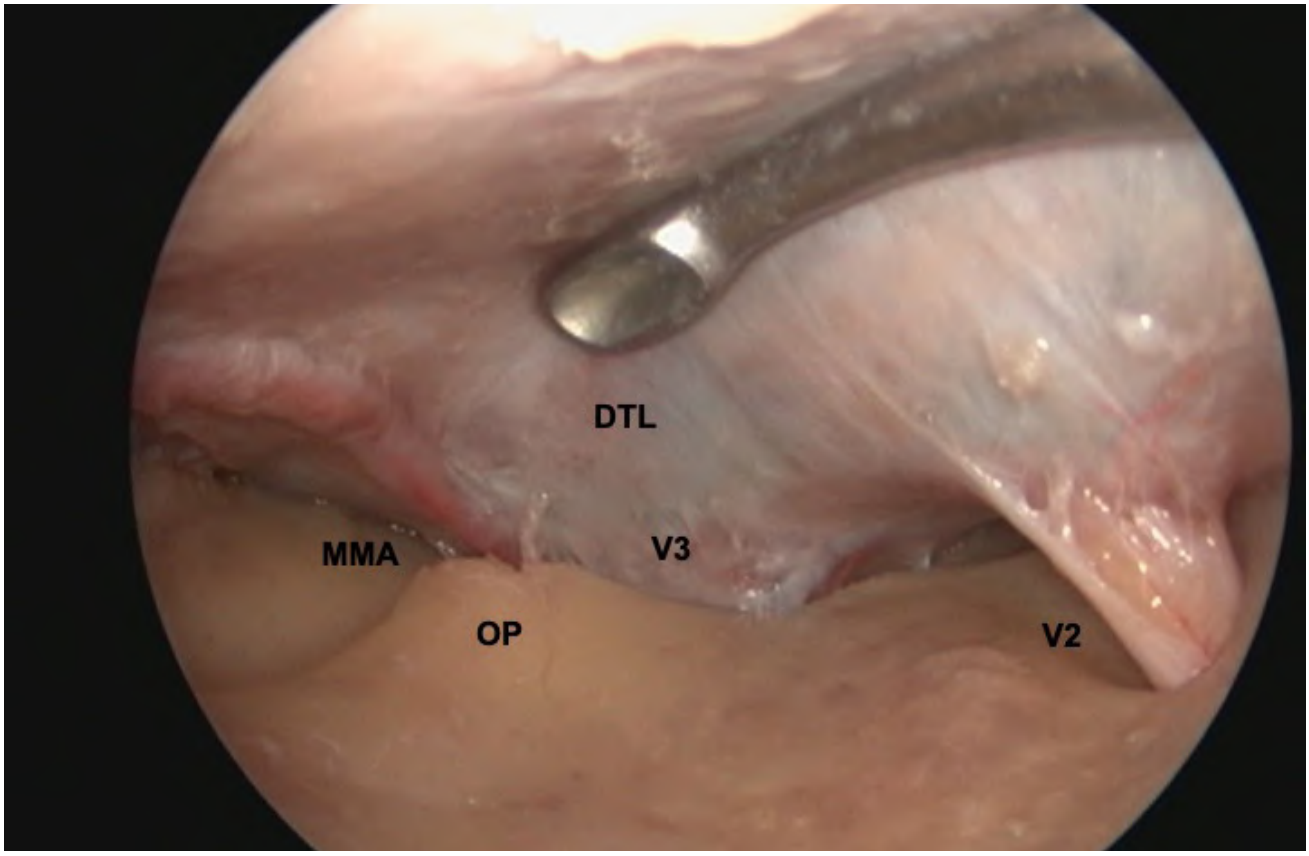

Fig. 6.- Visualization of the oval prominence (OP) on the floor of the right middle cranial fossa. DTL: dura mater of the temporal lobe; V2: maxillary nerve; V3: mandibular nerve; MMA: middle meningeal artery; PO: oval prominence.

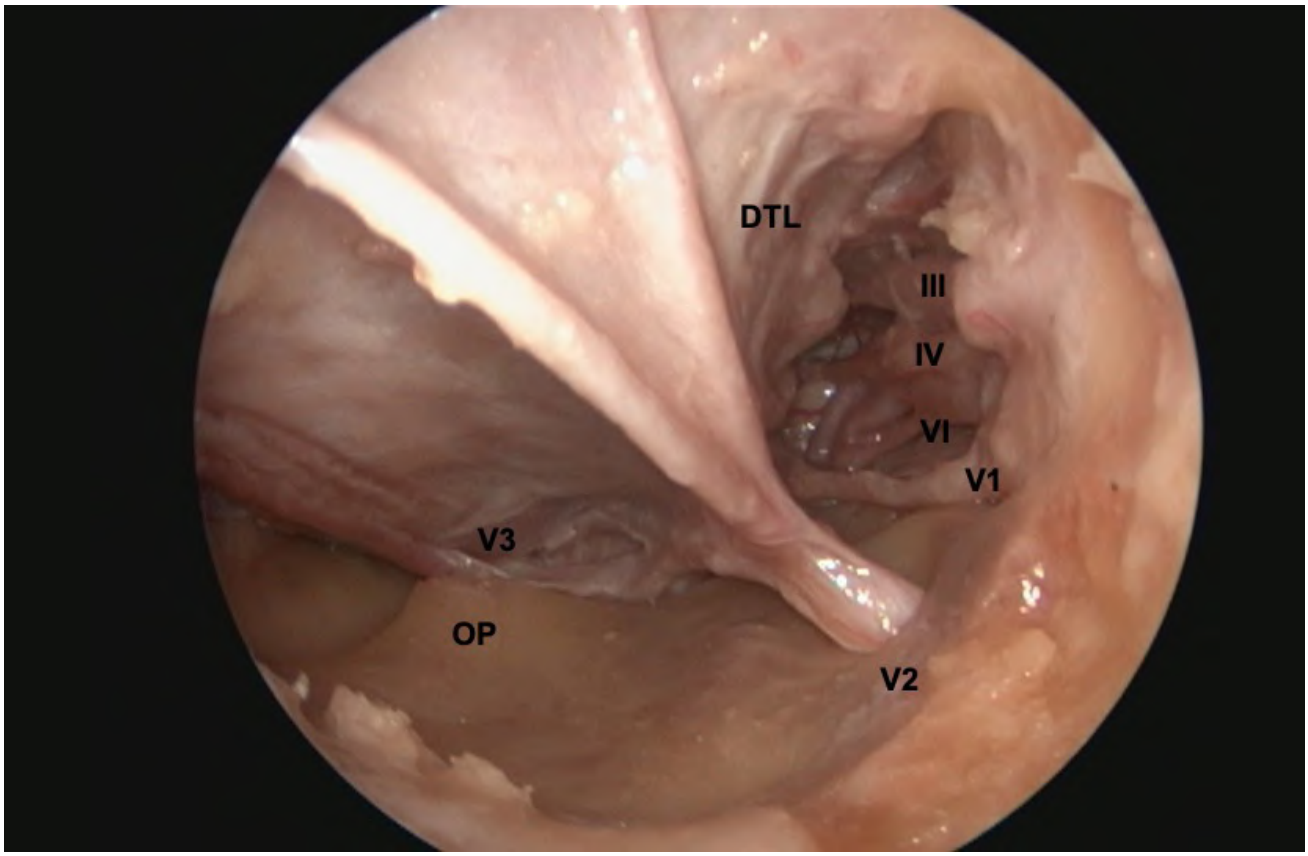

Fig. 7.- Lateral approach to the right cavernous sinus. DTL: dura mater of the temporal lobe; V2: maxillary nerve; V3: mandibular nerve; OP: oval prominence; Oculomotor nerves (III-IV-VI); V1: ophthalmic nerve.

perior. The lateral approach has the advantage of preserving the orbital rim without the need for reconstruction and avoids both craniotomy and traction of the brain contents. It also allows the palpebral fold to be used to minimise the possible cosmetic aspects caused by the scar. This technique can be used to treat certain lesions such as spheno-orbital meningiomas, osteomas, lesions on the lateral wall of the cavernous sinus, lesions of Meckel's cavum, vascular lesions and functional neurosurgical procedures (Andaluz et al., 2008; Abdel Aziz et al., 2011; Dallan et al., 2015; Lubbe et al., 2017; Di Somma et al., 2018; De Rosa et al., 2019; Suero Molina et al., 2021).

Our anatomical study shows in detail the different structures of the MCF that can be reached with an TTLEA, displacing the orbital contents medially without the need to open the periorbital cavity. The anatomical limits of this approach represent a triangular space defined superiorly and medially by the SOF, laterally by the temporalis muscle fascia and inferiorly and medially by the IOF (Fig. 1).

During dissection of the orbital lateral wall, we found foramina through which different structures enter and leave the orbit. On the anterolateral surface of the zygomatic bone we can see, through small bony ducts, the zygomatic-facial and zygomatic-temporal nerve branches. Both are branches of the zygomatic nerve which take their origin directly from the maxillary nerve in the pterygopalatine fossa. These nerves are accompanied by their arteries, which are branches from the lacrimal artery (ophthalmic artery). According to different studies, the zygomatic-temporal and zygomatic-facial vascular-nerve bundle are located approximately 4.3 mm to 9 mm away from the orbital margin (Krishnamurthy et al., 2011; Iwanaga et al., 2017, 2018). In our study, these measurements were located deeper than in the series reviewed. Both structures were located at an average distance of 11 mm and 16 mm, with the zygomatic-temporal foramen being located superior and posterior to the zygomatic-facial foramen. In depth, anterior to the lateral margin of the SOF, we can locate the meningo-orbital foramen (also called lacrimal, sphenofrontal, cranio-orbital or Hyrtl's orifice). The distance from the meningo-orbital foramen to the fronto-zygomatic suture is estimated to be between 25 mm and 31 mm (Macchi et al., 2016). It allows the passage of an anastomotic branch of the lacrimal artery to the MMA. Its prevalence is highly variable, ranging from 44 to 83%. In most cases it connects directly with the MCF and less frequently with the anterior cranial fossa (McQueen et al., 1995; Macchi et al., 2016). In our study, it was located in all cases at an average distance of 34 mm from the frontozygomatic suture, slightly more posterior than most of the data published in the different series. These differences and those found in the zygomatic vasculo-nerve bundles, can be explained by racial reasons or by differences in the measurement points at the level of the orbital rim. In our study they were calculated using the frontozygomatic suture as a reference. It is important to locate and cauterise all these small arteries that perforate the lateral orbital wall in order to safely advance the dissection in depth and to be able to reach the SOF. Its anterior margin is located approximately 34-41 mm from the lateral orbital rim (Dutton, 2011). Our data reflect a similar distance.

The MCF consists of the endocranial aspect of the greater wings of the sphenoid bone and the squamous and petrous parts of the temporal bone. The anterior margin of the floor of the MCF corresponds to the horizontal portion of the greater wing of the sphenoid which shows in the anterior-posterior direction, the foramen rotundum, the foramen ovale, the foramen spinosum, the foramen lacerum the trigeminal impression, the hiatuses for greater and lesser petrosal nerves and the arcuate eminence. In addition, two inconstant foramina can be found, the foramen venosum (sphenoidal emissary foramen or Vesalius' foramen) and the foramen petrosum (Arnold's foramen) (Rouvière and Delmas, 2005).

The foramen rotundum is located 3-4 mm posterior and inferior to the medial border of the SOF, and gives way to the maxillary nerve (V2), the foramen rotundum artery and small emissary veins (Rouvière and Delmas, 2005; Dutton, 2011; Gras Cabrerizo et al., 2017). It is the most anterior and medial structure located when performing subperiosteal dissection of the floor of the MCF.

Approximately 1 cm posterior and lateral to the foramen rotundum and 6 mm from Gasser's gan-

glion is located the foramen ovale (Rouvière and Delmas, 2005; Dutton, 2011). The main structures crossing the foramen ovale are the mandibular nerve (V3), the AMA, the lesser petrosal nerve and emissary veins (Kaplan et al., 2007). The AMA is present in more than 95% of cases as a branch of the first segment of the maxillary artery (mandibular segment) and in some cases may emerge directly from the MMA. It is predominantly an extracranial artery and only a small branch becomes intracranial, supplying the ganglion of Gasser and the dura mater of the FCM (Baumel and Beard, 1961; Dilenge and Géraud, 1975; Hur et al., 2012). This artery usually passes through the foramen ovale anterior or medial to the mandibular nerve(Baumel and Beard, 1961) (Figs. 3, 4). In 22% it may pass through the Vesalius' foramen (foramen venosum) located medial and anterior to the foramen rotundum (Tanoue et al., 2013; Leonel et al., 2020).

In the most of our cases, the AMA was located anterior and medial to the mandibular nerve (V3). Only in one case we found a foramen venosum. The location of the foramen ovale is an anatomical reference of great surgical relevance. Its identification makes it possible to safely approach lesions located in front of it, as both the internal carotid artery in its petrous portion and the pharyngotympanic tube are located posteriorly. In our study, we found a constant bony reference located anterior to the foramen ovale (oval prominence). This structure makes it possible to locate this foramen precisely and to preserve its contents. We have not found any reference to this anatomical structure in the series reviewed.

Approximately 3 mm posterior and lateral to the foramen ovale is placed the foramen spinosum, crossed by the middle meningeal artery (MMA) and vein and the meningeal branch of V3 (nervus spinosus). It may be absent unilaterally in 0.4% to 1% of cases (Krayenbühl et al., 2008). The MMA emerges from the first segment of the maxillary artery and, once is crosses the foramen spinosum, it divides into two branches (anterior and posterior). The anterior branch supplies the orbital region and the dura mater of the MCF, and can be anastomosed with the ophthalmic artery via the meningo-lagrimal artery through the meningo-orbital foramen (Rouvière and Delmas, 2005; Drake, 2011; Tanoue et al., 2013; Kornieieva et al., 2015).

The TTLEA has advantages over the classic approach using a pterional craniotomy alone or with its transzygomatic or orbitozygomatic variants (Drake, 2011). We avoid a skin incision in the frontotemporal region and a possible injury to the frontal branch of the facial nerve. It is not necessary to uninsert the temporalis muscle, thus avoiding discomfort at this level and the possible aesthetic defect due to atrophy of this muscle. Similarly, this pterional approach can also cause problems during mastication and at the temporomandibular joint.

To reach the most medial territory of this approach and thus to achieve the lateral wall of the cavernous sinus, it is necessary to locate and sectioning the meningo-orbital band. This anatomical structure represents the fusion of the fronto-temporal dura mater with the periorbita at the level of the lateral margin of the SOF. The transorbital approach allows to reach this structure without the need of retracting the temporal lobe if we compare with the frontotemporal approach. It is the anatomical reference that allows the cleavage plane to be found in order to perform an interdural dissection and separate the two layers that make up the lateral wall of the cavernous sinus, the external layer (dura mater) and the internal layer (periosteum) (Anania et al., 2022; Guizzardi et al., 2022). The external wall is thick while the inner layer is thin, semi-transparent and contains cranial nerves III, IV and V1. This procedure represents an alternative to the external approach with several advantages: a more direct and advantageous approach angle, no manipulation of the temporalis muscle and less manipulation of the temporal lobe and cranial nerves. Dallan et al. (2017) suggest its use for selected lesions such as trigeminal neurinomas and meningiomas lateral to the cavernous sinus. Our anatomical study provides relevant information for initiating these approaches and gaining greater experience.

The transpalpebral transorbital endoscopic lateral transorbital approach offers a wide and direct exposure of the MCF. It should be considered as an alternative to transcranial approaches in cer-

tain lesions invading the lateral region of the MCF, the lateral wall of the cavernous sinus or the infratemporal fossa. A detailed anatomical knowledge of the region is necessary to obtain the best surgical, aesthetic and functional results.

REFERENCES

ABDEL AZIZ KM, BHATIA S, TANTAWY MH, SEKULA R, KELLER JT, FROELICH S, HAPP E (2011) Minimally invasive transpalpebral "eyelid" approach to the anterior cranial base. *Neurosurgery*, 69 (Suppl. 2): 195-206.

ALPER MG (1995) Pioneers in the history of orbital decompression for Graves' ophthalmopathy. *Documenta Ophthalmologica*, 89(1-2): 163-171.

ANANIA P, MIRAPEIX LUCAS R, TODARO G, ZONA G, ASENCIO CORTES C, MUÑOZ HERNANDEZ F (2022) Anatomical meningo-orbital band evaluation and clinical implications: a cadaveric dissection study. *J Neurosurg Sci*, 66(3): 215-219.

ANDALUZ N, ROMANO A, REDDY LV, ZUCCARELLO M (2008) Eyelid approach to the anterior cranial base: Technical note. *J Neurosurg*, 109(2): 341-346.

BALAKRISHNAN K, MOE KS (2011) Applications and outcomes of orbital and transorbital endoscopic surgery. *Otolaryngol Head Neck Surg*, 144(5): 815-820.

BAUMEL JJ, BEARD DY (1961) The accessory meningeal artery of man. *J Anat*, 95(Pt 3): 386-402.

DALLAN I, CASTELNUOVO P, LOCATELLI D, TURRI-ZANONI M, ALQAHTANI A, BATTAGLIA P, HIRT B, SELLARI-FRANCESCHINI S (2015) Multiportal combined transorbital transnasal endoscopic approach for the management of selected skull base lesions: preliminary experience. *World Neurosurg*, 84(1): 97-107.

DALLAN I, DI SOMMA A, PRATS-GALINO A, SOLARI D, ALOBID I, TURRI-ZANONI M, FIACCHINI G, CASTELNUOVO P, CATAPANO G, DE NOTARIS M (2017) Endoscopic transorbital route to the cavernous sinus through the meningo-orbital band: A descriptive anatomical study. *J Neurosurg*, 127(3): 622-629.

DALLAN I, SELLARI-FRANCESCHINI S, TURRI-ZANONI M, DE NOTARIS M, FIACCHINI G, FIORINI FR, BATTAGLIA P, LOCATELLI D, CASTELNUOVO P (2018) Endoscopic transorbital superior eyelid approach for the management of selected spheno-orbital meningiomas: Preliminary experience. *Operative Neurosurg*, 14(3): 243-251.

DANDY WE (1941) Results following the transcranial operative attack on orbital tumors. *Arch Ophthalmol*, 25(2): 191-216.

DI SOMMA A, ANDALUZ N, CAVALLO LM, DE NOTARIS M, DALLAN I, SOLARI D, ZIMMER LA, KELLER JT, ZUCCARELLO M, PRATS-GALINO A, CAPPABIANCA P (2018) Endoscopic transorbital superior eyelid approach: Anatomical study from a neurosurgical perspective. *J Neurosurg*, 129(5): 1203-1216.

DILENGE D, GÉRAUD G (1975) Accessory meningeal artery. *Acta Radiol Diagnosis*, 16(347 suppl): 63-69.

DRAKE L (2011) *Terminología Anatómica – International Anatomical Terminology*. 2nd ed. Thieme Medical Publishers.

DUTTON JJ (2011) *Atlas of clinical and surgical orbital anatomy.* 2nd ed. Elsevier.

EROGLU U, SHAH K, BOZKURT M, KAHILOGULLARI G, YAKAR F, DOGAN I, OZGURAL O, ATTAR A, UNLU A, CAGLAR S, COHEN GADOL AA, UGUR HC (2019) Supraorbital keyhole approach: lessons learned from 106 operative cases. *World Neurosurg*, 124: e667-e674.

GRAS CABRERIZO JR, GRAS ALBERT JR, GARCIA-GARRIGOS E, ALOBID I, CASTELNUOVO P (2017) Nasal septum and nasal vascularization. Nasoseptal perforations: endoscopic repair techniques. Thieme, New York.

GUIZZARDI G, MOSTEIRO A, HOYOS J, FERRES A, TOPCZEWSKI T, REYES L, ALOBID I, MATAS J, CAVALLO LM, CAPPABIANCA P, ENSEÑAT J, PRATS-GALINO, DI SOMMA A (2022) Endoscopic transorbital approach to the middle fossa: qualitative and quantitative anatomic study. *Operative Neurosurg*, 23(4): e267-e275.

HUR MS, KIM HJ, LEE KS (2012) Unusual course of the accessory meningeal artery. *Korean J Phys Anthropol*, 25(4): 193.

IWANAGA J, WILSON C, WATANABE K, OSKOUIAN RJ, TUBBS RS (2017) Anatomical study of the zygomaticotemporal branch inside the orbit. *Cureus*, 9(9): e1727.

IWANAGA J, BADALONI F, WATANABE K, YAMAKI KI, OSKOUIAN RJ, TUBBS RS (2018) Anatomical study of the zygomaticofacial foramen and its related canal. *J Craniofacial Surg*, 29(5): 1363-1365.

KAPLAN M, EROL FS, OZVEREN MF, TOPSAKAL C, SAM B, TEKDEMIR I (2007) Review of complications due to foramen ovale puncture. *J Clin Neurosci*, 14(6): 563-568.

KOPPE M, GLEIZAL A, ORSET E, BACHELET JT, JOUANNEAU E, ROUGEOT A (2013) Superior eyelid crease approach for transobital neuroendoscopic surgery of the anterior cranial fossa. *J Craniofacial Surg*, 24(5): 1616-1621.

KORNIEIEVA M, HADIDY A, ZHURAVLOVA I (2015) Variability of the middle meningeal artery subject to the shape of skull. *J Neurol Surg Part B: Skull Base*, 76(06): 451-458.

KRAYENBÜHL N, ISOLAN GR, AL-MEFTY O (2008) The foramen spinosum: a landmark in middle fossa surgery. *Neurosurg Rev*, 31(4): 397-402.

KRISHNAMURTHY A, ROSHNI S, MURLIMANJU BV, NAYAK SR, JIJI PJ, SOMESH SM, PRABHU LV (2011) Foramina on the zygomatic bone: its clinical significance. *La Clinica terapeutica*, 162(5): 419-421.

LEONEL LCPC, PERIS-CELDA M, DE SOUSA SDG, HAETINGER RG, LIBERTI EA (2020) The sphenoidal emissary foramen and the emissary vein: Anatomy and clinical relevance. *Clin Anat*, 33(5): 767-781.

LUBBE D, MUSTAK H, TAYLOR A, FAGAN J (2017) Minimally invasive endo-orbital approach to sphenoid wing meningiomas improves visual outcomes – our experience with the first seven cases. *Clin Otolaryngol*, 42(4): 876-880.

MACCHI V, REGOLI M, BRACCO S, NICOLETTI C, MORRA A, PORZIONATO A, DE CARO R, BERTELLI E (2016) Clinical anatomy of the orbitomeningeal foramina: variational anatomy of the canals connecting the orbit with the cranial cavity. *Surg Radiol Anat*, 38(2): 165-177.

MCQUEEN C, DIRUGGIERO D, CAMPBELL J, SHOCKLEY W (1995) Orbital osteology: a study of the surgical landmarks. *Laryngoscope*, 105: 783-788.

MOE KS, BERGERON CM, ELLENBOGEN RG (2010) Transorbital neuroendoscopic surgery. *Neurosurgery*, 67 (Suppl. 1).

RAMOS-ZÚÑIGA R (1999) The trans-supraorbital approach. *Min Invasive Neurosurg*, 42(03): 133-136.

RIVKIN MA, TURTZ AR, MORGENSTERN KE (2013) Transorbital endoscopic removal of posterior lateral orbital mass. *Laryngoscope*, 123(12): 3001-3004.

ROSA AD, PINEDA J, CAVALLO LM, DI SOMMA A, ROMANO A, TOPCZEWSKI TE, SOMMA T, SOLARI A, ENSEÑAT J, CAPPABIANCA P, PRATS-GALINO A (2019) Endoscopic endo- and extra-orbital corridors for spheno-orbital region: anatomic study with illustrative case. *Acta Neurochirurg*, 161(8): 1633-1646.

ROUVIÈRE H, DELMAS A (2005) *Anatomía humana descriptiva, topográfica y funcional*. 11th ed. Masson. Barcelona.

SUERO MOLINA E, REVUELTA BARBERO J, EWELT C, STUMMER W, CARRAU R, PREVEDELLO D (2021) Access to Meckel's cave for biopsies of indeterminate lesions: a systematic review. *Neurosurg Rev*, 44(1): 249-259.

TANOUE S, KIYOSUE H, MORI H, HORI Y, OKAHARA M, SAGARA Y (2013) Maxillary artery: functional and imaging anatomy for safe and effective transcatheter treatment. *RadioGraphics*, 33(7): e209-e224.

WILSON DH (1971) Limited exposure in cerebral surgery. *J Neurosurg*, 34(1): 102-106.

Prevalence of accessory carpal ossicles - a CT-based survey

Ozkan Kose[1,2], Levent Sarikcioglu[2], Mehmet Baris Ertan[1], Faruk Aykanat[3], Omer Faruk Egerci[1], Cemil Gurses[4]

[1] *University of Health Sciences, Antalya Training and Research Hospital, Department of Orthopedics and Traumatology, Turkey*
[2] *Akdeniz University, Medical Faculty, Department of Anatomy, Turkey*
[3] *Sanko University, Medical Faculty, Department of Orthopedics and Traumatology, Turkey*
[4] *University of Health Sciences, Antalya Training and Research Hospital, Department of Radiology, Turkey*

SUMMARY

This observational study aimed to determine the prevalence of accessory carpal ossicles (ACO) using a computerized tomography examination. The digital imaging database of the authors' institution was retrospectively reviewed, and all wrist computerized tomography examinations for any indication were identified between 2014 and 2021. Patients with previous wrist surgery and severely impaired carpal anatomy, such as severe osteoarthritis or congenital or acquired deformities that may preclude evaluation and identification of accessory carpal ossicles, were excluded from the study. Four orthopedic surgeons reviewed the computerized tomography scans and identified patients with accessory carpal ossicles on two-dimensional (coronal, axial, and sagittal planes) and three-dimensional computerized tomography reconstructions. Two thousand two hundred thirteen patients, with a mean age of 36.8±12.8 years, were identified and included. Accessory carpal ossicles were detected in 156 (7.1%) subjects, with 186 ACOs identified. The most common accessory carpal ossicles were os praetrapezium (n:34, 1.536%), os triquetrum secundarium (n:28, 1.265%), os epitriquetrum (n:20, 0.903%), os hamuli proprium (n:18, 0.813%), os ulnostyloideum (n:16, 0.723%), os epilunatum (n:12, 0.542%) and os styloideum (n:11, 0.497%) respectively. The study provides valuable information on the prevalence and distribution of accessory carpal ossicles, which can aid in accurately diagnosing and managing wrist pathologies. Further research is warranted to explore the clinical significance and potential impact of rare accessory carpal ossicles on wrist disorders.

Key words: Accessory carpal ossicles – Anatomic variation – Carpal ossicles – Computerized tomography – Wrist

ABBREVIATIONS

CT: Computerized tomography

ACO: Accessory carpal ossicles

INTRODUCTION

Accessory ossicles are defined as small supernumerary bony structures located around the consistent elements of the human skeleton. These ossicles can be found in various locations,

Corresponding author:
Dr. Ozkan Kose. Varlık mah., Kazım Karabekir cd., 07100 Muratpasa, Antalya, Turkey. E-mail: drozkankose@hotmail.com - ORCID: 0000-0002-7679-9635

Submitted: October 18, 2023. **Accepted:** November 11, 2023

https://doi.org/10.52083/ZFNX1794

but the foot, ankle, and wrist are the most frequently observed anatomic sites (Keles-Celik et al., 2017; O'Rhailly, 1953). To date, twenty-five different accessory ossicles around the wrist have been described (O'Rhailly,1953; Pfitzner, 1900). Many accessory carpal ossicles (ACO) remain silent and do not impair the normal function of the wrist. However, in some instances, they might be the source of pain and other symptoms. For instance, the os styloideum, located on the dorsal aspect of the base of the 3rd metacarpal, is closely associated with carpal boss syndrome (Roulet et al., 2017). In the context of traumatic wrist injuries, ACOs can be confused with avulsion fractures during imaging examinations. Multiple studies have reported misdiagnosis of these ossicles as avulsion fractures (Yang et al., 1994; Bianchi et al., 1990; Weintraub et al., 2020). Thus, clinicians and radiologists should be aware of these normal variants to interpret radiographic workup and guide clinical management properly.

The description and nomenclature of these ossicles were established in the early 1900s through cadaveric dissections conducted by pioneering anatomists (Pfitzner, 1900; Schmidt and Freyschmidt, 1993; Keats and Anderson, 2012; Timins, 1999; Senecail et al., 2007). Since then, a limited number of studies have addressed the prevalence of ACO in contemporary literature (O'Rhailly, 1953; Gursoy et al., 2021; Bizarro, 1921; Bogart, 1932). All of these prevalence studies utilized direct radiography as the imaging method. However, due to the intricate anatomy of the wrist and the diminutive size of these ossicles, solely relying on two-view radiography, makes detection of these ossicles challenging. Alongside detection difficulties, the exact positioning of different ossicles that are proximate to one another is hard to discern due to superimposition. Based on these challenges, we hypothesized that the occurrence of these ossicles may be underreported in prior studies. This study aimed to determine the frequency of ACOs using advanced imaging techniques, specifically 2D and 3D computerized tomography wrist imaging, which were not available in earlier studies.

MATERIALS AND METHODS

Patients and study design

A retrospective review was conducted on the digital imaging archive to identify adult patients (>18 years of age) who underwent wrist CT scans between 2014 and 2021. A total of two thousand two hundred and thirteen individuals (696 females and 1517 males) were analyzed. Patients with a history of wrist surgery and those presenting with significantly altered carpal anatomy—such as severe osteoarthritis, congenital anomalies, or acquired deformities that could impede the evaluation and identification of accessory carpal ossicles—were excluded from the study. However, individuals with metacarpal, distal radial, or straightforward carpal bone fractures that did not hinder the identification of ACO were retained in the study. CT scans that failed to display all carpal bones within the field of view were also excluded. This research was conducted in alignment with the ethical standards set forth by the 1964 Declaration of Helsinki and its subsequent amendments. The Clinical Studies Ethics Committee approved the study protocol (Approval date/number: 06.01.2022 / 1-15).

Image acquisition

Wrist CT examinations were conducted using two distinct CT devices from the same manufacturer (Siemens go.Up, Siemens, Munich, Germany), situated in the radiology and emergency departments of the authors' institution. CT scans were captured with a tube voltage ranging from 120-130 kV and a tube current between 72-104 mA. The slice thickness varied from 0.5 to 1.5 mm. The field of view encompassed the distal radius, all carpal bones, and the proximal metacarpal bones, resulting in 100-350 axial sections.

Assessment of the CT examinations

Four orthopedic surgeons analyzed the CT scans, identifying patients with ACO. Radiological assessments were conducted on a digital workstation (Sectra Workstation IDS7; Sectra AB, Linköping, Switzerland). Both two-dimensional (in the coronal, axial, and sagittal planes) and three-dimensional (3D) reconstructions were

employed sequentially. Each reviewer optimized their assessment by adjusting screen contrast, illumination, magnification, and color settings. Subsequent evaluations of patients with accessory carpal ossicles were undertaken collaboratively by a radiologist and an orthopedic surgeon. The joint decision determined the nomenclature of the accessory ossicles, ensuring that any errors in evaluations and nomenclature during the initial review were rectified. As informed by prior research, 25 distinct accessory carpal ossicles were scrutinized (O'Rhailly, 1953; Pfitzner, 1900; Keats and Anderson, 2012; Schmidt and Freyschmidt, 1993). The nomenclature of the ossicles adhered to the definitions and anatomical references delineated in these studies (Fig. 1).

Statistical analysis

Descriptive statistics are provided as frequency and percentage for categorical data, and as mean ± standard deviation along with range for continuous data. The Kolmogorov-Smirnov test assessed data normality. Comparative analyses between independent groups were conducted using the Mann-Whitney U test and chi-square tests. A p-value of less than 0.05 was deemed statistically significant.

RESULTS

A total of 2,213 subjects, with a mean age of 36.8±12.8 years (range: 18-89 years), were included in the study. Male patients were significantly younger than females, with mean ages of 34.0±11.6 and 42.8±13.3 years, respectively (p=0.001). Out of the total participants, 1,517 (68.5%) were male and 696 (31.5%) were female. The study assessed 1,205 (54.5%) right wrist CTs and 1,008 (45.5%) left wrist CTs. ACOs were identified in 158 (7.1%) out of the 2,213 subjects. The frequency of ACO occurrence between genders was comparable (p=0.535) (Table 1).

Among the 158 patients with detected ACOs, a total of 186 individual ACOs were identified,

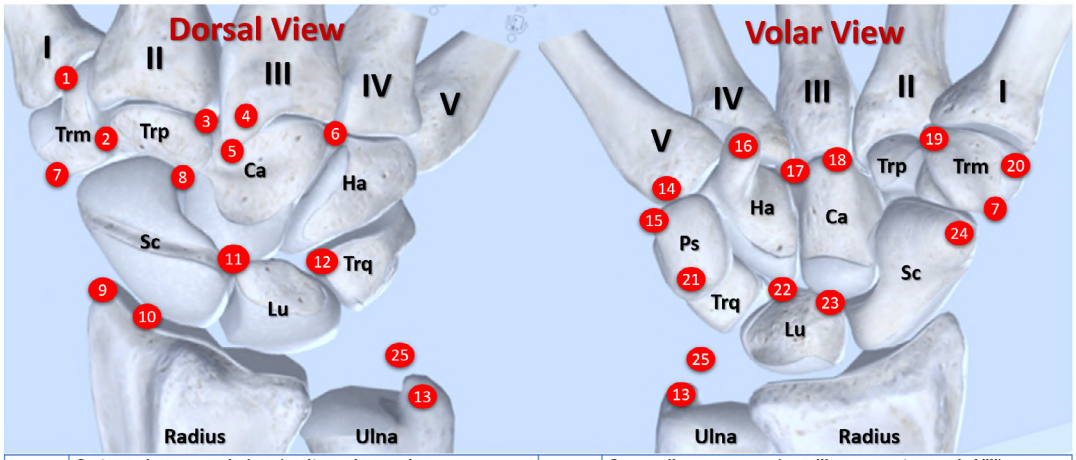

1	Os trapezium secundarium (multangulum majus secundarium, carpometacarpale II)	14	Os vesalianum manus (vesalii, carpometacarpale VIII)
2	Os trapezoideum secundarium (multangulum minus secundarium)	15	Os ulnare externum
3	Os parastyloideum (carpometacarpale III)	16	Os hamuli proprium
4	Os styloideum (carpometacarpale IV)	17	Os Gruberi (carpometacarpale VI)
5	Os metastyloideum	18	Os subcapitatum
6	Os capitatum secundarium (Carpometacarpale V)	19	Os praetrapezium (carpometacarpale I)
7	Os epitrapezium	20	Os paratrapezium (petrapezium)
8	Os carpi centrale	21	Os priforme secundarium (ulnare antebrachii, metapisoid)
9	Os radiostyloideum (persistent radial styloid)	22	Os hypotriquetrum
10	Os paranaviculare	23	Os hypolunatum (centrale III)
11	Os epilunatum	24	Os radiale externum (os parascaphoid)
12	Os epitriquetrum (epipyramis, centrale IV)	25	Os triquetrum secundarium (os triangulare - os intermedium antebrachii)
13	Os ulnostyloideum		

Fig. 1.- Schematic illustration of the carpus showing the various accessory bones and approximate locations. **(a)** Dorsal view. **(b)** Volar view. Abbreviations: I-V: First to fifth metacarpals, Sc: Scaphoid, Lu: Lunate, Trq: Triquetrum, Ps: Pisiforme, Ha: Hamate, Ca: Capitate, Trp: Trapezoid, Trm: Trapezium.

Table 1. Summary of demographic characteristics of the study population. Abbreviations, SD: standard deviation, Min: Minimum, Max: Maximum, ACO: Accessory carpal ossicle.

Variables	Total	Female	Male	p-value
Number of subjects (n, %)	2213 (100%)	696 (31.5%)	1517 (68.5%)	
Age (years)				0.001*
(Mean ± SD)	36.8±12.8	42.8±13.3	34.0±11.6	
(Min. – Max)	18-89	18-89	18-78	
Side (n, %)				0.019**
Right	1205 (54.5%)	356 (16.1%)	849 (38.4%)	
Left	1008 (45.5%)	340 (15.4%)	688 (30.2%)	
Frequency of ACO (n, %)	158 (7.1%)	46 (6.6%)	112 (7.4%)	0.535**

*Mann-Whitney-U test, ** Chi-square Test

Table 2. Frequency of accessory carpal ossicles (ACO) among the study population.

#	Name of the Ossicle	Frequency (n, %)	
		Within all cases	**Within ACOs**
1	***Os trapezium secundarium***	1 (0.045%)	0.538%
2	***Os trapezoideum secundarium***	1 (0.045%)	0.538%
3	***Os parastyloideum***	1 (0.045%)	0.538%
4	***Os styloideum***	11 (0.497%)	5.914%
5	***Os metastyloideum***	3 (0.135%)	1.613%
6	***Os capitatum secundarium***	1 (0.045%)	0.538%
7	***Os epitrapezium***	0	%0
8	***Os carpi centrale***	6 (0.271%)	3.226%
9	***Os radiostyloideum***	2 (0.094%)	1.075%
10	***Os paranaviculare***	0	0%
11	***Os epilunatum***	12 (0.542%)	6.452%
12	***Os epitriquetrum***	20 (0.903%)	10.753%
13	***Os ulnostyloideum***	16 (0.723%)	8.602%
14	***Os vesalianum manus***	1 (0.045%)	0.538%
15	***Os ulnare externum***	7 (0.316%)	3.763%
16	***Os hamuli proprium***	18 (0.813%)	9.677%
17	***Os Gruberi***	0	0%
18	***Os subcapitatum***	1 (0.045%)	0.538%
19	***Os praetrapezium***	34 (1.536%)	18.280%
20	***Os paratrapezium***	3 (0.135%)	1.613%
21	***Os psiforme secundarium***	3 (0.135%)	1.613%
22	***Os hypotriquetrum***	4 (0.180%)	2.151%
23	***Os hypolunatum***	10 (0.452%)	5.376%
24	***Os radiale externum***	3 (0.135%)	1.613%
25	***Os triquetrum secundarium***	28 (1.265%)	15.054%

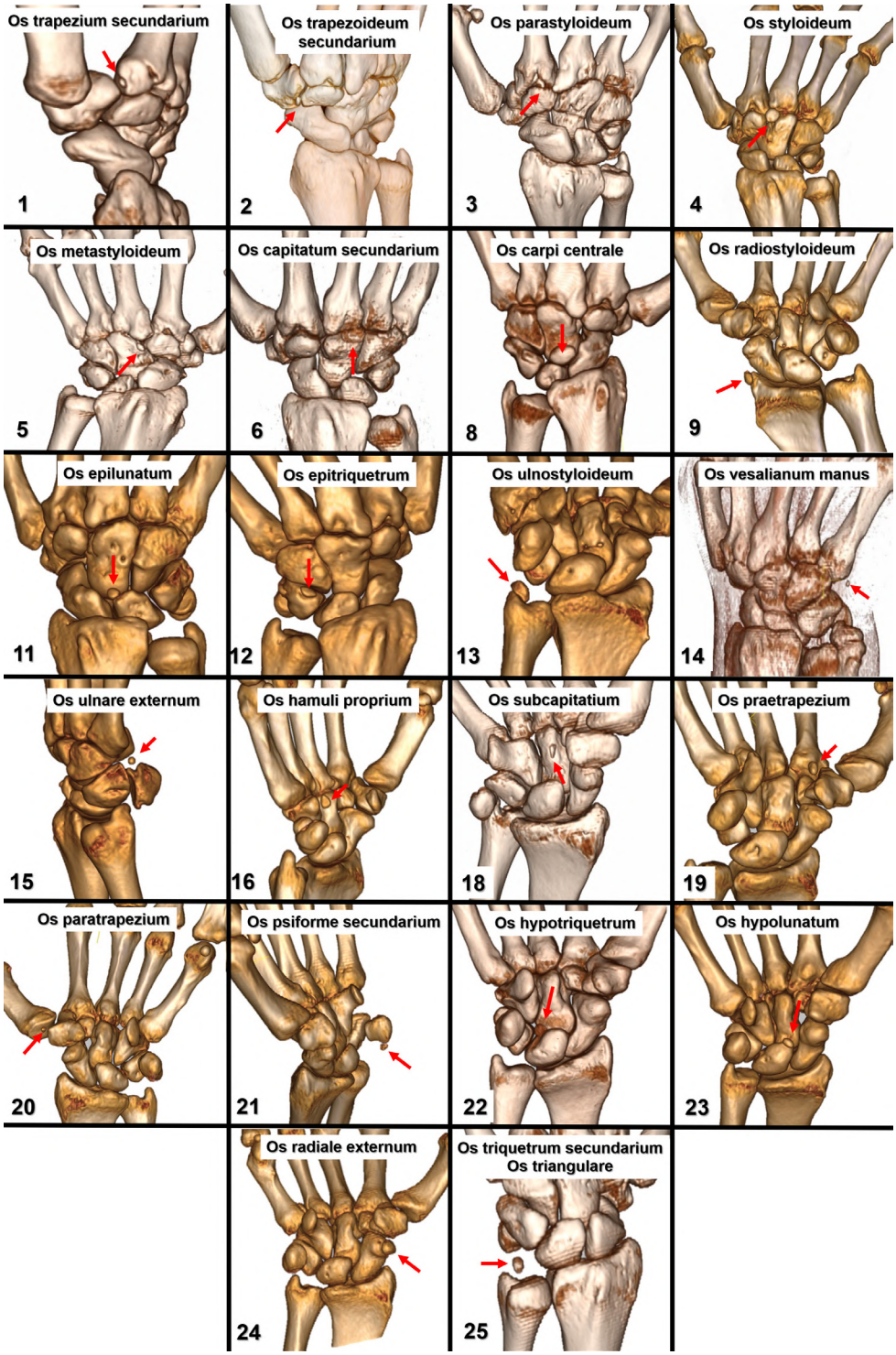

Fig. 2.- The representative 3D appearance of each detected accessory carpal ossicle.

ranging from 1 to 4 per patient. Specifically, four ossicles were found in two patients, three in four patients, two in 14 patients, and one bone in 139 patients. The most commonly observed ACOs included: os praetrapezium (n=34, 1.536%), os triquetrum secundarium (n=28, 1.265%), os epitriquetrum (n=20, 0.903%), os hamuli proprium (n=18, 0.813%), os ulnostyloideum (n=16, 0.723%), os epilunatum (n=12, 0.542%), and os styloideum (n=11, 0.497%), respectively. A comprehensive frequency and distribution of the ACOs are delineated in Table 2. A representative 3D visual representation of each detected ACO can be found in Fig. 2.

DISCUSSION

The present study comprehensively examines ACOs in a large cohort using advanced imaging techniques. Notably, the overall prevalence of ACOs in the studied population was 7.1%. Among the various ACOs identified, the most common ones were os praetrapezium, os triquetrum secundarium, os epitriquetrum, os hamuli proprium, os ulnostyloideum, os epilunatum, os styloideum, and os hypolunatum. The exact incidence of ACOs in the wrist remains uncertain due to the limited number of studies on this subject. To provide a context for our findings, we compared them with previous studies. Bogart (1932) examined 1452 wrist radiographs and documented an ACO incidence of 0.4%, while O'Rahilly (1953) examined 743 wrist radiographs and found a rate of 1.6%. Another study by Bizarro (1921) reported the presence of accessory bones in only four out of 100 wrist radiographs (4%). A more recent study by Gursoy et al. (2021) examined 1,146 digital wrist radiographs and detected ACOs at a higher rate of 9.7%, attributing the increased detection to improved image quality in digital radiography. In our study, while we observed a higher ACO rate than in previous studies, the number of ACOs detected was lower than that reported by Gürsoy et al. (2021). Besides the discrepancy in the frequency of ACOs, the distribution was also inconsistent. It is important to note that evaluating complex carpal bone anatomy solely based on direct radiographs is challenging due to superimposition and the relatively small size of the bones. Additionally, distinguishing between nonunion of avulsion fractures and traumatic calcifications can be difficult (O'Rahilly, 1953). Cross-sectional and three-dimensional examinations, such as computed tomography (CT), provide superior results. In our study, we employed CT as a screening method, which, to our knowledge, is the first study of its kind in the current literature. We consider the data obtained from CT to be more reliable for evaluating ACOs.

The exact etiology of these ossicles remains disputed, but few theories address the formation of certain ossicles. The first theory proposes that these structures are formed when there is a defect in the coalescence of secondary ossification centers with the main structure. In such instances, the accessory element complements the constant element, and they form the normal structure together. This theory can account for the presence of the os styloideum. In the initial stages of carpal embryological development, a primordial cartilaginous structure is typically observed at the site of the second metacarpal bone's styloid process. This eventually merges with the metacarpal to form the styloid process (Kootstra et al., 1974). A lack of fusion between these entities can lead to the emergence of the os styloideum. Notably, a fibrocartilaginous junction typically connects the ossicle to the metacarpal base. In a parallel manner, the os hamuli proprium originates from a fusion anomaly in the secondary ossification center located in the hook of the hamate bone (Greene and Hadied, 1981).

The second theory posits that these ossicles have a phylogenetic origin and they are atavistic remnants. Some of these ossicles consistently appeared in subspecies but regressed or disappeared entirely over the course of evolution. In most primates, the carpus comprises nine bones, compared to eight in humans. The ninth bone is named the "os carpi centrale". This bone locks and stabilizes the midcarpal joint, making the wrist suitable for weight-bearing. The upright posture of humans and the evolution of our forelimbs, once used for walking, into upper extremities are believed to be major factors behind the disappearance of the os carpi centrale (Kivell, 2016; Lewis, 1985). The os radiale externum and epitrapezium ossicles are thought to be remnants of the prepollex found in our mammalian ancestors' wrists (Le Minor 1994).

The third theory suggests that these ossicles arise from nonunion traumatic avulsion fractures or osseous metaplasia in surrounding soft tissues like the capsule and ligaments (O'Rahilly, 1953). A prime example is the os epitriquetrum. Triquetral fractures are the second most common carpal bone fractures, following scaphoid fractures. A large portion of triquetral fractures are dorsal cortical chip fractures. These can often go unnoticed in direct radiographs, and untreated cases might result in nonunion (Vigler et al., 2006; Suh et al., 2014). Due to the traction from the dorsal

triquetroscaphoid and radiotriquetral ligaments, these fragments can move radially from the triquetrum, resembling a distinct accessory bone. Pfitzner (1900) once labeled this fracture as an ACO without complete knowledge of the injury mechanism or radiological characteristics. We believe this labeling was a misinterpretation. An instance of ectopic calcification is the os triangulare. The triangular fibrocartilage complex (TFCC) frequently exhibits ectopic calcification due to both traumatic and non-traumatic degenerative wrist diseases and certain deposition diseases (Bade et al., 1996; Yang et al., 1995). Regrettably, such structures have sometimes been mistakenly classified as accessory elements in direct radiographs. O'Rahilly (1953) noted in a study of 743 wrist radiographs that 6% showed accessory calcific structures. Only 1.6% were genuine ACOs, while the remaining 4.4% were lesions resulting from trauma. As we gain a deeper understanding of the etiology of these structures, we expect modifications in the official list of ACOs.

The current study presents both strengths and limitations. Its primary strength lies in the methodology used to screen for the presence of ACOs, making it the most comprehensive study on the topic to date. However, there are notable limitations. The data were collected from a local institution, so the findings may not be generalizable to other ethnic groups. Four different observers reviewed The CT scans once, potentially leading to discrepancies in their assessments. Nonetheless, every observer noted any suspicious structure during their initial review, and a joint decision was made independently afterward. This process possibly enhances the reliability of our data. As a retrospective study, the detailed past medical history, especially regarding traumatic hand injuries of the patients, remained unknown.

In conclusion, this study represents a landmark in the literature on ACOs. Properly identifying these ossicles is crucial for precise diagnosis and intervention. While many of these ossicles are clinically insignificant and are often found incidentally during imaging, others can be associated with specific medical conditions and might be mistaken for fractures. Conducting comparable research on various ethnic populations would broaden our understanding of their distribution. Understanding the origins of these ossicles is crucial to accurately defining them.

ACKNOWLEDGEMENTS

The authors thank Dr. May, Dr. Unal, and Dr. Ergun for the data screening and entry.

Author contributions: Study conception and design: OK, LS, MBE Acquisition of data: OK, LS, CG, FA Analysis and interpretation of data: OK, LS, CG, Drafting of the manuscript: OK, LS, MBE, FA, CG Critical revision: OK, LS, MBE, FA, CG (Initials of authors' names). All authors accepted the final version of the manuscript.

Ethical approval: We confirm that we have read the Journal's position on issues involved in ethical publication and affirm that this report is consistent with those guidelines. The Institutional Review Board approved the study protocol (Date/Issue: 06.01.2022 / 1-15).

REFERENCES

BADE H, KOEBKE J, KLUMPP M (1996) Accessory ossifications in the ulnocarpal wrist region. *Ann Anat*, 178(3): 263-268.

BIANCHI S, ABDELWAHAB IF, FEDERICI E (1990) Unilateral os hamuli proprium simulating a fracture of the hook of the hamate: a case report. *Bull Hosp Jt Dis Orthop Inst*, 50(2): 205-208.

BIZARRO AH (1921) On sesamoid and supernumerary bones of the limbs. *J Anat*, 55(Pt 4): 256-268.

BOGART FB (1932) Variations of the bones of the wrist. *AJR Am J Roentgenol*, 28: 638-646.

GREENE MH, HADIED AM (1981) Bipartite hamulus with ulnar tunnel syndrome--case report and literature review. *J Hand Surg Am*, 6(6): 605-609.

GURSOY M, COBAN I, METE BD, BULUT T (2021) The incidence of accessory ossicles of the wrist: a radiographic study. *J Wrist Surg*, 10(5): 458-464.

KEATS TE, ANDERSON MW (2012) Atlas of normal Roentgen variants that may simulate disease, 9th ed. *Elsevier Health Sciences*, Philadelphia.

KELES-CELIK N, KOSE O, SEKERCI R, AYTAC G, TURAN A, GULER F (2017) Accessory ossicles of the foot and ankle: disorders and a review of the literature. *Cureus*, 9(11): e1881.

KIVELL TL (2016) The primate wrist. In: Kivell T, Lemelin P, Richmond B, Schmitt D (eds). *The Evolution of the Primate Hand. Developments in Primatology: Progress and Prospects*. Springer, New York, pp 17-54.

KOOTSTRA G, HUFFSTADT JC, KAUER JM (1974) The styloid bone. A clinical and embryological study. *Hand*, 6(2): 185-189.

LE MINOR JM (1994) The sesamoid bone of musculus abductor pollicis longus (os radiale externum or prepollex) in primates. *Acta Anat (Basel)*, 150(3): 227-231.

LEWIS OJ (1985) Derived morphology of the wrist articulations and theories of hominoid evolution: Part II. The midcarpal joints of higher primates. *J Anat*, 142: 151-172.

O'RAHILLY R (1953) A survey of carpal and tarsal anomalies. *J Bone Joint Surg Am*, 35-A(3): 626-642.

PFITZNER W (1900) Die morphologischen Elemente des menschlichen Handskelets. *Z Morph Anthropol*, 2: 77-157.

ROULET S, BACLE G, MARTEAU E, LAULAN J (2017) Surgical treatment of carpal boss by simple resection: Results in 25 cases at a mean of 8 years' follow-up. *Hand Surg Rehabil*. 36(2): 109-112.

SCHMIDT H, FREYSCHMIDT J (1993) Kohler/Zimmer borderlands of normal and early pathological findings in skeletal radiology, 4th edition. Thieme, New York.

SENECAIL B, PERRUEZ H, COLIN D (2007) Variations numériques et synostoses congénitales des os du carpe [Numerical variants and congenital fusions of carpal bones]. *Morphologie*, 91(292): 2-13.

SUH N, EK ET, WOLFE SW (2014) Carpal fractures. *J Hand Surg Am*, 39(4): 785-791.

TIMINS ME (1999) Osseous anatomic variants of the wrist: findings on MR imaging. *AJR Am J Roentgenol*, 173(2): 339-344.

VIGLER M, AVILES A, LEE SK (2006) Carpal fractures excluding the scaphoid. *Hand Clin*, 22(4): 501-516.

WEINTRAUB MD, HANSFORD BG, STILWILL SE, ALLEN H, LEAKE RL, HANRAHAN CJ, CHAN BY, SOLTANOLKOTABI M, KOBES P, MILLS MK (2020) Avulsion Injuries of the Hand and Wrist. *Radiographics*, 40(1): 163-180.

YANG ZY, GILULA LA, JONSSON K (1994) Os centrale carpi simulating a scaphoid waist fracture. *J Hand Surg Br*, 19(6): 754-756.

YANG BY, SARTORIS DJ, DJUKIC S, RESNICK D, CLOPTON P (1995) Distribution of calcification in the triangular fibrocartilage region in 181 patients with calcium pyrophosphate dihydrate crystal deposition disease. *Radiology*, 196(2): 547-550.

A cone beam computed tomographic study on foramen transversarium

Karthikeya Patil, Sanjay C.J., Mahesh K.P., Eswari Solayappan, Varusha Sharon Christopher, Namrata Suresh

Department of Oral Medicine and Radiology, JSS Dental College and Hospital, JSS Academy of Higher Education and Research, Mysuru – 570015, Karnataka, India

SUMMARY

The foramen transversarium is a vital feature found in the cervical vertebrae of the spine. It serves as a protective passageway for the vertebral artery and vertebral vein, supplying blood to the brain and spinal cord. Any compromise to these structures within the foramen can lead to severe neurological complications, emphasizing its clinical significance. The study was carried out on 83 subjects of typical cervical vertebrae. Among them were 42 males and 41 females. All the foramen transversaria were observed for any anatomical variations. The anteroposterior, transverse diameters of all the foramen transversaria and the distance between the medial margin of uncinate process to the foramen transversarium were measured. The average transverse diameter of typical cervical vertebrae and seventh cervical vertebrae were ± 0.84mm and 5.13 ± 1.22 mm respectively. The average anteroposterior diameters of typical and seventh cervical vertebrae were 4.84 ± 0.69 mm and 3.91 ± 1.17 mm respectively. The distance from medial border of uncinate process to foramen transversaria was 4.28 ± 0.77 mm in typical and 5.44 ± 1.28 mm in seventh cervical vertebrae. The incidence of double bubble foramen in typical cervical vertebrae was reported to be17.5%. The incidence of double foramen transversaria was 12.5% in the seventh cervical vertebrae. Osteophytes were obstructing the foramen transversarium and narrowing it in 25% of vertebrae. In cone beam computed tomography (CBCT), the foramen transversarium plays a pivotal role in precise imaging of the cervical spine. Its significance lies in providing clear visualization of anatomical structures and potential abnormalities, aiding in the accurate diagnosis and treatment planning for various spinal conditions, thus enhancing patient care.

Key words: Cone Beam Computed Tomography – Typical cervical vertebrae – Foramen transversarium – Osteophytes – Vertebrobasilar insufficiency

INTRODUCTION

A cluster of seven tiny bones, termed the cervical vertebrae, that are nestled in the neck area of the human spine are crucial to our daily existence and functional capacity. Given the extensive multitude of tasks they execute, these vertebrae are of paramount importance. The vertebral body, vertebral arch, vertebral foramen, articular facet, spinous process, and foramen transversarium

Corresponding author:
Dr Sanjay, C.J. Department of Oral Medicine and Radiology, JSS Dental College and Hospital, JSS Academy of Higher Education and Research Mysuru – 570015, Karnataka, India. Phone: +91 97425 65566. E-mail: drsanjaycj_dch@jssuni.edu.in - ORCID: 0000-0003-2830-1481

Submitted: October 4, 2023. **Accepted:** November 15, 2023

https://doi.org/10.52083/CJIY2659

(FT) are all defined by the CV as crucial anatomical adaption elements (Benzel, 2012). The foramen transversarium, also known as the vertebral artery foramen, is a recent structure that has garnered attention. It is a small but important anatomical feature, encountered notably in the first through sixth cervical vertebrae.

The foramen transversarium is a unique structure with bilateral openings, one on each side of the spine. It executes a multitude of necessary tasks. The sympathetic nerve plexus, vertebral artery, and vein all pass through the foramen transversarium. These blood vessels deliver oxygen-rich blood to the brain, supplying it with the resources it needs to function at its best. The sympathetic nerve fibres that travel via the foramen transversarium also assist in stabilising and supporting the cervical vertebrae, as well in regulating different bodily processes like blood pressure and heart rate (Chaiyamoon et al., 2021).

Any FT-related alterations can have a direct influence on the structure and shape of the neurovascular structures to which they are connected, resulting in vertebrobasilar ischemia, hearing impairment, and neurological symptoms inextricably linked to the vertebral artery or basilar artery (Zaw et al., 2021). The foramen transversarium in dry skulls is extensively discussed in the literature, albeit without the use of radiography. By using different imaging modalities, these variations of FT can be clearly seen radiographically. Cone beam computed tomography (CBCT) has recently attracted interest in this area.

In the entities of orthopaedics and radiology, cervical vertebral imaging using CBCT has become a useful diagnostic tool. Due to its high-resolution three-dimensional capabilities, CBCT has the unique advantage of rendering the cervical spine. This technique permits a comprehensive inspection of the cervical vertebrae, which is best suited for surgical planning, as it enables surgeons to precisely examine the anatomy and pathology of the cervical spine, impacting the precision of procedures and mitigating risk. Furthermore, cervical spine disorders, fractures, tumours, and degenerative changes can all be intercepted and monitored early with CBCT, which contributes to developing more effective and comprehensive treatment plans. So, the aim of the present study is to study the foramen transversarium from the stance of a radiologist in order to improve the process of diagnosis and therapy.

MATERIALS AND METHODS

The JSSDCH IEC Research Protocol Number: 21/2023 was approved by the institutional ethics committee. The volumetric images produced in the large view modes were generated using Planmeca ProMax 3D. A convenient sampling technique was used, assuming an absolute precision of 5% and a confidence level of 95%. A total of 83 CBCT scans, 42 males and 41 females, were utilised between May 2022 and June 2023.

Inclusion criteria

1. Ideal axial section of optimum diagnostic CBCT images of cervical vertebrae and closely associated structures.
2. Patients who underwent CBCT evaluation of:
    a. Mixed dentition analysis.
    b. Maxillary and mandibular arch pathologies.
    c. Pre and post treatment evaluation for maxillofacial implant placement.
    d. Pre-surgical planning for orthognathic surgery.
    e. Trauma involving maxilla and mandible.

Exclusion criteria

1. CBCT of axial images do not clearly depict the cervical region and not cover the sixth cervical region.
2. Images with developmental defects or pathology involving the cervical region.
3. Inadequate image quality, including images with exposure artefacts, subject artefacts, and inherent artefacts.

Radiographical images satisfying this inclusion criteria will be further analysed for the transverse diameter, antero-posterior diameter, distance from the medial border of the uncinate process to the foramen transversarium, and the prevalence of any accessory foramina and osteophytes (Figs. 1-3).

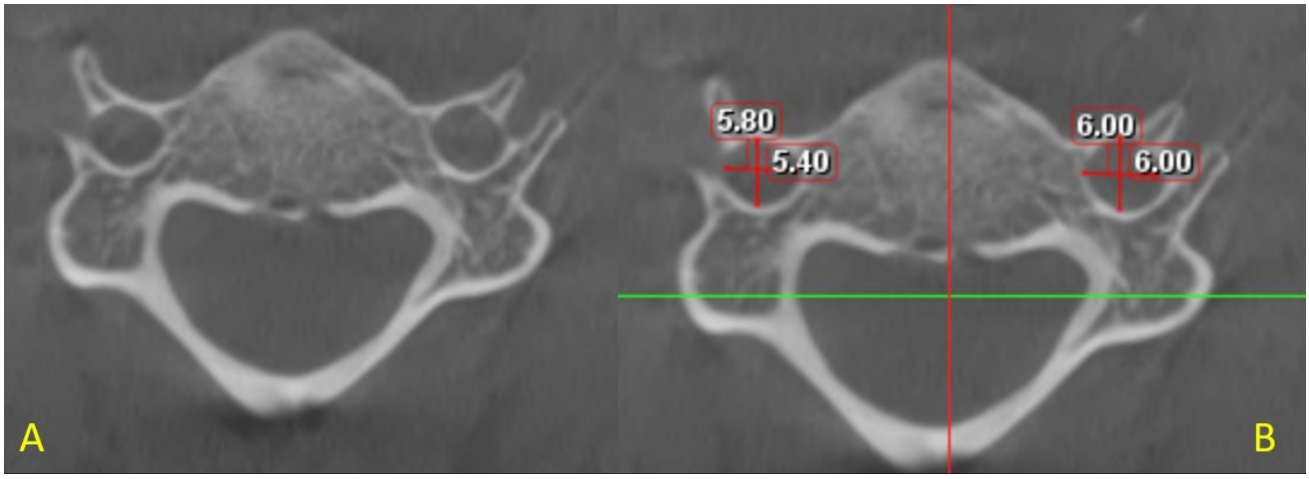

Fig. 1.- A: Transverse and anterior-posterior diameter of foramen transversarium in axial section. **B:** Transverse and anterior-posterior diameter of foramen transversarium measuring its dimension.

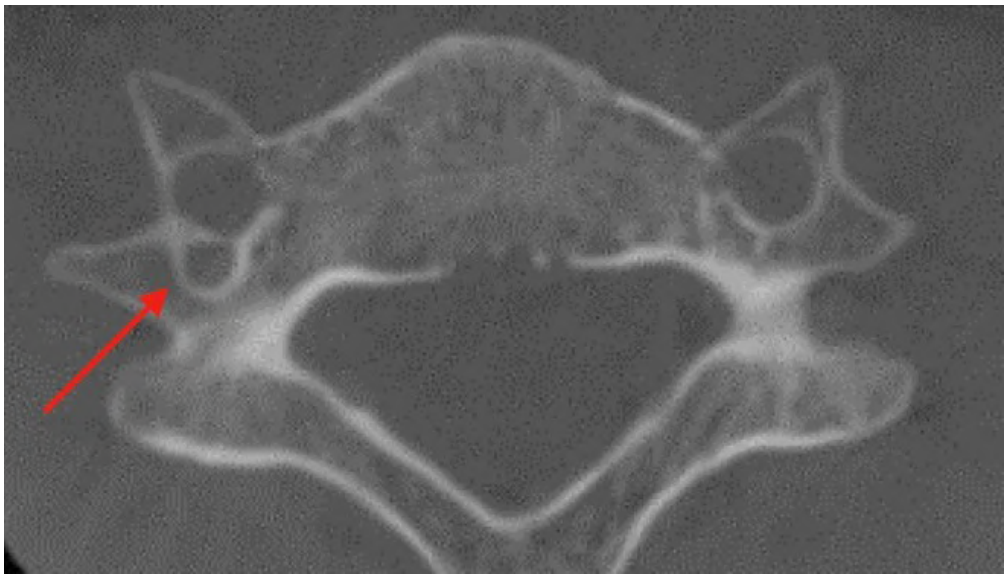

Fig. 2.- Accessory foramen transversarium (arrow).

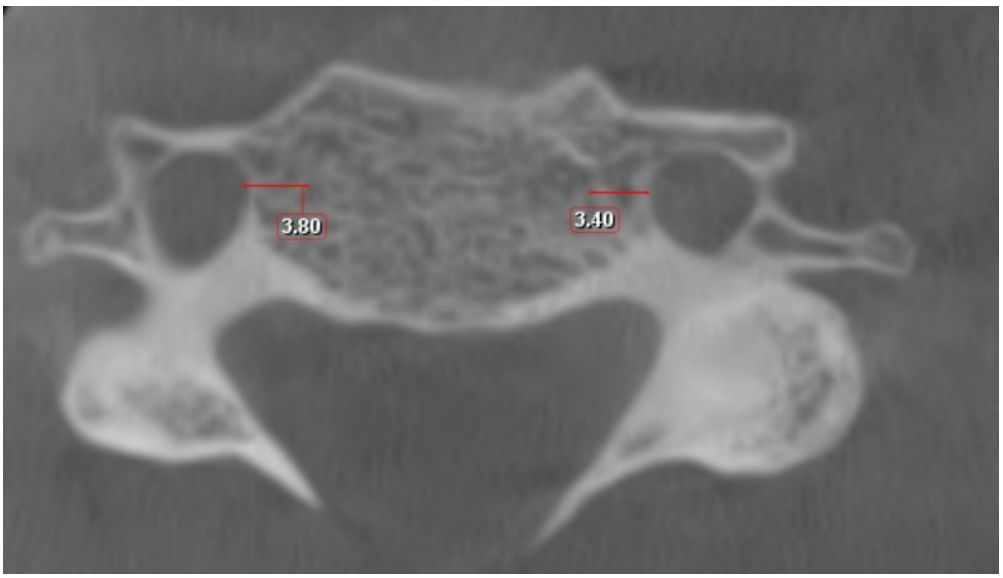

Fig. 3.- Distance from the medial process of the uncinate process to foramen transversarium.

Table 1. Mean and standard deviation.

Evaluated Parameters	Mean (mm)		Standard deviation (mm)	
	Right	Left	Right	Left
Transverse Diameter	5.993	6.066	0.747	0.707
Anterior- Posterior Diameter	5.363	5.488	0.656	0.660
Distance from the medial border of uncinate process to foramen transversarium	4.761	4.677	0.987	0.958

Statistical analysis

The SPSS 22.0 package was used to tabulate and analyse the gathered data. The application of descriptive statistics was rendered. A paired sample t-test was employed to assess the mean differences between the left and right sides or between the AP and transverse dimensions. It was done to calculate the mean, standard deviation, and P value. Also, the presence of the accessory foramen and the osteophytes obstructing the transverse foramen were qualitatively assessed.

RESULTS

The transverse diameter of the right transverse foramen in a typical cervical vertebra exhibited considerable variation, with a mean value of 5.99 ± 0.74 mm, while the anteroposterior diameter of the right transverse foramen had a mean diameter of 5.36 ± 0.65 mm. The average transverse diameter of the left transverse foramen was found to be 6.06 ± 0.7 mm, while the average antero-posterior diameter was measured to be 5.48 ± 0.66 mm. The estimation of the distance between the right medial border of the uncinate process and the foramen transversarium exhibited variability, with an average value of 4.76 ± 0.98 mm. Similarly, the measurement of the distance between the left medial border of the uncinate process and the foramen transversarium also displayed variability, with an average value of 4.67 ± 0.958 mm (Table 1).

Table 2. Qualitative analysis of accessory foramina and osteophytes.

	Total Number (N = 83)	Percentage
Accessory transverse foramina	15	18.07
Osteophytes	7	8.43

The accessory transverse foramen was identified as the most prevalent anomaly, observed in 15 individuals, accounting for 18.07% of the total sample. Osteophytes, the second most prevalent anomaly, manifested in 7 patients, accounting for 8.43% of the sample (Table 2).

A paired t-test was performed on a sample comprising 83 individuals with the purpose of comparing four measurements pertaining to the architectural characteristics of the cervical spine, specifically focusing on the differences between the right and left sides. The transverse foramen exhibited a discernible discrepancy in both transverse diameter (t-test of difference, T-value = -0.948, P value = 0.346) and antero-posterior diameter (t-test of difference, T-value = -1.37, P value = 0.174) between the right and left sides. None of the aforementioned distinctions exhibit statistical significance, as none of the p-values fall below the threshold of This finding indicates that there are no statistically significant differences between the right and left sides of the foramen transversarium in the studied population (Table 3).

Table 3. Paired t-test.

	t value	*p value*
Right vs Left Anterior - Posterior Diameter	-1.37	0.174
Right vs Left Transverse Diameter	-0.948	0.346
Right vs Left Uncinate Process to FT	0.96	0.34

DISCUSSION

Studying the morphology of FT is indispensable for diagnostic applications in a variety of ways in light of the impairment that might occur in the vertebral artery pathway. Vertebral artery com-

pression can manifest in neurological ailments like headaches, migraines, vertigo, and disturbances of the hearing. In any context, it's critical to understand the FT variations, especially for surgeons and neurosurgeons. The formation of the vertebral artery, the essential component of the FT, during embryogenesis may be substantially causally linked to the presence of these variations. The vertebral artery is developed by the fusion of the cervical intersegmentary arteries' longitudinal anastomosis with the primitive dorsal aorta. Furthermore, the disparities detected may be precipitated by developmental changes. According to the literature, stress and posture in the upright human figure the skeletal layout of the neck region (Taitz and Nathan, 1986).

As the angle of the head increases, vertebral artery stenosis, which induces the constriction, triggers Bow Hunter's stroke, a sign of vertebrobasilar insufficiency (Sarkar et al., 2014). The vertebrobasilar insufficiency (VBI), which provokes neck actions to nudge on the vertebral artery, is characterised by headache, migraine, and fainting spells (Kaya Özçora and Canpolat, 2017; Sangari et al., 2015). Cervical migraine, also known as Barré-Lieou syndrome, is a distinctive kind of migraine that originates in the neck. It is deemed that the causes of this condition comprise spasm of the vertebral artery and occlusion of the foramen transversarium (Tamura, 1989).

The two vertebral arteries are purportedly not of equal size in about 69% of cases; additionally, Sangari et al. (2015) report about 75% of unequal size. In the present study, the mean diameter of the right and left transverse foramen varied from the mean by 5.99 ± 0.74 mm and 6.06 ± 0.7 mm, respectively. Based on a study by Tellioglu et al. (2018), there is still a substantial positive association between the variation in C3-C6 vertebrae, despite the fact that there was no statistically significant difference between the dimensions of the right and left sides. The present study is concurrent with similar investigations by Cagnie et al. (2005), Taitz et al. (1978) and Zaw et al. (2021), all of which report that the left transverse foramen is larger than the right. The reason is that this is presumably because the arteries on the left side are frequently broader than those on the right side (Abd el-Bary et al., 1995; Gotlib and Thiel, 1985; Mitchell, 2004).

The C6 level was the most afflicted level in the present study, with 53% of the vertebrae having a duplicate foramen, followed by the C5 level with 31%; this is almost certain with Moreira et al. (2020) and Zibis et al. (2016). The primary anatomical difference most commonly noticed in our investigation was the double foramen, which Meckel first described in 1912. The double foramen transversarium is also known as foramen transversarium bipartitia. Relying on the vertebral artery's course, it could be unilateral or bilateral. The vertebral artery's tortuosity, along with embryological factors, is crucial in the development of FT bipartitia. However, the actual cause of the double FT is not well renowned (Ulusoy, 2019).

According to our report, the occurrence of the accessory foramen is approximately 18.07%, compared to 17.5% encountered by Yesender et al. (2017). At the level of C7, Taitz et al. (1978) presented three foramina in a single vertebra. No triple foramen was located during our analysis. This may well raise the probabilities of thrombus formation and embolisation in fenestrated or numerous vertebral arteries, which could lead to severe transient ischemic attacks (Ionete and Omojola, 2006).

Ostephytes, which are aberrant bone growths that can conceivably cause injuries to the sympathetic plexus, vertebral artery, and vein, are evidently existent inside the FT (Strek et al., 1998). The vertebral artery may get compressed as a consequence of elevated external constraint imposed by the cervical spine's deterioration (Cockerill et al., 2000). 8.43% of the vertebrae in the present study evinced osteophytes, which showed hardly a proclivity for the right or left side. Osteophytes were found in 5.7% of the vertebrae, predominantly in the C7 segment, according to a study, which is significantly less than the percentage reported (Das and Basu, 2022; Sanchis-Gimeno et al., 2019). Whenever the head revolves, the osteophyte triggers an inflammatory response that results in the development of a fibrous layer surrounding the VA, which hinders arterial advancement, compression or kinking are more likely to occur (Kuether et al., 1997).

The mean distance of the transverse foramen from the medial margin of the uncinate process in the present study was 4.76± 0.98 mm on the right side and 4.67± 0.95 mm on the left side, which was less than the study by Sangari et al. (2015), who reported it as 5.0 ± 0.87 mm on the right side and 5.0 ± 1.0 mm on the left. This is noteworthy because the medial edge of the uncovertebral joint may contribute as a robust landmark during anterior cervical disc surgery to prevent vertebral artery injury (Malik et al., 2010). It is possible to have a strong possibility of laceration of the vertebral arteries, particularly during lateral decompression to eliminate osteophytes from the uncinate process (Ebraheim et al., 1996).

Agenesis of the transverse foramen is often rare. However, our investigation did not find any evidence of the foramen transversarium being absent. Taitz et al. reported the absence of a foramen transversarium in four vertebrae. Kimura et al. (1985) recorded 18 instances, and Wysocki et al. (2003) reported one case.

CONCLUSION

This study concluded that, regardless of the lack of statistical significance, the left transverse foramen was larger than the right one. In 18.07% of the samples that were evaluated, an accessory foramen was located, and 8.43% of the samples revealed osteophytes. We opine that any values lower or higher may suggest abnormality. In this circumstance, it is posited to assess the foramen transversarium using cone-beam computed tomography (CBCT), an imaging modality that is embraced as the gold standard. The clinical significance of the foramen transversarium will be comprehended with further research in this field. This is pertinent to medical practitioners, since it exemplifies the value of detailed anatomical information when diagnosing and treating disorders involving the cervical spine. Recognising the importance of the foramen transversarium in vascular health, neurology, or orthopaedics is vital to delivering expedient patient treatment and ensuring people's livability.

DECLARATIONS

The authors declare that they have no known competing financial interests or personal relationships that could have appeared to influence the work reported in this paper. The Institutional Ethics Committee authorised the work as a descriptive retrospective study after it was proffered to them. Only subjects' respective masked radiographs were evaluated from the archives maintained in the department; no patients actively participated in the study. Hence, patient consent is not applicable for the study.

REFERENCES

ABD EL-BARY TH, DUJOVNY M, AUSMAN JI (1995) Microsurgical anatomy of the atlantal part of the vertebral artery. *Surg Neurol*, 44(4): 392-400; discussion 400-401.

BENZEL EC (2012) *The Cervical Spine*. Lippincott Williams & Wilkins. https://play.google.com/store/books/details?id=eII8vVpHE-wC

CAGNIE B, JACOBS F, BARBAIX E, VINCK E, DIERCKX R, CAMBIER D (2005) Changes in cerebellar blood flow after manipulation of the cervical spine using technetium 99m–ethyl cysteinate dimer. *J Manipulative Physiol Ther*, 28(2): 103-107.

CHAIYAMOON A, YANNASITHINON S, SAE-JUNG S, SAMRID R, THONGBUAKAEW T, IAMSAARD S (2021) anatomical variation and morphometric study on foramen transversarium of the upper cervical vertebrae in the Thai population. *Asian Spine J*, 15(5): 557-565.

COCKERILL W, ISMAIL AA, COOPER C, MATTHIS C, RASPE H, SILMAN AJ, O'NEILL TW (2000) Does location of vertebral deformity within the spine influence back pain and disability? European Vertebral Osteoporosis Study (EVOS) Group. *Ann Rheum Dis*, 59(5): 368-371.

DAS NK, BASU U (2022) Morphological features and anatomical variations of the foramen transversarium in cervical vertebrae: a study in Eastern Indian population. *Int J Sci Technol Res Arch*, 3(2): 213-227.

EBRAHEIM NA, LU J, BROWN JA, BIYANI A, YEASTING RA (1996) Vulnerability of vertebral artery in anterolateral decompression for cervical spondylosis. *Clin Orthop Rel Res*, 322: 146-151.

GOTLIB AC, THIEL H (1985) A selected annotated bibliography of the core biomedical literature pertaining to stroke, cervical spine, manipulation and head/neck movement. *J Can Chiropract Assoc*, 29(2): 80.

IONETE C, OMOJOLA MF (2006) MR angiographic demonstration of bilateral duplication of the extracranial vertebral artery: unusual course and review of the literature. *AJNR. Am J Neuroradiol*, 27(6): 1304-1306.

KAYA ÖZÇORA GD, CANPOLAT M (2017) stretch syncope: a rare case mimicking seizure. *J Pediat*, 11(4): 274-276.

KIMURA K, KONISHI M, HU SY (1985) Shape and size of the transverse foramina in Japanese. *Okajimas Folia Anat Japon*, 62(2): 123-131.

KUETHER TA, NESBIT GM, CLARK WM, BARNWELL SL (1997) Rotational vertebral artery occlusion: a mechanism of vertebrobasilar insufficiency. *Neurosurgery*, 41(2): 427-432; discussion 432-433.

MALIK SW, STEMPER BD, METKAR U, YOGANANDAN N, SHENDER BS, RAO RD (2010) Location of the transverse foramen in the subaxial cervical spine in a young asymptomatic population. *Spine*, 35(12): E514-E519.

MITCHELL J (2004) Differences between left and right suboccipital and intracranial vertebral artery dimensions: an influence on blood flow to the hindbrain? *Physiother Res Int*, 9(2): 85-95.

MOREIRA MOREIRA JJ, HERRERO CFPS (2020) Anatomical variations and morphometric features of the foramen transversarium in the cervical vertebrae of a latin American population: A Brazilianstudy. *World Neurosurg*, 137: e18-e26.

SANCHIS-GIMENO JA, QUILES-GUIÑAU L, LLIDO-TORRENT S, APARICIO L, NALLA S, MIQUEL-FEUTCH M (2019) Possible clinical implications of geographic differences in prevalence of double transverse foramen. *World Neurosurg*, 126: e570-e572.

SANGARI SK, DOSSOUS P-M, HEINEMAN T, MTUI EP (2015) Dimensions and anatomical variants of the foramen transversarium of typical cervical vertebrae. *Anat Res Int*, 2015: 391823.

SARKAR J, WOLFE SQ, CHING BH, KELLICUT DC (2014) Bow hunter's syndrome causing vertebrobasilar insufficiency in a young man with neck muscle hypertrophy. *Ann Vasc Surg*, 28(4): 1032.e1-1032.e10.

STREK P, REROŃ E, MAGA P, MODRZEJEWSKI M, SZYBIST N (1998) A possible correlation between vertebral artery insufficiency and degenerative changes in the cervical spine. *Eur Arch Oto-Rhino-Laryngol*, 255(9): 437-440.

TAITZ C, NATHAN H (1986) Some observations on the posterior and lateral bridge of the atlas. *Acta Anat*, 127(3): 212-217.

TAITZ C, NATHAN H, ARENSBURG B (1978) Anatomical observations of the foramina transversaria. *J Neurol Neurosurg Psych*, 41(2): 170-176.

TAMURA T (1989) Cranial symptoms after cervical injury. Aetiology and treatment of the Barre-Lieou syndrome. *J Bone Joint Surg*, 71-B(2): 283-287.

TELLIOGLU AM, DURUM Y, GOK M, KARAKAS S, POLAT AG, KARAMAN CZ (2018) Suitability of foramen magnum measurements in sex determination and their clinical significance. *Folia Morphol*, *77*(1): 99-104.

ULUSOY M (2019) Anatomical variations in foramen transversarium. *Eurasian J Med Invest*, https://doi.org/10.14744/ejmi.2019.15468

WYSOCKI J, BUBROWSKI M, REYMOND J, KWIATKOWSKI J (2003) Anatomical variants of the cervical vertebrae and the first thoracic vertebra in man. *Folia Morphol*, 62(4): 357-363.

YESENDER M, DEVADAS P, SARITHA S, VINILA BHS (2017) Study on the anatomical variations and morphometry of foramen transversaria of the subaxial cervical vertebrae. *Int J Anat Res*, 5(2.1): 3708-3712.

ZAW AK, OLOJEDE SO, LAWAL SK, OFFOR U, NAIDU ECS, RENNIE CO, AZU OO (2021) Preliminary study on foramen transversarium of typical cervical vertebrae in KwaZulu-Natal population: Age and gender related changes. *Transl Res Anat*, 22: 100099. https://www.sciencedirect.com/science/article/pii/S2214854X20300388

ZIBIS AH, MITROUSIAS V, BAXEVANIDOU K, HANTES M, KARACHALIOS T, ARVANITIS D (2016) Anatomical variations of the foramen transversarium in cervical vertebrae: findings, review of the literature, and clinical significance during cervical spine surgery. *Eur Spine J*, 25(12): 4132-4139.

Increased mucous cell population and modulation of Bax/Bcl-2 factors characterize *in vivo* gastroprotective activity of *Cissampelos owariensis* in rats

Oluwasegun Olatomide[1,2], Dayo Omotoso[1]

[1] *Department of Human Anatomy, Faculty of Basic Medical Sciences, Redeemer's University, Ede, Nigeria*
[2] *Department of Anatomy, College of Health Sciences, Igbinedion University, Okada, Edo State, Nigeria*

SUMMARY

The physiological integrity of the gastric mucosa is dependent on the balance between the mucosal protective and aggressive factors. Medicinal plants or their derivatives generally exhibit gastroprotective effect by promoting the protective factors against the aggressive factors of the gastric mucosa. The study was conducted to elucidate the gastroprotective mechanism of the methanol extract of *C. owariensis* (MECo) in rats. Twenty male Wistar rats were divided into four groups, which include control groups A and B – given distilled water – and treated groups C and D – animals given 100 and 300 mg/kg MECo respectively for 28 days. After the treatment period, gastric mucosal injury was induced for groups B-D by pyloric ligation method. The gastric tissue of animals was collected, processed for histology (haematoxylin and eosin technique), histochemistry (periodic acid-schiff technique) and immunohistochemical staining (for Bcl-2 & Bax proteins). The results of the gastric histomorphology showed prominent and widespread mucosal erosion in positive control group B compared to normal control group A, while treated groups C and D showed only mild or focal mucosal erosion. Furthermore, the histochemical results showed significant increase in mucous cell population in treated groups C and D compared to positive control group B. The immunostaining results showed significant up-regulation of anti-apoptotic Bcl-2 protein and down-regulation of pro-apoptotic Bax protein in the treated groups C and D compared to the control groups A and B. In conclusion, the findings of this study indicate that the increased mucous cell population and modulation of apoptotic signaling highlights the mechanism of gastroprotective activity of MECo.

Key words: *Cissampelos owariensis* – Gastroprotection – Mucous cell – Apoptosis – *In vivo*

INTRODUCTION

The gastrointestinal tract represents a collection of tissues which function to convey and digest ingested food substance, as well as absorb

Corresponding author:
Dr. Dayo Rotimi Omotoso. Department of Human Anatomy, Redeemer's University, Ede, Nigeria. Phone: +2348034779886. E-mail: dayohmts@gmail.com

Submitted: September 16, 2023. **Accepted:** November 20, 2023

https://doi.org/10.52083/QKPM8082

water, electrolytes, vitamins and other nutrients into the body (Barret et al., 2019). From the external aspect inward, the morphological composition of the tract includes serosa, muscular layers, submucosa and mucosa. Among the viscera of the tract, the stomach function as the major storage of ingested food substance, and as a site for churning or mixing the food substance with acidic gastric secretions to form a semi-fluid product known as chyme (Hall, 2016). Generally, the innermost mucosal layer of the gastrointestinal tract provides the protective covering against the digestive effect of the secretions or other toxic ingested substances. However, the gastric mucosal protection is functionally achieved by an equilibrium between the mucosal protective and aggressive factors (Omotoso and Eze, 2022).

Essentially, the gastric mucosa contains mucous and parietal cells which produce mucus and bicarbonate ions respectively. These in turn form a viscous layer of gel that constitutes the major protection for the mucosa against the acidic gastric secretions and digestive enzymes. Other contributing factors to the gastric mucosal protection include the microcirculation, prostaglandins, cyclooxygenase and epidermal growth factors (Bongu and Vijayakumar, 2012; De Lima et al., 2021). On the other hand, the mucosal aggressive factors include oxidative stress, ischaemia, exogenous factors such as bacteria, ethanol, non-steroidal anti-inflammatory drugs and endogenous factors such as elevated acidic gastric secretions, and bile acids (Sembulingam and Sembulingam, 2010). The mechanism of gastric mucosal injury or ulceration by most aggressive factors involves the induction of oxidation stress through the production of reactive oxygen species (ROS) and other free radicals (Ajeigbe et al., 2014). Therefore, there is a probable potency of antioxidants to mitigate the erosive effect of the aggressive factors on the gastric mucosa. These antioxidants include chemically synthesized compounds and naturally derived from medicinal plants.

Medicinal plants have been widely applied for diverse therapeutic purposes and their applications have been on a steady increase in recent years due to their wide accessibility, affordability and negligible adverse effects (Adelanwa and Tijani, 2013). Among the diverse medicinal plants is the *Cissampelos owariensis* (*C. owariensis*), which is a twiner plant commonly found in tropical regions especially sub-Saharan African countries. It belongs to the menispermaceae family, which comprises about 70 genera and 450 species (Akande et al., 2013). It has been reported to exhibit a wide range of therapeutic activities, which include the treatment of dysentery, diarrhoea, enteritis, colic and intestinal worm infections (Ekeanyanwu et al., 2012; Erhirhie et al, 2015). In our previous study, the gastroprotective potential of the methanol extract of the *C. owariensis* against the erosive effect of prolonged exposure to acidic gastric secretions (a potent gastric mucosal aggressive factor) has been reported (Omotoso et al., 2019b). However, the mechanism of its gastroprotective has not been fully elucidated in contrast to the anti-ulcer activity of another species of the same family – *Cissampelos mucronata* –which has been previously described and linked with its cytoprotective and antispasmodic mechanisms (Nwafor and Okoye, 2005).

The aim of this study was to elucidate the *in vivo* gastroprotective mechanism of the methanol extract of *C. owariensis* (MECo) through assessment of the role of gastric mucous cell and apoptotic signaling factors, which include the anti-apoptotic Bcl-2 and pro-apoptotic Bax proteins using rat model.

MATERIALS AND METHODS

Study Reagents

The reagents used for the study were of analytical grade and procured from Sigma-Aldrich Chemical Company (St. Louis, MO, USA) except the primary and secondary antibodies that were procured from Abcam, Cambridge, Massachusets, USA.

Experimental animals

This study involved twenty (20) adult male Wistar rats with a weight range of 140-170 g. They were sourced from the Central Animal House facility of the School of Basic Medical Sciences, Igbinedion University, Okada, Edo State, Nigeria. The animals were housed at the facility throughout the study period and kept in standard animal cages under hygienic conditions, room temperature of 25 ± 2°C and twelve (12) hour light/dark cy-

cle. They were fed with standard animal feed and access to drinking water was ensured throughout the study period. The study was approved by the Research and Ethical Committee, School of Basic Medical Sciences, Igbinedion University, Okada, Edo Sate, Nigeria (11/013413/HSC). The experimental procedures were conducted in compliance with international guidelines for handling and care of experimental animals.

Plant material collection and extraction

The plant material was collected from the suburb of the Okada community in Edo State, Nigeria. Following the verification of the plant, the leaves were detached and air-dried for three weeks. With the aid of mechanical grinder, the dried leaves were pulverized into powder form. The powdered plant material was infused into methanol for seventy-two (72) hours, filtered and the filtrate was evaporated through a rotary evaporator. The alcohol-based extractio, adopted in the current study essentially exhibits the potency for extracting more phytochemicals, especially those with antioxidant properties than aqueous-based extraction (Safarzaei et al, 2020). The extract residue was cooled and kept in a refrigerated chamber until its use for the study.

Experimental design

The animals were randomly divided into four groups, which include control groups A and& B and treated groups C and D. Each group comprised five animals (n=5). The normal control group-A animals were given distilled water (5 ml/kg body weight) and not induced by pyloric ligation. The positive control group-B animals were given distilled water (as in group A) and induced by pyloric ligation. The treated groups C and D were given 100 and 300 mg/kg MECo respectively and induced by pyloric ligation. The treatment period was 28 days and the administration was carried out via oral route using an orogastric gavage coupled to a calibrated syringe.

Pyloric-ligation method of inducing gastric mucosal injury

At the end of the treatment period, the animals were fasted for 24 hours but allowed free access to water. Animals were anaesthetized by intraperitoneal injection of Ketamine/Xylazine (50 mg/kg at ratio 1:1). The pylorus of the stomach of the animals in groups B to D was accessed in the abdominal cavity via a small midline abdominal incision. The pylorus was gently pulled up, ligated and returned into the cavity. The abdomen was closed and a five (5)-hour observatory period followed (Shay et al., 1945). Thereafter, the animals were euthanized and stomach tissue harvested for subsequent examination

Tissue processing, histological and histochemical staining

The stomach tissue was fixed using 10% neutral buffered formalin, dehydrated using ascending grades of alcohol (70%, 90% and absolute alcohol), cleared using xylene and embedded in paraffin to form tissue blocks. The tissue blocks were sectioned using rotary microtome at 5 µ, and tissue sections were mounted on slides for histological and histochemical staining.

For histological staining using haematoxylin and eosin (H & E) technique, the tissue sections were dewaxed using xylene and hydrated using descending grades of alcohol (100%, 90%, and 70% alcohol) and distilled water. They were stained in haematoxylin, washed in running water, differentiated and blued using 1% acid alcohol and tap water respectively, and rinsed in water. The counter-staining of tissue sections was done using eosin. The sections were rinsed in water, dehydrated using alcohol, cleared using xylene and mounted using distrene polystyrene xylene (DPX) (Fischer et al., 2008).

For histochemical staining using the periodic acid-schiff (PAS) technique, the tissue sections were dewaxed using xylene and hydrated using alcohol to distilled water. Sections were treated with 0.5% periodic acid, rinsed in water, treated with schiff's reagent. The tissue sections were rinsed in water, counterstained in haematoxylin and rinsed in water. Dehydration of sections was done using alcohol, clearing using xylene and mounting using DPX (McManus, 1948). The quantification of the mucous cell population within the gastric tissue sections was conducted using the image-J software. This was achieved by creating

uniformly-defined count areas on the tissue section in each of the five replicates per group using grid-lines. The mucous cell count for three uniformly selected count areas was recorded in each replicate and the mean value of mucous cell count was determined for each group.

Immunohistochemical staining for Bax and Bcl-2 proteins

Tissue sections were hydrated using alcohol and water and antigen retrieval was done using citric acid solution (pH 6.0) in a microwave (at 100 Watts). Equilibration was done using running water to displace the hot citric acid; tissue sections were then exposed to peroxidase block, rinsed in phosphate buffer saline (PBS). Non-specific proteins in sections were blocked using Nevocastra protein block. Tissue sections were rinsed in PBS and incubated in primary antibody (prepared with 1 in 100 dilution ratio). They were rinsed with PBS, treated with secondary antibody and further rinsed with PBS. The polymer was added to the tissue sections and rinsed with PBS. Tissue sections were treated with 3,3-diaminobenzidine (DAB) substrate, rinsed with water, counterstained with haematoxylin and further rinsed with water. Dehydration was done using alcohol, clearing with xylene, and mounting with DPX (Omotoso and Eze, 2022). The quantification of the protein distribution within the gastric tissue sections was conducted using the image-J software.

Statistical analysis

The data derived during this study were analyzed using IBM-SPSS (version 22) and statistical results were presented as mean ± standard error of mean (SEM). Comparison of statistical mean values was done using one-way analysis of variance (ANOVA), with $p < 0.05$ and $p < 0.01$ considered as statistical significant levels.

RESULTS

Histological study

The gastric tissues of the study animals showed varying histomorphology. The normal control group (Fig. 1A) presented normal gastric histomorphology that shows the component parts of the gastric mucosal glands, which include gastric pits, isthmus, neck and base. The positive control group (Fig. 1B) showed intense mucosal erosion

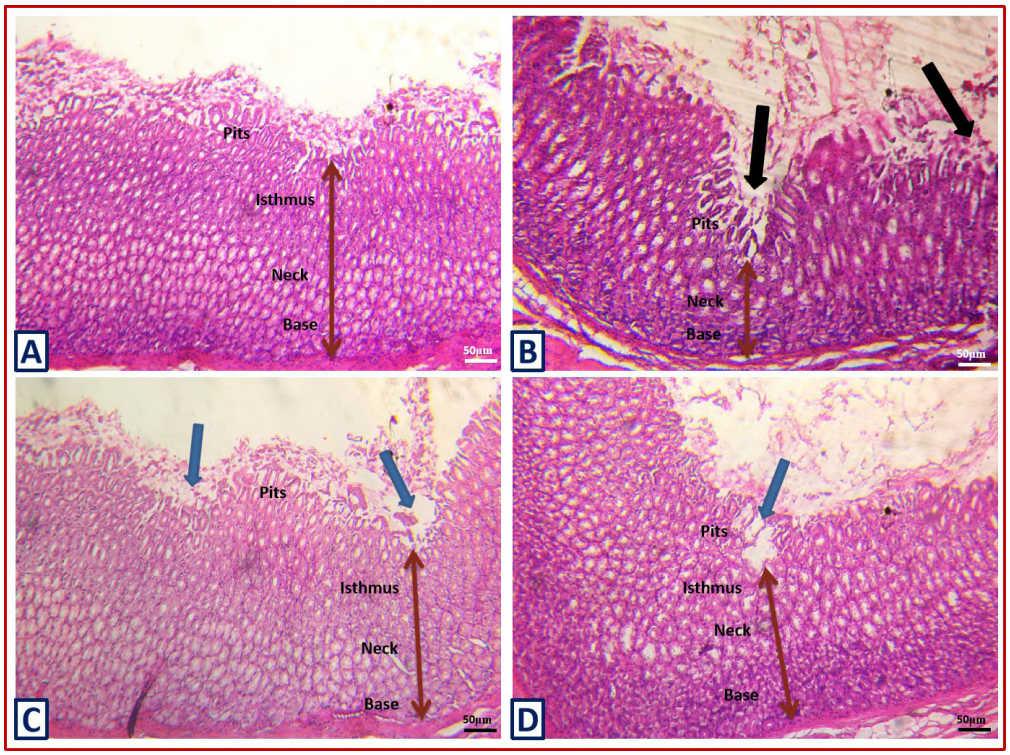

Fig. 1.- Photomicrograph of stomach tissue of experimental animals showing normal gastric histomorphology in control group A, intense mucosal erosion (black arrow) in positive control group B and mild focal mucosal erosion in treated groups C and D (H&E, X100). Double end red arrow indicates the minimum mucosal layer thickness. Scale bars: 50 µm.

with significant reduction of the mucosal isthmus due to the exposure to the gastric acid secretion. However, the pre-treatment with *C. owariensis* resulted into mild or focal mucosal erosion in the gastric histomorphology of groups C and D after exposure to the gastric acid secretion (Fig. 1C, 1D).

Histochemical study

The PAS staining of the gastric tissues revealed the distribution of the mucous cells of gastric mucosa of study animals. The normal control group presented normal distribution of the surface and neck mucous cell population (Fig. 2A). The positive control group (Fig. 2B) showed significant decline of the mucous cell population following the exposure to the gastric acid secretion. However, the pre-treatment with *C. owariensis* resulted into significant increase of the mucous cell population which include the surface and neck cells (Fig. 2C, D).

Immunohistochemical study

The immunostaining of the gastric tissues revealed the distribution of the anti-apoptotic Bcl-2 protein within the gastric tissues of the study animals. The Bcl-2 protein distribution of the positive control group-B animals showed significant decline compared to the normal control group A. However, the pre-treatment with *C. owariensis* resulted into significant increase of the Bcl-2 protein distribution compared to the control groups A and B (Fig. 3).

The immunostaining of the gastric tissues further revealed the distribution of the pro-apoptotic Bax protein within the gastric tissues of the study animals. The Bax protein distribution of the positive control group B animals showed significant increase compared to the normal control group A. However, the pre-treatment with *C. owariensis* resulted into significant decline of the Bax protein distribution compared to the positive control groups B (Fig. 4).

DISCUSSION

The physiological integrity of the gastric mucosa has been described to be dependent on the balance between the mucosal protective factors (which include increase mucous cell population or mucus secretion) and mucosal aggressive factors (which result into oxidative stress and apop-

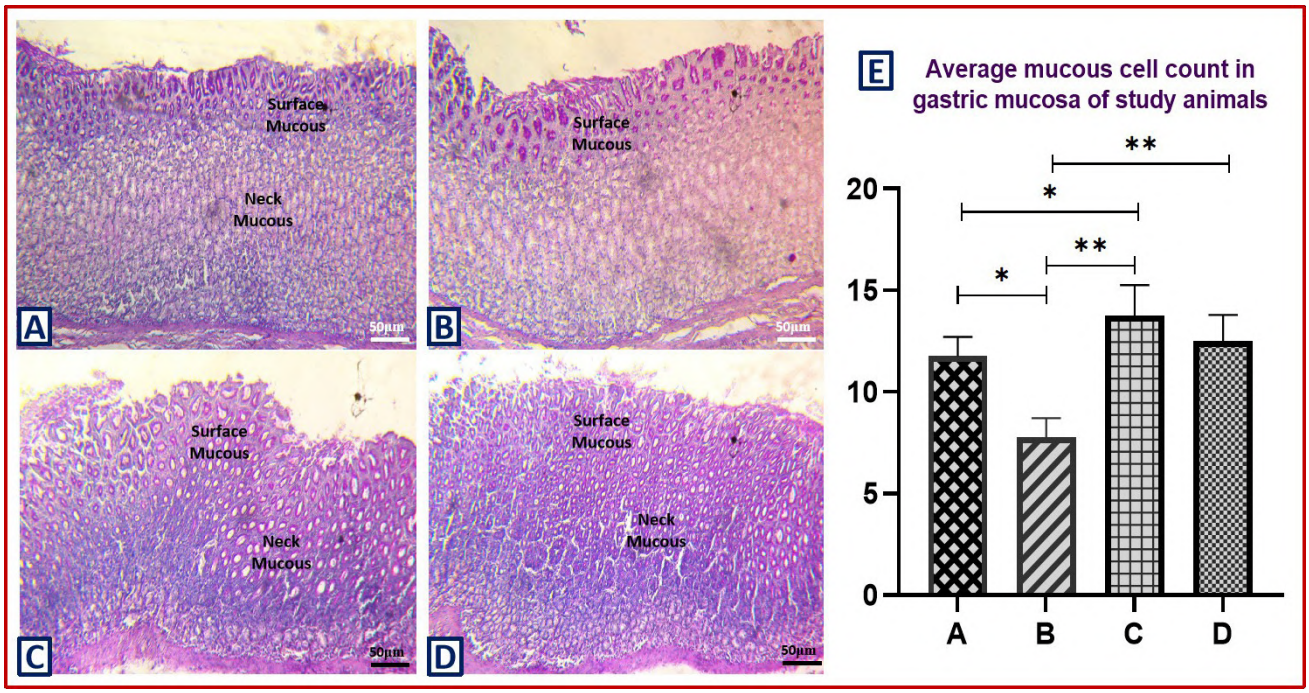

Fig. 2.- A-D: Histochemical staining of gastric tissue of groups A-D animals showing the mucous cell population (surface and neck mucous cells) within the gastric mucosa (PAS, X100). **E:** Evaluation of mucous cell distribution in the gastric mucosa of experimental animals in groups A–D using five replicates per group. (*,** indicate significant difference at $p < 0.05$ (0.0212) and $p < 0.01$ (0.0032) respectively). Scale bars: 50 µm.

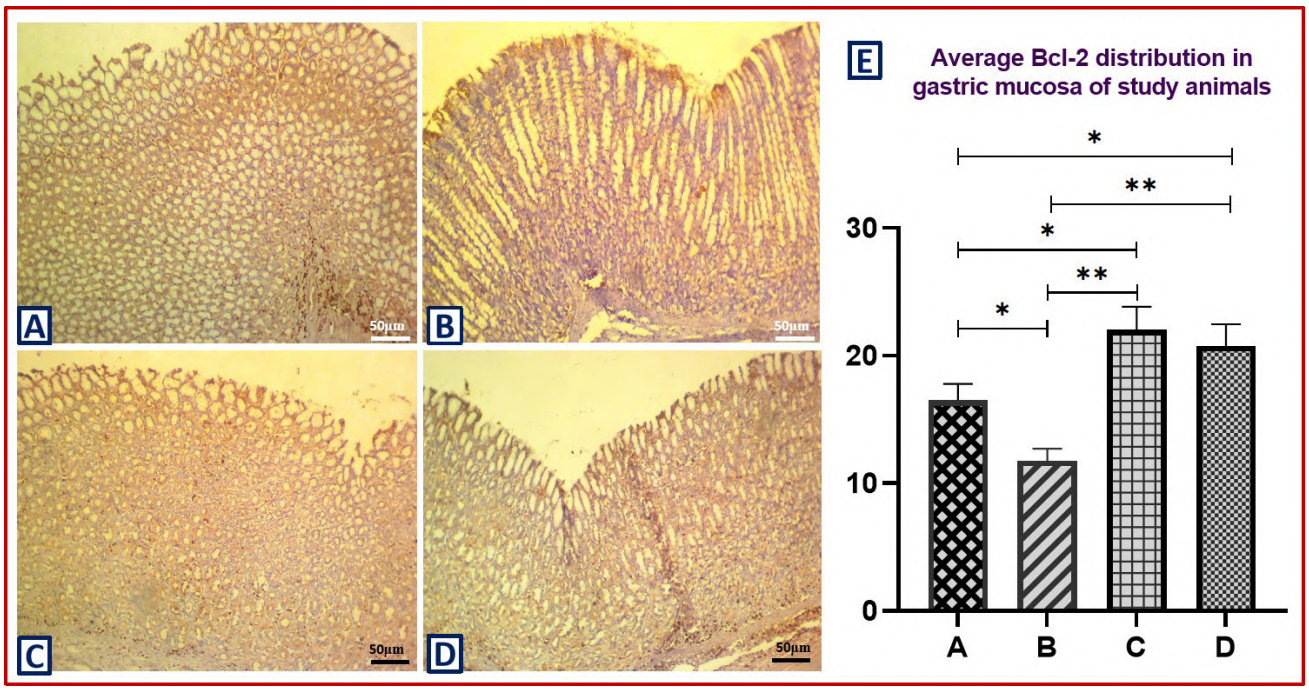

Fig. 3.- A-D: Immunostaining of gastric tissue of groups A-D animals showing Bcl-2 protein distribution indicated by dark-brown coloration. **E:** Evaluation of Bcl-2 protein expression in gastric mucosa of groups A-D animals using five replicates per group (*,** indicate significant difference at $p < 0.05$ (0.0344) and $p < 0.01$ (0.0048) respectively). Scale bars: 50 µm.

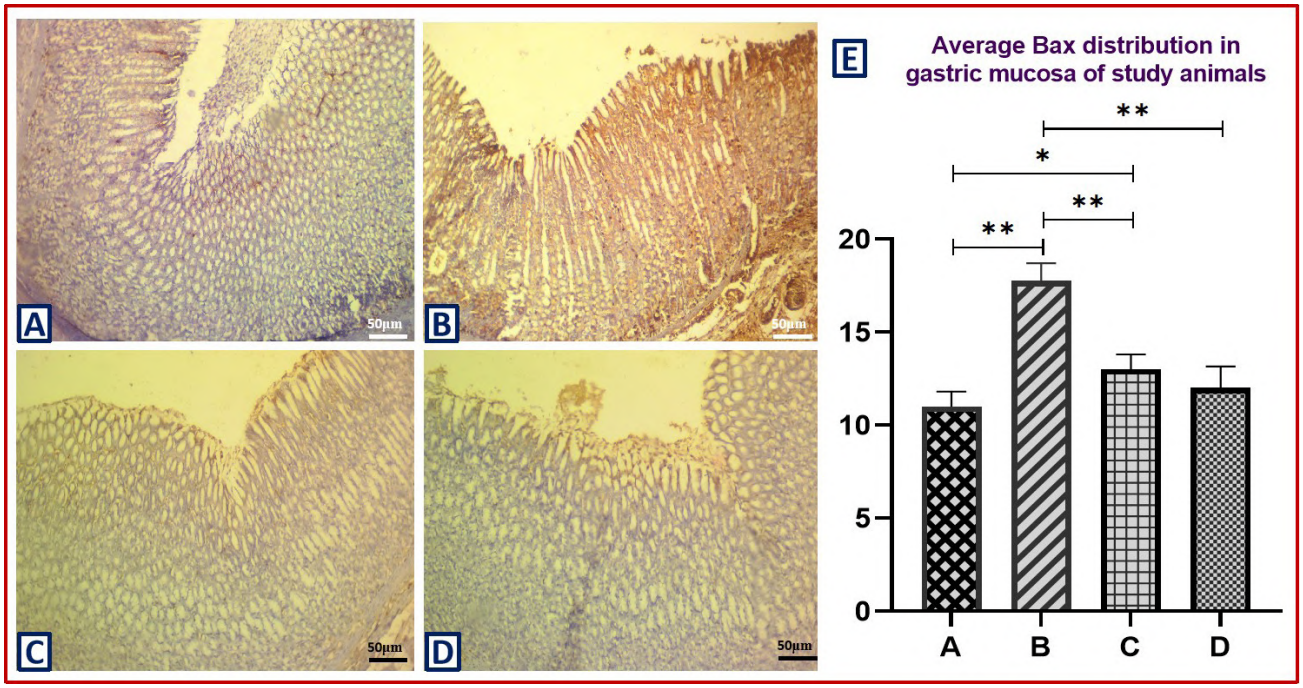

Fig. 4.- A-D: Immunostaining of gastric tissue of groups A-D animals showing Bax protein distribution indicated by dark-brown coloration. **E:** Evaluation of Bax protein expression in gastric mucosa of groups A-D animals using five replicates per group (*,** indicate significant difference at $p < 0.05$ (0.0134) and $p < 0.01$ (0.0037) respectively). Scale bars: 50 µm.

tosis) (Gryko et al., 2014; De Lima et al., 2021). Medicinal plants or their derivatives generally exhibit gastroprotective effect by promoting the protective factors against the aggressive factors of the gastric mucosa. This is indicated in the current study whereby MECo exhibited gastroprotective effect against the gastric mucosal aggressive factor (acidic gastric secretion). Based on the his-

tological results of this study (Fig. 1), the gastric histomorphology of the positive control group-B animals showed prominent and widespread mucosal erosion compared to the normal control group A. However, the gastric histomorphology of treated groups C and D revealed mild or focal mucosal erosion which indicates the gastroprotective effect of MECo. Previous studies on the phytochemical analysis of *C. owariensis* have reported the presence of bioactive compounds which include flavonoids, alkaloids, tannins and saponin. These are secondary metabolites that provide the therapeutic activity of the extract which include reparation of tissue histomorphology following exposure to toxicants (Ekeanyanwu et al., 2012; Omotoso et al., 2019a).

According to the histochemical results of this study (Fig. 2), the mucous cell population showed significant ($p < 0.05$) increase among the animals of groups C and D, which were pre-treated with MECo compared to the animals of control groups A and B. Essentially, the mucous cells of gastric mucosa produce alkaline mucus, which contributes to the formation of a layer of protective gel that protects the mucosal surface against the erosive effects of gastric mucosal aggressive factors (Sembulingam and Sembulingam, 2010). In previous studies, the functional impairment of mucus secretion had been associated with increased mucosal injury, while elevated gastric mucus secretion, usually due to increase in the mucosal cell population, enhanced the gastric mucosal protection (Zakaria et al., 2015; Ige et al., 2016). The increase in the mucous cell population among the treated groups C and D in the current study would enhance a physiological elevation of mucus secretion, which would in turn mitigate the erosive effect of the acidic gastric secretion. Previous studies have similarly reported the increase in gastric mucus production as one of the gastroprotective mechanism which helps to preserve the mucosal protective covering (Nwangwu et al., 2013; Chantharangsikul et al., 2016; Kim et al., 2019; Kim et al., 2020).

Furthermore, the exposure to aggressive factors results into gastric ulceration or injury through induction of oxidative stress and stimulation of apoptosis. Hence, the modulation of apoptotic signaling pathway plays an important role in determining the physiological integrity of the gastric mucosa. The B-cell lymphoma-2 (Bcl-2) protein family regulates apoptosis through interaction with mitochondrial function leading to mitochondrial membrane permeabilization and activation of the caspase signaling cascades. The members of the protein family include the anti-apoptotic Bcl-2 protein and pro-apoptotic Bax protein (Kale et al., 2018). According to the result of the current study (Fig. 3), there was a significant ($p < 0.05$) increase in the anti-apoptotic Bcl-2 protein in the gastric tissue of the treated groups C and D compared to the control groups A and B. Conversely, there was a significant ($p < 0.05$) increased level of the pro-apoptotic Bax protein in the gastric tissue of the positive control group B compared to the normal control group A and treated groups C and D (Fig. 4).

Therefore, the findings of this study concluded that the gastroprotective mechanisms of MECo include the upregulation of anti-apoptotic and down-regulation of pro-apoptotic signaling factors. According to the studies by Arab et al. (2015) and Liu et al. (2018), gastroprotective mechanisms involve the inhibition of pro-apoptotic signaling factors, which include Bax/Bak expressions and activation of anti-apoptotic signaling factors like Bcl-2/Bcl-X_L. This outcome was further corroborated by the findings of Zhou et al. (2020), Raish et al. (2021) and Fu et al. (2021), which showed that the inhibition of Bax and activation of Bcl-2 signaling as significant contributory mechanisms during the gastroprotective activity of gallic acid, sinapic acid and *Periplaneta americana* extract respectively. Moreover, previous studies have reported that the anti-apoptotic effects of therapeutic drug candidates such as paeonol, irbesartan and betaine-homocysteine significantly contribute to their gastroprotective activity in rat model (Hafez et al., 2018; Shahin et al., 2018; Gundogdu et al., 2022).

CONCLUSION

The findings of this study indicated that a significant increase in the mucous cell population, up-regulation of anti-apoptotic (Bcl-2) and down-regulation of pro-apoptotic (Bax) protein

expression and distribution within the gastric mucosa characterize *in vivo* gastroprotective activity of the methanol extract of *C. owariensis* in rat model.

REFERENCES

ADELANWA EB, TIJJANI AA (2013) An ethno medical survey of the flora of Kumbotso local government area of Kano State. *Nig J Pharmaceut Sci,* 12: 1-9.

AJEIGBE KO, ONIFADE AA, OMOTOSO DR, ENITAN SS, OLALEYE SB (2014) Anti-ulcerogenic activity of *Aspilia africana* leaf extract: roles of gastric acid, oxidative stress and neutrophil infiltration. *Afr J Biomed Res,* 17(3): 193-201.

AKANDE R, OKWUTE SK, ILIYA I, EFIOM OO (2013) Chemical constituents and anti-tuberculosis activity of the root extracts of Cissampelos owariensis (P. Beauv.) Menispermaceae. *Afr J Pure Appl Chem,* 7: 21-30.

ARAB HH, SALAMA SA, OMAR HA, ARAFA EA, MAGHRABI IA (2015) Diosmin protects against ethanol-induced gastric injury in rats: novel anti-ulcer actions. *Plos One*, 10(3): e0122417.

BARRET KE, BARMAN SM, BROOKS HL, YUAN J (2019) Ganong's Review of Medical Physiology, 26th edition. McGraw-Hill Education, New York, pp 1041-1050.

BONGU S, VIJAYAKUMAR S (2012) Animal models in experimental gastric ulcer screening-a review. *Int J Pharmacol Screen Method,* (2): 82-87.

CHANTHARANGSIKUL G, KITPATI W, SOONTHORNCHAREONNON N, SAILASUTA A, ITHARAT A, SUVITAYAVAT W (2016) Mucus secretion stimulation: A mechanism in gastroprotective effect of *Zingiber officinale. Thai J Pharmaceut Sci*, 40(1): 1-8.

DE LIMA CAA, DE LIMA RS, DE SOUZA JB, GRACA ADS, THOMAZZI SM, BATISTA JS, ESTEVAM CDS (2021) Gastroprotective mechanisms. Available at: www.intechopen.com/chapters/79812. doi: 10.5772/intechopen.101631.

EKEANYANWU RC, UDEME AA, ONUIGBO AO, ETIENAJIRHEVWE OF (2012) Anti-diabetic effect of ethanol leaf extract of *Cissampelos owariensis* (lungwort) on alloxan induced diabetic rats. *Afr J Biotechno*l, 11: 6758-6762.

ERHIRHIE OE, MOKE EG, CHINWUBA P (2015) Cissampelos owariensis: Experimental review. *Phar Innov J,* 3: 75-77.

FISCHER AH, JACOBSON KA, ROSE J, ZELLER R (2008) Heamatoxylin and eosin staining of tissue and cell sections. *CSH Protoc*, pdb.prot4986. doi: 10.1101/pdb.prot4986.

FU S, CHEN J, ZHANG C, SHI J, NIE X, HU Y, FU C, LI X, ZHANG J (2021) Gastroprotective effects of *Periplaneta americana* L. extract against ethanol-induced gastric ulcer in mice by suppressing apoptosis-related pathways. *Front Pharmacol,* 12: 798421.

GRYKO M, PRYCZYNICZ A, ZAREBA K, KĘDRA B, KEMONA A, GUZIŃSKA-USTYMOWICZ K (2014) The expression of Bcl-2 and BID in gastric cancer cells. *J Immunol Res,* 2014: 953203.

GUNDOGDU AC, KAR F, OZBAYER C (2022) Investigation of the gastroprotective effect of Betaine-Homocysteine homeostasis on oxidative stress, inflammation and apoptosis in ethanol induced ulcer model. *J Investig Surg,* 35(11-12): 1806-1817.

HAFEZ HM, MORSY MA, MOHAMED MZ, ZENHOM NM (2018) Mechanisms underlying gastroprotective effect of paeonol against indomethacin-induced ulcer in rats. *Hum Exp Toxicol,* 38(5): 510-518.

HALL JE (2016) Guyton and Hall Textbook of Medical Physiology, 13th edition. Elsevier, Philadelphia, pp 760-809.

IGE AO, ADEWOYE EO, OKWUNDU NC, ALADE OE, ONUOBIA PC (2016) Oral magnesium reduces gastric mucosa susceptibility to injury in experimental diabetes mellitus. *Pathophysiol,* 23(2): 87-93.

KALE J, OSTERLUND EJ, ANDREWS DW (2018) Bcl-2 family proteins: changing partners in the dance towards death. *Cell Death Diff,* 25: 65-80.

KIM Y, PARK HJ, KIM H, SONG J, LEE D (2019) Gastroprotective effects of paeonia extract mixture HT074 against experimental gastric ulcers in rats. *Evid Based Complement Alternat Med,* 2019: 3546258.

KIM Y, PARK HJ, KIM H, SONG J, LEE D (2020) Gastroprotective effects of inulae flos on HCl/Ethanol induced gastric ulcers in rats. *Molec,* 25(23): 5623.

LIU W, YANG M, CHEN X, LI L, ZHOU A, CHEN S, YOU P, LIU Y (2018) Mechanisms of antiulcer effect of an active ingredient group of modified Xiao Chaihu decoction. *Evid Based Complement Alternat Med,* 2018: 5498698.

MCMANUS JFA (1948) Histological and histochemical uses of periodic acid. *Stain Technol,* 23(3): 99-108.

NWAFOR SV, OKOYE CF (2005) Antiulcer properties of the ethanol root extract of *Cissampelos mucronata. Pharmaceut Biol*, 43(5): 396-403.

NWANGWU S, AJEIGBE K, OMOTOSO D, JOSIAH S, OLAYANJU A, BOLAJI A (2013) Acid buffering effects of aqueous leaf extract of *Ocimum gratissimum* L. in the rabbit stomach. *Turk J Gastroenterol,* 24(3): 204-210.

OMOTOSO DR, EZE GI (2022) Assessment of gastroprotective activity of aqueous leaf extract of *Ageratum conyzoides* L.: Role of mucous cells, anti-apoptotic (Bcl-2) and tumor suppressor (p53) proteins. *J Herbmed Pharmacol,* 11(2): 245-252.

OMOTOSO DR, LAWAL OS, OLATOMIDE OD, OKOJIE IG (2019a) Nephroprotective effect of *Cissampelos owariensis* extract on renal histomorphology of Wistar rats during exposure to carbon tetrachloride induced nephropathy. *Asian J Biol,* 8(4): 1-10.

OMOTOSO DR, UWAGBOR V, LAWAL OS, OLATOMIDE OD, OKOJIE IG (2019b) Gross and histo-morphological study of anti-ulcerogenic effects of *Cissampelos owariensis* (P. Beauv.) methanolic extract in Wistar rats. *J Biomed Sci*, 8(3): 1-5.

RAISH M, SHAHID M, BIN JARDAN YA, ANSARI MA, ALKHARFY KM, AHAD A, ABDELRAHMAN IA, AHMAD A, AL-JENOOBI FI (2021) Gastroprotective effect of sinapic acid on ethanol-induced gastric ulcer in rats: Involvement of Nrf/HO-1 and NF-κB signaling and antiapoptotic role. *Front Pharmcol,* 12: 622815.

SAFARZAEI A, SARHADI H, HADDAD KHODAPARAST MH, SHAHDADI F, DASHIPOUR AR (2020) Optimization of aqueous and alcoholic extraction of phenolic and axtioxidant compunds from *Caper (Capparis spinosa)* roots by assisted by ultrasound waves. *Sahedan J Res Med Sci,* 22(4): e100747.

SEMBULINGAM K, SEMBULINGAM P (2010) Essentials of Medical Physiology. 5th edition. Jaypee Brothers Medical Publishers Ltd, United States, pp 218-226.

SHAHIN NN, ABDELKADER NF, SAFAR MM (2018) A novel role of irbesartan in gastroprotection against indomethacin-induced gastric injury in rats: Targeting DDAH/ADMA and EGFR/ERK signaling. *Sci Rep,* 8: 4280.

SHAY JP, KOMOROV SA, FELS SS, MERANZE D, GRUNSTEIN M, SIPLET H, FELES SS, KOMROV S, FELS S, GRUENTEIN M, MERAZE D, FRUESTEIN M, KAMAROV SA, MREANZE D, MERAAZE D, GRUEUNSTEIN H (1945) A simple method for the uniform production of gastric ulceration in the rat. *Gastroenterol,* 5: 43-61.

ZAKARIA ZA, BALAN T, MAMAT SS, MOHTARRUDIN N, KEK TL, SALLEH MZ (2015) Mechanisms of gastroprotection of methanol extract of *Melastoma malabathricum* leaves. *BMC Compl Med Therap,* 15: 135.

ZHOU D, YANG Q, TIAN T, CHANG Y, LI Y, DUAN L-R, LI H, WANG S-W (2020) Gastroprotective effect of gallic acid against ethanol-induced gastric ulcer in rats: Involvement of the Nrf/HO-1 signaling and anti-apoptosis role. *Biomed Pharmacother,* 126: 110075.

Morphometric analysis of the mastoid process using cone beam computed tomography

Karthikeya Patil[1], Sanjay C.J.[1], Varusha Sharon Christopher[1], Eswari Solayappan[1], Sharath Niranjan[1], Deepa B.V.[2]

[1] Department of Oral Medicine and Radiology, JSS Dental College and Hospital, JSS Academy of Higher Education and Research, Mysuru – 570015, Karnataka, India

[2] Department of Oral and Maxillofacial Surgery, JSS Dental College and Hospital, JSS Academy of Higher Education and Research, Mysuru – 570015, Karnataka, India

SUMMARY

The sexual dimorphism of the mastoid process, as demonstrated by cone beam computed tomography (CBCT), is not well examined in forensic anthropology or clinical diagnostics. The mastoid region can be precisely imaged in three dimensions using CBCT, which reveals minute anatomical variations between males and females. These characteristics can help forensic professionals identify the sex of unidentified human remains, helping to solve crimes and aid in the search for missing persons. Moreover, recognising sexual dimorphism in the mastoid process in clinical settings can help with precise patient identification and individualised medical treatments, highlighting the important function of CBCT in both the forensic and medical areas.

Key words: Mastoid pneumatisation – Cone beam computed tomography – Sexual dimorphism – Forensic sciences – Morphology

INTRODUCTION

The human skull holds a wealth of information that can aid in determining the sex of an individual, providing valuable insights in fields such as forensic science, anthropology, archaeology, and medicine. This method of sex determination is based on the observation of sexually dimorphic traits as they manifest in the skull. These traits are influenced by hormonal, genetic, and functional factors, making the analysis of skull morphology a powerful tool for identifying the sex of skeletal remains (Bertsatos et al., 2020).

In forensic investigations, the identification of human remains is of paramount importance. The skull is often one of the best preserved parts of a skeleton, making it a prime structure for sex determination. By analysing various features, forensic experts can establish the sex of the individual, aiding in the process of identifying missing persons, civil cases, extensive antemortem injuries, high-intensity explosions, or postmortem mutilation by animals. The mastoid process of the skull has attracted attention from various researchers,

Corresponding author:
Dr Sanjay C.J. Department of Oral Medicine and Radiology, JSS Dental College and Hospital, JSS Academy of Higher Education and Research, Mysuru – 570015, Karnataka, India. Phone: +91 97425 65566. E-mail: drsanjaycj_dch@jssuni.edu.in - Orcid: 0000-0003-2830-1481

Submitted: October 7, 2023. **Accepted:** November 22, 2023

https://doi.org/10.52083/XIOD6609

because of its protected position at the base of the skull and relatively compact structure; it usually remains in one piece (Franklin et al., 2012).

Since mastoid provides valuable information for sex determination, it is essential to recognise that it is not a foolproof method. There is variability within populations, and some individuals may exhibit traits that are atypical for their sex. Advances in technology, such as three-dimensional imaging, continue to refine and enhance the accuracy of sex determination based on skull morphology, and Cone Beam Computed Tomography (CBCT) is one such modality that has gained recent interest.

CBCT is an imaging device that uses a cone shaped X-ray beam. The X-ray source and detector rotate around a field of interest for the patient. The received images are transferred to a computer that performs primary reconstructions, which can be viewed as 2D multiplanar reformatted slices or in 3D. The advancements in oral and maxillofacial radiology, together with the availability and affordability of CBCT devices, have led to an increase in scanning addressability in the field of dentistry, including forensics (Baban and Mohammad, 2023).

Several researchers have evaluated various aspects of the mastoid process for their usefulness in sexual dimorphism, which is primarily determined through dry skull exploration (Gupta et al., 2022; İnceoğlu et al., 2021; Sushmitha et al., 2020). Studies using CBCT are extremely rare, as are those including the Indian population. The purpose of this study is to assess all the metrics in axial, sagittal, and coronal sections, as well as the 3D-rendered imagery for all conceivable findings in the mastoid process that may demonstrate sexual dimorphism in order to build up the body of knowledge.

MATERIALS AND METHODS

This is a descriptive retrospective study performed on 64 subjects, comprising 32 males and 32 females. The study samples were selected by a simple purposive sampling method and were homogenous in origin. Ethical clearance was obtained from the institutional ethical committee.

Objectives of the study

The aim of the study is to analyse the morphology of the mastoid process by using the area of the mastoid triangle, the area of the intermastoid triangle, mastoid volume, bimastoid distance, and mastoid height, that is, to find out if any difference exists between the area of the mastoid triangle, the area of the intermastoid triangle, mastoid volume, bimastoid distance, and mastoid height between males and females.

If established, a further aim is to apply these findings to forensic uses.

Inclusion criteria

- CBCT images with optimum diagnostic quality.
- CBCT images clearly showing the morphology of the base of the skull.

Exclusion criteria

- Image with presence of any developmental anomaly/ central pathology involving the base of the skull.
- Image with any evidence of previous surgery, fracture, or healed fracture of the base of the skull.
- Non-diagnostic CBCT images, including partial images or presence of artefacts in the mastoid region.

Radiographs satisfying the inclusion criteria were subjected to analysis for the following landmarks in axial, coronal, sagittal, and 3D-rendered images in Planmeca Romexis 5.3 (3D software):

- Area of the mastoid triangle using Heron's formula (a mathematical formula to calculate the area of the triangle in terms of the length of the sides), which will be measured using the porion, asterion, and mastoidale as landmarks (Fig. 1A).

$$\Delta = \sqrt{s\,(s-a)\,(s-b)\,(s-c)}$$

a, b and c are the lengths of the sides and s = (a +5 b + c) ÷ 2

- Area of the intermastoid triangle using Heron's formula, which will be measured using the bilateral mastoidales and menton. (Fig. 1B).

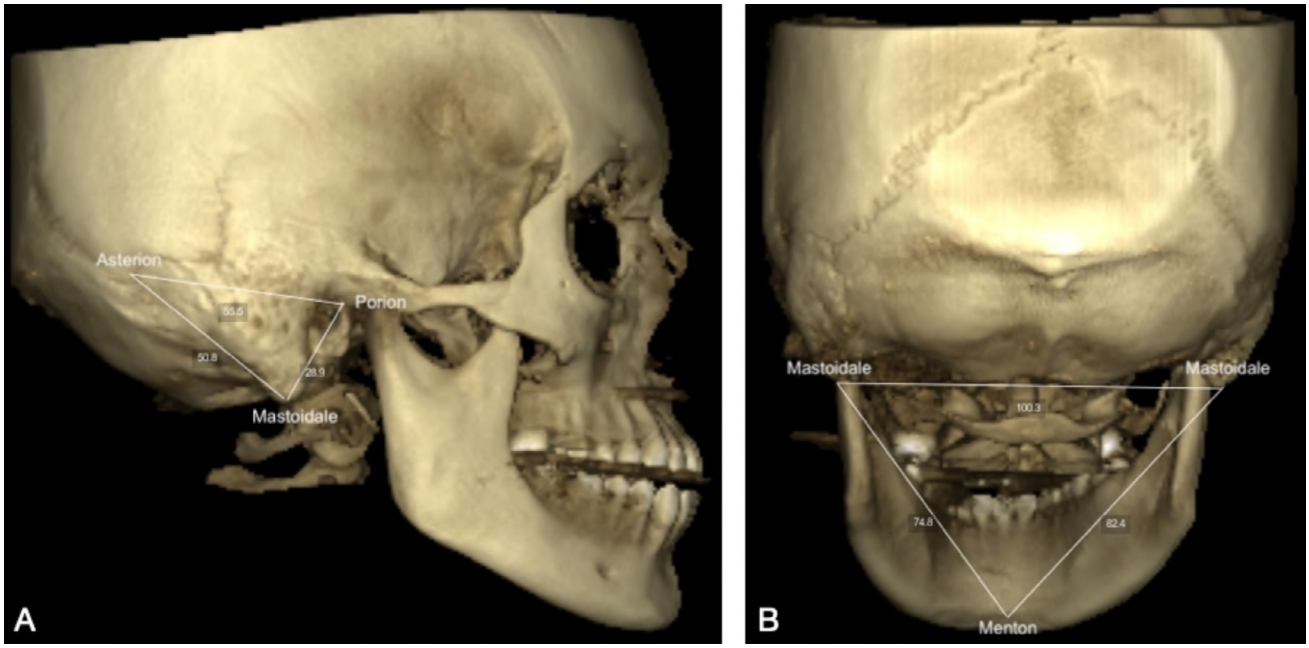

Fig. 1.- A. Area of the mastoid triangle that is measured using the porion, asterion, and mastoidale as landmarks. **B.** Area of the intermastoid triangle that is measured using the bilateral mastoidales and menton.

- Mastoid volume, which will be measured using:
  - True mastoid height (TMH)–a vertical line from the mastoid tip to the tegmen mastoidium measured on a coronal plane (Fig. 2A).
  - Maximal oblique sagittal diameter (OSD): maximal long axis diameter of the mastoid measured on an axial plane (Fig. 2B).
  - Maximal oblique coronal diameter (OCD): maximal short axis diameter of the mastoid measured on the axial plane (Fig. 2B).
  - Formula for calculating the volume used = TMH x OSD X OCD X 0.52 (Allam and Allam, 2016).
- Bimastoid length – the distance between the right and left mastoidale. (Fig. 3).
- Mastoid height from the Frankfurt plane (Fig. 4).

Each of these measurements was repeated twice by the same observer at an interval of 15 days. An

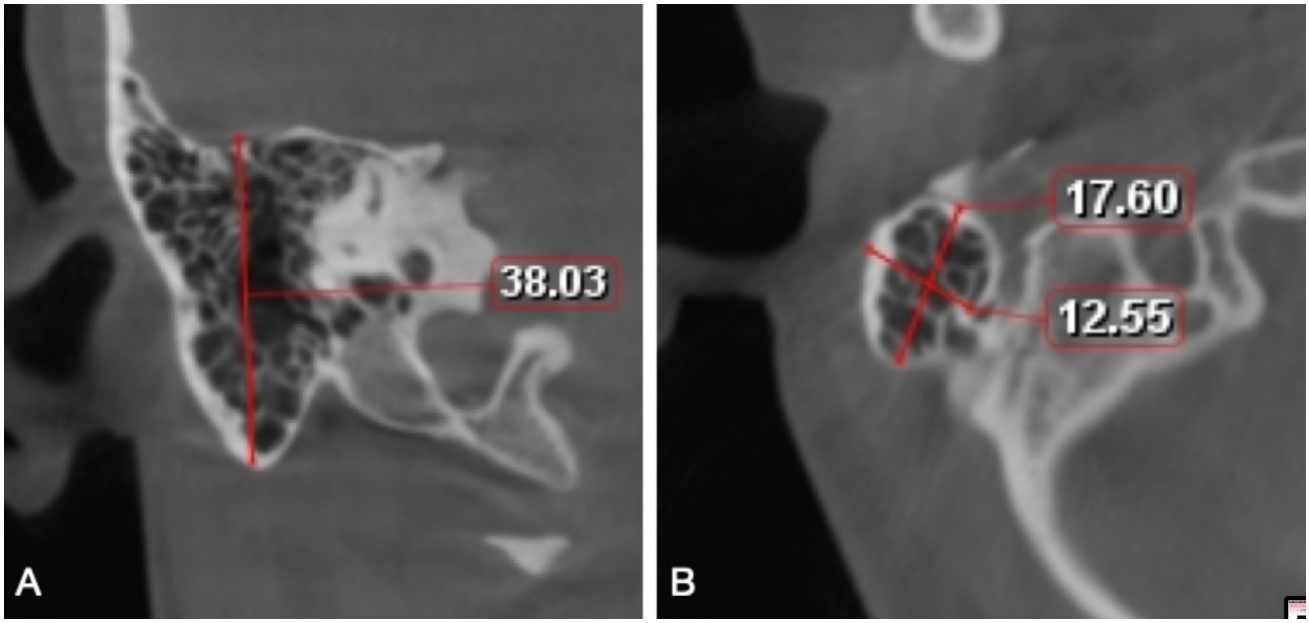

Fig. 2.- Cone Beam Computed Tomography (CBCT) images of right mastoid; **A:** True mastoid height that is measured axially in CBCT with vertical line from the mastoid tip to the tegmen mastoidium. **B:** Maximal oblique sagittal diameter (OSD)- maximal long axis diameter of the mastoid; and Maximal oblique coronal diameter (OCD)- maximal short axis diameter of the mastoid measured in coronal section of CBCT.

Fig. 3.- Bimastoid length- distance between the right and left mastoidale.

Fig. 4.- Mastoid height from the Frankfurt plane.

average of these measurements was taken into consideration to avoid intra-examiner variations.

Statistical analysis

The collected data was tabulated and statistically analysed, and a comparison was made between different age and sex groups. The mean value, SD, *p* value, and t value were calculated separately. The collected data were then subjected to descriptive statistics and the Kolmogorov-Smirnov test to establish normality. As the data were normally distributed, a two-tailed t test for independent samples was performed. A *p* value of less than or equal to 0.05 was considered statistically significant. The statistical analysis was performed using SPSS software version 23.0.

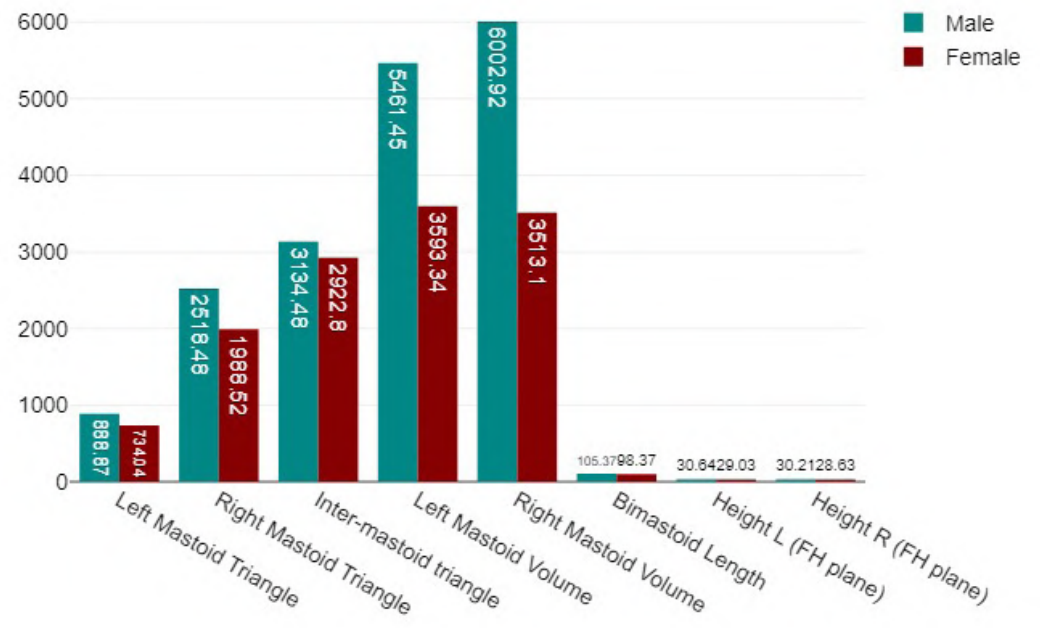

Fig. 5.- Graph depicting the descriptive statistics of all the parameters analysed.

Table 1. Descriptive statistics.

	Sex	N	Mean	Std. Deviation	Std. Error Mean
Area of Left Mastoid Triangle	Male	32	888.87 mm^2	164.39 mm^2	29.06
	Female	32	734.04 mm^2	147.91 mm^2	26.15
Area of Right Mastoid Triangle	Male	32	2518.48 mm^2	367.57 mm^2	64.98
	Female	32	1988.52 mm^2	385 mm^2	68.06
Area of Inter-mastoid Triangle	Male	32	3134.48 mm^2	461.07 mm^2	81.51
	Female	32	2922.8 mm^2	488.72 mm^2	86.39
Volume of Left Mastoid	Male	32	5461.45 mm^3	2891.33 mm^3	511.12
	Female	32	3593.34 mm^3	2023.67 mm^3	357.74
Volume of Right Mastoid	Male	32	6002.92 mm^3	3149.39 mm^3	556.74
	Female	32	3513.1 mm^3	1954.88 mm^3	345.58
Bimastoid length	Male	32	105.37 mm	4.53 mm	0.8
	Female	32	98.37 mm	6.12 mm	1.08
Left Mastoid Height	Male	32	30.64 mm	8.64 mm	1.53
	Female	32	29.03 mm	7.21 mm	1.27
Right Mastoid Height	Male	32	30.64 mm	8.64 mm	1.53
	Female	32	29.03 mm	7.21 mm	1.27

RESULTS

Out of the 64 subjects scrutinised, 32 (50%) were male and 32 (50%) were female. The mean, standard deviation, and standard error mean were estimated with descriptive statistics, which are depicted in Fig. 5 and Table 1.

Table 2. Independent t test.

	t	df	p
Area of Left Mastoid Triangle	3.96	62	<.001
Area of Right Mastoid Triangle	5.63	62	<.001
Area of Inter-mastoid Triangle	1.78	62	0.08
Volume of Left Mastoid	2.99	62	0.004
Volume of Right Mastoid	3.8	62	<.001
Bimastoid length	5.2	62	<.001
Left Mastoid Height	0.81	62	0.422
Right Mastoid Height	0.83	62	0.452

A two-tailed t test for independent samples showed the following differences between males and females with respect to the dependent variables: area of the mastoid triangle, volume of the mastoid triangle, and bimastoid length were statistically significant, whereas the area of the intermastoid triangle and the height of the mastoid process with relation to the Frankfurt plane were not statistically significant between both sexes, as elaborated in Table 2.

DISCUSSION

The mastoid process is a bony projection located behind the ear, specifically at the base of the skull's temporal bone. This anatomical structure has garnered attention in the fields of forensic anthropology and physical anthropology as a sexually dimorphic trait that can aid in sex determination, particularly when analysing skeletal remains. The size and shape of the mastoid process can exhibit differences between males and females, contributing to the overall assessment of an individual's sex (Paiva and Segre, 2003). Numerous authors have suggested the same. In general, the mastoid process tends to be more prominent and larger in males if compared to females. This difference arises due to various factors, including hormonal influences, muscle attachment points, and biomechanical demands associated with sexual dimorphism (Schulter-Ellis, 1979).

Most of the mastoid dimensions observed in the study had significant sexual dimorphism, such as the area of the mastoid triangle, mastoid volume, and bimastoid length, except for the area of the intermastoid triangle and mastoid height. The literature also shows significant sexual dimorphism among many racial and ethnic groups (Allam and Allam, 2016; Bhayya et al., 2018; Gupta et al., 2012; Kemkes and Göbel, 2006), which also assessed various parameters involving the mastoid with similar significant results of sexual dimorphism.

Using the xerographic approach, Paive and Segre identified and characterised the mastoid triangle on dry skulls in a population in Sao Paulo, Brazil. They did this by calculating the areas of the left and right mastoid triangles, then amplifying the two areas to determine the overall area (de Paiva and Segre, 2003). In dry skulls, the area of the mastoid triangle is a highly scrutinised indicator of sexual dimorphism. The mastoid, asterion, and porion were considered markers in the majority of studies for this analysis. Kemkes and Gobel (2006) reported that only 65% of the skulls could succinctly discern the right gender using discriminant function analysis. The mastoid triangle area in the Saudi population demonstrated sexual dimorphism, according to Madadin et al. (2015), which was all in line with the current study, because the techniques used were comparable and the subjects shared an ethnic origin.

We attempted to analyse the area of the intermastoid triangle that has not previously been studied. The study's findings, however, were not significant in terms of sexual dimorphism. However, a study by Sobhani et al. (2021) using the intermastoid triangle's shape showed a considerable sexual dimorphism in shape, with a discriminant analysis accuracy of 88.8%. This conflict can be due to the methods adopted, as the application used for the analysis was third-party software, so images had to be imported accordingly.

The same technique adopted by Allam et al., who used tMH, OCD, and OSD to measure the volume, was used to analyse the volume of the mastoid triangle (Allam and Allam, 2016). They scrutinised over 80 samples using MDCT (Multi-Detector Computed Tomography) belonging to the Egyptian population. They encountered positive results for sexual dimorphism, which is concurrent with the present study. They reported a mean of 13.09 ± 3.6 cm^3 and 8.43 ± 3.3 cm^3 in males and females, respectively. The similarity between the studies might be due to the similar method of calculation used in both the studies. The sexual dimorphic trait exhibited by the volume of the mastoid process can be validated with similar a study presented by Sumati and Patnaik (2015).

Bimastoid diameter has been previously analysed by Okumus (2021), who scrutinised 200 CBCT images of 100 male and 100 female subjects. He found significant sexual dimorphism, which is in accordance with our study. Marinescu et al. (2014) reported that the accuracy rate for bimastoid diameter was 73%, and the measurements showed a significant difference in the Romanian population. In addition, Jain et al. (2013) reported that the accuracy rate for bimastoid diameter was 75%, and that its availability for sex determination was relatively high in an Indian population, which is similar to the present population involved in the study.

The average mastoid height was reported to be 24.5 mm in female skulls and 29.7 mm in male skulls by Passey et al. (2021) in their study on 70 adult skulls (44 male and 26 female skulls). Sumati and Patnaik (2015) revealed that the mean mastoid height was 28.3 mm in male skulls and 23.18 mm in female skulls in their study of 60 adult human skulls. They came to the conclusion that, after stepwise discriminant function analysis, mastoid height was shown to be the best sex determinant. Mastoid height with the Frankfurt plane as a reference point, however, was not statistically significant for sex estimation, which led to contradictory findings in the current study. This may be due to the variability of the landmarks considered for the study despite being of the same ethnic origin.

Any study based on the mastoid's dimensions is very dependent on the population being investigated, because numerous factors influence the shape and size of the mastoid bone in various populations, which makes it impossible to extrapolate from the results of a study conducted in one demography to another. It is urged that similar research be done on a larger database and that these limitations be taken into account when applying

the study's conclusions. The very small sample size of the present study is a drawback, and larger-scale studies are advised to investigate their function in sex estimation. The use of a single type of CBCT device with a defined FOV (Field of Vision) and voxel size is another restriction. The resolution of the image may be affected by using a different machine or changing study conditions, leading to varying findings.

CONCLUSION

The mastoid bone could be efficiently used in sex discrimination via unidentified bone remains, and is preferable in forensic medicine and anthropology. Area of the mastoid triangle, volume of the mastoid triangle, and bimastoid diameter are the most efficient determinants with high accuracy. Studies on the mastoid process for sex determination have contributed valuable insights to the field of forensic anthropology. While the mastoid process can be a helpful indicator of sex, it is not used in isolation. Instead, it is integrated with other cranial and postcranial traits to create a comprehensive assessment of an individual's sex. Furthermore, the significance of population-specific variation highlights the importance of developing accurate reference standards for various populations.

REFERENCES

ALLAM FAFAB, ALLAM MFAB (2016) Sex discrimination of mastoid process by anthropometric measurements using multidetector computed tomography in Egyptian adult population. *Egypt J Forensic Sci*, 6(4): 361-369.

BABAN MTA, MOHAMMAD DN (2023) the accuracy of sex identification using cbct morphometric measurements of the mandible, with different machine-learning algorithms—a retrospective study. *Diagnostics*, 13(14): 2342.

BERTSATOS A, CHOVALOPOULOU M-E, BRŮŽEK J, BEJDOVÁ Š (2020) Advanced procedures for skull sex estimation using sexually dimorphic morphometric features. *Int J Legal Med*, 134(5): 1927-1937.

BHAYYA H, AVINASH TEJASVI ML, JAYALAKSHMI B, REDDY MM (2018) Craniometric assessment of gender using mastoid process. *J Indian Acad Oral Med Radiol*, 30(1): 52.

DE PAIVA LAS, SEGRE M (2003) Sexing the human skull through the mastoid process. *Revista Do Hospital Das Clinicas*, 58(1): 15-20.

FRANKLIN D, CARDINI A, FLAVEL A, KULIUKAS A (2012) The application of traditional and geometric morphometric analyses for forensic quantification of sexual dimorphism: preliminary investigations in a Western Australian population. *Int J Legal Med*, 126(4): 549-558.

GUPTA AD, BANERJEE A, KUMAR A, RAO SR, JOSE J (2012) discriminant function analysis of mastoid measurements in sex determination. *J Life Sci Royal Dublin Soc*, 4(1): 1-5.

GUPTA N, KALASKAR A, GUPTA N, KALASKAR R, KULKARNI R (2022) Cone beam computed tomographic study of gender determination by mastoid process. Available at SSRN: https://doi.org/10.2139/ssrn.4127802

İNCEOĞLU A, BAHŞI İ, ORHAN M, YALÇIN ED, İNCEOĞLU F (2021) The radiological evaluation of the mastoid process and its implications for surgical approaches. *Cureus*, 13(7): e16101.

JAIN D, JASUJA OP, NATH S (2013) Sex determination of human crania using Mastoid triangle and Opisthion-Bimastoid triangle. *J Forensic Legal Med,* 20(4): 255-259.

KEMKES A, GÖBEL T (2006) Metric assessment of the "mastoid triangle" for sex determination: a validation study. *J Forensic Sci*, 51(5): 985-989.

MADADIN M, MENEZES RG, AL DHAFEERI O, KHAROSHAH MA, AL IBRAHIM R, NAGESH KR, RAMADAN SU (2015) Evaluation of the mastoid triangle for determining sexual dimorphism: A Saudi population based study. *Forensic Sci Int*, 254: 244.e1-e4.

MARINESCU M, PANAITESCU V, ROSU M, MARU N, PUNGA A (2014) Sexual dimorphism of crania in a Romanian population: Discriminant function analysis approach for sex estimation. *Rom J Leg Med*, 22(1): 21-26.

OKUMUŞ Ö (2021) Determination of age and sex using bimastoid diameter: A cone beam computed tomography study. *Odovtos Int J Dental Sci*, 24(2): 157-163.

PAIVA LAS DE, SEGRE M (2003) Sexing the human skull through the mastoid process. *Revista Do Hospital Das Clinicas*, 58(1): 15-20.

PASSEY J, PANDEY S, PASSEY N, SINGH R, SINGH R, KUMAR A (2021) Radiographic evaluation of mastoid parameters for sexual differentiation in North Indian population. *Cureus*, 13(6): e16011.

SCHULTER-ELLIS FP (1979) Population differences in cellularity of the mastoid process. *Acta Oto-Laryngol*, 87(5-6): 461-465.

SOBHANI F, SALEMI F, MIRESMAEILI A, FARHADIAN M (2021) Morphometric analysis of the inter-mastoid triangle for sex determination: Application of statistical shape analysis. *Imaging Sci Dentistry*, 51(2): 167-174.

SUMATI, PATNAIK VVG (2015) Reliability of supramastoid crest in sex determination by logistic and probit regression. *Indian J Forensic Med Toxicol*, 9(1): 184-187.

SUSHMITHA S, GOPAL S, KUMAR M (2020) Mastoid and magnum – hidden key in forensics – A retrospective three-dimensional cone-beam computed tomographic study. *Int J Forensic Odontol*, 5(2): 62.

Effect of oxytocin receptor antagonist (GSK-221-149-A) on mandibular bone porosity in peri-menopausal rats

Ahmed S. Ahmed[1,2], Liju S. Mathew[2], Marwa M. Mona[3], Omaima K. Docmac[1], Hoda A. Ibrahim[4], Amira M. Elshamy[4], Ehab M. Hantash[1], Rasha A. Elsisy[5]

[1] Anatomy and embryology department, College of Medicine, Tanta University. Tanta 31511, Egypt

[2] Biomedical Sciences department, College of Medicine, Gulf Medical University. Ajman 4184, United Arab Emirates

[3] Medical biochemistry and molecular biology department, College of medicine, kafrelsheikh University. Kafrelsheikh 33516, Egypt

[4] Medical biochemistry and molecular biology department, College of Medicine, Tanta university. Tanta 31511, Egypt

[5] Anatomy and embryology department, College of medicine, kafrelsheikh University. Kafrelsheikh 33516, Egypt

SUMMARY

The period of peri-menopause (PMP) is characterized by hormonal fluctuations that impact the strength and health of bones. Oxytocin (OX), a small peptide known to be present in bone tissue, is the focus of this study. The objective of this research is to gain a better understanding of how OX precisely functions in the remodeling process of the mandibular bone. This understanding is seen as a crucial step in preventing the loss of both cortical and trabecular bone during the PMP. The current findings indicate that OX plays a role in preserving both compact and trabecular bone tissues, enhancing the mineral-to-matrix ratio, and regulating bone markers. Furthermore, it reduces porosity in both cortical and trabecular bone levels. Interestingly, these effects are reversed when an oxytocin receptor antagonist (GSK-221,149-A) is introduced, suggesting that OX's bone-preserving action is primarily mediated through the oxytocin receptor, rather than other mechanisms.

Key words: GSK-221-149-A – Mandibular bone – Estradiol – Peri-menopausal – Oxytocin

INTRODUCTION

The peri-menopause period (PMP) is associated with sex hormone fluctuations affecting strength of skeletal system in females (Marongiu, 2019). The decline in estradiol (E2) levels has a noticeable impact on the activity of bone cells, leading to an overactive state of osteoclasts coupled with reduced activity of osteoblasts (Allan et al., 2010; Nordstrom et al., 2015). This imbalance results in higher bone resorption, which manifests as an increased occurrence of bone fractures. Research findings indicate that the prevalence of hip bone fractures rises significantly in females aged over 50, with up to a 20% increase when compared to middle-aged females (Kim et al., 2020). Since the cortical part of the bone contributes more significantly to its strength than the trabecular part

Corresponding author:
Rasha A. Elsisy. Anatomy and embryology department, Faculty of Medicine, kafrelsheikh University, El-Geish Street, Kafrelsheikh 33516, Egypt. Cell Phone: +01274337050. E-mail: rasha_saleh2014@med.kfs.edu.eg - Orcid: 0000-0003-3230-4474.

Submitted: October 21, 2023. **Accepted:** November 27, 2023

https://doi.org/10.52083/XMJO8562

(Naqvi et al., 2020), the higher rate of bone fractures with age can be attributed to the diminished presence of orthophosphate ions [(PO4)3-] and carbonate [H2CO3] within the bone cortex. This leads to alterations in the microstructure and thickness of the bone (Akkus et al., 2004; Ahmed et al., 2015; Long et al., 2020; Fañanas-Baquero et al., 2021).

Oxytocin (OX) receptors have been detected in various bone cells, including osteoclasts and osteoblasts (Cheng et al., 2020), and studies have shown that OX can enhance the anabolic activity of these bone cells (Colicci et al., 2002; Tamma et al., 2009; Abbasi et al., 2019). In females during the peri-menopausal period (PMP), there is typically a decrease in estrogen plasma levels, which is reflected in reduced OX levels and the down-regulation of its receptor (Breuil et al., 2011; Colaianni et al., 2014a). There is a clear need to develop alternative therapies that can effectively reduce the prevalence of osteopenia or osteoporosis in females during the PMP (Ferreira et al., 2015). In albino Wistar rats, the peri-menopausal phase, characterized by lower estrogen plasma levels, typically occurs around twenty months of age (Nicola et al., 2016). The primary objective of the current study is to investigate the precise mechanism through which OX operates in the remodeling of the mandibular bone. This research aims to take a crucial step toward preventing the loss of cortical and trabecular bone during the PMP.

MATERIALS AND METHODS

Chemicals and animals

Unless stated otherwise, chemicals and kits were sourced from Sigma-Aldrich (USA). In terms of the animals used, thirty female albino Wistar rats aged twenty months were employed. These rats were individually housed and provided with an ample supply of food and water, maintaining a room temperature of 25°C. Following the protocol outlined by Marcondes et al. (2002), vaginal secretions were examined daily for a period of two weeks. Only rats displaying peri-estropause phases were included in the present research project. The study was conducted in accordance with the Animal Research: Reporting of In Vivo Experiments (ARRIVE) guidelines.

Experimental design

The animals were given a two-week period to adapt, after which they were evenly distributed into three groups. Control group (C-group) was treated with normal saline (0.9% NaCl) (1 ml / kg bw / day), intraperitoneal injection (i.p.) only for two days. Oxytocin group (OX-group) was treated with OX (200 µg / Kg bw / day), i.p., only for two days. Retosiban (GSK-221,149-A) group (RS-group), received RS by oral gavage (5 mg / Kg bw / day) for two days. After four weeks, animals were euthanized by injecting sodium pentobarbital i.p., then samples of blood were centrifuged for 20 minutes (10 x 1000 rpm). Plasma was gathered for subsequent analysis. The mandibles were dissected and divided in half using a large pair of scissors. The right half was preserved in saline at -20°C for additional investigations, while the left half was immersed in formalin for fixation.

Histopathological and immunohistochemistry examinations

In accordance with protocol described by Tucker et al. (2016), the mandibular neck was cut into 1cm3 cubes and fixed in 10% formalin (48 hours). Tissue sections (5 µm) were processed and stained with hematoxylin and eosin (H&E) (Tucker et al., 2016). Histopathologists unaware to the aim of our study were consulted for examinations. Non-overlapping fields were analyzed using the software ImageJ 1.24.

Immunohistochemistry was done following the protocol of Ervolino, et al. (2019). Diluted 1ry antibody were used [Goat anti-osterix (Osx) (1:1000), rabbit anti-runt-related transcription factor 2 (RUNX-2) (1:10000), rabbit anti- periostin (PER) (1:10000), goat anti-osteopontin (OPN) (1:100000), goat anti-osteocalcin (OCN) (1:200), rabbit anti-sclerostin (SOST) (1:10000), rabbit anti-bone morphogenetic protein (BMP) (1:200), and goat anti-tartrate-resistant acid phosphatase (TRAP) (1:200)]. Secondary antibodies were alkaline phophatase (Abcam, USA). Scoring was done in accordance with Stringhetta-Garcia et al. (2016) [Negative immunoreactivity (IR) = 0, mild IR = 1, moderate IR = 2 and sever IR = 3].

Bone tissue homogenate Western blotting (W.B.)

W.B. was used in order to estimate alkaline phosphatase (ALP) and TRAP in accordance with protocol described by Peres-Ueno et al. (2020). Briefly, one hundred milligrams of bone tissue were homogenate using Argos Flexi-fuge microcentrifuge (Stellar-scientific, USA) then centrifuged. Supernatants were blotted into polyvinylidene fluoride (PVDF) membranes (Merck, Germany) using Trans-Blot® electrophoretic transfer Cell (BioRad USA). 5% milk solution was used to block PVDF membranes, which were then incubated with the primary antibodies [anti-alkaline phosphatase (ALP) antibody (1:200) and anti-TRAP antibodies (1:400)] (Abcam, UK) for 12 hours. Subsequently, blots were incubated with horseradish peroxidase (HRP) secondary antibodies 1:5000 dilution (Abcam, UK) for 60 min. at 25°C. Bands were imaged using iBright™ Imaging Systems (Thermo-fisher, USA) and quantified were analyzed using the software ImageJ 1.24.

Raman microspectroscopy (RMSS), microtomography (micro-CT) and Dual-energy X-ray absorptiometry (DXA) examinations

Mineral composition of bone tissue was analyzed by chemical analysis technique (Raman microspectroscopy) (CRAIC Technologies, USA) following protocol described by Fernandes et al. (2020). Using SkyScan (Bruker, UK), microtomography examinations were performed (analysis was done for 20 slices in mandibular neck) following protocol described by Stringhetta-Garcia et al. (2017). Bone mineral density (BMD) was assessed by Sunlight MiniOmni™ (Beam-med, USA). The equipment was calibrated to small animals following manufacturer protocol.

Biomechanical compression bending (BCB) examinations

EMIC DL3000 (Instron, Brazil) was used to evaluate of the biomechanical characteristics of the mandible. The mandibular ramus was placed vertically. Compression was applied to mandibular head to evaluate bone stiffness.

Statistical analysis

Data analysis was performed using Statistical Package for Social Sciences (SPSS) software, version 20 (SPSS Inc., USA). To validate the statistical significance of differences between groups, a one-way analysis of variance (ANOVA) was conducted. Post hoc Tukey-Kramer testing was employed for comparing groups. The data were presented as mean ± standard deviation, and a probability value was deemed significant if it was lower than 0.05.

RESULTS

Retosiban and oxytocin administration effect on mandibular neck histopathological and immunohistochemical changes in peri-estropause rats

C-group and OX-group showed healthy tissue. Compact bone was organized as parallel condensed lamellae with minimal thinning surrounding a central trabecular bone area which was formed of branching and anastomosing irregular trabeculae rich in blood vessels. RS-group showed reduction of the bone matrix with an obvious thinning of compact bone in addition to perforations and disconnection of trabecular bone trabeculae (Fig. 1 A-C).

A significant increase of compact bone tissue area in addition to a non-significant change of trabecular bone areas were noticed in OX-group as compared to the control group, while RS-group showed a significant decrease of both compact and trabecular bone areas (by 27% and 50% respectively) as compared to the control (Fig. 1D).

By examination of either compact (Fig. 2) or trabecular (Fig. 3) bone sections stained with anti-Osx, anti-RUNX-2 (plays a cell proliferation regulatory role in cell cycle entry and exit in osteoblasts), anti-PER (member of the matricellular protein family) and anti-BMP antibodies (plays important roles in a wide array of processes during formation and maintenance of bone); OX-group and RS-group showed strong and negative reactions respectively, while C-group showed weak reaction. In bone sections stained with anti-OPN, anti-OCN, anti-SOST and anti-TRAP antibodies, OX-group and RS-group showed weak and strong reactions respectively, while C-group showed weak reaction. Statistical analysis showed that OX-group and RS-group showed significant increase and decrease respectively of Osx, RUNX-2, PER and BMP bone immunoreactivity compared to the control values. OX-group

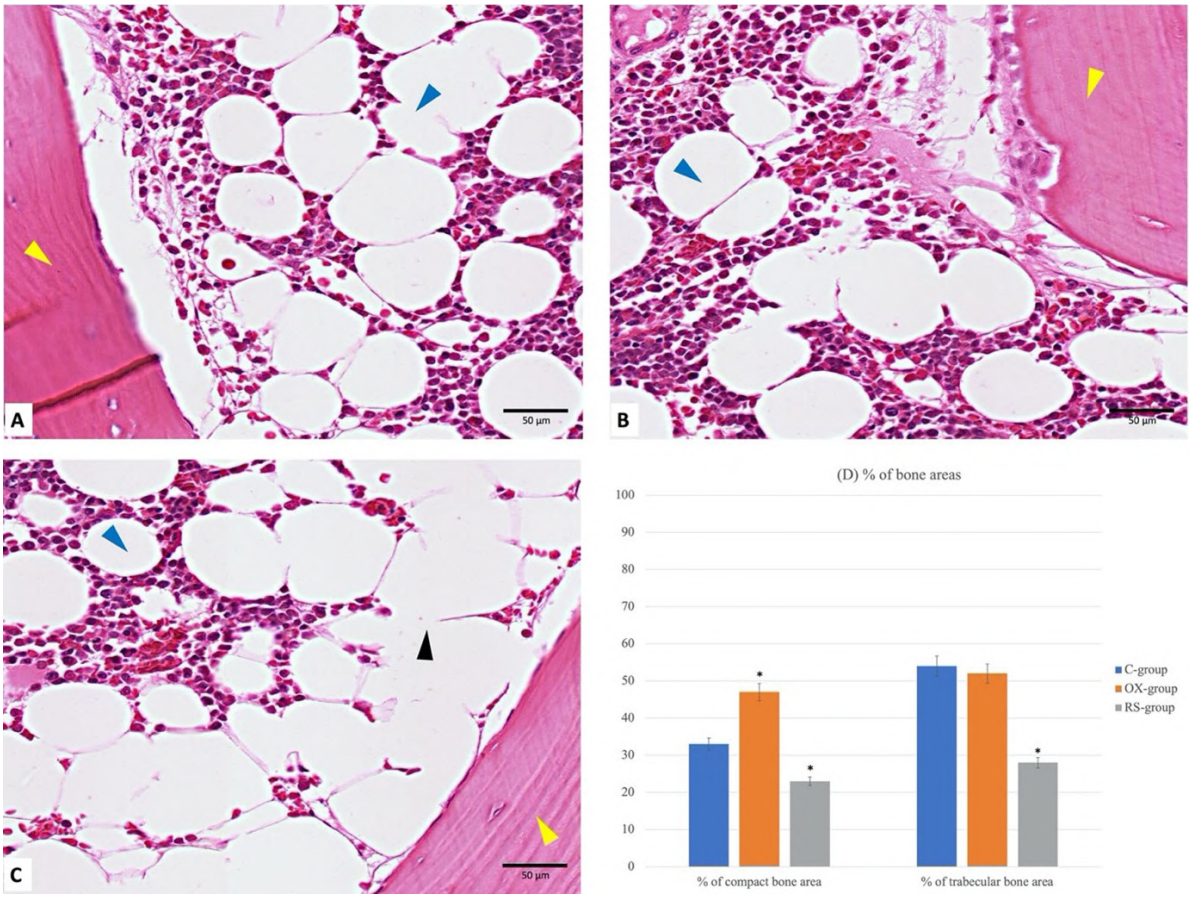

Fig. 1.- (A-C) Mandibular neck tissue stained with hematoxylin and eosin (X 1000), (n=20). Scale bars = 50 µm. C-group (A) and OX-group (B) showed normal bone histological architecture. Compact bone was organized as parallel condensed lamellae with minimal thinning surrounding a central trabecular bone area which is formed of branching and anastomosing irregular trabeculae rich in blood vessels. RS-group (C) showed reduction of the bone matrix with an obvious thinning of compact bone in addition to perforations and disconnection of trabecular bone trabeculae. (Note: Yellow arrow = compact bone, Blue arrow = trabecular bone, Black arrow = disconnected trabeculae). **(D)** Represents % of compact and trabecular bone areas. * Significant ($p < 0.05$) difference in comparison to C-group. Data are expressed in mean ± standard deviation and probability value is considered significant if <0.05, (n=20).

showed non-significant difference of OPN, OCN, SOST and TRAP bone immunoreactivity. A significant increase of bone immunoreactivity was noticed in RS-group compared to C-group (Fig. 4 A-B).

Retosiban and oxytocin administration effect on mandibular bone turnover markers in peri-estropause rats

A significant increase of ALP activity in addition to a significant decrease of TRAP activity were recorded in OX-group as compared to the control values. RS-group showed a significant decrease of ALP activity in addition to a significant increase of TRAP activity as compared to C-group (Fig. 5 A-C).

Retosiban and oxytocin administration effect on mineral / matrix ratio in peri-estropause rats

OX-group presented a significant increase of bone-mineral/matrix ratio in addition to a significant drop of B-type carbonate as compared to the control values. RS-group showed a significant drop of both bone-mineral/matrix ratio and crystallinity, in addition to a significant rise of B-type carbonate values as compared to the control values (Fig. 6 A-C).

Retosiban and oxytocin administration effect on cortical bone area and % of trabecular bone volume in peri-estropause rats

OX-group presented a significant increase of the area of cortical bone and % of trabecular bone volume with a significant drop of % of cortical porosity and number of trabeculae as compared to control values. On the other hand, RS-group showed a significant decrease of % of trabecular bone volume and cortical bone area in addition to a significant rise % of cortical porosity as compared to control values (Fig. 7 A-D).

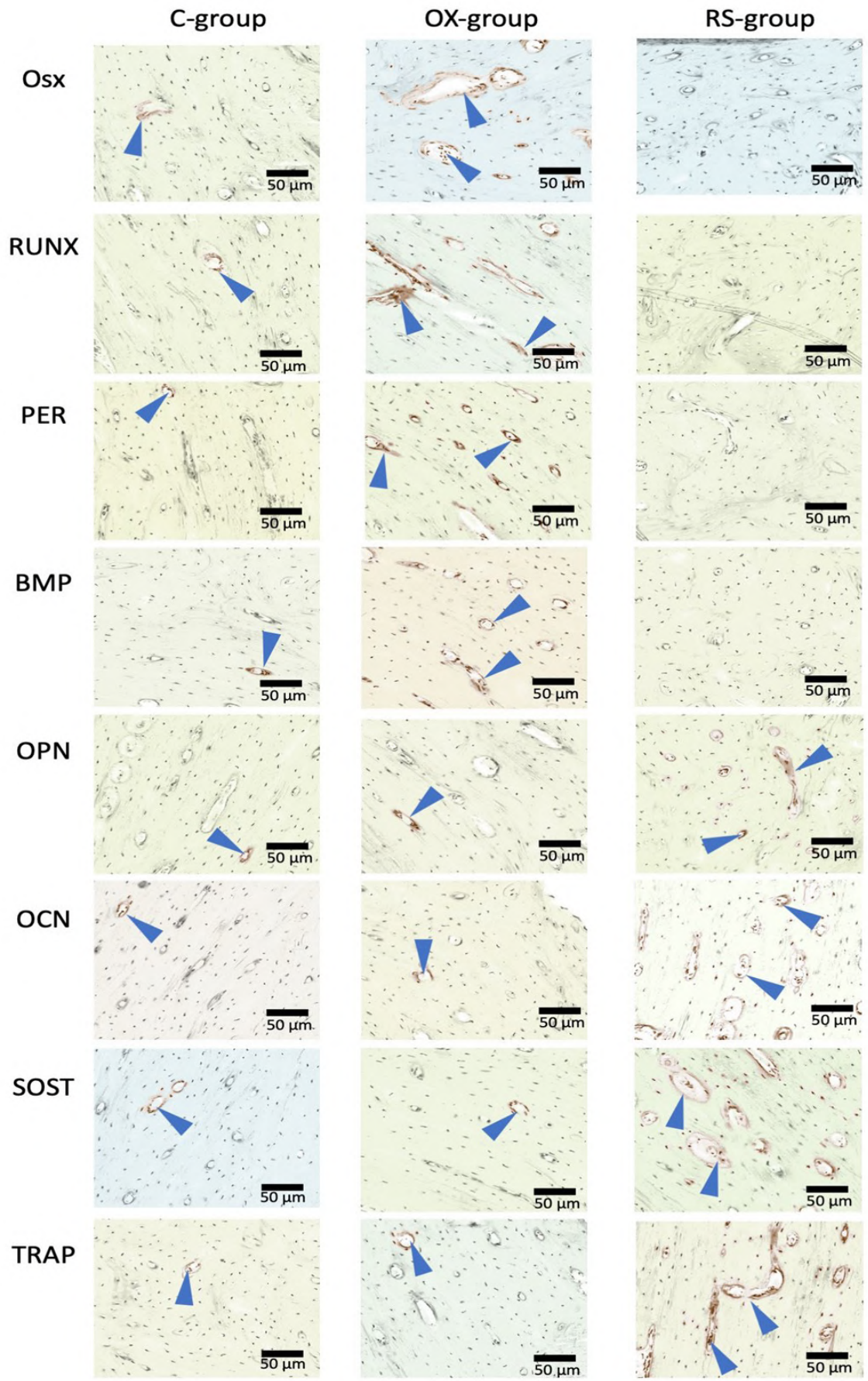

Fig. 2.- Mandibular neck compact bone stained immunohistochemically (X 1000), (n=20). Scale bars = 50 µm. By examination of compact bone sections stained with anti-Osx, anti-RUNX-2, anti-PER and anti-BMP antibodies; OX-group and RS-group showed strong and negative reactions respectively while C-group showed weak reaction. By examining compact bone sections stained with anti-OPN, anti-OCN, anti-SOST and anti-TRAP antibodies; OX-group and RS-group showed weak and strong reactions respectively while C-group showed weak reaction (Note: Immune-positive areas are labelled with blue arrows).

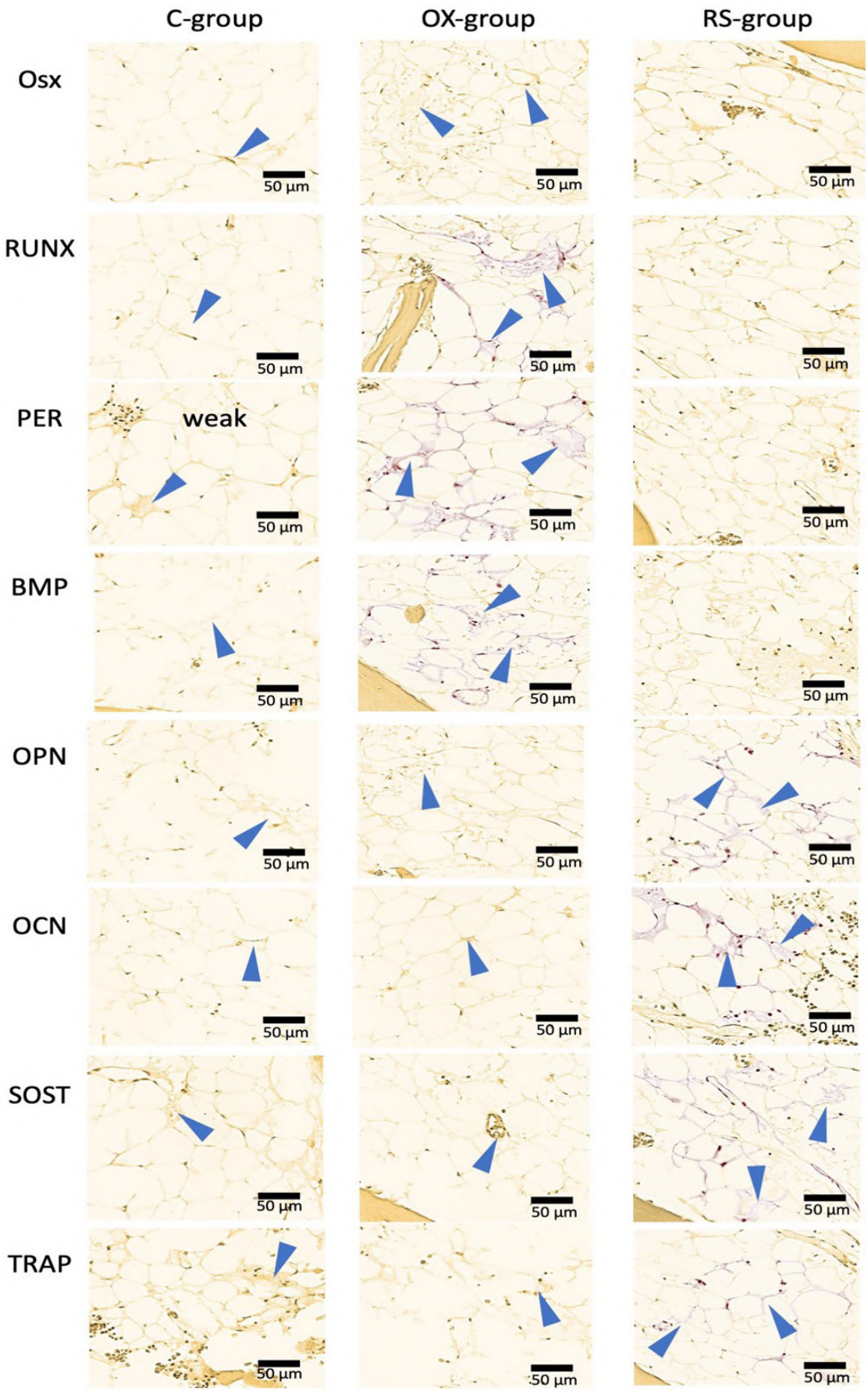

Fig. 3.- Mandibular neck trabecular bone stained immunohistochemically (X 1000), (n=20). Scale bars = 50 µm. By examination of trabecular bone sections stained with anti-Osx, anti-RUNX-2, anti-PER and anti-BMP antibodies; OX-group and RS-group showed strong and negative reactions respectively while C-group showed weak reaction. By examining of trabecular bone sections stained with anti-OPN, anti-OCN, anti-SOST and anti-TRAP antibodies; OX-group and RS-group showed weak and strong reactions respectively while C-group showed weak reaction (Note: Immune-positive areas are labelled with blue arrows).

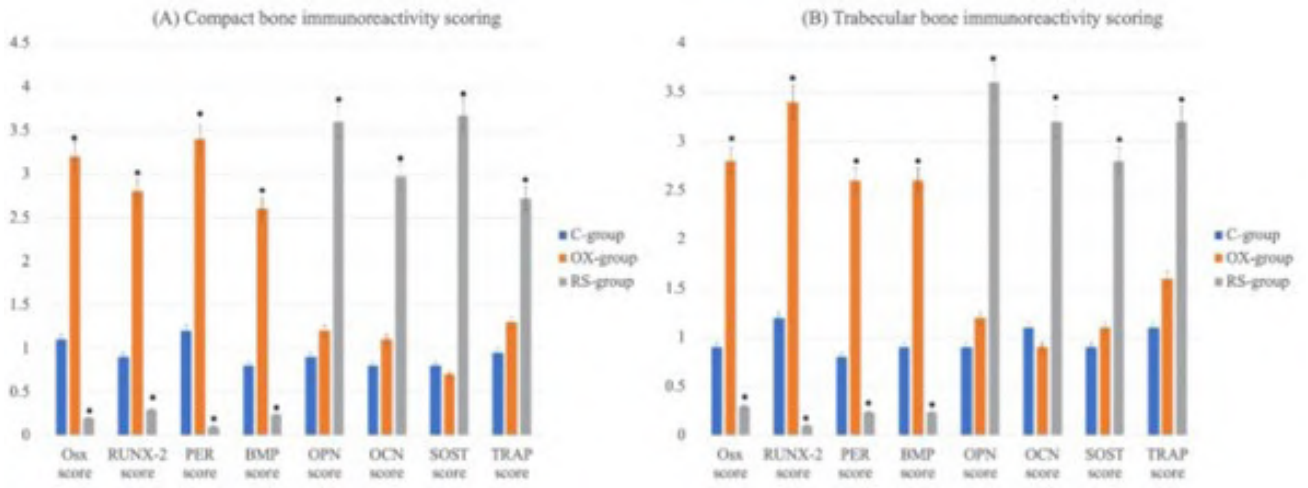

Fig. 4.- Effect of retosiban and oxytocin administration on mandibular neck compact **(A)** and trabecular **(B)** bone immunoreactivity in peri-estropause rats. Statistical analysis showed that OX-group and RS-group showed significant ($p < 0.05$) increase and decrease (of Osx, RUNX-2, PER and BMP bone immunoreactivity) respectively as compared to C-group. OX-group showed non-significant difference (of OPN, OCN, SOST and TRAP bone immunoreactivity) as compared to C-group, while RS-group showed significant ($p < 0.05$) increase (of bone immunoreactivity) as compared to C-group. * Significant ($p < 0.05$) difference in comparison to C-group. Data are expressed in mean ± standard deviation and probability value is considered significant if <0.05, (n=20).

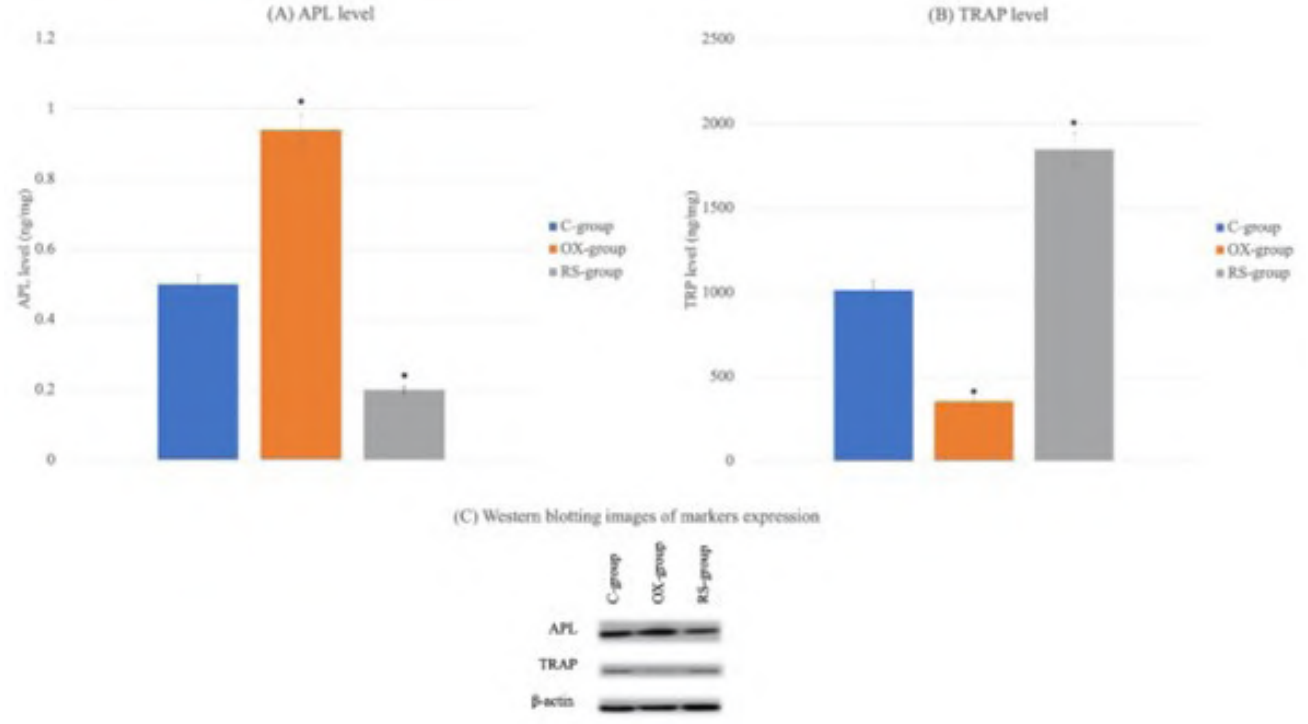

Fig. 5.- Effect of retosiban and oxytocin administration on mandibular bone APL **(A)** and TRAP **(B)** levels in peri-estropause rats. OX-group showed a significant increase of ALP activity in addition to a significant decrease of TRAP activity as compared to C-group. RS-group showed a significant decrease of ALP activity in addition to a significant increase of TRAP activity as compared to C-group. **(C)** Represents Western blot images of markers expression. * Significant ($p < 0.05$) difference in comparison to C-group. Data are expressed in mean ± standard deviation and probability value is considered significant if <0.05, (n=20).

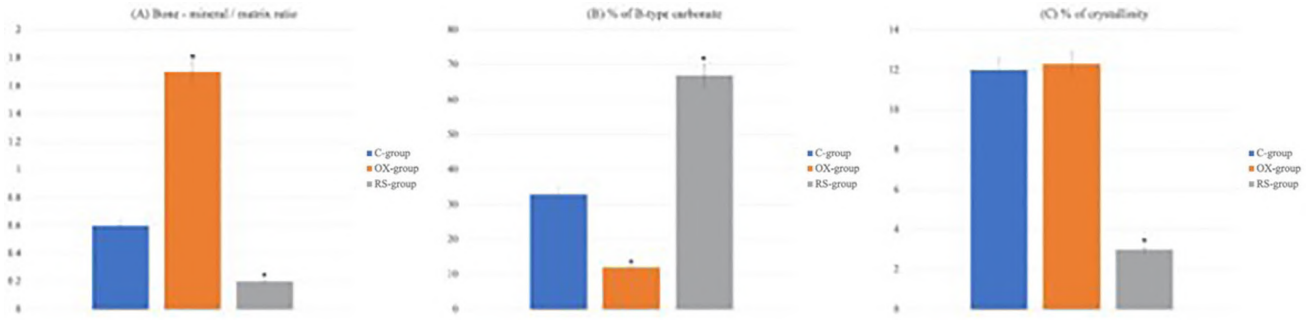

Fig. 6.- Effect of retosiban and oxytocin administration on mineral / matrix ratio in peri-estropause rats. OX-group showed a significant ($p < 0.05$) increase of bone - mineral / matrix ratio **(A)** in addition to a significant ($p < 0.05$) decrease of B-type carbonate **(B)** with non-significant change of crystallinity **(C)** as compared to C-group. On the other hand, RS-group showed a significant ($p < 0.05$) decrease of both bone - mineral / matrix ratio and crystallinity in addition to a significant ($p < 0.05$) increase of B-type carbonate as compared to C-group. * Significant ($p < 0.05$) difference in comparison to C-group. Data are expressed in mean ± standard deviation and probability value is considered significant if <0.05, (n=20).

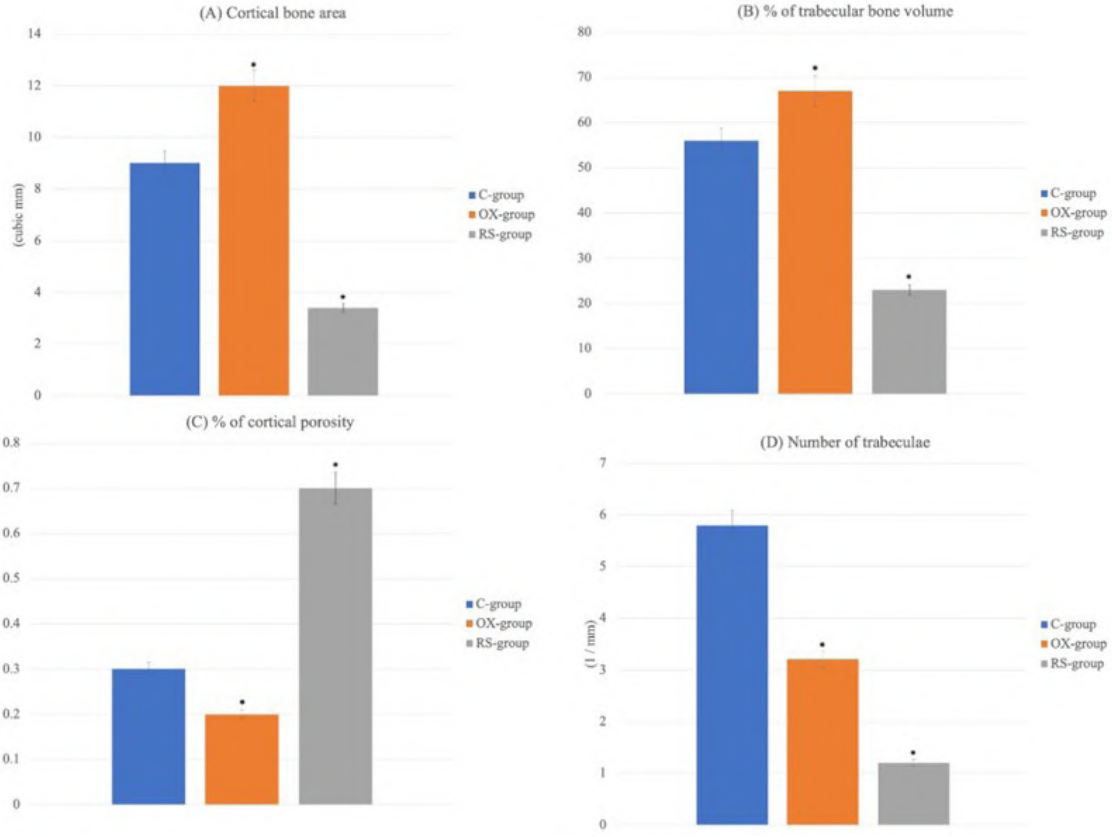

Fig. 7.- Effect of retosiban and oxytocin administration on cortical bone area and % of trabecular bone volume in peri-estropause rats. Microtomography results showed that; OX-group represents a significant ($p < 0.05$) increase of cortical bone area **(A)** and % of trabecular bone volume **(B)** in addition to a significant ($p < 0.05$) decrease of % of cortical porosity **(C)** and number of trabeculae **(D)** as compared to C-group. On the other hand, RS-group showed a significant ($p < 0.05$) decrease of cortical bone area and % of trabecular bone volume in addition to a significant ($p < 0.05$) increase % of cortical porosity as compared to C-group. * Significant ($p < 0.05$) difference in comparison to C-group. Data are expressed in mean ± standard deviation and probability value is considered significant if <0.05, (n=20).

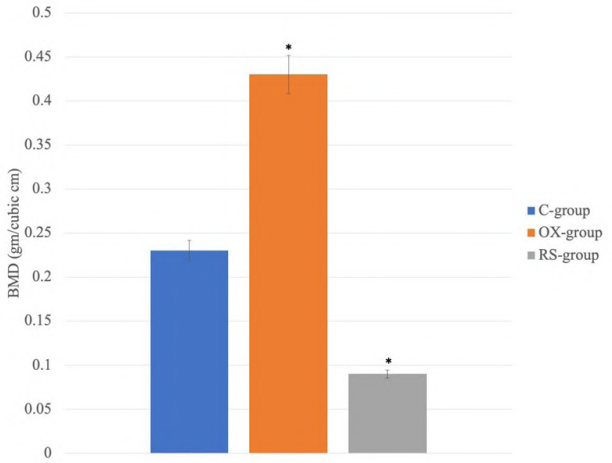

Fig. 8.- Effect of retosiban and oxytocin administration on BMD in peri-estropause rats. OX-group showed a significant ($p < 0.05$) increase of BMD as compared to C-group. On the other hand, RS-group showed a significant ($p < 0.05$) decrease of BMD as compared to C-group. * Significant ($p < 0.05$) difference in comparison to C-group. Data are expressed in mean ± standard deviation and probability value is considered significant if <0.05, (n=20).

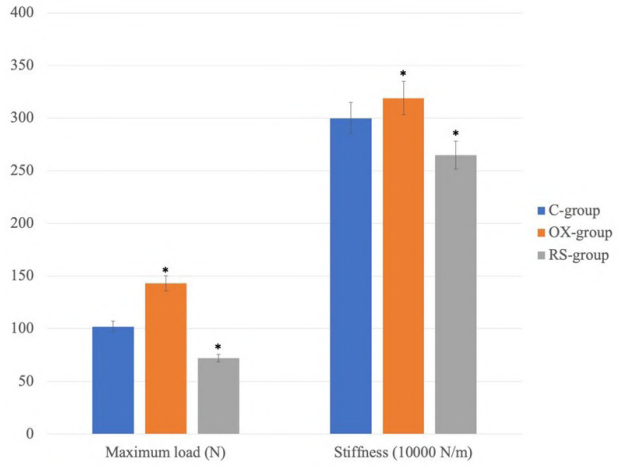

Fig. 9.- Effect of retosiban and oxytocin administration on mandibular bone stiffness in peri-estropause rats. OX-group showed a significant ($p < 0.05$) increase of maximum load and stiffness as compared to C-group. On the other hand, RS-group showed a significant ($p < 0.05$) decrease of same parameters as compared to C-group. * Significant ($p < 0.05$) difference in comparison to C-group. Data are expressed in mean ± standard deviation and probability value is considered significant if <0.05, (n=20).

Retosiban and oxytocin administration effect on BMD in peri-estropause rats

OX and RS groups showed a significant rise and drop of BMD respectively as compared to the control values (Fig. 8).

Retosiban and oxytocin administration effect on mandibular bone stiffness in peri-estropause rats

EMIC DL3000 (Instron, Brazil) was used in order to evaluate the biomechanical characteristics of the mandible. OX-group showed a significant rise of maximum load and stuffiness as compared to control group. On the other hand, RS-group showed a significant drop of same parameters as compared to control group (Fig. 9).

DISCUSSION

Marongiu (1) linked the reduction in bone stiffness during the peri-menopausal period (evidenced by an increased susceptibility to fractures) to the fluctuations in sex hormone levels. In addition to OX's direct impact on bone, the connection between OX and steroid sex hormones, particularly estrogen, was elucidated by Colaianni et al. (2011). They reported that OX's influence on bone in response to estrogen operates through an autocrine loop, where OX is locally released from bone marrow osteoblasts via a non-genomic, Erk-dependent pathway. Furthermore, OX serves as a mediator for estrogen's effects on bone by influencing the expression of oxytocin receptors through genomic mechanisms. Di Benedetto et al. (2014) outlined the mechanism by which OX operates on its own receptors (OTR) in the skeletal system, involving translocation to the nucleus of osteoblasts. This translocation process is the primary mechanism responsible for osteoblast differentiation.

The current study explored the impact of OX on bone during the peri-estropause period. In the OX-treated group, there was an observed increase in ALP activity, which is an osteoblastic marker, along with a significant decrease in TRAP activity, a marker associated with osteoclasts. These findings align with the research by Naylor and Eastell (2012). Conversely, the RS-group exhibited the opposite trend in these parameters. Colli et al. (2012) noted that OX's peripheral effects in older rats were linked to substantial increases in ALP and osteocalcin, suggesting enhanced osteogenesis coupled with reduced bone resorption activity following OX administration. Furthermore, Colaianni et al. (2014b) pointed out that oxytocin's influence on skeletal tissue is also mediated by its impact on osteoclasts. This finding is consistent with Nicola et al. (2016) research, which highlighted the altered activity of both osteoblasts and

osteoclasts during the perimenopausal period.

In present results, OX-group showed a strong immunohistochemical reaction of bone sections indicating increased expression of Osx, RUNX-2. These are osteogenesis markers indicating osteoblast differentiation as reported by Tamma et al. (2009), in addition to PER and BMP proteins, while RS-group showed negative reactions. This comes in the same context as, Stringhetta-Garcia et al. (2016) who noticed the ability of PER protein to interact with collagen (type I), resulting in better bone quality. Fernandes et al. (2020) reported the role of PER in osteogenesis, mineralization which results in better bone quality and thickness reflected directly on bone strength. Kim et al. (2015) reported the role of down-regulated PER in bony fractures of postmenopausal women, in addition to the peripheral role of OX in a greater osteoblastic activity. Santos et al. (2018) reported the in vitro effect of OX in activating bone marrow derived mesenchymal stem to differentiate into osteoblasts. In the same line, Tamma et al. (2009) reported that OX induced osteoblast development toward a mineralizing phenotype through increasing of bone morphogenetic protein2 (Bmp-2). On the other hand, they added that despite OX stimulate osteoclastogenesis, it was found that OX treatment can inhibits bone resorption of mature osteoclasts.

Following the examination using Raman microspectroscopy, the OX-treated group exhibited an increase in the mineral-to-matrix ratio, along with a reduction in carbonate (B-type), aligning with findings from other authors (Bi et al., 2011; Khalid et al., 2018; Burr, 2019). Ge et al. (2019) also reported that OX was observed to stimulate mineral formation and the deposition of Ca2+.

In the current study, OX-group represented an increase of cortical and trabecular bones in addition to a decrease of % of cortical porosity and number of trabeculae, which was reflected as an increased bone stiffness as reported by Kazakia et al. (2013). According to Vilayphiou et al. (2016), it is commonly observed that aging leads to heightened porosity and reduced strength in bones. They also noted that evaluating cortical porosity can serve as a predictive measure for future fractures.

In conclusion, Oxytocin plays a crucial role in enhancing bone density and mineralization in both compact and trabecular bone by promoting osteoblast differentiation and regulating bone turnover markers. Additionally, it contributes to improved bone strength. These effects were negated by Retosiban (GSK-221,149-A), suggesting that Oxytocin's anabolic impact on bone in peri-estropause rats is most likely mediated through oxytocin receptor mechanisms rather than other pathways.

STATEMENT OF ETHICS

The Research and Ethics Committee, Kafrelsheikh University, Egypt approved the study protocol (MKSU 65-2-14).

REFERENCES

ABBASI N, AZIZPOUR Y, AZIZI M, KARIMI E, AIDY A, ASADOLLAHI K (2019) The effects of mumie extract on cell proliferation and enzyme expression of human osteoblast-like cells (MG63). *J Stem Cells Regen Med,* 15(2): 18-23.

AHMED L, SHIGDEL R, JOAKIMSEN R, ELDEVIK O, ERIKSEN E, GHASEM-ZADEH A, BALA Y, ZEBAZE R, SEEMAN E, BJØRNEREM Å (2015) Measurement of cortical porosity of the proximal femur improves identification of women with nonvertebral fragility fractures. *Osteoporos Int*, 26: 2137-2146.

AKKUS O, ADAR F, SCHAFFLER M (2004) Age-related changes in physicochemical properties of mineral crystals are related to impaired mechanical function of cortical bone. *Bone*, 34: 443-453.

ALLAN CM, KALAK R, DUNSTAN CR, MCTAVISH KJ, ZHOU H, HANDELSMAN DJ, SEIBEL MJ (2010) Follicle-stimulating hormone increases bone mass in female mice. *Proc Natl Acad Sci USA*, 107(52): 22629-22634.

BI X, PATIL C, LYNCH C, PHARR G, MAHADEVAN-JANSEN A, NYMAN J (2011) Raman and mechanical properties correlate at whole bone- and tissue-levels in a genetic mouse model. *J Biomech*, 44: 297-303.

BREUIL V, AMRI E, PANAIA-FERRARI P, TESTA J, ELABD C, ALBERT-SABONNADIÈRE C, ROUX CH, AILHAUD G, DANI C, CARLE GF, EULLER-ZIEGLER L (2011) Oxytocin and bone remodelling: relationships with neuropituitary hormones, bone status and body composition. *Joint Bone Spine*, 78: 611-615.

BURR D (2019) Changes in bone matrix properties with aging. *Bone,* 120: 85-93.

CHENG L, ZHU Y, KE D, XIE D (2020) Oestrogen-activated autophagy has a negative effect on the anti-osteoclastogenic function of oestrogen. *Cell Proliferation,* 53(4): e12789.

COLAIANNI G, DI BENEDETTO A, ZHU LL, TAMMA R, LI J, GRECO G, PENG Y, DELL'ENDICE S, ZHU G, CUSCITO C, GRANO M, COLUCCI S, IQBAL J, YUEN T, SUN L, ZAIDI M, ZALLONE A (2011) Regulated production of the pituitary hormone oxytocin from human and murine osteoblasts. *Biochem Biophys Res Commun*, 411: 512-515.

COLAIANNI G, SUN L, ZAIDI M, ZALLONE A (2014a) Oxytocin and bone. *Am J Physiol*, 307: 970-977.

COLAIANNI G, TAMMA R, DI BENEDETTO A, YUEN T, SUN L, ZAIDI M, ZALLONE A (2014b) The oxytocin-bone axis. *Neuroendocrinology,* 26(2): 53-57.

COLLI V, OKAMOTO R, SPRITZER P, DORNELLES R (2012) Oxytocin promotes bone formation during the alveolar healing process in old acyclic female rats. *Arch Oral Biol*, 57: 1290-1297.

COLUCCI S, COLAIANNI G, MORI G, GRANO M, ZALLONE A (2002) Human osteoclasts express oxytocin receptor. *Biochem Biophys Res Commun*, 297: 442-445.

DI BENEDETTO A, SUN L, ZAMBONIN C, TAMMA R, NICO B, CALVANO C, COLAIANNI G, JI Y, MORI G, GRANO M, LU P, COLUCCI S, YUEN T, NEW MI, ZALLONE A, ZAIDI M (2014) Osteoblast regulation via ligand-activated nuclear trafficking of the oxytocin receptor. *Proc Natl Acad Sci*, 111(46): 16502-16507.

ERVOLINO E, STATKIEVICZ C, TORO L, DE MELLO-NETO J, CAVAZANA T, ISSA J, DORNELLES RC, MILANEZI DE ALMEIDA J, NAGATA MJ, OKAMOTO R, APARECIDO CASATTI C, GOUVEIA GARCIA V, THEODORO L (2019) Antimicrobial photodynamic therapy improves the alveolar repair process and prevents the occurrence of osteonecrosis of the jaws after tooth extraction in senile rats treated with zoledronate. *Bone,* 120: 101-113.

FAÑANAS-BAQUERO S, ORMAN I, APARICIO F, DE MIGUEL S, MERINO J, YAÑEZ R, FERNANDEZ SAINZ Y, SÁNCHEZ R, DESSY-RODRÍGUEZ M, ALBERQUILLA O, ALFARO D, ZAPATA A, BUEREN JA, SEGOVIA JC, QUINTANA-BUSTAMANTE O (2021) Natural estrogens enhance the engraftment of human hematopoietic stem and progenitor cells in immunodeficient mice. *Haematologica*, 106(6): 1659-1670.

FERNANDES F, STRINGHETTA-GARCIA C, PERES-UENO M, FERNANDES F, NICOLA A, CASTOLDI R, OZAKI G, LOUZADA MJQ, CHAVES-NETO AH, ERVOLINO E, DORNELLES R (2020) Oxytocin and bone quality in the femoral neck of rats in periestropause. *Sci Rep*, 10(1): 7937.

FERREIRA L, DE NICOLA A, ANSELMO-FRANCI J, DORNELLES R (2015) Activity of neurons in the preoptic area and their participation in reproductive senescence: Preliminary findings. *Exp Gerontol*, 72: 157-161.

GE B, LIU H, LIANG Q, SHANG L, WANG T, GE S (2019) Oxytocin facilitates the proliferation, migration and osteogenic differentiation of human periodontal stem cells in vitro. *Arch Oral Biol*, 99: 126-133.

KAZAKIA G, NIRODY J, BERNSTEIN G, SODE M, BURGHARDT A, MAJUMDAR S (2013) Age- and gender-related differences in cortical geometry and microstructure: Improved sensitivity by regional analysis. *Bone*, 52: 623-631.

KHALID M, BORA T, GHAITHI A, THUKRAL S, DUTTA J (2018) Raman spectroscopy detects changes in bone mineral quality and collagen cross-linkage in staphylococcus infected human bone. *Sci Rep*, 8: 9417.

KIM B, RHEE Y, KIM C, BAEK K, MIN Y, KIM D, AHN SH, KIM H, LEE SH, LEE SY, KANG M, KOH J (2015) Plasma periostin associates significantly with non-vertebral but not vertebral fractures in postmenopausal women: Clinical evidence for the different effects of periostin depending on the skeletal site. *Bone*, 81: 435-441.

KIM HN, PONTE F, NOOKAEW I, OZGUREL SU, MARQUES-CARVALHO A, IYER S, WARREN A, AYKIN-BURNS N, KRAGER K, SARDAO VA, HAN L, DE CABO R, ZHAO H, JILKA RL, MANOLAGAS SC, ALMEIDA M (2020) Estrogens decrease osteoclast number by attenuating mitochondria oxidative phosphorylation and ATP production in early osteoclast precursors. *Sci Rep*, 10(1): 11933.

LONG H, HU CT, PRIJATEL J, WENG C (2020) Antrodia cinnamomea is a potentially effective complementary medicine for adjuvant therapy against breast cancer with bone metastasis: A case report. *Medicine (Baltimore)*, 99(27): 20808.

MARCONDES F, BIANCHI F, TANNO A (2002) Determination of the estrous cycle phases of the rats: some helpful considerations. *Braz J Biol*, 62: 609-614.

MARONGIU R (2019) Accelerated ovarian failure as a unique model to study peri-menopause influence on Alzheimer's disease. *Front Aging Neurosci*, 11: 242.

NAQVI S, PANADERO PÉREZ JA, KUMAR V, VERBRUGGEN A, MCNAMARA L (2020) A novel 3D osteoblast and osteocyte model revealing changes in mineralization and pro-osteoclastogenic paracrine signaling during estrogen deficiency. *Front Bioeng Biotechnol*, 8: 601.

NAYLOR K, EASTELL R (2012) Bone turnover markers: use in osteoporosis. Nature reviews. *Rheumatology*, 8: 379-389.

NICOLA A, LEITE C, NISHIKAVA M, DE CASTRO J, ANSELMO-FRANCI J, DORNELLES R (2016) The transition to reproductive senescence is characterized by increase in A6 and AVPV neuron activity with attenuation of noradrenaline content. *Exp Gerontol*, 81: 19-27.

NORDSTROM P, GUSTAFSON Y, MICHAELSSON K, NORDSTROM A (2015) Length of hospital stay after hip fracture and short-term risk of death after discharge: a total cohort study in Sweden. *BMJ*, 350: h696.

PERES-UENO M, FERNANDES F, BRITO V, NICOLA Â, STRINGHETTA-GARCIA C, CASTOLDI R, MENEZES AP, CIARLINI PC, LOUZADA MJQ, PENHA OLIVEIRA SH, ERVOLINO E, CHAVES-NETO AH, DORNELLES R (2020) Effect of pre-treatment of strength training and raloxifene in periestropause on bone healing. *Bone*, 134: 115285.

SANTOS L, SINGULANI M, STRINGHETTA-GARCIA C, OLIVEIRA S, CHAVES-NETO A, DORNELLES R (2018) Oxytocin effects on osteoblastic differentiation of bone marrow mesenchymal stem cells from adult and aging female Wistar rats. *Exp Gerontol*, 113: 58-63.

STRINGHETTA-GARCIA C, SINGULANI M, SANTOS L, LOUZADA M, NAKAMUNE A, CHAVES-NETO A, ROSSI AC, ERVOLINO E, DORNELLES R (2016) The effects of strength training and raloxifene on bone health in aging ovariectomized rats. *Bone*, 85: 45-54.

STRINGHETTA-GARCIA C, MORAIS S, FERNANDES F, PEREZ-UENO M, ALMEIDA R, LOUZADA MJQ, CHAVES-NETO AH, ERVOLINO E. DORNELLES R (2017) Effects of strength training and raloxifene on femoral neck metabolism and microarchitecture of aging female Wistar rats. *Sci Rep*, 7(1): 14410.

TAMMA R, COLAIANNI G, ZHU LL, DIBENEDETTO A, GRECO G, MONTEMURRO G, PATANO N, STRIPPOLI M, VERGARI R, MANCINI L, COLUCCI S, GRANO M, FACCIO R, LIU X, LI J, USMANI S, BACHAR M, BAB I, NISHIMORI K, YOUNG LJ, BUETTNER C, IQBAL J, SUN L, ZAIDI M, ZALLONE A (2009) Oxytocin is an anabolic bone hormone. *Proc Natl Acad Sci*, 106 (17): 7149-7154.

TUCKER D, FOLEY J, HAYES-BOUKNIGHT S, FENTON S (2016) Preparation of high-quality hematoxylin and eosin-stained sections from rodent mammary gland whole mounts for histopathologic review. *Toxicol Pathol*, 44(7): 1059-1064.

VILAYPHIOU N, BOUTROY S, SORNAY-RENDU E, VAN RIETBERGEN B, CHAPURLAT R (2016) Age-related changes in bone strength from HRpQCT derived microarchitectural parameters with an emphasis on the role of cortical porosity. *Bone*, 83: 233-240.

A study of macrodontia of the permanent maxillary central incisors among Delta State University students in Abraka, Nigeria

Ese Anibor, Okoro Ogheneyebrorue Godswill, Rosemary Obaremi

Department of Human Anatomy and Cell Biology, Delta State University, Abraka, Nigeria
Department of Human Anatomy, Achievers University, Owo, Ondo State, Nigeria

SUMMARY

Macrodontia (or megadontia) is a rare dental anomaly characterized by excessive enlargement of all tooth structures, and in few cases may be associated with morphological anomalies. The goal of this study was to find out how common macrodontia of the maxillary central incisors was among Delta State University students in Abraka. The Research and Ethical Committee of the Department of Human Anatomy and Cell Biology, Delta State University, Abraka, gave approval for this study. A descriptive cross-sectional survey with a representative sample of 102 subjects was conducted (58 female and 44 male). The method used was a simple random sampling technique. The age and sex of each subject were obtained using a data form, and intra-oral measurements of the mesio-distal width of the maxillary right central incisors were taken. Results were arranged according to age and sex to ascertain the occurrence of sexual dimorphism; independent sample t test and chi-square test were used as inferential statistical tools. The prevalence of macrodontia was 35.3%; there was a significant sex difference, as p value was <0.05; there was no significant difference within the age groups, as p-value was > 0.05. The mean mesio-distal width was 8.54±0.25 mm in those who did not have macrodontia and 9.63±0.54 mm in those who did have macrodontia. Macrodontia of central incisors is dominant amid Delta State University learners in Abraka.

Key words: Macrodontia – Incisors – Prevalence – Maxillary – Delta State – Nigeria

INTRODUCTION

Proliferation, condensation, adhesion, migration, differentiation, and secretion are all regulated by reciprocal and sequential interactions between epithelial and mesenchymal cells during tooth development. These events result in the development of a functional tooth organ (Sharma et al., 2014). Tooth development, also known as odontogenesis, is a complex process in which tooth cells form, grow, and erupt into the mouth.

Macrodontia (also known as Megadontia) is a rare dental condition (Dugmore, 2001; Rootkin-Gray and Sheehy, 2001; Garib and Peck, 2006). This is the excessive enlargement of all tooth structures, which

Corresponding author:
Okoro Ogheneyebrorue Godswill. Department of Human Anatomy and Cell Biology, Delta State University, Abraka, Nigeria. Phone: +2347033314640. E-mail: thomasgodswill23@gmail.com.

Submitted: October 13, 2023. **Accepted:** December 5, 2023

https://doi.org/10.52083/PVZF3619

may be associated with morphological anomalies in some cases (O'Sullivan, 2000; Dugmore, 2001; Nemes and Albert, 2006). Such anomaly can be categorized as follows: true generalized (large percentage of dentition), relative generalized (entire dentition), and isolated macrodontia of single tooth (Nemes and Albert, 2006; Dugmore, 2001). In addition, hormonal imbalances, such as pituitary gigantism, can cause generalized macrodontia (Nemes and Albert, 2006). Macrodontia of a single tooth is a rare occurrence, but it has been reported frequently in mandibular molars and premolars (Kumar et al., 2009). The incisors, third molars, and second mandibular premolars may be affected. It is defined by excessive growth of the mesiodistal and faciolingual tooth dimensions, as well as an increase in the occlusal crown area (Dugmore, 2001). Macrodontia can also be seen in pairs. Macrodontia is mostly found in incisors and canines, according to some authors (Dugmore, 2001). The goal of this study was to find out how common Macrodontia of the maxillary central incisors was among Delta State University students in Abraka.

MATERIALS AND METHODS

Most of the subjects in this present study were females (n=58, 57%), while a minority wasmales (n=44, 43%) (Fig. 1). This observational cross-sectional study was conducted in Delta State University, Abraka and included male and female students of the Delta State University, in Abraka. One hundred and two subjects (44 males and 58 females) were used and the cluster sampling technique was adopted. Information on age and sex was taken from the students within the age of 17 to 31years (Fig. 2) who gave their consent. The width of the maxillary right central incisors was determined intra-orally and recorded. The width of the maxillary right central incisors was measured as the greatest mesio-distal width between the contact points of the teeth (maxillary right central and lateral incisors). Each measurement was taken twice, then averaged so as to minimize bias error. All measurements were taken using a divider with a fixing device which was placed on a centimeter rule to take the readings. Proper precautions were taken to ensure sterilization of the divider before and after use with the aid of autoclave.

The anthropometric measurements that were taken include:

- Maxillary right central incisor width: mesio-distal width of the right maxillary central incisor.

When the mesio-distal width of the crown of the permanent central incisor is larger than 9 mm then the term macrodontia is applicable.

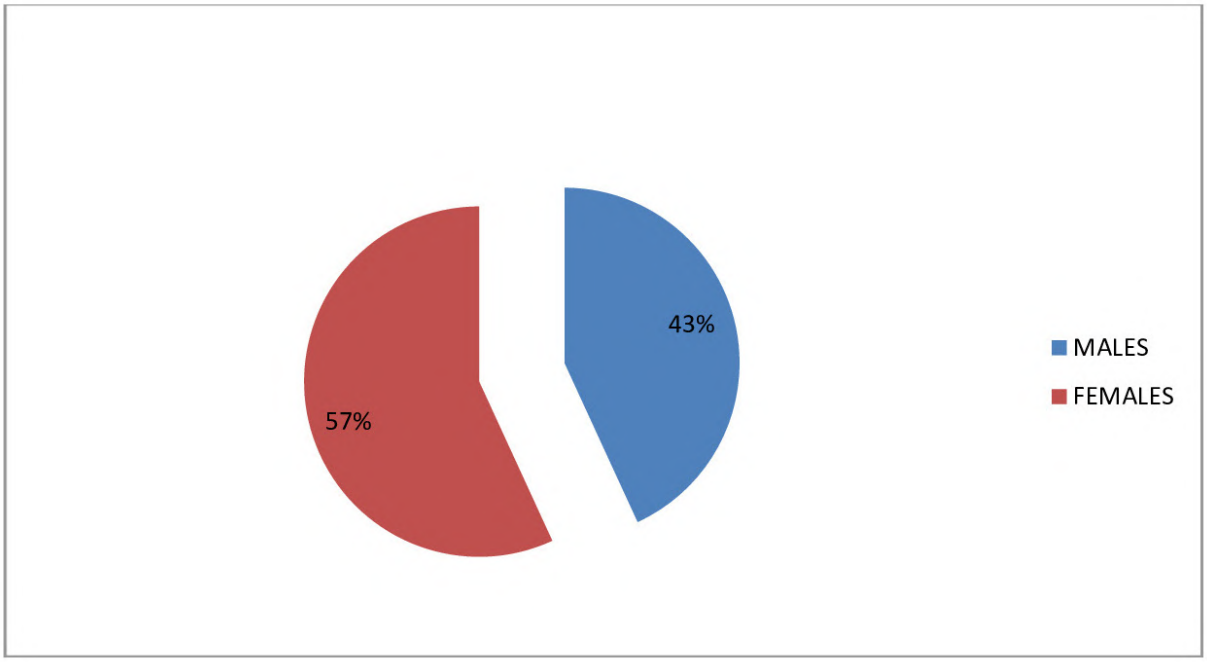

Fig. 1.- Gender of respondents.

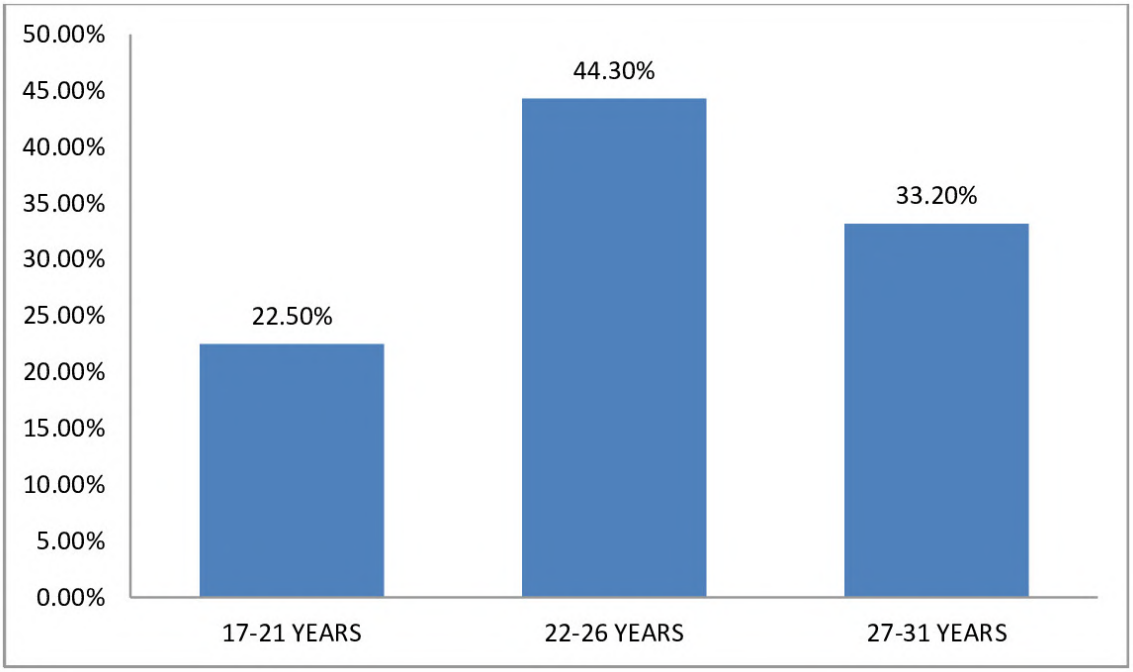

Fig. 2.- Age group of respondents.

Ethical clearance for this study was obtained from the Research and Ethical Committee of the Department of Human Anatomy and Cell Biology, Delta State University, Abraka, before the research was done. The subjects were told the nature and objectives of the study and only those who gave their consent were included in the study. The ethical clearance letter is attached in the appendix.

With the help of Statistical Package for Social Sciences (SPSS), version 22, the data were statistically analyzed using frequency distribution for descriptive statistics, with independent sample t-test, and Chi-square test employed for inferential statistics. A statistically significant P- value of less than 0.05 was used.

RESULTS

The results showed that the age range between 17 and 21years had a frequency of 23, with a percentage of 22.50%; the age range between 22 and 26 years had a frequency of 45, with a percentage of 44.3%; the age range between 27 and 31 years had a frequency of 34, with a percentage of 33.2%. Hence the age range between 22 and 26 showed the highest frequency.

The mean mesio-distal width for those not observed with macrodontia was found to be 8.54±0.25 mm, while that for those observed with macrodontia was 9.63±0.54 mm (Table 1).

Table 1. Values of mesiodistal width found in the present study.

VARIABLES	N	Mesiodistal width (mm)	T-Test	P-Value	Inference
STUDY GROUP					
Not observed Observed	66 36	8.54±0.25 9.63±0.54	-13.37	0.001	Significant
GENDER					
Male not observed Female not observed	19 47	8.69±0.23 8.48±0.30	2.71	0.009	Significant
Male observed Female observed	24 12	9.76±0.56 9.37±0.33	2.24	0.031	Significant

Table 2. Presence and frequency of macrodontia in the present study.

Variables	Frequency (%)	Chi-Square	P-value	Inference
Presence of Macrodontia				
Observed Not observed	36 (35.3) 66 (64.7)	8.82	0.003	Significant
Age group				
17-21 22-26 27-31	6 (16.7) 15 (41.7) 15 (41.7)	4.50	0.105	No significant
Presence of Macrodontia and Gender				
Male Female	24 (23.5) 12 (11.8)	24.92	0.001	Significant

The results also show that, amid the 102 subjects, macrodontia was observed in 36 persons, with a percentage of 35.3%, and was not observed in 66 persons, with a percentage of 64.7%; p-value shows that there was significant gender difference. The prevalence within the age groups is notable: the 17-to-21-year group was 6 (16.17%), the 22-to-26-year group was 15 (41.7%), and the 27-to-31-year group was 15 (41.7%), with a p-value indicating that there was no significant difference. Findings also show the prevalence within sex to be: 24 male (23.5%) and 12 female (11.8%); p-value revealed that there was a significant difference between sex (Table 2).

DISCUSSION

This present study showed that macrodontia was observed in 36 (35.3%) and was not observed in 66 (64.7%) persons. It also showed that 23.5% of males had macrodontia and 11.8% of females had macrodontia. This study further showed that there was a significant difference between sex (P-value=0.001), but there was no significant difference between the age groups (p- value=0.105). The mean values of the mesio-distal width were 8.54±0.25 mm for those not observed with macrodontia, and 9.63±0.54 mm for those observed with macrodontia.

Previous reports regarding macrodontia outcomes revealed notable difference compared to this current study. Vishnudev (2016) did research on the prevalence and distribution of selected developmental dental anomalies among patients visiting K.S.R. institute of dental science and research, and showed that out of 94,507 patients sampled (46,337 males and 48,170 females), 23 males and 18 females, had macrodontia (0.04%). P value indicated that the dental anomalies were statistically independent of sex. A similar study done by Supreetha and Sreelatha (2017) showed presence of dental anomalies in 21 (53.85%) males and 18 (46.15%) females, 5.71% with macrodontia. Vishnudev (2016) did a study on the prevalence of developmental dental anomalies among an adult population of Jazan, Saudi Arabia, and the result was remarkably lower, as macrodontia was noted in 0.6%. There was no significant sex difference with respect to prevalence of dental anomalies, as P value was > 0.05 (Almandey et al., 2010). The differences in the various studies may be due to ethnicity /race, sample size or sampling technique.

The present examination demonstrated a high dominance of macrodontia of the maxillary central incisors among Delta State University students, with a value of 35.3%. There was a notable sex distinction in the occurrence of macrodontia of the maxillary central incisors (p<0.05), but there was no significant dissimilarity between the age groups.

ACKNOWLEDGEMENTS

The author expresses gratitude to the Delta State University, Abraka, Nigeria.

REFERENCES

ALMANDEY AH, ANTHONAPPA RP, KING NM, AND FUNG CW (2010) KBG Syndrome: Clinical features and specific dental findings. *Pediat Dentistry*, 32(5): 439-444.

DUGMORE CR (2001) Bilateral macrodontia of mandibular second premolars: a case report. *Int J Pediat Dentistry*, 11(1): 69-70.

GARIB DG, PECK S (2006) Extreme variations in the shape of mandibular premolars. *Am J Orthod Dentofacial Orthop*, 130(3): 317-323.

KUMAR H, PRABHU N, CAMERON A (2009) KBG syndrome: review of the literature and findings of 5 affected patients. *Oral Surg Oral Med Oral Pathol Oral Radiol Endod*, 108(3): e72-79.

NEMES JA, ALBERTH M (2006) The Ekman-Westborg and Julin trait: report of a case. *Oral Surg Oral Med Oral Pathol Oral Radiol Endod*, 102(5): 659-662.

O´SULLIVAN EA (2000) Multiple dental anomalies in a young patient: a case report. *Int J Pediat Dentistry*, 10(1): 63-66.

ROOTKIN-GRAY VF, SHEEHY EC (2001) Macrodontia of a mandibular second premolar: a case report. *Am Soc Dentistry Children*, 68(5-6): 347-349.

SHARMA A, SHARMA S, SINGH VP (2014) Concomitant hypodontia and unusual dental anomalies in family. *J Health Specialties*, 2: 82-85.

SUPREETHA C, SREELATHA SV (2017) Vetting of selected dental anomalies associated with anterior teeth. *J Med Radiol Pathol Surg*, 4: 1-5.

VISHNUDEV PV (2016) Prevalence and distribution of selected developmental dental anomalies among patients visiting K.S.R. Institute of dental science and research, Tiruchengode. Masters thesis K.S.R. Institute of Dental Science and Research, 19-20.

The relationship of medial sigmoid depression and sigmoid notch morphology with vertical and sagittal growth patterns in Turkish population

Ali Cantürk Gürleyük[1], Defne Yalçin Yeler[2], İlknur Eninanç[2], Hasan Yeler[2]

[1] *Darıca Oral and Dental Health Center, Kocaeli, Turkiye*

[2] *Oral and Maxillofacial Radiology, Faculty of Dentistry, Sivas Cumhuriyet University, Sivas, Turkiye*

SUMMARY

Medial sigmoid depression (MSD) is an anatomical variation located just below the deepest point of the sigmoid notch (SN). The etiology of MSD is unknown. It has been reported that increased maximum bite force affects the occurrence of MSD, and vertical growth pattern affects SN morphology. The aim of this study was to investigate the effects of these malocclusions on the presence and morphology of MSD and SN, since bite force can change with vertical and sagittal growth patterns. This is the first study to investigate the effects of vertical growth pattern on the presence and morphology of MSD, and the effects of sagittal growth pattern on SN morphology. Panoramic and lateral cephalometric radiographs of a total of 634 (427 female, 207 male) patients aged from 18 to 35 years (mean 19.58) were included in this retrospective study. MSD and SN shapes, SN depth and width were evaluated on panoramic radiographs. Mann Whitney-U, Kruskal-Wallis and Chi-square tests were used for data analysis.

Sagittal and vertical growth patterns were not significantly associated with the presence and shape of MSD ($p>0.05$). SN depth was greater in individuals with class III malocclusion, and both SN depth and width were lower in hyperdivergent individuals. There was no significant relationship between SN shapes and vertical and sagittal growth patterns ($p>0.05$). SN depth is affected by both vertical and sagittal growth pattern, and SN width is affected only by vertical growth pattern. The presence of MSD was not associated with growth pattern.

Key words: Medial sigmoid depression – Sigmoid notch – Vertical growth pattern – Skeletal malocclusion – Panoramic radiography

INTRODUCTION

The sigmoid notch (SN) is a deep gap above the mandibular ramus that separates the condyle and the coronoid process (Tassoker et al., 2017). Anterior to the deepest point of the sigmoid notch, there is an anatomical variation known as medial sigmoid depression (MSD) (Carvalho et al., 2001).

Corresponding author:
Ali Cantürk Gürleyük, DDS, PhD. Darıca Oral and Dental Health Center, Kocaeli, Turkiye. Phone: +90 262 655 77 00; Fax: +90 262 655 38 00. E-mail: alicangrlyk@gmail.com - Orcid: 0000-0001-6862-9735

Submitted: October 19, 2023. **Accepted:** December 5, 2023

https://doi.org/10.52083/EDUF7397

Posterior and medial attachments of the temporal muscle are inserted into this area (Özkan and Sessiz Ak, 2021).

Although the exact etiology of MSD is unknown, it has been stated that it may be a developmental or congenital variation (Özkan and Sessiz Ak, 2021). In addition, there are various studies showing that the presence of MSD is associated with dental and skeletal sagittal malocclusions (Carvalho et al., 2001; Dalili and Mohtavipour, 2003; Sudhakar et al., 2014).

In one study, greater occurrence of MSD was reported in association with increased maximum bite force (Adisen et al., 2018). Since the MSD region is an attachment site for some temporal muscle fibers, a number of studies suggested that the presence of MSD may also be correlated with temporal muscle activity (Adisen et al., 2018; Storey, 1975). EMG (electromyography) studies have demonstrated that temporal muscle activity was lower in hyperdivergent patients and higher in hypodivergent patients compared to normodivergent subjects (García-Morales et al., 2003; Ueda et al., 1998). The sigmoid notch (SN) allows for the passage of the masseteric nerve and artery, which innervates and supplies nutrients to the masseter muscle, respectively (Ishwarkumar et al., 2019). To the best of our knowledge, there is only one study which investigated the relationship between SN morphology and vertical growth pattern, showing that hyperdivergent individuals have a more concave SN than normodivergent individuals (Ferrario et al., 1999). No study has been identified in the literature on the relationship between sagittal growth pattern and SN morphology and the association of vertical growth pattern with the presence and morphology of MSD.

Therefore, the aim of this study was to evaluate the relationship of MSD and SN with the vertical and sagittal growth patterns of the face.

MATERIALS AND METHODS

This retrospective study was approved by Sivas Cumhuriyet University Ethics Committee for Non-Invasive Studies (14.04.2021, No. 2021-04/49). All procedures followed were in accordance with the ethical standards of the responsible committee on human experimentation (institutional and national) and with the Helsinki Declaration of 1975, as revised in 2008. Due to the retrospective nature of this study, a signed informed consent was not required.

For this study, lateral cephalometric and panoramic radiographs taken before orthodontic treatment at Sivas Cumhuriyet University Faculty of Dentistry between January 2018 and January 2021 were used. A total of 634 radiographs were included in the study. The exclusion criteria were the presence of artifacts, positioning errors, cysts, any pathology involving the area of interest and patients with prior orthodontic treatment.

The Orthopantomograph OP200D (Instrumentarium Dental, Tuusula, Finland) device was used to obtain the panoramic radiographs. The radiographs were taken at 66 kVp, 10 mA dose values and in P1 mode, including the temporomandibular joint. Lateral cephalometric radiographs were taken using Ortoceph OC200D (Instrumentarium Dental, Tuusula, Finland) device at dose parameters of 85 kVp and 13 mA.

Images were reviewed on a 8 GB RAM computer with a 23.6-inch Full HD IPS LED screen, Intel i5 processor, Windows 7 operating system and Cliniview 10.1 software in a semi-lit and quiet room. Measurements and examinations on all radiographs were examined by a researcher with 4 years of experience. Intra-observer agreement was assessed by evaluating 158 (25%) randomly selected radiographs two weeks apart.

ANB and SN-GoGn angles were used to determine sagittal and vertical skeletal patterns on cephalometric radiographs. Sagittal relationships of the jaws were classified as Class I ($0^{o}<ANB<4^{o}$), Class II ($ANB>4^{o}$) and Class III ($0^{o}<ANB$). The vertical growth pattern was classified as hypodivergent ($SN\text{-}GoGn<28^{o}$), normodivergent ($28^{o}<SN\text{-}GoGn<36^{o}$) and hyperdivergent ($SN\text{-}GoGn>36^{o}$) (Schudy, 1965). MSD location was evaluated separately for the right and left ramus, and MSD shapes were classified as semilunar, teardrop, circular, and triangular, as described by Carvalho et al. (2001) (Fig. 1).

SN width (SNW) and SN depth (SND) measurements were made on panoramic radiographs as

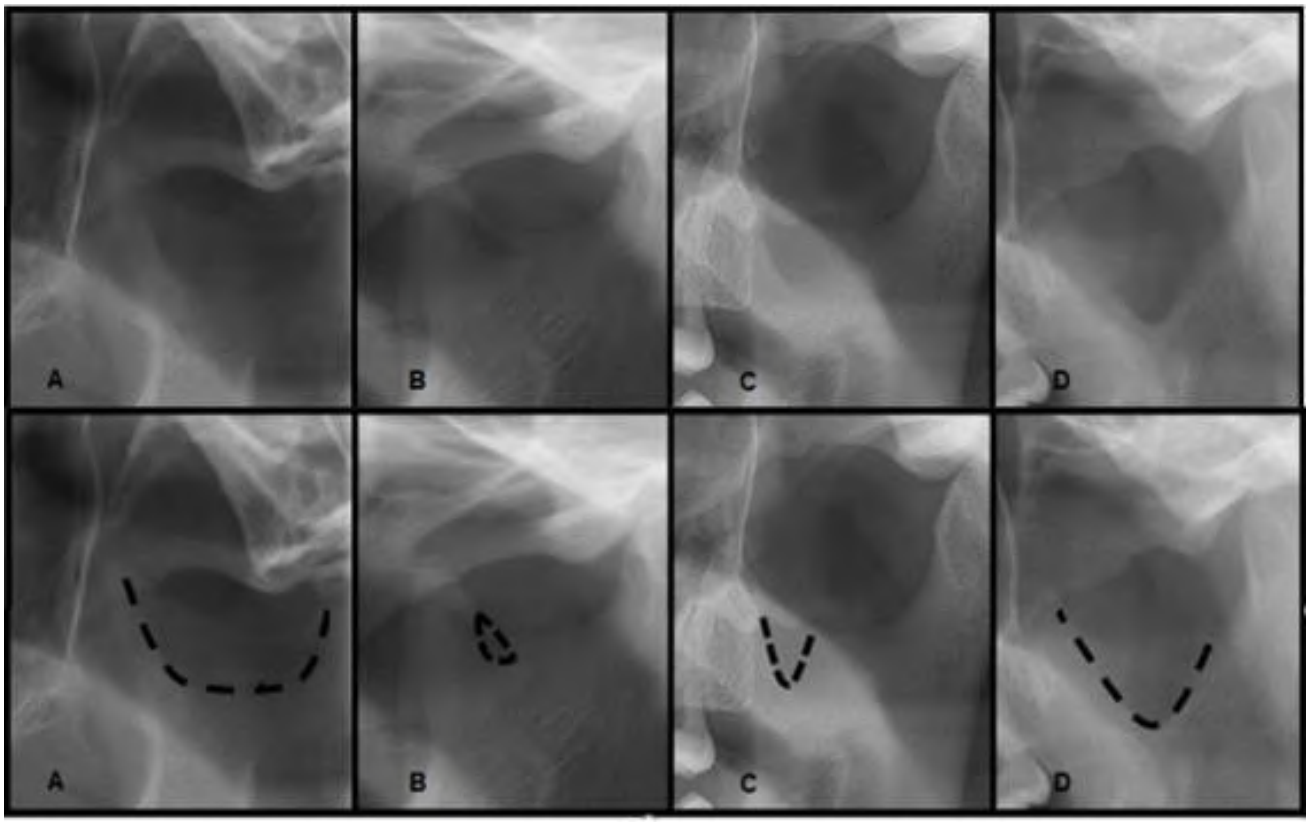

Fig. 1.- MSD Shapes. **A**: Semilunar, **B**: Circular, **C**: Teardrop, **D**: Triangular.

millimeters (mm). SNW was considered as the distance between the highest points of the condyle and coronoid process. SND was measured as the length of the perpendicular line drawn from the SN width line to the deepest point of SN (Fig. 2).

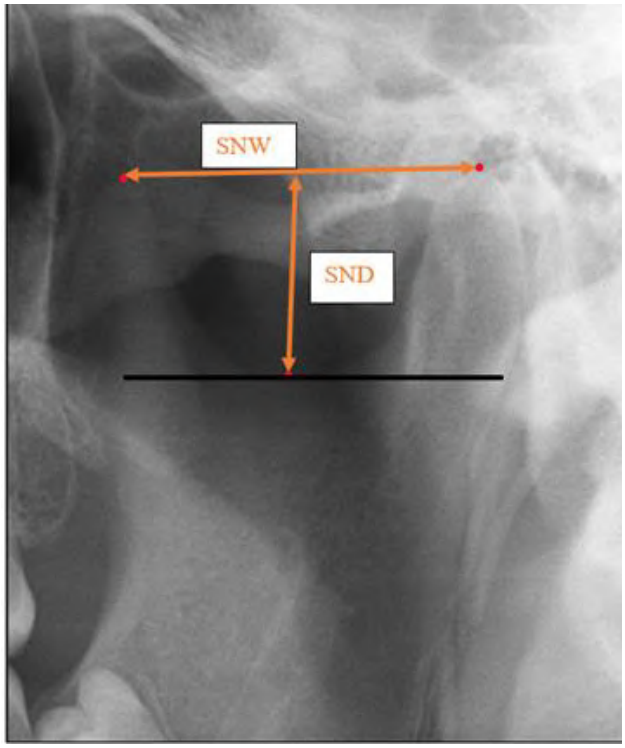

Fig. 2.- Measurement of SN depth (SND) and SN width (SNW).

SN morphology was classified as round, wide and sloping, as reported by Shakya et al. (2013) (Fig. 3).

Statistical analysis

The study data were analyzed using SPSS software package, version 22.0 (IBM Corp., Armonk, NY, USA). Chi-square test was used for categorical variables and Kruskal-Wallis test for numerical data. Pairwise comparisons were made using Dunn's test. Mann-Whitney U test was used to examine the distribution of measurements by sex. Intra-observer agreement was assessed using Kappa statistics and Intra-class Correlation Coefficient. A p value lower than 0.05 was considered statistically significant.

RESULTS

The mean age of 634 patients included in the study was 19.58 ± 3.58 years (mean ± SD). 427 (67.4%) individuals were female and 207 (32.6%) were male. Intra-observer agreement was found to be excellent (0.852-0.988) for categorical and numerical variables.

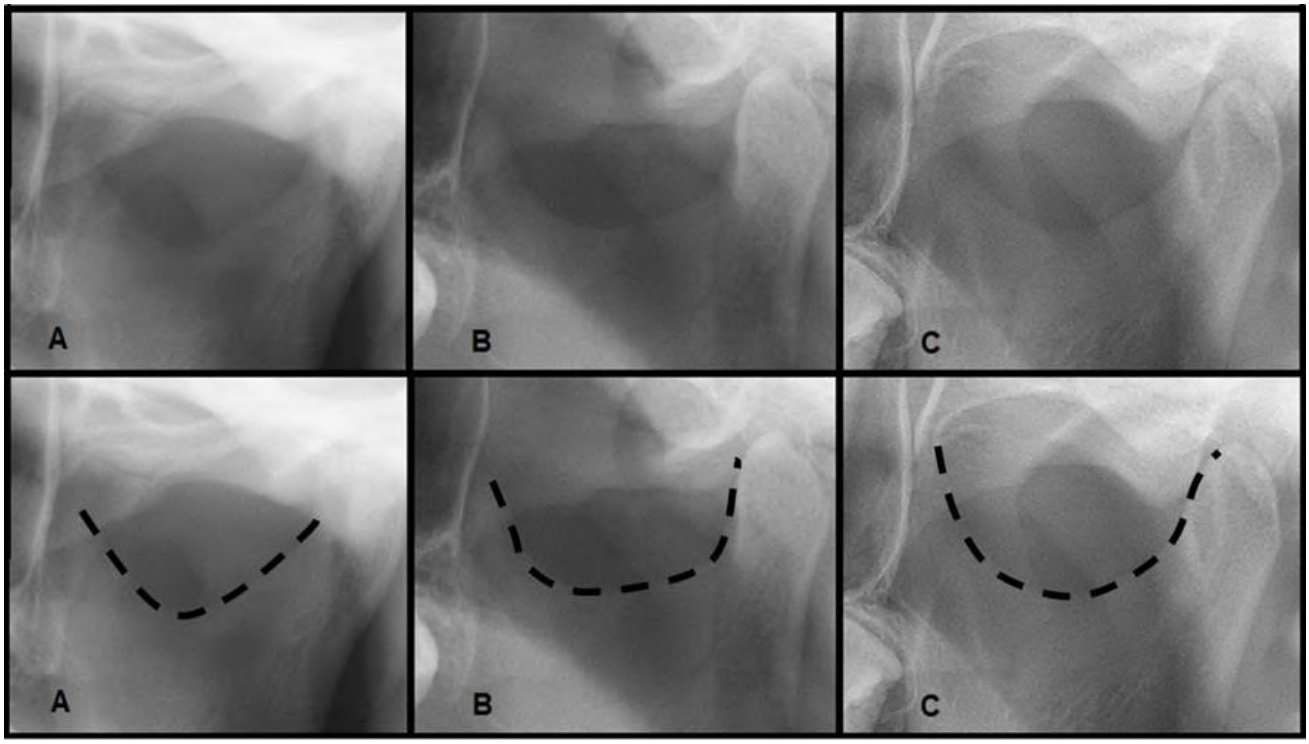

Fig. 3.- SN shapes. **A**: Sloping, **B**: Wide, **C**: Round.

When the vertical growth pattern was examined on cephalometric radiographs, hypodivergent growth pattern was observed in 142 (22.4%) individuals, normodivergent growth pattern in 251 (39.6%) individuals and hyperdivergent growth pattern in 241 (38%) individuals (Table 1). With regard to sagittal growth pattern, class-I relationship was observed in 298 (47%) individuals, class-II relationship in 238 (37.5%) individuals and class-III relationship in 98 (15.5%) individuals.

MSD was detected in 138/634 (21.8%) radiographs included in the study. The presence of MSD was not significantly associated with sex and sagittal/vertical growth patterns (p>0.05) (Table 1). With respect to MSD location, unilateral location was more common, and sex x and sagittal/vertical growth pattern did not show an effect on unilateral and bilateral location (p>0.05) (Table 1).

Among four MSD shapes (semilunar, triangular, circular and teardrop), semilunar shape was the most common (46.3%), followed by triangular (29.2%), circular (13.6%) and teardrop (10.7%) shapes, respectively (Table 2). MSD shape was not significantly associated with sex and sagittal/vertical growth pattern (p>0.05) (Table 2).

Table 1. MSD presence and location by sex and sagittal/vertical growth pattern

	Present	**Unilateral Right**	**Unilateral Left**	**Bilateral**	**p**
Male (n=207)	37 (17.9%)	9 (4.3%)	12 (5.8%)	16 (7.7%)	0.121
Female (n=427)	101 (%23.7)	32 (7.5%)	18 (4.2%)	51 (11.9%)	
Hypodivergent (n=142)	32 (22.5%)	10 (7%)	10 (7%)	12 (8.5%)	0.651
Normodivergent (n=251)	51 (20.3%)	17 (6.8%)	9 (3.6%)	25 (10%)	
Hyperdivergent (n=241)	55 (22.8%)	14 (5.8%)	11 (4.6%)	30 (12.4%)	
Class I (n=298)	58 (19.5%)	17 (5.7%)	14 (4.7%)	27 (9.1%)	0.741
Class II (n=238)	60 (25.2)	17 (7.1%)	13 (5.5%)	30 (12.6%)	
Class III (n=98)	20 (20.4%)	7 (7.1%)	3 (3. %1)	10 (10.2%)	
Total (n=634)	138 (21.8%)	41 (6.5%)	30 (4.7%)	67 (10.6%)	

Chi-square test

**Statistically significant if p<0.05*

Table 2. Distribution of MSD shapes by sex and sagittal/vertical growth pattern

		Semilunar	Triangular	Circular	Teardrop	p
Male (n=207)	Right	17 (68%)	4 (16%)	1 (4%)	3 (12%)	0.071
	Left	14 (50%)	5 (17.9%)	6 (21.4%)	3 (10.7%)	0.355
Female (n=427)	Right	37 (44.6%)	29 (34.9%)	12 (14.5%)	5 (6%)	0.071
	Left	27 (39.1%)	22 (31.9%)	9 (13%)	11 (15.9%)	0.355
Hypodivergent (n=142)	Right	14 (63.6%)	5 (22.7%)	2 (9.1%)	1 (4.5%)	0.863
	Left	9 (40.9%)	7 (31.8%)	3 (13.6%)	3 (13.6%)	0.791
Normodivergent (n=251)	Right	19 (45.2%)	15 (35.7%)	5 (11.9%)	3 (7.1%)	0.863
	Left	14 (41.2%)	8 (23.5%)	8 (23.5%)	4 (11.8%)	0.791
Hyperdivergent (n=241)	Right	21 (47.7%)	13 (29.5%)	6 (13.6%)	4 (9.1%)	0.863
	Left	18 (43.9%)	12 (29.3%)	4 (9.8%)	7 (17.1%)	0.791
Class I (n=298)	Right	21 (47.7%)	15 (34.1%)	5 (11.4%)	3 (6.8%)	0.924
	Left	18 (43.9%)	12 (29.3%)	2 (4.9%)	9 (22%)	0.152
Class II (n=238)	Right	26 (55.3%)	12 (25.5%)	5 (10.6%)	4 (8.5%)	0.924
	Left	17 (39.5%)	13 (30.2%)	10 (23.3%)	3 (7%)	0.152
Class III (n=98)	Right	7 (41.2%)	6 (35.3%)	3 (17.6%)	1 (5.9%)	0.924
	Left	6 (46.2%)	2 (15.4%)	3 (23.1%)	2 (15.4%)	0.152
Total (n=1264)		95 (46.3%)	60 (29.2%)	28 (13.6%)	22 (10.7%)	

Chi-square test.
**Statistically significant if p<0.05*

SND and SNW were significantly associated with vertical growth pattern on both right and left sides (p<0.05). Right and left SND were greatest in hypodivergent individuals, followed by normodivergent and hyperdivergent individuals, respectively (p<0.05).

When SNW measurements were compared, it was seen that hyperdivergent individuals had shorter SNW than hypodivergent individuals (p<0.05) (Table 3).

There was a significant relationship between sagittal growth pattern and SND (p<0.05), and class-III individuals had deeper SN than class-II individuals (p<0.05). No significant association was found between sagittal growth pattern and SNW (p>0.05) (Table 3). When the morphometric measurements (SND and SNW) were compared between the sexes, males showed higher values for all parameters (p<0.05) (Table 3).

There was no statistically significant difference among SN shapes in terms of vertical and sagittal growth patterns (p>0.05). SN morphology was round in 64.2%, wide in 19.8% and sloping in 16% of the individuals. Round type was more common in males (69.1%) and wide type was more common in females (22.3%), and this difference was significant for right SN (p<0.05) (Table 4).

DISCUSSION

Studies conducted in different populations reported a widely variable prevalence of MSD, ranging from 5% to 70% (Carvalho et al., 2001; Divya and Mahima, 2006; Honing, 1991; Özkan and Sessiz-Ak, 2021). Previous studies have shown that the presence of MSD is much higher on dry human mandibles than on panoramic radiographs (Byung-Cheol, 1991; Carvalho et al., 2001; Divya and Mahima, 2006; Langlais et al., 1983). While Langlais et al. (1983) explained this finding by the fact that the MSD region may not always be imaged due to focal trough of the panoramic radiography device, Carvalho et al. (2001) argued that the difference in anatomical, and radiographic examinations may be due to the inability to adequately visualize the relatively shallow depressions rather than the image layer. However, it has also been suggested that this may be caused by superposition of anatomical structures such as the lateral

Table 3. Morphometric parameters by sex and sagittal and vertical growth patterns

	SN Depth (SND)		SN Width (SNW)	
	Right	**Left**	**Right**	**Left**
Male	13.03±1.98	13.54±2.40	28.85±3.20	28.77±4.30
Female	12.53±1.94	12.64±1.87	27.98±3.24	27.68±3.33
p#	**<0.001***	**<0.001***	**0.004***	**<0.001***
Hypodivergent	13.48±1.73	13.40±1.76	28.87±3.03	28.61±4.03
Normodivergent	12.84±1.84	13.03±2.05	28.72±3.17	28.24±3.59
Hyperdivergent	12.33±2.13	12.54±2.25	27.41±3.30	27.49±3.57
p§	**<0.001***	**<0.001***	**<0.001***	**0.008***
Class I	12.91 2.16	13.00 2.10	28.34 3.44	28.13 3.54
Class II	12.47 1.61	12.63 2.14	28.32 2.93	27.88 3.63
Class III	13.16 2.13	13.42 1.86	27.86 3.38	28.13 4.32
p§	**0.003***	**<0.001***	0.229	0.830

 # Mann-Whitney U test
§ Kruskal-Wallis Test
** Statistically significant if p<0.05*

pterygoid plate, air space of the nasopharynx or soft palate (Byung-Cheol, 1991). Although the use of panoramic radiography allows a larger sample size to be studied, it may have led to underestimation of the MSD prevalence in the current study as well. However, since this will affect all groups similarly in terms of vertical (hyperdivergent, normodivergent, hypodivergent) and sagittal growth patterns (classes I, II, III), it is believed that its effect on the results would be minimal. The use of CBCT in future studies would provide more valid results in terms of true MSD prevalence.

Table 4. SN shapes by sex and sagittal/vertical growth pattern

		Round	**Sloping**	**Wide**	**p**
Male (n=207)	Right	148 (71.5%)	32 (15.5%)	27 (13%)	0.008*
	Left	138 (66.7%)	35 (16.5%)	34 (16.4%)	0.340
Female (n=427)	Right	262 (61.4%)	65 (15.2%)	100 (23.4%)	0.008*
	Left	265 (62.1%)	71 (16.7%)	91 (21.3%)	0.340
Hypodivergent (n=142)	Right	93 (65.5%)	21 (14.8%)	28 (19.7%)	0.646
	Left	93 (65.5%)	25 (17.6%)	24 (16.9%)	0.819
Normodivergent (n=251)	Right	157 (62.5%)	45 (17.9%)	49 (19.5%)	0.646
	Left	158 (62.9%)	44 (17.5%)	49 (19.5%)	0.819
Hyperdivergent (n=241)	Right	160 (66.4%)	31 (12.9%)	50 (20.7%)	0.646
	Left	152 (63.1%)	37 (15.4%)	52 (21.6%)	0.819
Class I (n=298)	Right	189 (63.4%)	47 (15.8%)	62 (20.8%)	0.580
	Left	183 (61.4%)	53 (17.8%)	62 (20.8%)	0.657
Class II (n=238)	Right	151 (63.4%)	36 (15.1%)	51 (21.4%)	0.580
	Left	154 (64.7%)	41 (17.2%)	43 (18.1%)	0.657
Class III (n=98)	Right	70 (71.4%)	14 (14.3%)	14 (14.3%)	0.580
	Left	66 (67.3%)	12 (12.2%)	20 (20.4%)	0.657
Total (n=1268)		813 (64.1%)	203 (16%)	252 (19.9%)	

Chi-square Test
**Statistically significant if p<0.05*

In a study by Özkan and Sessiz-Ak (2021) on 1000 panoramic radiographs from a representative Turkish population, the prevalence of MSD was reported at 23.4%, with a significant increase in the prevalence with age ($p<0.05$). In the present study, the prevalence of MSD was 21.8%, which is similar to that reported by Özkan and Sessiz-Ak (2021). The large differences among populations with regard to the presence of MSD suggest that genetic factors may also be involved. In this study, the age range was narrow, precluding the ability to examine the relationship between MSD and age.

The association between temporal muscle activity and the vertical growth pattern of the face has been reported in the literature, with EMG studies showing reductions in temporal muscle activity and maximum bite force in hyperdivergent individuals, and increases thereof in hypodivergent individuals (García-Morales et al., 2003; Ueda et al., 1998). It has also been stated that muscle activity may affect the presence and shape of the MSD, due to the attachment of some of the temporal muscle fibers to the MSD area (Adisen et al., 2018; Al-Sadhan, 2021; Storey, 1975). The aforementioned results led to the question as to whether MSD occurs more commonly in hypodivergent patients with greater temporal muscle activity.

The present study attempted to find an answer to this question and no significant association was found between the vertical growth of the face and the presence of MSD. This suggests that, contrary to what is expected, temporal muscle activity may not strongly affect the shape of MSD. However, the significant increase in the prevalence of MSD in individuals with high maximum bite force (Adisen et al., 2018) suggests that environmental factors and masticatory forces may also be involved in the occurrence of MSD.

Very few studies in the literature evaluated the relationship between the presence of MSD and sagittal skeletal and dental malocclusions and yielded differential results (Carvalho et al., 2001; Dalili and Mohtavipour, 2003; Sudhakar et al., 2014; Adisen et al., 2018) In only one study, the prevalence of MSD was found to be higher in individuals with class II malocclusion, which is related to the sagittal growth pattern ($p<0.05$) (Carvalho et al., 2001), with no significant associations found in other studies (Dalili and Mohtavipour, 2003; Sudhakar et al., 2014; Adisen et al., 2018). However, in the current study, the presence of MSD was more common in individuals with skeletal class-II malocclusion ($p>0.05$), albeit non-significantly. In addition, the presence of MSD was not be associated with vertical malocclusion and sex, and a comparison could not be made because this is the first study to investigate this relationship. In the presence of MSD, this should be taken into consideration before orthognathic surgery, because since the bone structure in this region is very thin, there is an increased risk of complications, and the fixation of the fracture line cannot be achieved.

Carvalho et al. (2001) reported that the most common MSD morphology is the triangular shape. Contrastingly, separate studies have reported that the most common form of MSD is the semilunar type (Dalili and Mohtavipour, 2003; Divya and Mahima, 2006; Sudhakar et al., 2014; Adisen et al., 2018). Sudhakar et al. (2014) reported that there was no significant relationship between MSD shapes and sagittal growth pattern in their study on 300 panoramic radiographs. In line with former studies, the most common MSD morphology was semilunar type in the present study, with no significant association of MSD shapes with sex, and vertical and sagittal growth patterns.

To the best of our knowledge, there is only one study that investigated the relationship between SN morphology and vertical growth pattern. In their morphological study using Fourier analysis on lateral cephalometric radiographs of 45 girls, Ferrario et al. (1999) reported that more concave SN was observed in hyperdivergent individuals. In contrast, SN shapes did not differ significantly in relation to vertical growth pattern in the current study ($p>0.05$). On the other hand, as shown by SND and SNW measurements, sigmoid notches were significantly shallower and narrower in hyperdivergent individuals and significantly deeper and wider in hypodivergent individuals, which are consistent with the findings reported by Ferrario et al. (1999). Additionally, it was observed that the morphometric properties of SN are affected by the vertical growth pattern to a greater extent compared to its morphological features.

In the present study, no association was found between the SN morphology and the sagittal growth pattern, and a comparison could not be made due to lack of similar studies. However, SND was greater in individuals with class III malocclusion ($p<0.05$). This may be due to the increased condyle height in class III individuals as demonstrated by various studies (Hasebe et al., 2019; Noh et al., 2021).

In their study on 149 panoramic radiographs and 51 dry mandibles from the South African and Indian populations, Ishwarkumar et al. (2019) reported that the width of SN was greater in males ($p<0.05$). In a study from Saudi Arabia on 240 panoramic radiographs, males (14.01 mm) were found to have a deeper sigmoid notch than females (13.75 mm) ($p<0.05$) (Al-Gunaid, 2020). Likewise, in the current study, SND and SNW were found to be significantly higher in males ($p<0.05$), and to the best of our knowledge, this is the first study to report the dimensions of SN in the Turkish population.

CONCLUSION

In conclusion, SN depth is affected by both vertical and sagittal growth patterns, and SN width is affected only by vertical growth pattern. The presence of MSD was not found to be associated with growth pattern. Further studies in which the relationship of MSD with vertical and sagittal growth patterns is investigated in a wider range of age groups and muscle activities are evaluated using EMG would provide valuable findings.

ACKNOWLEDGEMENTS

The authors thank to Dr. Esra Gültürk for support on statistical analysis.

Author Contributions

All authors have contributed to writing and reviewing the manuscript, conceptualizing of the work. In addition, ACG acquired and analyzed data; DY and IE overviewed the coordination of the work.

REFERENCES

ADISEN MZ, OKKESIM A, MISIRLIOGLU M (2018) A possible association between medial depression of mandibular ramus and maximum bite force. *Folia Morphol*, 77(4): 711-716.

AL-GUNAID TH (2020) Sex-related variation in the dimensions of the mandibular ramus and its relationship with lower third molar impaction. *J Taibah Uni Med Sci*, 15(4): 298-304.

AL-SADHAN R (2021) CT Study of the medial depression of the human mandibular ramus. *Int J Morphol*, 39(6): 1570-1574.

BYUNG-CHEOL K (1991) The medial sigmoid depression: Its anatomic and radiographic considerations. *J Korean Acad Oral Maxillofac Radiol*, 21(1): 7-13.

CARVALHO IMM, DAMANTE JH, TALLENTS RH, RIBEIRO-ROTTA RF (2001) An anatomical and radiographic study of medial depression of the human mandibular ramus. *Dentomaxillofac Radiol*, 30(4): 209-213.

DALILI Z, MOHTAVIPOUR ST (2003) Frequency of medial sigmoid depression in panoramic view of orthodontic patients based on facial skeletal classification. *J Guilan Uni Med Sci* 12(45): 16-23.

DIVYA A, MAHIMA VG (2006) An anatomic and radiological study of medial sigmoid depression in human mandibular ramus. *Rajiv Gandhi Uni Health Sci*. Dental Thesis Guide.

FERRARIO VF, SFORZA C, DE FRANCO DJ (1999) Mandibular shape and skeletal divergency. *Eur J Orthod*, 21(2): 145-153.

GARCÍA-MORALES P, BUSCHANG PH, THROCKMORTON GS, ENGLISH JD (2003) Maximum bite force, muscle efficiency and mechanical advantage in children with vertical growth patterns. *Eur J Orthod*, 25(3): 265-272.

HASEBE A, YAMAGUCHI T, NAKAWAKI T, HIKITA Y, KATAYAMA K, MAKI K (2019) Comparison of condylar size among different anteroposterior and vertical skeletal patterns using cone-beam computed tomography. *Angle Orthod*, 89(2): 306-311.

HONING JF (1991) Identificacion anatomica de radiolucencias subsemilunares circulares en la rama ascendente mandibular. *Electromedica*, 59: 58-63.

ISHWARKUMAR S, PILLAY P, DE GAMA BZ, SATYAPAL KS (2019) Osteometric and radiological study of the mandibular notch. *Int J Morphol*, 37(2): 491-497.

LANGLAIS RP, GLASS BJ, BRICKER SL, MILES DA (1983) Medial sigmoid depression: A panoramic pseudoforamen in the upper ramus. *Oral Surg Oral Med Oral Pathol*, 55(6): 635-638.

NOH KJ, BAIK HS, HAN SS, JANG W, CHOI YJ (2021) Differences in mandibular condyle and glenoid fossa morphology in relation to vertical and sagittal skeletal patterns: A cone-beam computed tomography study. *Korean J Orthod*, 51(2): 126-134.

ÖZKAN G, SESSİZ-AK R (2021) Evaluation of the frequency of medial sigmoid depression using panoramic radiographs: A retrospective study. *J Dent Fac Atatürk Uni*, 30(4): 552-556.

SCHUDY FF (1965) The rotation of the mandible resulting from growth: Its implications in orthodontic treatment. *Angle Orthod*, 35(1): 36-50.

SHAKYA S, ONGOLE R, NAGRAJ SK (2013) Morphology of coronoid process and sigmoid notch in orthopantomograms of South Indian population. *World J Dent*, 4(1): 1-3.

STOREY E (1975) Growth and remodeling of bone and bones. Role of genetics and function. *Dent Clin N Am*, 19(3): 443-455.

SUDHAKAR S, NAVEENKUMAR B, PRABHAT MPV, NALINI J (2014) Characteristics of medial depression of the mandibular ramus in patients with orthodontic treatment needs: A panoramic radiography study. *J Clin Diag Res*, 8(11): ZC100-ZC104.

TASSOKER M, KABAKCI ADA, AKIN D, SENER S (2017) Evaluation of mandibular notch, coronoid process, and mandibular condyle configurations with cone beam computed tomography. *Biomed Res*, 28(19): 8327-8335.

UEDA HM, ISHIZUKA Y, MIYAMOTO K, MORIMOTO N, TANNE K (1998) Relationship between masticatory muscle activity and vertical craniofacial morphology. *Angle Orthod*, 68(3): 233-238.

Expression analysis of leptin in nephrogenesis and renal carcinogenesis

Priyanka Parmesh[1], Roshni Sadashiv[2], U.S. Dinesh[3], Anil Bargale[4]

[1] *Dept. of Pathology, SDM University, SDM College of Medical Sciences & Hospital, Dharwad, India*
[2] *Dept. of Anatomy, SDM University, SDM College of Medical Sciences & Hospital, Dharwad, India*
[3] *Dept. of Pathology, SDM College of Medical Sciences& Hospital, Dharwad, India*
[4] *Dept. of Biochemistry, SDM College of Medical Sciences& Hospital, Dharwad, India*

SUMMARY

The complex phenomenon of renal development involves several signaling molecules. Any alteration in the developmental process could largely influence the organogenesis, thus predisposing to several adulthood diseases. Leptin is a pleiotropic gene secreted by adipose cells. However, the purview of its actions is much beyond merely the extent of human adipose reserve. It regulates several cellular mechanisms such as cell proliferation, inflammation, vasculogenesis, and the production of collagen fibres. Further leptins are thought to play a putative role in embryogenesis and tumorigenesis. The aim of thIS study was to investigate the localization of the protein in fetal and cancer kidney in an attempt to understand the role of the protein in fetal kidney development and in renal cancer.

Leptin expression was evaluated by subjecting tissue sections from paraffin-embedded blocks of renal tissues (fetal, adult and cancer) to immunohistochemistry staining. The tissues were scored based on the staining pattern and percentage of immunoreactive cells. The tissues were subjected to haematoxylin and eosin stain before performing immunohistochemistry. The images were analyzed and photographed. Mild staining for leptin was observed in the tubules of fetal and adult kidneys. Mild to moderate staining was seen in membranes of renal cell carcinoma tissues. It appears such that leptin may not be a key factor or rather a temporary factor in the developmental process of the kidney. The low levels of leptin in normal adult renal tissues may be physiologically significant. The role of leptin in the renal cell carcinoma progression is sceptible.

Keywords: Leptin – Renal cell carcinoma – Kidney – Nephrogenesis – Immunohistochemistry

INTRODUCTION

Leptin, a16kDa hormone is produced in the intrauterine life. Its varying concentration in the systemic tissues has been identified in the foetal and neonatal life in mice (Reynolds and Vickers,

Corresponding author:
Dr. Roshni Sadashiv. Dept. of Anatomy, SDM University, SDM College of Medical Sciences & Hospital, Dharwad, Karnataka, India. Phone: +91 9480242975; Fax: 0836 2461651. E-mail: drroshnisadashiv@gmail.com

Part of this work was presented at the meeting: 'International Conference on Biomedical and Clinical Research', organized by SHRI Dharmasthala Manjunatheshwara University in Dharwad, India on November 21-22, 2022.

Submitted: November 2, 2023. **Accepted:** December 20, 2023

https://doi.org/10.52083/MYAZ1507

2019) Physiologically the hormone is greatly associated with appetite and body mass index. However, the purview of its actions is much beyond merely the extent of human adipose reserve. It is thought to be involved in the biological processes of cell proliferation, angiogenesis, and reproduction. Leptin plays a role in implantation and is also produced by the trophoblastic cells indicated by its presence in the placenta, amniotic fluid, and umbilical cord (Biesianda et al., 2016).

Though leptin is primarily secreted by the adipocytes of white adipose tissue, its localization and function in other gestational tissues still need to be elucidated (Lappas et al., 2005). Leptin receptors have been localized in the central nervous tissue, lung tissue, and several other peripheral tissues (Prince et al., 2007). The definitive human kidney begins its development in the fifth week of gestational life. It is formed by an interaction between the metanephric blastema cells and a diverticulum of the mesonephric duct, the ureteric bud[5]. Several genes have been identified by experimental studies on cell lines and animal models, which are responsible for the cascade of events during nephrogenesis. Any mutations in the signaling molecules or disruptions in the epigenetic pathway could largely dispose the adult kidney to diseases such as cancer (Patel and Dressler, 2013). Our previous work on foetal renal tissues has highlighted certain less-known genes in nephrogenesis and renal cancer (Sadashiv et al., 2019).

Owing to the different cell types in the human kidney, the current study aimed to localize the expression status of leptin in foetal, adult, and cancer kidneys to check if leptin may have a role in kidney development and cancer.

MATERIALS AND METHODS

Representative samples of autopsied foetal kidney n=30, adult kidney (cadaveric) n=30, and renal cell carcinoma (biopsy tissues) n=30, consisted of paraffin-embedded tissue blocks collected from the Department of Pathology after approval from the institutional review board. Prior to performing immunohistochemistry, the tissues were subjected to conventional H&E staining. The histogenesis of developing foetal kidneys at different gestational ages and the diagnostic confirmation of the renal cancer tissues were done by clinical pathologists.

Four µm thick sections were taken on positively charged slides. Overnight incubation at 37ºC and deparaffinization with repeated washes of xylene (10 mins each) was followed by rehydration of tissues with graded alcohol. The slides were then washed with running water (10 mins) and distilled water (5 mins), following which antigen retrieval with citrate buffer at 95ºC was done and cooled at room temperature.

Peroxidase block was carried out for 10-15 mins and washed in phosphate buffer solution (PBS) for 5 mins and incubated with primary antibody (anti-leptin rabbit polyclonal antibody (in 1: 250 dilutions with reagent –antibody diluents as per manufacturer's instructions, {Wuhan Fine Biotech Co. Ltd, Wuhan, China} for 45 min. Subsequently, tissues were incubated with poly excel target binder for 15 to 20 mins and washed with PBS for 5 mins. Incubation was done with H.R.P for 15 to 20 mins, washed with PBS for 5 mins, and developed with DAB (diaminobenzidine) chromogen for 5-8 mins. Sections were counterstained with haematoxylin after washing with running water. Every staining run contained a slide treated with tris buffer in place of the leptin antibody as a negative control. Sections of benign breast lesion with ductal epithelial cells displaying cytoplasmic positivity was used as positive controls.

Immunoreactivity score (IRS)-classification scoring systems were used as shown in Table 1 (Fuhrman et al., 1982). For statistical purposes, the results of IRS scores were divided as follows:

Negative, mild staining = negative expression of leptin

Moderate, strong staining = positive expression of leptin

Table 1. Leptin expression in PCT cells and RCC.

Group	0	+1	+2	+3	P-value
Fetal Kidney (n=30)	27	3	—	—	
Adult Kidney (n=30)	0	22	8	—	<0.0001
RCC (n=30)	0	10	15	5	

IHC scoring for leptin antibody (0=Absent, +1=Mild, +2= Moderate, +3=Strong)

RESULTS

Expression of leptin in fetal renal tissues: as depicted in Fig. 1a and 1b, the histological sections of fetal kidney at early gestational ages showed cortex with precursors of mature glomeruli such as the renal vesicle (rv), comma, S-shaped bodies in the nephrogenic zone, and branching ureteric bud (ub). The deeper cortex demonstrated sections of developing proximal convoluted tubules (PCT), distal convoluted tubules (DCT), and thick ascending limbs of loops of Henle (LOH) (Fig. 2a, 2b). The medulla presented with developing collecting duct and blood vessels. Beyond 36 weeks of gestation, definitive glomeruli, and mature forms of the renal tubules could be demonstrated. Immunohistochemistry staining with anti-leptin antibody showed mild staining (+1) n=3 to the absence of immunoreactive cells in the PCTs' of fetal kidney from 14 weeks to beyond 36 weeks of gestation (p=<0.0001) (Fig. 2c, 2d). However, all the other cellular components of the kidneys from 14 weeks to 39 weeks were immunonegative (Figs. 1b, 2c, 2d).

Expression of leptin in adult renal tissue: adult PCT were identified by the presence of highly eosinophilic brush-bordered cuboidal epithelial cells with small lumens as shown in Figure 3a and 3b as stained with hematoxylin and eosin stain. The adult renal kidney showed mild immunopositivity in the cytoplasm of proximal convoluted tubules (+1) n=22 (Fig. 3c, 3d). The cells of the glomeruli (mesangial, podocytes, and endothelial cells), juxta glomerular apparatus, distal convoluted tubules, and loop of Henle cells were found to be immunonegative to leptin antibodies.

Expression of leptin in renal cell cancer tissue: The H and E stain showed various grades of conventional renal cell carcinoma. (Fig. 4a, 4b, 4c). The tissues were graded according to Fuhrman et al (Fuhrman et al., 1982). The conventional renal carcinoma tissues of clear cells and papillary variants showed mild to moderate cytosolic and membranous expression of leptin (+2) (n= 15), p=<0.0001) as demonstrated in Figs. 4d, 4e, 4f, 4g, 4h and 4i. Strong expression of leptin was found in fewer tissues of grade 3 renal cell carcinomatous tissues (n=5) (Fig. 4i). The proximal convoluted tubules in the normal renal cortical area adjacent to the carcinomatous tissue showed moderate staining for leptin (+2) as shown in Fig. 4d. The summary of the results is shown in Table 1.

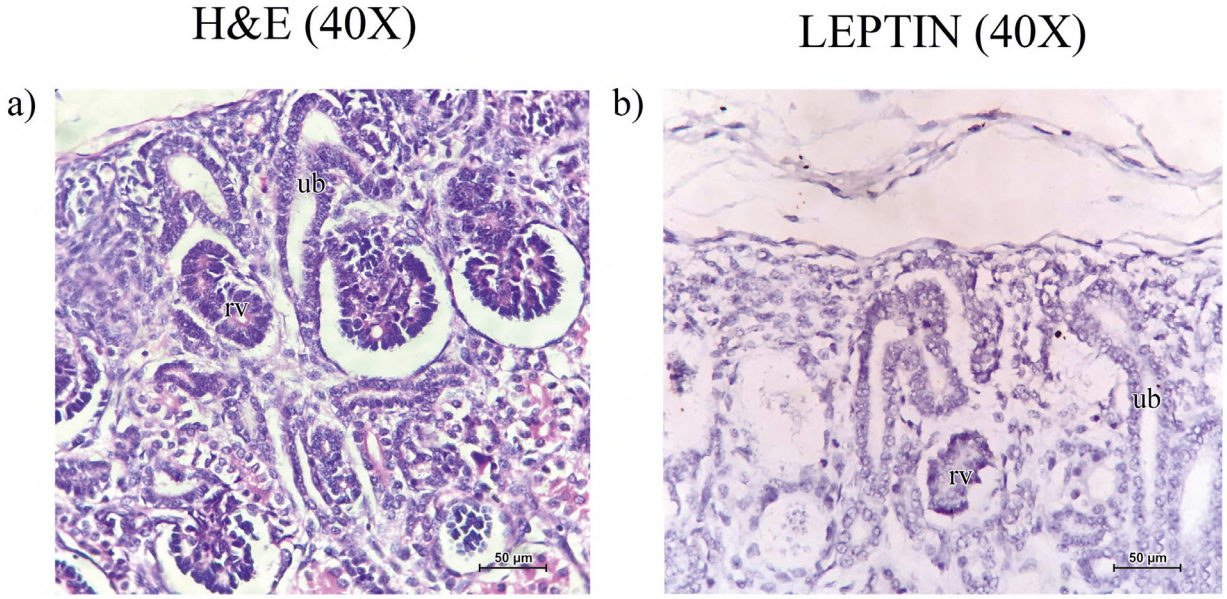

Fig. 1.- a) and **b)** show the nephrogenic zone in fetal kidney. rv, renal vesicle., ub, ureteric bud. Fig. 1b demonstrates the absence of leptin in the nephrogenic zone. Scale bars = 50 µm.

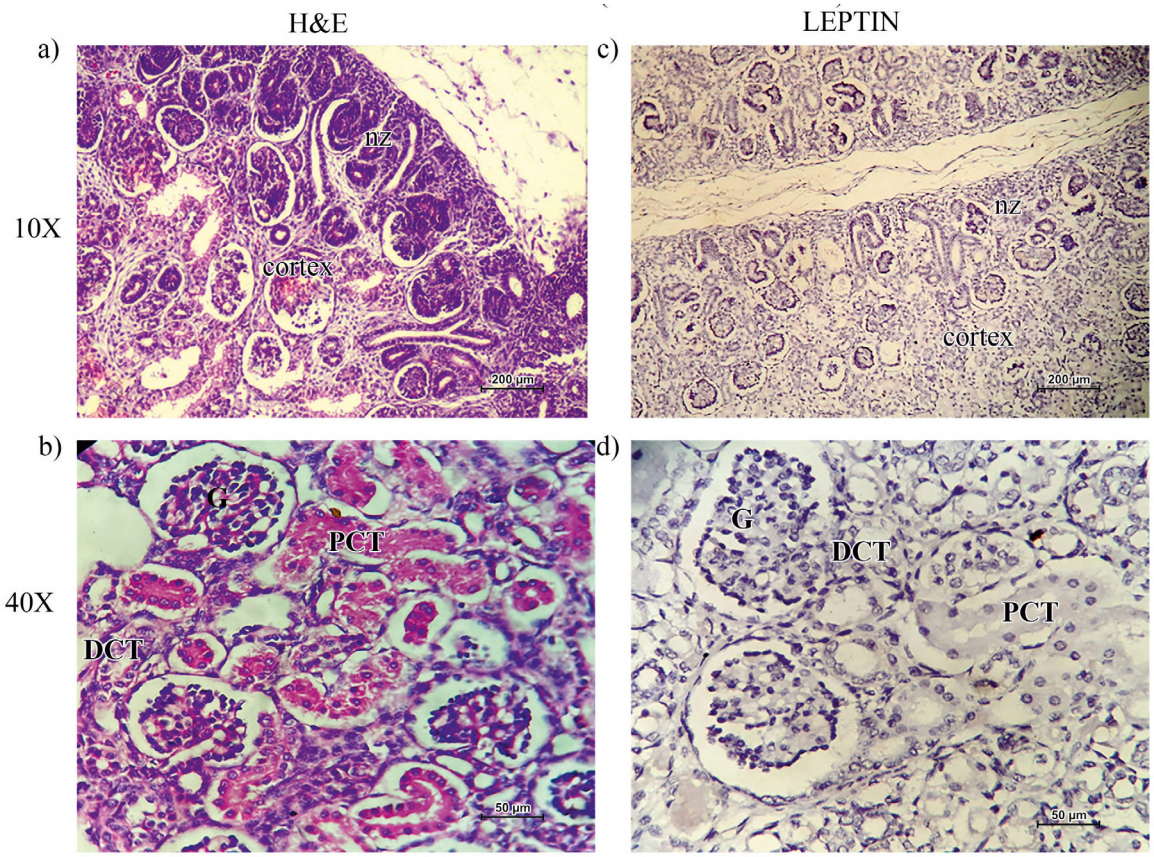

Fig. 2.- a) and **b)** demonstrate H&E sections of the fetal kidney showing the nephrogenic zone, PCT, DCT, and glomerulus (G). **c)** and **d)** demonstrate immunonegative expression of leptin in renal components. Scale bars: a, c = 200 µm; b, d = 50 µm.

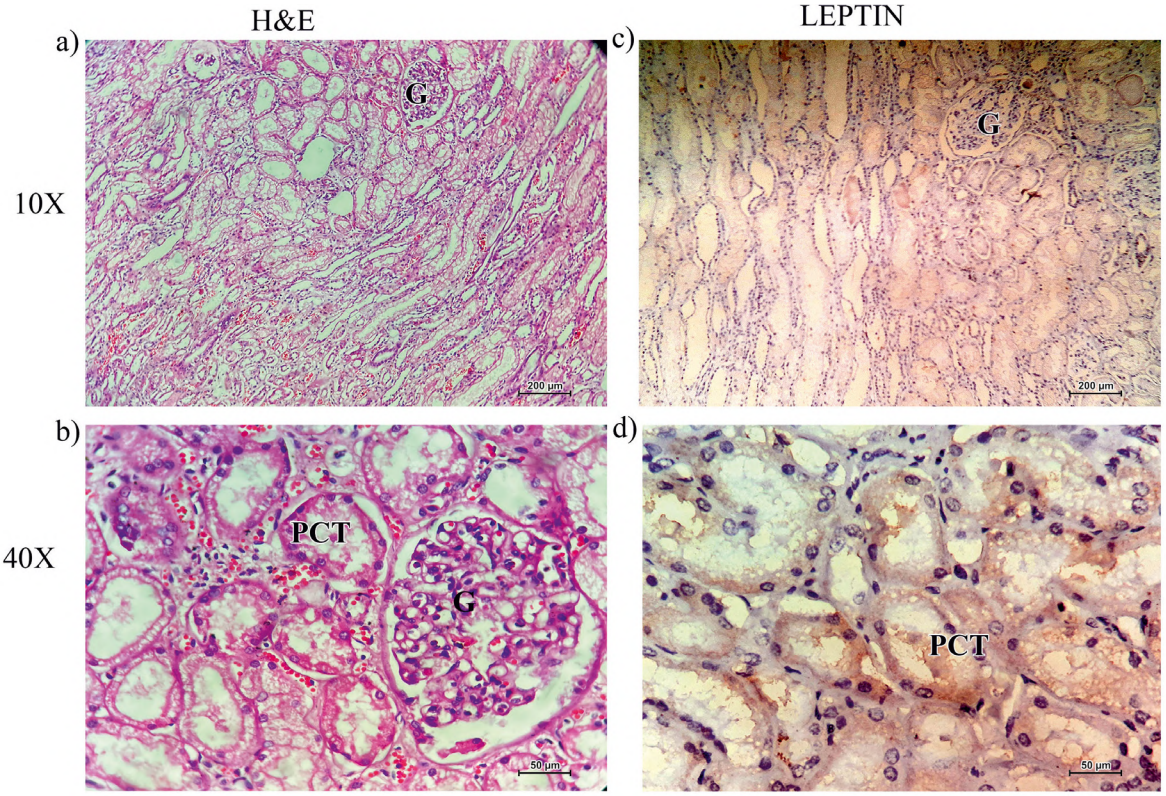

Fig. 3.- a) and **b)** show H&E sections of the adult kidney. **c)** and **d)** showing immunopositive expression of leptin in the PCTs. Scale bars: a, c = 200 µm; b, d = 50 µm.

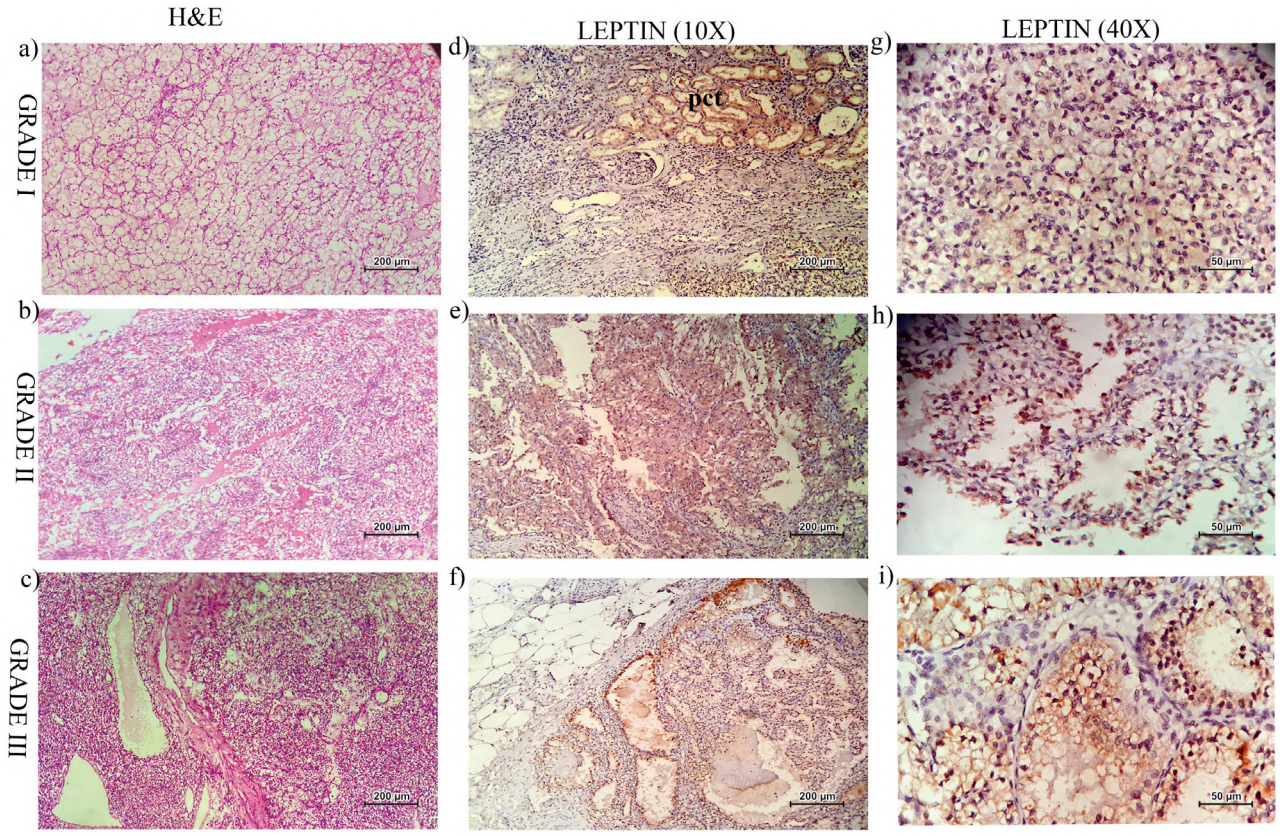

Fig. 4.- a), **b)** and **c)** show H&E sections of various grades of conventional renal cell carcinoma. **d), e), f), g), h)** and **i)** show increased expression of leptin in RCC tissues. Scale bars: a-f = 200 µm; g-i = 50 µm.

DISCUSSION

Studies on experimental animal models have revealed the potential benefit of reversing post-natal consequences by manipulating the leptin signalling pathways during early life stages. A study on maternal LP (low protein) rat models showed the effect of leptin administration enhanced the growth of the foetal pancreas. Similar results showed the growth of tissues such as kidneys, spleen, liver, and ovaries in the leptin-treated piglets with intra-uterine growth reduction. Though its expression has been demonstrated in the foetal tissues and foetal membranes its role still remains unclear (Reynolds and Vickers, 2019).

Leptin is thought to be produced by the placenta and secreted into the foetal and maternal circulation. Foetal leptin is also secreted by foetal adipose tissue and the foetal vascular endothelium (Tsai et al., 2015). The effect of leptin is largely through its transmembrane receptors having six spliced isoforms (OB-Ra-f). The positive expression of leptin in the PCT of human adult kidneys, as in the case of the current study, indicated its possible biological role in adult renal tissue. This could be attributed to the presence of the long form of the leptin receptor (OB-Rb) and short isoform OB-Raw with adequate signaling properties within the renal tissues, as stated by earlier studies. The OB-Rb is essential for intracellular signal transduction however the precise effect of the OB-Rb still remains to be explored (Ja Young Seol et al., 2007; Hoggard et al., 1997).

Contrarily, previous studies also show that with the exception of murine foetal brain and lung tissues, OB-Rb expression was not demonstrated in other tissues such as the liver, kidney, and adrenal gland even in their primitive forms (Hoggard et al., 1997). Thus, reflecting various roles of leptin in adult tissues that are redundant in the foetus.

A study conducted on leptin and various receptors in different segments of the nephron revealed the expression of leptin primarily in the PCT. The other components included the DCT, the loop of Henle, and the collecting duct (Hamma et al., 2004). A former study on rat models showed the PCT cells' uptake, internalization, and deg-

radation of 125I-leptin. The leptin is thought to be filtered by the glomeruli before metabolic degradation in the tubules. The study indicated the presence of megalin, a member of the low-density lipoprotein family at the apical membranes of PCT cells. The Megalin receptors bind to leptin in a Ca2+-dependent manner and tend to reabsorb, metabolize its ligand into endocytic compartments before recycling to the cell surface and thus help in leptin clearance. However, other tubular compartments or glomerular cells did not show the uptake of leptin (Hamma et al., 2004).

Leptin is known to be associated with tumorgenicity in several carcinomas. Leptin is bound to its Ob-RB receptor and is known to undergo a conformational change. This allows the activation of the Janus tyrosine kinase 2 (JAK2) pathway resulting in the phosphorylation of tyrosine residues of the receptor. It also activates the transcription 3 (STAT3) pathway (Ja Young Seol et al., 2007). While the long-form receptor is thought to signal through the Janus kinase pathway, the short-forms regulate the mitogen-activated protein kinase pathway (Tsai et al., 2015). It is also hypothesized to behave like a mitogenic agent in the cellular proliferation and differentiation of various types of cancer (Ja Young Seol et al., 2007). On the contrary, though the short isoform Ob-Ra is observed to activate mitogen-activated protein kinase (MAPK) signal transduction it fails to show proliferative behaviour or signal transduction in the peripheral tissues like the kidney (Harwick et al., 2001).

Studies show that serum leptin is an indicator of progression and survival in breast carcinoma. IHC expression of leptin in breast tumours of invasive ductal carcinoma is associated with tumour characteristics. It is used as a primary therapeutic target against breast carcinoma. Positive immunostaining of colorectal carcinoma (CRC) is associated with tumour size, lymph vascular invasion, distant metastasis, and recurrence in CRC (Al-Maghrabi et al., 2018). The decrease in serum leptin after colectomy indicates a definite association with CRC (Wang et al., 2016). Leptin is also associated with other Gastrointestinal (GI) tumours such as Barret's oesophagus and oesophageal adenocarcinoma (Clemons et al., 2013). Studies have observed that leptin is associated with an increased risk of progression of hepatocellular carcinoma, prostate carcinoma, pancreatic carcinoma, and gall bladder carcinoma (Jimenez-Cortegana et al., 2021).

Renal cell carcinoma (RCC) is the most common and accounts for 80-85% of malignant kidney tumours. Renal cell carcinoma is derived from the tubular lining epithelial cells of the kidney. The most common subtype of RCC is clear cell RCC (ccRCC) arising from the epithelial cells of PCT (Fan et al., 2021). Other subtypes of RCC are papillary cell RCC accounting for 15 to 20%, and chromophobe RCC accounting for 15% (Fan et al., 2021). A few proven etiological factors for RCC are alcoholism, tobacco smoking, obesity, hypertension, and genetic disorders like Von-Hippel Landau syndrome (Perumal et al., 2019). World Health Organization (WHO) has predicted that adiposity accounts for 24% of kidney malignancies (Ljungberg et al., 2011).

Studies performed with respect to serum leptin levels and RCC elucidated overlapping and controversial results. A case-control study done by Spyridopoulos et al. (2009) showed that low circulating leptin will lead to an increased risk of RCC while Liao et al showed that the more the serum concentration of leptin, more is the risk of RCC. The study could not explain the pro-carcinogenic effect of leptin in RCC (Spyridopoulos et al., 2009; Liao et al., 2013). Several other studies indicated serum leptin does not correlate with the progression of the disease in RCC (Perumal et al., 2019).

A few studies opined Acyl-coenzyme A: cholesterol acyl transferase (ACAT) is an important mediator that converts the free cholesterol into cholesterol esters inside the cell. Thus, the untoward (toxic) effects of free cholesterol on the tumour cells are controlled and thus have a protective effect on the latter. It is demonstrated that ACAT is increased in ccRCC when compared to normal renal tubular cells (Gebhard et al., 1987; Pinthus et al., 2011). Hongo et al. (2009) showed that ACAT activity is increased in the presence of leptin and proposed that leptin promotes RCC development. Studies also showed that there is no difference in the increase of leptin between clear-cell and non-clear-cell RCC and between the early and advanced stages of RCC (Drabkin

and Gemmill, 2010). According to a meta-analysis study, serum leptin was not associated with RCC. However, it was observed that the serum leptin levels are significantly elevated in non-clear cell RCC (Perumal et al., 2019). These authors showed that there is no relation between serum leptin and RCC development and progression (Perumal et al., 2019). However, in another study, no association was found between tumour characteristics and the IHC expression of leptin and its receptor. But the study found that nuclear expression of leptin was associated with overall survival (Zhu et al., 2018). Fan et al. (2021) studied RCC cell lines and Western blot and it was in accordance with similar results in the nuclear expression of leptin was associated with overall survival. The study by Ng et al. (2018) suggested that the level of Ob and ObR expression is higher in RCC than in normal tissues. It was observed that ccRCC shows strong cytoplasmic immunostaining. The above studies support our finding that PCT is specific for ccRCC. A study done by Perumal et al. (2020) demonstrated that there is no differential expression between ccRCC and adjacent kidney tissue. This was in contrary to our findings that demonstrated higher expression of leptin in ccRCC than in the adjacent tissue. Our study observed a graded increase in the expression of IHC from grade 1 to grade 3. While other studies done on breast cancer cell lines also showed high leptin association in high-grade/ stage tumors (Ishikawa et al., 2004). Further, the expression of leptin in other variants of renal neoplasms such as chromophobe, collecting duct carcinoma, and renal oncocytoma has been sparsely studied. Elesawy et al. (2020) observed that renal oncocytoma shows differential nuclear staining; chromophobe RCC shows no nuclear localization. Ng et al. (2018) demonstrated that nuclear expression of leptin is higher in renal oncocytoma compared to an eosinophilic variant of chromophobe RCC and an eosinophilic variant of clear cell RCC. Normally leptin stains mainly cytoplasm in non-cancerous tissues (Ng et al., 2018). The current study demonstrates that leptin is specific for PCT, we believe that the leptin biomarker can be used to distinguish the eosinophilic variant of chromophobe RCC, renal oncocytoma with Eosinophilic variant of clear cell RCC. Since the morphological overlap in renal malignancy is common, the scope for core needle biopsy (CNB) is limited. Leptin IHC can be used to distinguish the clear cell RCC from others. We emphasize that leptin IHC can be used pre-operative use in CNB will be valuable. In dilemma, it can also be used for the diagnosis of oncocytoma, chromophobe RCC, an eosinophilic variant of RCC.

CONCLUSION

The present study demonstrated leptin immunolocalized in the cytoplasm of the proximal convoluted tubules (+1) of the adult kidney and in the tumour cells (membranous) of conventional renal cell carcinoma (+2). However, leptin was not found to be localized in any of the renal components of the foetal kidneys. It was neither expressed in the nephrogenic zone nor neither in the developing proximal convoluted tubules. The proximal convoluted tubules are thought to be the source of the development of clear RCC. Thus, leptin may not participate in the development of human kidneys. Leptin expression in the PCT of the normal adult kidney, its enhanced expression in the PCT of the renal tissue adjacent to the carcinomatous tissue, and its overexpression in the cancerous cells indicate dysregulation of the leptin signalling pathways. Since the expression of leptin is observed to be absent in the fetal their expression in the renal tumor cells is indicative of an aberrant expression pattern unlikely to be due to reactivation of a repressed gene in the process of normal embryonic development.

ACKNOWLEDGEMENTS

The authors sincerely thank those who donated their bodies to science so that anatomical research could be performed. Results from such research can potentially increase mankind's overall knowledge that can improve patient care. Therefore, these donors and their families deserve our highest gratitude.

REFERENCES

AL-MAGHRABI JA, QURESHI IA, KHABAZ MN (2018) Expression of leptin in colorectal adenocarcinoma showed significant different survival patterns associated with tumor size, lymphovascular invasion, distant metastasis, local recurrence, and relapse of disease in the western province of Saudi Arabia. *Medicine*, 97: e12052.

BERGEN HT, CHERLET TC, MANUEL P, SCOTT JE (2002) Identification of leptin receptors in lung and isolated fetal type II cells. *Am J Respir Cell Mol Biol*, 27(1): 71-77.

BIESIADA LA, GŁOWACKA E, KREKORA M, SOBANTKA S, KROKOCKA A, KRASOMSKI G (2016) The impact of excessive maternal weight on the nutritional status of the fetus - the role of leptin. *Arch Med Sci*, 12(2): 394-401.

CLEMONS NJ, PHILLIPS WA, LORD RV (2013) Signaling pathways in the molecular pathogenesis of adenocarcinomas of the esophagus and gastroesophageal junction. *Cancer Biol Ther*, 14: 782-795.

DRABKIN HA, GEMMILL RM (2010) Obesity, cholesterol, and clear-cell renal cell carcinoma (RCC). *Adv Cancer Res*, 107: 39-56.

ELESAWY YF, AMER SI, EESA AN (2020) The reliability of leptin immunostain use for differentiating renal oncocytoma and chromophobe renal cell carcinoma. *Kasr Al Ainy Med J*, 26(1): 5.

FAN WL, YEH YM, LIU TT, LIN WM, YANG TY, LEE CW, LIN TC (2021) Leptin is associated with poor clinical outcomes and promotes clear cell renal cell carcinoma progression. *Biomolecules*, 11(3): 431.

FUHRMAN SA, LASKY LC, LIMAS C (1982) Prognostic significance of morphologic parameters in renal cell carcinoma. *Am J Surg Pathol*, 6: 655-663.

GEBHARD RL, CLAYMAN RV, PRIGGE WF, FIGENSHAU R, STALEY NA, REESEY C, BEAR A (1987) Abnormal cholesterol metabolism in renal clear cell carcinoma. *J Lipid Res*, 28(10): 1177-1184.

HAMA H, SAITO A, TAKEDA T, TANUMA A, XIE Y, SATO K, KAZAMA JJ, GEJYO F (2004) Evidence indicating that renal tubular metabolism of leptin is mediated by megalin but not by the leptin receptors. *Endocrinology*, 145(8): 3935-3940.

HARDWICK JC, VAN DEN BRINK GR, OFFERHAUS GJ, VAN DEVENTER SJ, PEPPELENBOSCH MP (2001) Leptin is a growth factor for colonic epithelial cells. *Gastroenterology*, 121(1): 79-90.

HOGGARD N, HUNTER L, DUNCAN JS, WILLIAMS LM, TRAYHURN P, MERCER JG (1997) Leptin and leptin receptor mRNA and protein expression in the murine fetus and placenta. *Proc Natl Acad Sci USA*, 94(20): 11073-11078.

HONGO S, WATANABE T, ARITA S, KANOME T, KAGEYAMA H, SHIODA S, MIYAZAKI A (2009) Leptin modulates ACAT1 expression and cholesterol efflux from human macrophages. *Am J Physiol*, 297: E474-482.

ISHIKAWA M, KITAYAMA J, NAGAWA H (2004) Enhanced expression of leptin and leptin receptor (OB-R) in human breast cancer. *Clin Cancer Res,* 10(13): 4325-4331.

JA YOUNG SEOL, SOON YOUNG CHOI, NARI LEE (2007) Establishment of a stable cell line expressing mouse leptin receptor (OB-Rb) in human embryonic kidney 293 cell and preadipocyte 3t3l-1 cell. *Cancer Prev Res*, 12: 240-245.

JIMÉNEZ-CORTEGANA C, LÓPEZ-SAAVEDRA A, SÁNCHEZ-JIMÉNEZ F, PÉREZ-PÉREZ A, CASTIÑEIRAS J, VIRIZUELA-ECHABURU JA, DE LA CRUZ-MERINO L, SÁNCHEZ-MARGALET V (2021) Leptin, both bad and good actor in cancer. *Biomolecules*, 11(6): 913.

KAEMMERER D, PETER L, LUPP A, SCHULZ S, SÄNGER J, BAUM RP, PRASAD V, HOMMANN M (2012) Comparing of IRS and Her2 as immunohistochemical scoring schemes in gastro-enteropancreatic neuroendocrine tumors. *Int J Clin Exp Pathol*, 5(3): 187-194.

LAPPAS M, YEE K, PERMEZEL M, RICE GE (2005) Release and regulation of leptin, resistin and adiponectin from human placenta, fetal membranes, and maternal adipose tissue and skeletal muscle from normal and gestational diabetes mellitus-complicated pregnancies. *J Endocrinol*, 186(3): 457-465.

LIAO LM, SCHWARTZ K, POLLAK M, GRAUBARD BI, LI Z, RUTERBUSCH J, ROTHMAN N, DAVIS F, WACHOLDER S, COLT J, CHOW WH, PURDUE MP (2013) Serum leptin and adiponectin levels and risk of renal cell carcinoma. *Obesity (Silver Spring)*, 21(7): 1478-1485.

LJUNGBERG B, CAMPBELL SC, CHO HY, JACQMIN D, LEE JE, WEIKERT S, KIEMENEY LA (2011) The epidemiology of renal cell carcinoma. *Eur Urol*, 60(4): 615-621.

NG KL, DEL VECCHIO SJ, SAMARATUNGA H, MORAIS C, RAJANDRAM R, VESEY DA, WOOD ST, GOBE GC (2018) Leptin and its receptor: can they help to differentiate chromophobe renal cell carcinoma from renal oncocytoma? *Pathology*, 50(5): 504-510.

PATEL SR, DRESSLER GR (2013) The genetics and epigenetics of kidney development. *Semin Nephrol*, 33(4): 314-326.

PERUMAL K, HUIN WK, YAP NY, ONG TA, GOBE GC, RAJANDRAM R (2019) Role of leptin as a biomarker for early detection of renal cell carcinoma? No evidence from a systematic review and meta-analysis. *Med Hypotheses*, 129: 109239. Erratum in: *Med Hypotheses*, 131: 109284 (2019).

PERUMAL K, MUN KS, YAP NY, RAZACK AHA, GOBE GC, ONG TA, KUPPUSAMY S, RAJANDRAM R (2020) A Study on the immunohistochemical expressions of leptin and leptin receptor in clear cell renal cell carcinoma. *Biomed Res Int*, 4: 3682086.

PINTHUS JH, WHELAN KF, GALLINO D, LU JP, ROTHSCHILD N (2011) Metabolic features of clear-cell renal cell carcinoma: mechanisms and clinical implications. *Can Urol Assoc J*, 5(4): 274-82.

PRICE KL, LONG DA, JINA N, LIAPIS H, HUBANK M, WOOLF AS, WINYARD PJ (2007) Microarray interrogation of human metanephric mesenchymal cells highlights potentially important molecules in vivo. *Physiol Genomics*, 28(2): 193-202.

REYNOLDS C, VICKERS M (2019) The role of adipokines in developmental programming: evidence from animal models. *J Endocrinol*, 242: T81-T94.

SADASHIV R, BANNUR BM, SHETTY P, DINESH US, RANI H, VISHWANATHA J, DESHPANDE SK, BARGALE A, SARATHKUMAR, RUIKAR K (2019) Differential expression pattern of annexin A2 during nephrogenesis and kidney carcinoma. *Rom J Morphol Embryol*, 60(3): 895-904.

SPYRIDOPOULOS TN, PETRIDOU ET, DESSYPRIS N, TERZIDIS A, SKALKIDOU A, DELIVELIOTIS C, CHROUSOS GP (2009) Obesity and Cancer Oncology Group. Inverse association of leptin levels with renal cell carcinoma: results from a case-control study. *Hormones*, 8: 39-46.

TSAI PJ, DAVIS J, BRYANT-GREENWOOD G (2015) Systemic and placental leptin and its receptors in pregnancies associated with obesity. *Reprod Sci,* 22(2): 189-197.

WANG D, GAO L, GONG K, CHAI Q, WANG G (2016) Increased serum leptin level in overweight patients with colon carcinoma: A cross-sectional and prospective study. *Mol Clin Oncol*, 6: 75-78.

ZHU H, LI W, MAO S, WANG L (2018) Association between leptin level and renal cell carcinoma susceptibility and progression: A meta-analysis. *J Cancer Res Ther*, 14(4): 873-880.

The relationship between optic nerve and Onodi cells on CT scan

Lam Huyen Tran, Nguyen Le Vinh Thuan

Department of Otolaryngology, University of Medicine and Pharmacy at Ho Chi Minh City, Ho Chi Minh City, Vietnam

SUMMARY

The Onodi cells, also known as sphenoethmoidal air cells, are a variant of the most posterior ethmoid cells and are closely related to the optic canal. The presence of Onodi cells may increase the risk of optic nerve injury and result in confusion with sphenoid sinuses during endoscopic sinus surgery, leading to the oversight of sphenoid sinus pathology. The aim of the study was to examine the characteristics of Onodi cells and their relationship with the optic nerve on CT scans. A cross-sectional study was conducted, analyzing CT scans of paranasal sinuses in 196 posterior ethmoid air cells from 98 patients (30 males and 68 females) aged 18 or older, without abnormalities in the paranasal sinuses and optic nerve anatomy.

The prevalence of Onodi cells was 38.78%, with 26.32% on the left, 44.74% on the right, and 28.94% bilaterally. Onodi cell pneumatization was observed in the order of Type I > Type II > Type III on both sides. The most common relationship between Onodi cells and the optic nerve was Type A on both sides. The incidence of the optic nerve bulging into Onodi cells was 50%, and the exposure of the optic nerve into Onodi cells was 7.89%. The study investigated the prevalence and relationship between Onodi cells and the optic nerve. CT scans proved to be a crucial diagnostic tool in providing essential information about Onodi cells before surgery.

Key words: Onodi cells – Optic nerve – Posterior ethmoid air cells

INTRODUCTION

Onodi cells, also known as sphenoethmoidal air cells, are the most posterior ethmoidal cells which pneumatized superiorly, laterally, or superolaterally and closely associated with the optic nerve (Stammberger and Kennedy, 1995). The presence of the optic nerve, whether or not there is dehiscence in the Onodi cell, *may* increase the risk of optic nerve injury during endoscopic sinus surgery. Additionally, the potential confusion of Onodi cells with sphenoid sinuses during surgery can lead to incomplete endoscopic sinus procedures (Chmielik and Chmielik, 2017).

It is evident that accurately determining the presence of Onodi cells and their relationship with the optic nerve preoperatively is essential. Therefore, we conducted the study: "The relationship between the Optic Nerve and Onodi Cells on CT Scan."

Corresponding author:
Lam Huyen Tran. 194/46 Vo Van Tan Street, District 3, Ho Chi Minh City, Vietnam
Nguyen Le Vinh Thuan. 91 Tan Vinh Street, District 4, Ho Chi Minh City, Vietnam

Submitted: December 7, 2023. **Accepted:** December 22, 2023

https://doi.org/10.52083/UWJI9217

MATERIALS AND METHODS

Study Population

The study sample comprised 96 patients aged 18 and above who underwent paranasal sinus CT scans at Nguyen Tri Phuong Hospital in Ho Chi Minh City, Vietnam, from January 2023 to June 2023. The research obtained approval from both the Institutional Review Ethics Committee and the Ethical Committee of the involved hospital. All participants in the study provided their informed consent to participate by affixing their signatures on the informed consent form.

Exclusion criteria affected patients with a history of facial trauma, malignant facial diseases, or previous surgeries in the paranasal sinus area.

Research Method

A cross-sectional study was performed using a 64-slice multidetector scanner with a slice thickness of 0.625 mm. Subjects under 18 years old, with a history of facial trauma, malignant facial diseases, or previous surgeries in the paranasal sinus area, were excluded from the study (Fig. 1).

All CT scans were conducted in a supine position, and axial slices were parallel to the hard palate bone, ranging from the anterior border of the frontal sinus to the posterior border of the sphenoid sinus. The slice thickness was 0.625 mm, using a bone window (W 2000 L 350), a matrix of 512×512, and technical parameters of 120KV and 330mAs.

The relationship between the Onodi cells and the optic nerve was assessed based on Chmielik's classification (Chmielik and Chmielik, 2017):

- Type A: there was no contact between the wall of the ethmoid cell and optic nerve canal.
- Type B: the wall of the ethmoid cell was adjacent to the optic nerve canal wall on the distance maximum 2 mm (measuring in axial and sagittal planes), not extending laterally or supero- laterally.
- Type C: the wall of the ethmoid cell was adjacent to the optic nerve canal wall within distance >2 mm in the axial and/or sagittal plane extending laterally or supero-laterally without bulging of the optic nerve canal into the ethmoid bone.

Fig. 1.- Onodi cells on the coronal section (red arrow).

Fig. 2.- A: Onodi cell type I. **B:** Onodi cell type II. **C:** Onodi cell type III.

- Type D: the wall of the ethmoid cell was adjacent to the optic nerve canal wall for a distance of more than 5 mm (measuring in axial or sagittal plane) extending supero-laterally with bulging. The bulging was defined as the protrusion of the optic nerve into the ethmoid cell visualised in two planes. The very thin slice thickness guaranteed not missing any bulging of the optic nerve canal.
- Types C and D are defined as a close relationship between the posterior ethmoid cells and the optic nerve.

The Onodi cells are defined according to the Stammberger and Kennedy (1995) standard: they are posterior ethmoid cells pneumatized superiorly, laterally, or superior-laterally to the sphenoid sinus and have a close relationship with the optic nerve (Type C or D). Paranasal sinus CT scans are analyzed in all three planes: coronal, axial, and sagittal, to avoid missing Onodi cells.

The pneumatization pattern of Onodi cells is assessed based on Thimmaiah's classification (Thimmaiah and Anupama, 2017). In the coronal plane, the location of the sphenoid sinus is iden-

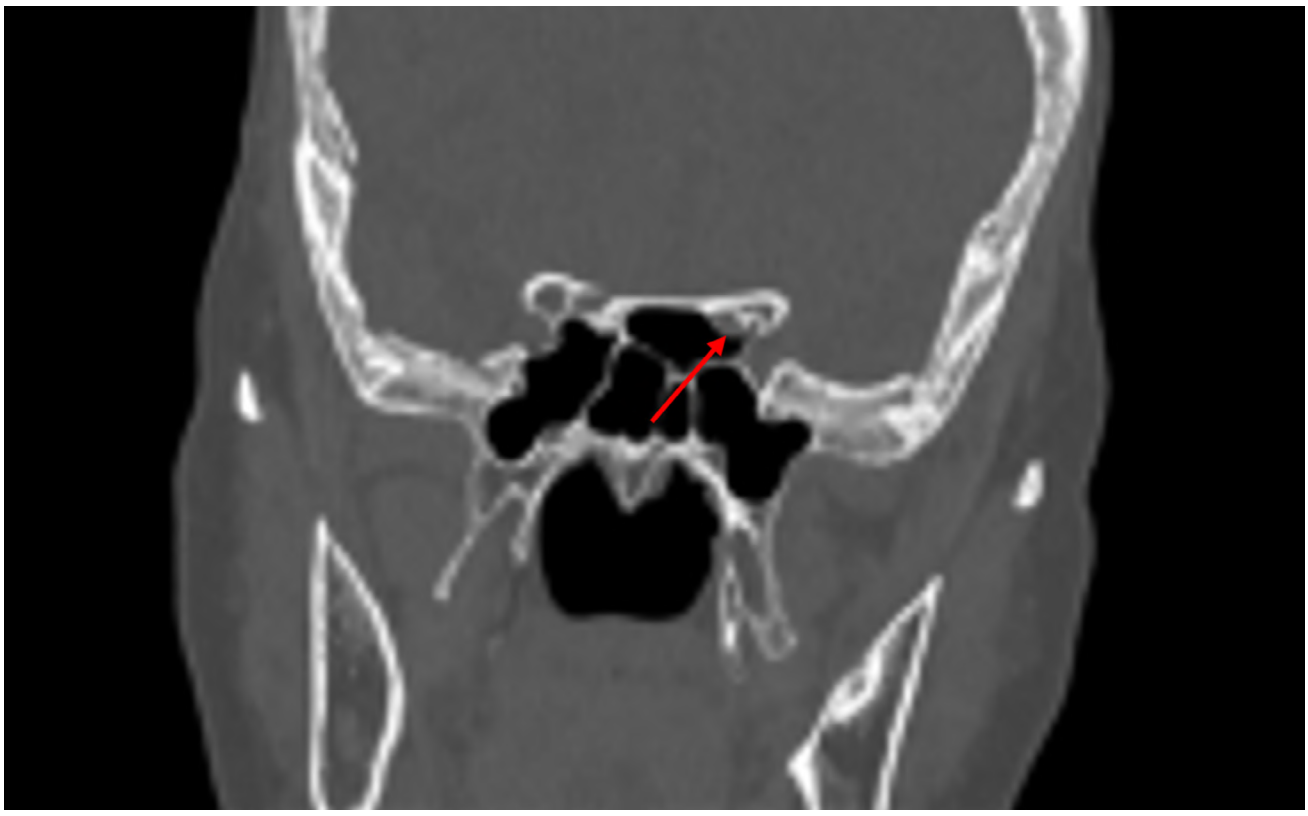

Fig. 3.- Protrusion of the optic nerve into the Onodi cell (red arrow).

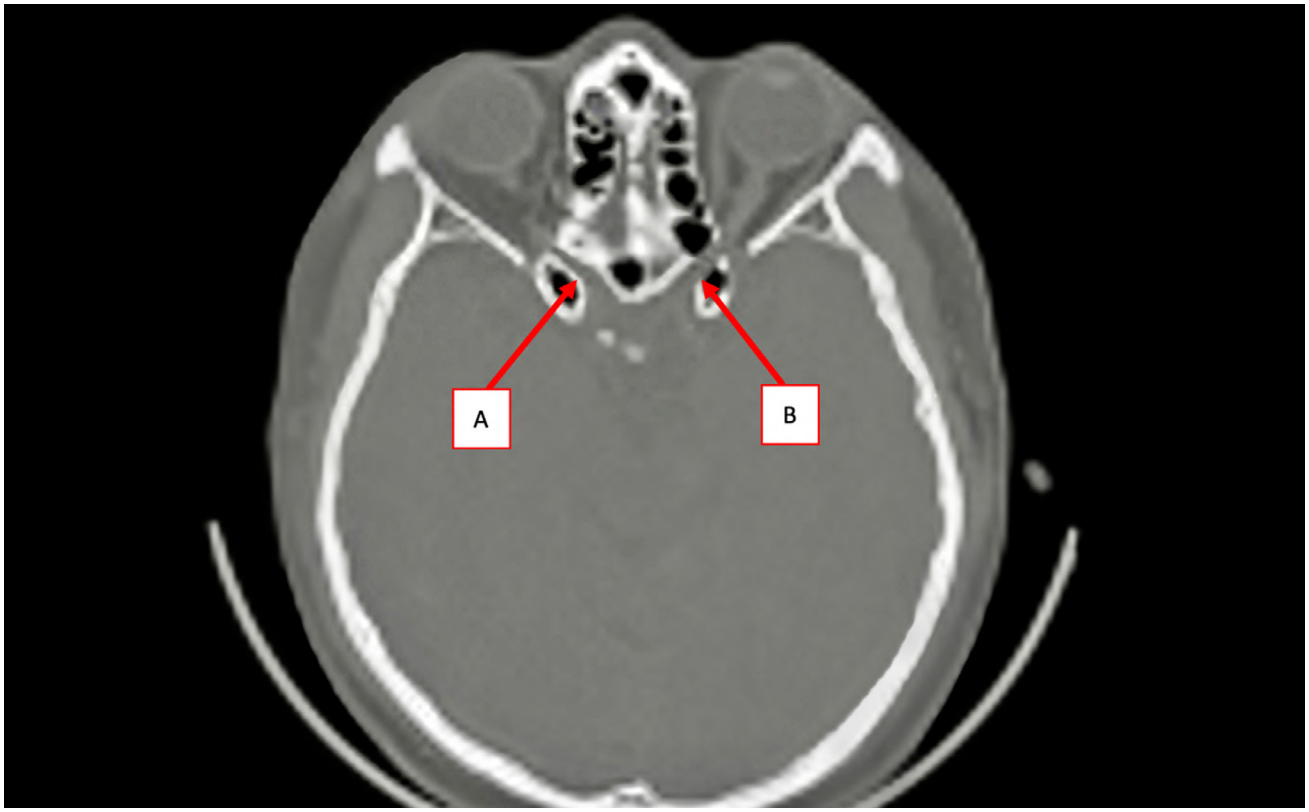

Fig. 4.- Protrusion of the optic nerve into Onodi cells on both sides, with the right optic nerve having bony coverage (A) and the left optic nerve lacking bony coverage - exposed into the Onodi cell (B).

tified, and the section where Onodi cells have the largest cross-sectional area and are related to the sphenoid sinus is determined. A horizontal line is drawn at the highest point of the sphenoid sinus at that section, and the position of Onodi cells is evaluated in relation to the drawn line (Fig. 2):

- Type I: if Onodi cells are observed above or laterally to the sphenoid sinus.
- Type II: if Onodi cells are observed both above and below the drawn line.
- Type III: if Onodi cells are observed below the drawn line.

The protrusion of the optic nerve is assessed according to Chmielik's study (Chmielik and Chmielik, 2017): it refers to the bulging of the optic nerve into the cavity of Onodi cells, evaluated on two sections (Figs. 3, 4). It must be meticulously analysed on each section to ensure that no optic nerve protrusion is overlooked.

Exposure of the optic nerve into the cavity of Onodi cells is noted when there is a protrusion of the optic nerve into the cavity of Onodi cells, and there is no bony wall covering.

RESULTS

The study analysed CT scans of 196 posterior ethmoid air cell systems and optic nerve relationships from 96 patients (30 males and 68 females). The average age was 47.15 ± 15.22 years, ranging from 19 to 88 years, with no history of facial trauma, malignant facial conditions, or prior surgery in the adjacent nasal sinus area.

The study observed the presence of Onodi cells in 38 patients (38.78%). Among these cases, Onodi cells were identified on the right side in 17 out of 38 cases (44.74%), on the left side in 10 out of 38 cases (26.32%), and bilaterally in 11 out of 38 cases (28.94%). In the male group, Onodi cells were noted in 13 out of 30 cases (43.33%): 4 cases on the left (30.77%), 4 cases on the right (30.77%), and 5 cases bilaterally (38.46%). In the female group, Onodi cells were identified in 25 out of 68 cases (36.76%): 6 cases on the left (24%), 13 cases on the right (52%), and 6 cases bilaterally (24%). The correlation between posterior ethmoid cells and the optic nerve is presented in Table 1.

Table 1. The correlation between posterior ethmoid cells and the optic nerve.

Type	Left (%)	Right (%)
A	73.46	66.32
B	5.1	5.1
C	11.22	13.26
D	10.22	15.32
Total	100	100

Regarding the pneumatization types of Onodi cells, on the left side, Type I was observed in 47.61%, Type II in 42.86%, and Type III in 9.53%. On the right side, Type I accounted for 60.71%, Type II for 35.71%, and Type III for 3.58%.

The study also noted that the rate of optic nerve protrusion into the Onodi cells was 50%, and the rate of exposure of the optic nerve into the Onodi cells was 7.89%. Comparison of the prevalence rate of Onodi cells with previous studies is exposed in Table 2.

DISCUSSION

Onodi cells are closely related to vital anatomical structures such as the optic nerve and the internal carotid artery, and they can be confused with the sphenoid sinus during surgery. Therefore, the detection of Onodi cells prior to nasal sinus surgeries is crucial for minimising complications and avoiding missing sphenoid sinus pathology during the procedure.

Previous studies have indicated varying prevalence rates of Onodi cells and their association with the optic nerve. However, most of these studies utilized one or two sectional views for assessment. For instance, Delano's study (Delano et al., 1996) showed that only 3% of posterior ethmoid cells were associated with the optic nerve, but this study only analysed coronal sections. Until now, there has been no consensus on the method of evaluating Onodi cells on CT scans. According to Hoang et al. (2010), the assessment of paranasal sinus on CT scans should involve all three sectional views.

In some studies, the detection rate of Onodi cells was higher when evaluated in multiple sectional views compared to a single sectional view (Weinberger et al., 1996; Driben et al., 1998). Therefore, our study assessed all three sectional views (coronal, axial, and sagittal) to prevent overlooking Onodi cells during CT scan analysis (Hui et al., 2022).

Numerous previous studies have reported a considerable variation in the prevalence of Onodi cells, ranging from 3.4% to 65.3% (Delano et al., 1996; Yanagisawa et al., 1998; Kasemsiri et al., 2011; Tomovic et al., 2012; Pham Thy and Pham Ngoc, 2012; Ozturan et al., 2013; Toan, 2013; Chmielik et al., 2014; Sarita Choudhary et al., 2014; Wada et al., 2015; Seung-Ju et al., 2015; Senturk et al., 2016; Chmielik and Chmielik, 2017; Nguyen et al., 2018). In our study, the observed rate of Onodi cells was 38.78%, distributed by gender as 34.21% in males and 65.72% in females, with no statistically significant difference between the two genders.

Table 2. Comparison of the prevalence rate of Onodi cells with previous studies.

Authors	Location	Year	Sample Size	Prevalence Rate
Thiên	Vietnam	2008	289	21%
Kasemsiri et al.	Thailand	2011	187	49,5%
Seung-Ju et al.	South Korea	2015	129	47,3%
Sarita et al.	India	2014	100	31%
Chmielik and Chmielik	Poland	2017	196	39,8%
Nguyen Thi et al.	Vietnam	2018	120	25,42
Nair and Ibrahim	India	2021	201	42,8%
Özdemir et al.	Germany	2019	508	21,2%
Le Nhat Vinh	Vietnam	2021	400	19,6%
Liuling Hui et al.	China	2022	273	60,4%
Our study	Vietnam	2023	98	38,78%

The prevalence rate of Onodi cells in our study was higher than in some previous studies, such as Sarita Choudhary et al. (2014) (31%), Ozdemir et al. (2019) (21.2%), and Vinh (2021) (19.6%) studies. However, it was quite similar to Chmielik and Chmielik's (2017) study in Poland in 2017, partly due to the use of similar criteria for analysing Onodi cells.

According to Chmielik's study, among the four types of relationships between Onodi cells and the optic nerve, types C and D are considered Onodi cells with a close relationship to the optic nerve. In the context of endoscopic sinus surgery, injuries to the optic nerve are more likely to occur with types C and D, especially when the optic nerve lacks bony covering (Chmielik and Chmielik, 2017). In our study, type A had the highest prevalence, accounting for 73.46% on the left and 66.32% on the right, followed by types C, D, and the lowest was type B, with no statistically significant difference between the left and right sides.

It can be observed that in both studies, type A consistently had the highest prevalence. However, the two dangerous types that often lead to optic nerve injuries during surgery (types C and D) still accounted for a considerable proportion, with 14.8% for type C and 25% for type D in Chmielik's study, and 12.24% for type C and 12.77% for type D in our study.

The pneumatization types of Onodi cells were classified into three types according to Thimmaiah's classification (Thimmaiah and Anupama, 2017), where type I had the highest prevalence, followed by type II, and the least was type III. This is quite similar to Nair and Ibrahim's study (Nair and Ibrahim, 2021), but differs from Thimmaiah's study, which reported type II as the most prevalent, followed by type I and type III. This difference may be attributed to variations in anatomical structures and pneumatization processes of the Onodi cell system among different ethnic groups.

Our study recorded that 50% of cases exhibited the optic nerve protruding into the Onodi cell, which is lower than the findings of Vinh (2021) (59.9%). In both studies, when Onodi cells were present, the prevalence of optic nerve protrusion was relatively high. The study also noted that 7.89% of cases involved the exposure of the optic nerve into the Onodi cell, which is the most dangerous type, leading to optic nerve injury during endoscopic sinus surgery.

Due to its close association with many important anatomical structures, especially the optic nerve, identifying the characteristics of Onodi cells before surgery is crucial. The presence of the optic nerve, whether or not there is dehiscence in the Onodi cell, *may* increase the risk of optic nerve injury, particularly when the surgeon fails to recognize their presence on preoperative CT scans. Evaluating Onodi cells on all three coronal, axial, and sagittal planes can help reduce the likelihood of overlooking these cells and provide a better assessment of their relationship with the optic nerve.

CONCLUSION

In this study, we reported the prevalence, characteristics, and relationship of Onodi cells with the optic nerve. CT scan proved to be a selected imaging diagnostic method that provides crucial information about Onodi cells before surgery.

ACKNOWLEDGEMENTS

We thank Dr. Nguyen Huu Dung and Dr. Do Hai Thanh Anh for useful discussions. We thank Nguyen Tri Phuong hospital for support.

REFERENCES

CHMIELIK ACL, BOGUSLAWSKA-WALECKA R (2014) The prevalence and CT detection of onodi cell types. *The European Congress of Radiology*, 1-15.

CHMIELIK LP, CHMIELIK A (2017) The prevalence of the Onodi cell - Most suitable method of CT evaluation in its detection. *Int J Pediatr Otorhinolaryngol*, 97: 202-205.

DELANO MC, FUN FY, ZINREICH SJ (1996) Relationship of the optic nerve to the posterior paranasal sinuses: a CT anatomic study. *AJNR Am J Neuroradiol*, 17(4): 669-675.

DRIBEN JS, BOLGER WE, ROBLES HA, CABLE B, ZINREICH SJ (1998) The reliability of computerized tomographic detection of the Onodi (Sphenoethmoid) cell. *Am J Rhinol*, 12(2): 105-111.

HOANG JK, EASTWOOD JD, TEBBIT CL, GLASTONBURY CM (2010) Multiplanar sinus CT: a systematic approach to imaging before functional endoscopic sinus surgery. *AJR Am J Roentgenol*, 194(6): W527-536.

HUI L, HUNG KF, YEUNG AWK, VON ARX T, LEUNG YY, BORNSTEIN MM (2022) Anatomical variations of the ethmoid sinuses and their association with health or pathology of the ethmoid and maxillary sinuses in a Southern Chinese population: An analysis using cone-beam computed tomography. *Imaging Sci Dent*, 52(1): 109-115.

KASEMSIRI P, THANAVIRATANANICH S, PUTTHARAK W (2011) The prevalence and pattern of pneumatization of Onodi cell in Thai patients. *J Med Assoc Thai*, 94(9): 1122-1126.

NAIR S, IBRAHIM A (2021) The importance of cribriform-lamella angle in endoscopic sinus surgery. *Indian J Otolaryngol Head Neck Surg*, 73(1): 66-71.

NGUYỄN THỊ THÚY AN , LÊ VĂN PHƯỚC, LÂM HUYỀN TRÂN (2018) Khảo sát đặc điểm lồi ống thần kinh thị vào lòng các xoang sau trên phim MSCT vùng mũi xoang. *Y Học TP Hồ Chí Minh*, 22(1): 96-101.

ÖZDEMIR A, BAYAR MULUK N, ASAL N, ŞAHAN MH, INAL M (2019) Is there a relationship between Onodi cell and optic canal? *Eur Arch Otorhinolaryngol*, 276(4):1057-1064.

OZTURAN O, YENIGUN A, DEGIRMENCI N, AKSOY F, VEYSELLER B (2013) Co-existence of the Onodi cell with the variation of perisphenoidal structures. *Eur Arch Otorhinolaryngol*, 270(7): 2057-2063.

PHẠM THY THIÊN LMT, PHẠM NGỌC HOA (2012) Khảo sát tần suất các biến thể tế bào sàng trên phim chụp cắt lớp điện toán ở người trưởng thành. *Y Học TP Hồ Chí Minh*, 16(1): 226-230.

SARITA CHOUDHARY NP, VINEETA TEWARI, MD. SHAKEEL SIDDIQUI, MRINAL RANJAN SRIVASTAVA (2014) CT study of sphenoethmoid (Onodi) cell and its clinical importance. *Int J Adv*, 2.

SENTURK M, GULER I, AZGIN I, SAKARYA EU, OVET G, ALATAS N, TOLU I, ERDUR O (2016) The role of Onodi cells in sphenoiditis: results of multiplanar reconstruction of computed tomography scanning. *Braz J Otorhinolaryngol*, 83(1): 88-93.

SEUNG-JU LEE, YONG-KYUNG KANG, EUN-SUB LEE, JI-SUN KIM (2015) Prevalence of Onodi cells in Korean based on computed tomography. Korean *J Otolaryngol Head Neck Surg*, 58(12): 855-858.

STAMMBERGER HR, KENNEDY DW (1995) Anatomic Terminology G. Paranasal sinuses: anatomic terminology and nomenclature. *Ann Otol Rhinol Laryngol*, Suppl, 167: 7-16.

THIÊN PT (2008) Khảo sát tế bào sàng bướm trên phim chụp cắt lớp điện toán. *Đại học Y Dược TPHCM*.

THIMMAIAH VT, ANUPAMA C (2017) Pneumatization patterns of onodi cell on multidetector computed tomography. *J Oral Maxilofac Radiol*, 5(3): 63-66.

TOÀN HT (2013) Khảo sát tế bào sàng bướm ở bệnh nhân viêm xoang sàng. Luận văn bác sĩ nội trú chuyên ngành *Tai Mũi Họng Đại học Y Dược TPHCM*.

TOMOVIC S, ESMAEILI A, CHAN NJ, CHOUDHRY OJ, SHUKLA PA, LIU JK, ELOY JA (2012) High-resolution computed tomography analysis of the prevalence of Onodi cells. *Laryngoscope*, 122(7): 1470-1473.

VINH LN (2021) Khảo sát các dạng tế bào sàng bướm trên CT scan mũi xoang. Luận văn bác sĩ chuyên khoa II, Đại học Y khoa Phạm Ngọc Thạch.

WADA K, MORIYAMA H, EDAMATSU H, HAMA T, ARAI C, KOJIMA H, OTORI N, YANAGI K (2015) Identification of Onodi cell and new classification of sphenoid sinus for endoscopic sinus surgery. *Int Forum Allergy Rhinol*, 5(11): 1068-1076.

WEINBERGER D, ANAND V, AL-RAWI M, CHENG H, MESSINA A (1996) Surgical anatomy and variations of the Onodi cell. *Am J Rhinol Allergy*, 10(6): 365-370.

YANAGISAWA E, WEAVER EM, ASHIKAWA R (1998) The Onodi (sphenoethmoid) cell. *Ear Nose Throat J*, 77(8): 578-580.

Aberrant origin of the left vertebral artery: clinical case and scientific literature

Cristina Mesas[1,2], Francisco Quiñonero[1,2], Gloria Perazzoli[1,2], Kevin Doello[2,3]

[1] *Department of Anatomy and Embryology, University of Granada, Granada 18071, Spain*

[2] *Institute of Biopathology and Regenerative Medicine (IBIMER), Biomedical Research Center (CIBM), Granada 18100, Spain*

[3] *Medical Oncology Service, Virgen de las Nieves Hospital, 18014 Granada, Spain*

SUMMARY

The variants in the origin of the trunks of the aortic arch are very heterogeneous. Among them, it is worth highlighting the variants that involve the origin of the vertebral artery and more specifically the left vertebral artery. We present the case of a 62-year-old patient in whom an aberrant vertebral artery was incidentally described in a computed tomography for oncological evaluation. This anatomical variant is asymptomatic in up to 5% of cases and can give rise to clinical problems of a vascular nature.

Key words: Vertebral artery – Anatomical variant – Aberrant – Computed tomography

INTRODUCTION

The aortic arch is an important structure in the human cardiovascular system, responsible for supplying oxygen-rich blood to the upper extremities and head. Three branches emerge from the aortic arch: the brachiocephalic trunk, the left common carotid artery, and the left subclavian artery. Under normal conditions, the left vertebral artery emerges from the left subclavian artery medial to the thyrocervical trunk and supplies blood to the upper part of the spinal cord, brainstem, and cerebellum. It ascends through the transverse foramina of all but the seventh cervical vertebrae and enters the posterior cranial fossa through the foramen magnum (Frankel and Roselli, 2023; Min et al., 2023). However, this structure does not always present the same anatomy in all individuals. Anatomical variants of the aortic arch are relatively common and may have clinical implications in some cases.

Anatomical variants of the aortic arch refer to any deviation from the normal structure and placement of the main branches of the aorta. These variants may imply a variation in the number, size, position and origin of the branches (Nandi et al., 2022). The presence of anatomical variants of the aortic arch may have important clinical implications in some patients, as they may affect blood perfusion to the upper extremities, head, and body. In addition, these variants can affect the interpretation of radiological studies, since the variation in the position and origin of the branches can make these structures similar to other pathologies (Case et al., 2015; Meester et al., 2023). Vertebral arteries are among thosemain arteries that supply blood to the spinal cord and brain.

Corresponding author: Dr. Kevin Doello. Medical Oncology Service, Virgen de las Nieves Hospital, 18014 Granada, Spain.E-mail: kdoello@correo.ugr.es

Submitted: October 10, 2023. **Accepted:** November 29, 2023

https://doi.org/10.52083/EWNO7926

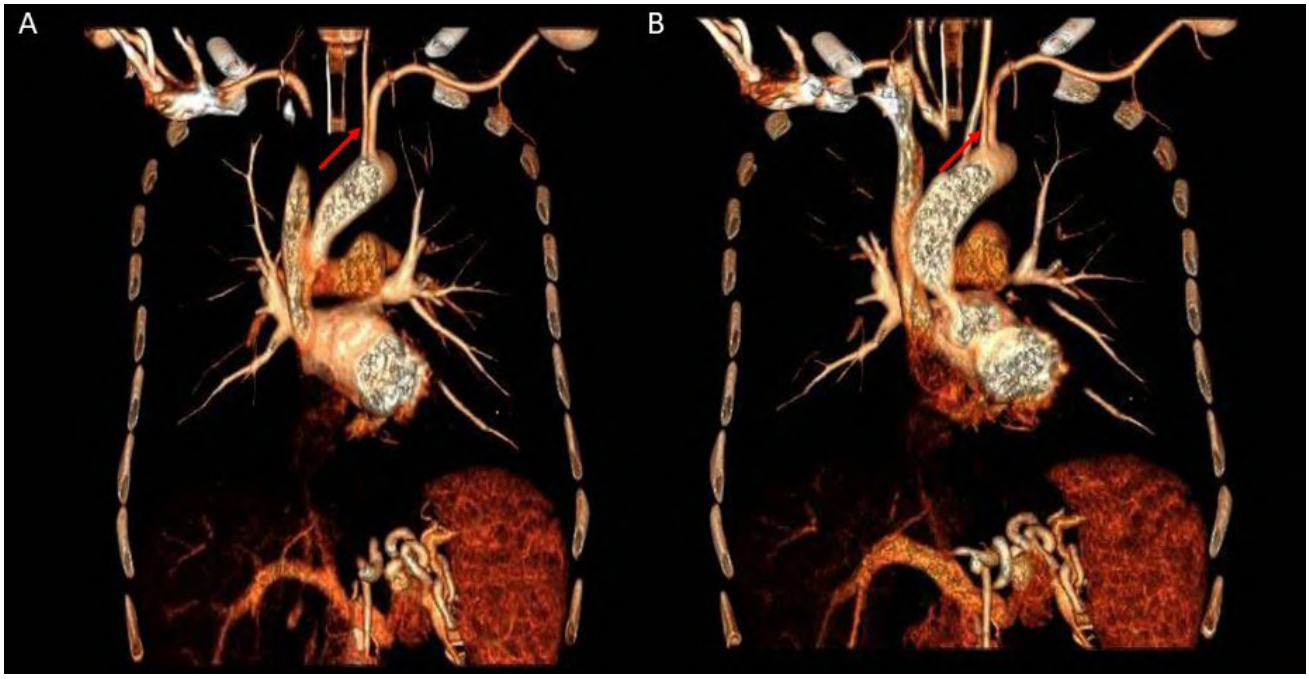

Fig. 1.- Coronal CT vascular reconstruction showing aberrant origin of left vertebral artery (red arrow) from aortic arc (**A** and **B**, different coronal views).

In terms of the embryological origin of the vertebral artery, cervical intersegmental arteries appear from the aortic arch. The first to sixth dorsal intersegmental arteries are anastomosed, and the inferior end is linked to the seventh dorsal intersegmental artery. The first portion of the left vertebral artery develops near the origin of the dorsal branch of the seventh cervical intersegmental artery. In order to go into the foramen transversarium of the sixth cervical vertebra, the artery follows a vertical and dorsal course (Magklara et al., 2020).

Normally, this artery arises from the left subclavian artery. However, in some cases, vertebral arteries may aberrantly originate directly from the aortic arch. One of the anatomical variants is known as aberrant origin of the left vertebral artery and is one of the most common variants of the aortic arch. More exactly, this aberrant origin comprises the types 3 and 4 of the classification of aortic arch trunks variants (Popieluszko et al., 2018). Although this anatomic variant may be asymptomatic in some patients, in others it may be associated with significant clinical complications.

CASE REPORT

This case concerns a 62-year-old male patient, a drinker and smoker, with no other personal history of interest. In 2017, the patient presented hoarseness and odynophagia, and an otorhinolaryngology examination was performed, which revealed a lesion in the left vocal cord that was pathologically diagnosed as squamous cell carcinoma of the larynx. In the CT corresponding to the extension study, an anatomical variant (Fig. 1) was observed by chance, consisting of the existence of an aberrant origin of the left vertebral artery directly from the aortic arch instead of originating from the left subclavian artery, which would be the usual origin. In fact, the left vertebral artery is originated from the aortic arch between the origin of the left carotid artery and the origin of the left subclavian artery. Furthermore, this arterial variant has a larger arterial diameter and penetrates through the transverse vertebral foramina, starting from the fifth cervical vertebra (Fig. 2). The patient had no symptoms in this regard. The final stage of his laryngeal tumor was T3N0M0. Due to the fact that the treatment with total laryngectomy would have been very mutilating, in this case a chemotherapy treatment based on cisplatin and radiotherapy for 2 months was decided. As of today, the patient is in complete response to treatment, that is, there is absence of any detectable cancer after completion of treatment and without signs of tumor relapse.

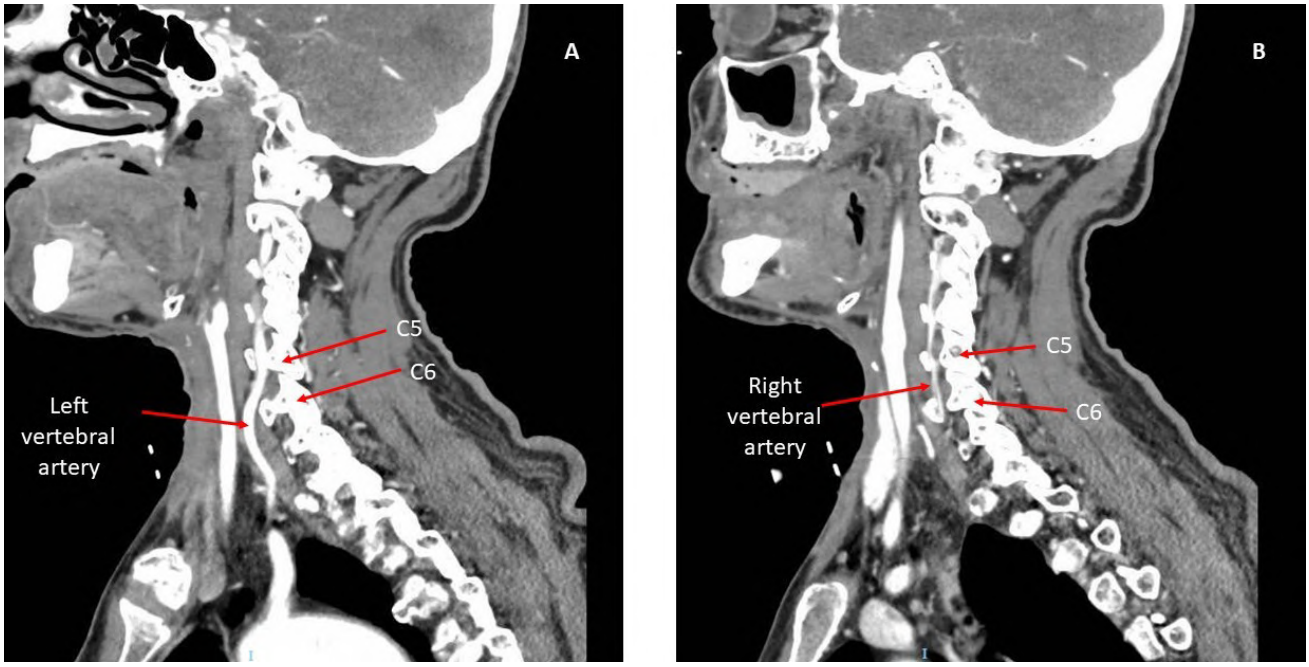

Fig. 2.- Sagittal CT with arterial intravenous contrast that show the entrance of left vertebral artery in transverse foramina in the fifth cervical vertebra (**A**) and in the sixth cervical vertebra in the case of right vertebral artery (**B**).

DISCUSSION

The existence of anatomical variations in the vertebral artery can be a problem when performing cervical surgeries on patients with degenerative diseases, tumors, infectious diseases or trauma, among others. In these procedures, an injury to the vertebral artery can be disastrous for the patient, since it can cause uncontrollable bleeding, syndromes associated with neck swelling such as dyspnea, and delayed hemorrhage from a pseudoaneurysm (Elnaggar et al., 2021). Regarding other studies that have described these malformations, it is worth highlighting the one published by Yuan et al., 2016, where it is indicated that most of the patients with alterations of the origin of the vertebral artery are asymptomatic and only 5.5% present some symptomatology derived from it.

According to different authors (Popieluszko et al., 2018; Adachi, 1928; Lippert et al., 1985; George et al., 2016), the variants of the origin of the aortic trunks are classified into 7 types. Of these, subtypes 3 and 4 are those in which the left vertebral artery originates directly from the aortic arch. Of them, subtype 3 would be the one that would correspond to the case described, since the rest of the aortic trunks originate in the usual way and the left vertebral artery would be the one that originates independently in the aortic arch before the origin of the left subclavian artery. Alterations in the origin of the left vertebral artery are present in 2.8% of the population, and subtype 3 is the third most common anomaly of the origin of the aortic trunks. Moreover, this case presents another variant, which consists of the left vertebral artery having a larger diameter than the right and penetrating the transverse foramina of the cervical vertebrae starting from the fifth vertebra. This anatomic variation is only present in approximately 3.3% of the population (Shin et al., 2014).

Finally, Ibrahim et al. (2021) describe the difficulty of aortic surgery in these patients, since they require different surgical strategies, and the risk of complications would be greater.

CONCLUSION

In conclusion, the aberrant origin of the left vertebral artery from the aortic arch is a rare anatomical variant that may be associated with various pathologies and complications. Their knowledge is important to avoid diagnostic errors and to plan safe surgical and radiological procedures.

ETHICAL CONSIDERATIONS

This clinical case has been carried out following the guidelines of the Virgen de las Nieves Hospital in Granada and the Helsinki protocol, with authorization for its publication being confirmed.

REFERENCES

ADACHI B (1928) Das Arteriensystem der Japaner. Verlag der Kaiserl Jap Univ, Kyoto, 1.

CASE D, SEINFELD J, FOLZENLOGEN Z, KUMPE D (2015) Anomalous right vertebral artery originating from the aortic arch distal to the left subclavian artery: a case report and review of the literature. *J Vasc Interv Neurol*, 8(3): 21-24.

ELNAGGAR ME, ABDULJAWAD H, ASSIRI A, EBRAHIM WH (2021) Anomalous origin of right vertebral artery from right common carotid artery. *Radiol Case Rep*, 16(6): 1574-1579.

FRANKEL WC, ROSELLI EE (2023) Strategies for complex reoperative aortic arch reconstruction in patients with congenital heart disease. *Semin Thorac Cardiovasc Surg*, 26: 81-88.

GEORGE B, BRUNEAU M (2016) Vertebral Artery. In*:* Tubbs RS, Shoja MM, Loukas M (eds). *Bergman's Comprehensive Encyclopedia of Human Anatomic Variation*. 2nd ed. Wiley Blackwell, USA, pp 487-500.

IBRAHIM M, CHUNG JCY, LINDSAY TF, OUZOUNIAN M (2021) Commentary: Aberrant vertebral arteries in aortic repair: Small but mighty! *JTCVS Techniques*, 7: 57-58.

LIPPERT H, PABST R (1985) Aortic arch. In: *Arterial Variations in Man: Classification and Frequency*. JF Bergmann-Verlag, Munich, Germany.

MAGKLARA EP, PANTELIA ET, SOLIA E, PANAGOULI E, PIAGKOU M, MAZARAKIS A, SKANDALAKIS P, TROUPIS T, FILIPPOU D (2021) Vertebral artery variations revised: origin, course, branches and embryonic development. *Folia Morphol*, 80(1): 1-12.

MEESTER JAN, HEBERT A, LOEYS BL (2023) Structural genomic variants in thoracic aortic disease. *Curr Opin Cardiol*, 38(3): 157-161.

MIN X, HU Z, WANG Z, XIA J (2023) Surgical treatment of double aortic arch malformation combined with descending aortic arch dissection in adults: A case series. *J Cardiothorac Surg*, 18(1): 174.

NANDI D, SHAW M, TAXAK A, KUMAR S (2022) Anomalous origin of right vertebral artery from aortic arch distal to origin of left subclavian artery in a patient with aneurysm of aortic arch and type B dissection of aorta. *BMJ Case Reports*, 15(3): e248004.

POPIELUSZKO P, HENRY BM, SANNA B, HSIEH WC, SAGANIAK K, PĘKALA PA, WALOCHA JA, TOMASZEWSKI KA (2018) A systematic review and meta-analysis of variations in branching patterns of the adult aortic arch. *J Vasc Surg*, 68(1): 298-306.

SHIN HY, PARK SK, JUNG GS, CHOI YS (2014) Variations in entrance of vertebral artery in Korean cervical spine: MDCT based analysis. *Korean J Pain*, 27(3): 266-270.

TROUTMAN DA, BICKING GK, MADDEN NJ, DOMER GS (2013) Aberrant origin of left vertebral artery. *J Vasc Surg*, 58(6): 1670.

YUAN SM (2016) Aberrant origin of vertebral artery and its clinical implications. *Braz J Cardiovasc Surg*, 31(1): 52-59.

Labial ankyloglossia - a case report on fusion of frenums

Sanjay CJ[1], Karthikeya Patil[1], Varusha Sharon Christopher[1], Vikram Jain[2]

[1] Department of Oral Medicine and Radiology, JSS Dental College and Hospital, JSS Academy of Higher Education and Research, Mysuru – 570015, Karnataka, India

[2] Department of Orthodontics and Dentofacial Orthopeadics, Farooqia Dental College and Hospital, Mysuru – 570021, Karnataka, India

SUMMARY

Labial ankyloglossia is a rare condition where the lingual frenum is found to be continuous with the labial frenum. It is a rare condition that can have a significant impact on a patient's quality of life. Early recognition and appropriate intervention can lead to substantial improvements in speech, oral hygiene, and overall well-being. This case report underscores the importance of considering labial ankyloglossia as a differential diagnosis in patients with lip-related issues and highlights the potential benefits of surgical correction in improving lip function and aesthetics.

Key words: Ankyloglossia – Lingual frenum – Labial frenum – Oral hygiene

INTRODUCTION

A frenum, which is additionally known as a frenulum, is a slender band of connective tissue found in the human body that serves as a stabilising or anchoring agent pertaining to specific bodily structures (Gottsegen, 1954). There are several distinct kinds of frenums located throughout the body, but a selection of the more prevalent ones includes the frenulum of the genitalia, the lingual frenum (under the tongue), and the labial frenum (within the lips). In order to preserve the normal range of motion and practicality in their respective locations, these structures are indispensable.

Clinical significance is attributed to frenum fusions in the oral cavity, which pertain to the tethering locations of the lingual or labial frenum. Variations in these frenula, including taut or loose attachments, can result in a number of functional and dental problems. The lingual frenum and lower labial frenum fused together, resulting in significant tongue hypomobility, make this case report individualistic.

CASE REPORT

The chief complaint of a 9-year-old boy who came to the outpatient facility was that he was having trouble swallowing and communicating. An intraoral examination revealed a tongue tie. The lingual frenum was positioned near the tip of the tongue and was thick and fibrous. It was connected anteriorly along the floor of the mouth

Corresponding author: Dr Karthikeya Patil. Department of Oral Medicine and Radiology, JSS Dental College and Hospital, JSS Academy of Higher Education and Research, Mysuru – 570015, Karnataka, India. Phone: +91 94498 22498. E-mail: dr.karthikeyapatil@jssuni.edu.in - ORCID: 0000-0002-7941-2467

Submitted: November 4, 2023. **Accepted:** December 28, 2023

https://doi.org/10.52083/LLMP7366

Fig. 1.- 'V' shaped notch seen in the floor of the mouth with the fusion of labial and lingual frenum in the lower arch.

with the mandibular labial frenum. The young toddler was unable to stick out his tongue. When the tongue was raised towards the palate, it displayed a typical 'V' shaped notch (Fig. 1). The tongue was unintentionally thrust out when the lower lip was pulled outward by the pull of the labial frenum. Similarly, the lower lip pulled forward as the tongue retruded into the floor of the mouth (Fig. 2). Blanching was seen over the frenum upon forcing the lip and tongue apart forcibly. Because of the fusion of the frenums, there were missing teeth in the lower anterior region. In addition to malnourishment, the patient had bad dental hygiene.

DISCUSSION

Labial ankyloglossia is a rare type of ankyloglossia where the frenulum attaches the lower lip to the gum, limiting the mobility of the lip and tongue. This condition can cause difficulties with breastfeeding, speech, and oral hygiene. Ankyloglossia can be classified into four classes based on Kotlow's assessment, with Class I being mild ankyloglossia and Class IV being complete ankyloglossia. However, there is no consensus on the best classification system for ankyloglossia, and individual evaluation and treatment discussions based on each patient's circumstances are recommended (Chaubal and Dixit, 2011). Only two such cases of labial ankyloglossia have been reported to the best of our knowledge (Bahadure et al., 2016; Chandrashekar et al., 2014).

Ankyloglossia typically becomes apparent in the first trimester of pregnancy, at the very beginnings of embryonic development. Like a multitude of other structures in the body, the lingual frenum sets up through a convoluted procedure of tissue growth and differentiation. From the base of the tongue to the floor of the mouth, the lingual frenum fosters an annular band of connective tissue. It encompasses an assembly of mesenchymal and epithelial cells that self-organize and

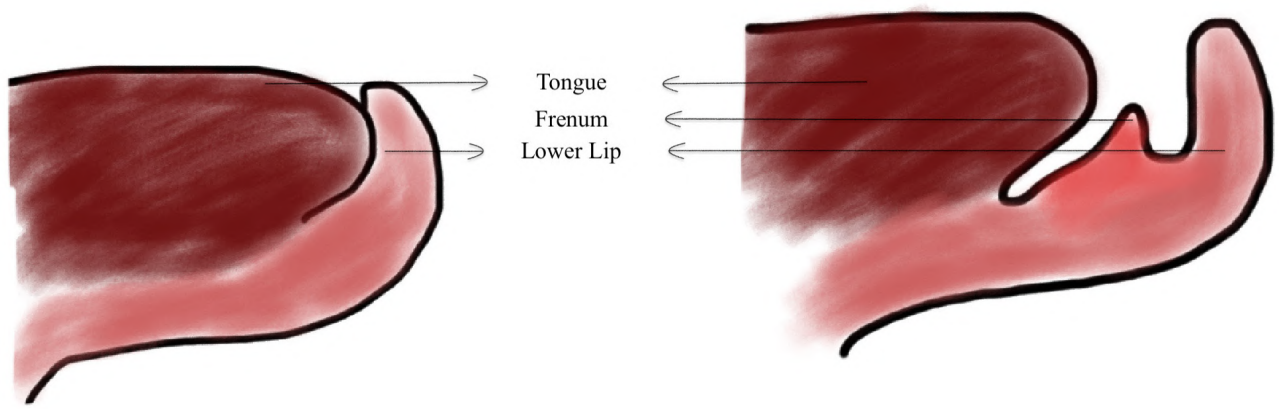

Fig. 2.- Tongue first develops fused to the floor of the mouth. Later, its anterior and inferior margin retracts, and the frenulum is the remnant of its most anterior attachment. Ankyloglossia is caused by an unusually short, thick lingual frenulum.

are proficient in forming the frenum framework (Kummer, 2023). The absence of permanent teeth and the fusion of the tongue tip to the lower lip in this instance indicate that the area where the first brachial arches fused has not developed normally. The normal development of the tongue and lip have been demonstrated in Fig. 2.

Although its precise causes are enigmatic, ankyloglossia can manifest as the consequence of both hereditary and environmental factors. An attachment characterised by being either tight or short could stem from genetic predispositions that affect the lingual frenum's structure. The moment of onset of ankyloglossia may also be susceptible to environmental variables or genetic changes (Suter and Bornstein, 2009).

Male-to-female ratios spanning from 1:1 to 3:1 continually demonstrated in multiple studies. X-linked or autosomal dominant inheritance may be postulated by the aforementioned findings. The disparities between ankyloglossia cases that strike sporadically and those that are familial impede this understanding. Unlike familial occurrences, most cases of ankyloglossia are assumed to be random and to have a greater male predisposition. There have been also reports of teratogen or environment-related causes of ankyloglossia (Klockars and Pitkäranta, 2009).

Ankyloglossia typically manifests alone in a familial pattern, but it can also surface syndromically in conditions like Ehlers-Danlos syndrome and oro-facio-digital syndrome. In certain familial patterns, male-to-male transfer provides partial vulnerability for an autosomal dominant inheritance pattern. An X-linked pattern is observed in other genes attributed to ankyloglossia, such as TBX22 mutations, which are also linked to cleft palate. As one of the multitudes of birth malformations linked to congenital Zika syndrome, the lingual frenulum was additionally observed to be aberrant, either non-existent or positioned posteriorly (Mintz et al., 2005).

Given the child's age, the severity, and the commonality of the condition, tongue-tie in newborns and children can have a wide array of repercussions. The most scrutinised area of this is how tongue-tie hinders an infant's ability to breastfeed. A synchronised peristaltic process and the establishment of a robust seal between the mother's nipple and the baby's oral cavity are requisites for effective breastfeeding. This seal facilitates the generation of an intraoral vacuum. The vantage point of the tongue matters for each of these phases (Hogan et al., 2005).

Disputes pertaining to dental health, orthognathic development, and oral hygiene are additionally posed by the tongue's tethering caused by this very particular kind of labial ankyloglossia. For one to clean the teeth after meals and remove any remaining food particles that may contribute to caries, tongue mobility is imperative. It is believed that a tight lingual frenulum is linked to a higher risk of dental caries because it limits the tongue's capacity to effectively reach and regularly clean every tooth. Apart from dental cavities,

a few investigations have linked issues related to appropriate occlusion and craniofacial development to the lingual frenulum (Messner and Lalakea, 2000).

The mainstays of alleviating ankyloglossia are surgical procedures such as frenotomies, frenectomy, and frenuloplasty. Based on the extant literature, there is no surgical technique that is preferred above the others. The patient's age and peculiar characteristics of the ankyloglossia usually ascertain the surgical course of treatment. Additionally, with the goal of enhancing suction and preventing scar repudiation, some research indicates that myofunctional treatment may be helpful both before and after surgery. It should be mentioned that opinions regarding whether tongue ties require surgical intervention and whether they can be managed with observation are still being debated. More investigations and research are required to develop an improved line of treatment (Baker and Carr, 2015).

This case study concludes by emphasising the need for diagnosing and treating labial ankyloglossia, a disorder that, despite being relatively uncommon, can significantly affect a patient's oral health and overall quality of life. This example highlights the value of early detection and treatment for cases of labial ankyloglossia, which will ultimately give patients a more functional and comfortable oral environment. The greatest possible outcomes for patients in the future will be ensured by ongoing research and clinical experience in this area, which will further refine our understanding and treatment options for this ailment.

REFERENCES

BAHADURE RN, JAIN E, SINGH P, PANDEY R, CHUK R (2016) Labial ankyloglossia: A rare case report. *Contemp Clin Dentist*, 7(4): 555-557.

BAKER AR, CARR MM (2015) Surgical treatment of ankyloglossia. *Oper Tech Otolaryngol Head Neck Surg*, 26(1): 28-32.

CHANDRASHEKAR L, KASHINATH KR, SUHAS S (2014) Labial ankyloglossia associated with oligodontia: a case report. *J Dentist*, 11(4): 481-484.

CHAUBAL TV, DIXIT MB (2011) Ankyloglossia and its management. *J Indian Soc Periodontol*, 15(3): 270-272.

GOTTSEGEN R (1954) Frenum position and vestibule depth in relation to gingival health. *Oral Surg Oral Med Oral Pathol*, 7(10): 1069-1078.

HOGAN M, WESTCOTT C, GRIFFITHS M (2005) Randomized, controlled trial of division of tongue-tie in infants with feeding problems. *J Paediat Child Health*, 41(5-6): 246-250.

KLOCKARS T, PITKÄRANTA A (2009) Inheritance of ankyloglossia (tongue-tie). *Clin Genet*, 75(1): 98-99.

KUMMER AW (2023) ankyloglossia: typical characteristics, effects on function, and clinical implications. *Seminars Speech Language*, 44(4): 217-229.

MESSNER AH, LALAKEA ML (2000) Ankyloglossia: controversies in management. *Int J Pediat Otorhinolaryngol*, 54(2-3): 123-131.

MINTZ SM, SIEGEL MA, SEIDER PJ (2005) An overview of oral frena and their association with multiple syndromic and nonsyndromic conditions. *Oral Surg Oral Med Oral Pathol Oral Radiol Endodontics*, 99(3): 321-324.

SUTER VGA, BORNSTEIN MM (2009) Ankyloglossia: facts and myths in diagnosis and treatment. *J Periodontol*, 80(8): 1204-1219.

The utility of soft-preservation in Medical Education: Current trends & future directions

Michael Leake[1], Aslam Ejaz[2], Romal Patel[2], Joy Y. Balta[3,4]

[1] Division of Anatomy, Department of Biomedical Education and Anatomy, College of Medicine, The Ohio State University, Columbus, Ohio

[2] Department of Surgery, Wexner Medical Center, The Ohio State University, Columbus, Ohio

[3] Anatomy Learning Institute, College of Health Sciences, Point Loma Nazarene University, San Diego, California

[4] Division of Anatomy, Department of Surgery, University of California, San Diego, California

SUMMARY

The future of Medical Education (ME) must be evaluated in light of the increasing variety and availability of educational models and embalming techniques for student and physician education and training. To evaluate the viability and sustainability of the different learning models, research and data on the diverse teaching modalities will be assessed from the perspectives of training residents and physicians. A literature review was conducted to provide an overview of the diversity of soft-preservation techniques presently available. It was shown that ME is optimized using soft-preservation techniques, but that many are limited in their present ability to accurately reflect the live human anatomy, and that more research must be done to identify the optimal preservation technique given unique educational needs. The aggregation of current research study results will aid educational programs in identifying the modalities of training most appropriate for their curriculum, and help in identifying models that can be utilized long-term to improve ME.

Key words: Medical Education – Simulation – Body donors – Soft preservation

INTRODUCTION

Medical Education

Medical Education (ME) can take on a variety of forms, depending upon the medical specialty. For practicing physicians, the scope of ME encompasses educational activities that aid medical professionals in maintaining, further developing, or increasing their professional and interpersonal knowledge and skills (AAMCE, 2022). While one's medical specialty may largely influence the specific set of Continuing Medical Education (CME) requirements, the overarching purpose is to aid physicians in continuing their life-long learning and to facilitate the enhancement of medical care to their patients and the medical field as a whole (University of Buffalo, 2018).

However, prior to being trusted with autonomy within the clinical setting, it is vital that physicians

Corresponding author: Dr. Joy Y. Balta. Anatomy Learning Institute, College of Health Sciences, Point Loma Nazarene University, San Diego, California, USA. E-mail: joy.balta@gmail.com

Submitted: May 26, 2023. **Accepted:** November 11, 2023

https://doi.org/10.52083/SNUW7660

be well-practiced and competent in their skillset. While the process of medical training is long and arduous, in many ways a physician's technical proficiency is intimately linked with their amount of experience. Under ideal circumstances without real-world consequences, physicians would be able to practice on live patients. However, this is not feasible for legal and ethical reasons, as well as the premise of providing optimal care for patients. As such, identifying training methods that appropriately and accurately mirror live medical circumstances is vital for preparing physicians to practice autonomously. Such a model is referred to as simulation-based training (Al-Elq, 2010).

Simulation refers to artificially representing real world circumstances and settings. In the context of ME, simulation-based training involves the recreation of clinical scenarios to promote the acquisition of clinical skills through deliberate and repeated opportunities to practice, while also removing the direct consequences of practising on real patients under high-risk settings. Under simulated conditions, trainees and inexperienced medical professionals can learn without fear of harming their patients, focusing less on the consequences of their mistakes, but directing their attention primarily to the acquisition of skills and knowledge for future application (Al-Elq, 2010).

Forms of Simulation-Based Training

One of the primary modalities of simulation-based training involves the use of models. Simulation-based learning models can be categorized into several different classifications based on their resemblance to reality. Low-fidelity models include static models without realism or scenario-based context, while medium-fidelity educational tools have more resemblance to reality with basic life function characteristics (pulse, heart sounds, and breathing sounds), and high-fidelity simulators incorporate manikins that reproduce physical signs and physiological readings on monitors (Al-Elq, 2010).

More recently, virtual and augmented reality show promise in multiple realms of medicinal and surgical education. Neurosurgery is one of the medical fields that has benefited from integrating virtual reality into their training and practice. A study by Bernardo (2017) provided an overview of the current future utility of virtual reality simulators in neurosurgical training. By simulating three-dimensional scenes and evoking a comparable sensory experience similar to real life experiences, neurosurgeons were able to begin to learn complex tactile and often unnatural surgical skills/procedures through intuition, repetition, and direct computer/teacher feedback.

Another simulation model that has been utilized particular in surgical settings is the animal model. Being able to practice these skills and techniques in-vivo in the animal model facilitates procedural learning in a safe environment, sparing the negative consequences of practising on live patients (Bergmeister et al., 2020). However, while these simulation models can represent reality and can aid training physicians in the acquisition and practice of vital clinical and surgical skills, they cannot fully replicate it (Al-Elq, 2010). A study by Carey et al. (2014) highlighted that the primary limiting factor of simulation models is their lack of translatability to live conditions. They subsequently asserted that the next best option for simulating procedures was on human body donors due to its approximation of live tissue. Venne et al. (2020) similarly concluded that in addition to the initial expense of simulation models, the artificial modalities could not fully reflect the immense variability and intricacy of the live human anatomy. This is usually highlighted in the anatomical variations present in the human body along with the morbidity and causes of death that could only be appreciated when working with body donors (Konschake and Brenner, 2014; Balta et al., 2022). Therefore, the human body donor model remains in many ways the gold standard for ME and the acquisition of clinical and procedural knowledge. Human body donors have been used for anatomical education for centuries and their utility in clinical education has expanded over the years. For this reason, many of the studies investigating the use of body donors in clinical education would rely primarily on experiences in anatomical dissection (Balta et al., 2022).

Human Body Donor Model

Human body donors have been used in numerous medical fields to aid in procedural skills ac-

quisition to overcome the initial learning curve, as well as to replace learning on live human patients (Porzionato et al., 2014; Yiasemidou et al., 2017; Watanabe et al., 2019; Nagase et al., 2022). One way in which human body donors have been utilized in internal medicine resident education is by simulating arthrocentesis (Gould et al., 2020). The study highlighted that, after the completion of a skills lab with human body donors, there was a 70% increase in confidence in performing arthrocentesis procedures. It was additionally noted that prior data and literature had shown that internal medicine program graduates had previously not felt adequately prepared to provide competent care to their patients in such procedures (Gould et al., 2020).

However, while studies have shown the potential of the human body donor model in ME, there is a significant constraint associated with the availability of unembalmed human body donors, limiting their viability as a continued and sustainable ME resource. While simulation would ideally be performed on unembalmed human body donors, the rate of decomposition of the human body makes this unsustainable for longitudinal ME. This rapid rate of decomposition has led programs to rely upon embalming techniques to prolong the viability and utility of each human body post-mortem.

Human Body Donor Embalming

While unembalmed human body donors initially reflect the color, texture, and tensile strength of unembalmed tissue, and seem like the obvious choice for simulating live operating conditions, their rapid decomposition following thawing presents many potential problems (Macchi et al., 2003; Hayashi et al., 2015). To avoid these issues, embalmed human bodies have been utilized to maintain desired anatomical properties, while minimizing the risk of infection and tissue desiccation as well as costs, and also maximizing body utility for teaching, educational, or surgical experiences (Hayashi et al., 2015).

Embalming is the process of exposing a subject to chemicals after death to prevent decay (Balta et al., 2015). Traditionally, chemical such as formaldehyde, glutaraldehyde, phenol, glycerin, bronopol, ethanol, and glycol have been utilized in embalming. However, each chemical and combination of chemicals offers unique benefits and drawbacks in quality of tissue, specifically in tissue appearance, texture, and flexibility. As such, it is vital that users assess each embalming method and identify the technique most optimal given their unique needs (Balta et al., 2018).

Types of Embalming Techniques

In discussing the utility of varying embalming techniques, it is important to define terms that have historically been ambiguously understood. When referring to a human body donor that has not been chemically treated, the appropriate term is an unembalmed human body donor. When an embalming solution produces a human body donor with joint flexibility less than that of the unembalmed body, the donor is described as "hard-fixed." In addition to hard-fixation, there is also an embalming technique known as "soft-preservation." Soft-preserved human body donors are defined as donors that have equal or more joint range of motion than that of the unembalmed human body donor (Balta et al., 2015).

Hard-fixation is the most common embalming technique, and it generally relies upon high concentrations of formaldehyde. Formaldehyde is one of the most common and important chemicals in embalming. Initially introduced in the late 19th century, it has been utilized consistently in human body donor embalming due to its low cost and wide availability. Working with formaldehyde is considered hazardous due to the carcinogenic impact on a living body and therefore strict exposure levels continue to be imposed (Balta et al., 2015). Human body donors embalmed with formaldehyde are often referred to as formalin-fixed. While formalin-fixation does offer excellent results in terms of eliminating potentially harmful bacteria, fungi, and other organisms, its high concentrations also result in extreme soft-tissue changes on the human body donor (Hayashi et al., 2015).

Formalin-fixed human body donors typically do not exhibit their normal tissue qualities, including color, texture, flexibility, elasticity, and pliability (Balta et al., 2015). The resultant tissues

often take on a greyish hue, appearing noticeably different compared to their former state, and are pervaded by a pungent, potentially carcinogenic, and unpleasant odor (Balta et al., 2015; Hayashi et al., 2015). While this may be sufficient for learning basic human anatomy, surgeons have questioned how realistic embalmed human body donors are and have sought ways of better emulating live tissue. This concern has resulted in interest in soft-preservation techniques, including Thiel-preservation, Saturated Salt Solution (SSS), Imperial College of London – Soft Preservation (ICL-SP), N-vinyl-2-pyrrolidone, and Modified Larssen Solution (MLS) techniques, which purportedly better resemble live tissue (Balta et al., 2015).

SOFT-PRESERVATION

Soft-preservation was first pioneered by Walter Thiel in 1992 with the advent of Thiel- preservation to better preserve tissue characteristics, including color, texture, pliability, and structural integrity (Thiel, 1992a, 1992b). Another adaptation of the Thiel method was published in 2022 (Thiel, 2002). However, as new soft-preservation techniques had been developed and become more readily utilized the variety of different applications have also increased, particularly within ME (Balta et al., 2015).

Thiel-Preservation in ME

By a significant margin, the most heavily and diversely researched/utilized soft-preservative method is the Thiel-preservation technique which preserves a deceased human body for over a year as indicated in Table 1. With the solution being first implemented at the University of Graz, one of the first dealings was utilizing this technique as a learning and training model for arthroscopic surgery (Grechenig et al., 1999).

In the practice of thoracic endovascular aortic repair (TEVAR) and endovascular abdominal repair (EVAR), McLeod et al. (2017) simulated procedures utilizing Thiel-preserved human body donors in conjunction with extracorporeal pulsatile ante-grade flow into the aorta. It was concluded that, in conjunction with the perfusion of the aorta, Thiel-preserved human body donors appropriately simulated aortic endovascular procedures both anatomically and physiologically, and additionally had potential in interventional radiologic training and medical device testing (McLeod et al., 2017).

Thiel-preserved human body donors have also been assessed as a viable training model in the context of upper and lower urinary tract endoscopy training. Bele and Kelc (2016) determined that, while there were limitations to the model in comparison to performing the procedure on live patients, the model was suitable as a simulation model for the initial training of urethrocystoscopy and ureteroscopy. The primary drawbacks of the preservation technique were that the bladder mucosa lacked visible vessels, making the model unsuitable for clinically identifying mucosal abnormalities, as well as the lack of muscle tonus, which made ureteroscopy more difficult, although still possible (Bele and Kelc, 2016).

In the context of head and neck preservation, Miyake et al. (2020) sought to evaluate the Thiel-preservation method for head and brain surgery training. Thiel-preservation is known for being able to preserve tissue's natural color, flexibility, and plasticity, but generally causes brain softening, limiting Thiel-preservation in the context of intra-cranial procedure practice. However, when used in conjunction with intra-cerebral ventricular formalin injection, the brain yielded suitable elasticity for surgical simulation. The ability of the brain to be appropriately mobilized and to develop the needed surgical field suggested that the method could be used to improve head and brain human body donor surgical training (Miyake et al., 2020). Additionally, Humbert et al. (2022) utilized Hammer's modified Thiel technique to evaluate the preservation method in comparison to formalin-fixed and frozen heads. Assessing the models, surgeons ranked the modified Thiel-preservation technique the best for quality of dissection, tissue identification, submandibular and parotid gland dissections, and otologic surgery involving the skin/eardrum, bone and muscle tissue. The modified technique was only not preferred for endonasal dissection. These results showed that the use of modified preservation technique can improve the quality of head and neck surgical anatomy

education similar to the findings of other studies (Feigl et al., 2007; Humbert et al., 2022).

In a study performed by Yiasemidou et al. (2017), researchers sought to evaluate Thiel-preserved human body donors as high-fidelity simulators over multiple surgical training specialties. It was determined that in examining the preserved donors over a broad range of specialties, anatomical accuracy and tissue properties were rated very positively, apart from preservation of the brain, eyes, and blood vessels (Yiasemidou et al., 2017). Several studies have also demonstrated the benefits of working with Thiel embalmed donors for ultrasound guided punctures and cricothyroidotomy (Benkhadra et al., 2008, 2009; Heymans et al., 2016).

In evaluating Thiel versus formalin-embalmed human body donors for thyroid surgery, Eisma et al. (2011) determined that the Thiel-preserved human body donors better represented real life surgical conditions. In assessing both the Thiel-preserved and formalin-embalmed human body donors, Thiel-preserved donors were preferred in all aspects including tissue quality (quality of skin, fat, muscle, blood vessels, and nerves), procedure perception (surgical position of the patient for the operation, designing the incision for the operation, making the incision, raising subplatysmal flaps, and retraction), and identification of structures (identification of muscular structures, vessels, the recurrent laryngeal nerve, and parathyroid glands) (Eisma et al., 2011).

In seeking to identify a suitable model for representing structures of the ear, Alberty et al. (2002) determined that Thiel-preservation effectively simulated temporal bone surgical training. Specifically in evaluating surgical techniques on external and middle ear structures, the structure and consistency of tissues of the auditory canal, tympanic cavity, and mastoid were regarded as comparable to live tissue, while the cartilage of the auricle was considerably softened (Alberty et al., 2002).

Additionally, Bailey et al. (2021) sought to improve ME through the utilization of Thiel-preserved human body donors. It was determined that the soft-preserved bodies were incredibly valuable for not only practising physical examinations and increasing participant confidence in performing Lachman tests, but also because live standardized patients (SPs) cannot reproduce physical examinations findings.

In a study performed by Hölzle et al. (2011), Thiel-preserved human body donors were evaluated in the context of dental education and for the teaching of oral surgery and implantology. Results indicated that even after weeks, the body maintained life-like tissue properties with the same high quality of tissue, particularly within the maxillary sinus membrane, mucosa, bone, and nerves, making the soft-preservation technique ideal for practising such oral procedures (Hölak et al., 2011).

In comparing fresh-frozen and Thiel-preserved human body donors for their suitability in biomedical education and research purposes, a study by Gatt et al. (2019) demonstrated there were no statistically significant differences identified between the two models regarding the kinematics and kinetics of the embalmed feet. It was concluded that such results indicated that the kinematic and kinetic properties of fresh-frozen and Thiel-preserved human body donor feet were not dissimilar, suggesting that they could be interchangeable in ME and research (Gatt et al., 2019).

In assessing Thiel-preserved human body donors in tropical weather, Reddy et al. (2017) sought to modify and improve the utility of the soft-preserved bodies in non-temperate climates. Generally, while Thiel-preserved human body donors have been accepted and effectively used in temperate climates, their use in tropical locations has been limited due to the poor short-term preservation outcomes. However, utilizing a modified Thiel-preservation technique, the soft-preserved bodies were successfully used for various surgical simulation exercises, making the use of Thiel-preserved human bodies more accessible and sustainable in tropical countries and locations (Reddy et al., 2017).

Thiel-preservation has also been evaluated in veterinary anatomy education. In a study conducted by Nam et al. (2020), while Thiel-preserved tissues were the most expensive embalming method, they also were superior to formalin-fixed

bodies for joint and muscle movement, lack of offensive/irritating odor, preference by students for identifying anatomical structures, and maintaining muscle and internal organ color and texture comparable to living animals.

Thiel-preserved human body donors have been also evaluated for their viability in laparoscopic, endoscopic, and microsurgical procedures. Porzionato et al. (2014) identified Thiel embalmed human body donors as being viable learning models for teaching transanal/transrectal and transvaginal Natural Orifice Transluminal Endoscopic Surgery (NOTES). Additionally, Rashidian et al. (2019) found that for training laparoscopic liver surgery the Thiel-preserved human body donors were considered to be superior to other training modalities, including proctoring in the operating room, virtual reality, video training, and practice on pigs. A study by Ruiz-Tovar et al. (2019) determined that Thiel-preserved human body donors were the optimal method for the simulation of laparoscopic bariatric surgery over other teaching modalities, including virtual reality simulators and practice on animal models, owing to the body's ability to simulate life-like elasticity of the tissues necessary for laparoscopic bariatric surgery simulation. For evaluating Thiel-preserved human body donors in laparoscopic Roux-en-Y gastric bypass procedures, Zevin et al. (2012) concluded that the model was superior to both the porcine model and virtual reality simulation by offering tactile practice, preserving tissue color and consistency comparable to real life, and allowing participants to practise patient positioning. And in a study performed by Odobescu et al. (2019), Thiel-preserved human body donors were regarded positively as high-fidelity simulation models for training surgeons the basics of nerve repair, preserving the fascicles, perineural, and epineural sheaths well.

While the soft-preservation of human body donors has been studied most utilizing the Thiel-preservation technique, in seeking to further improve ME and surgical skills training different soft-preservation techniques have been invented and studied, including the Saturated Salt Solution (SSS).

Saturated Salt Solution in ME

In seeking to identify an ideal human body donor embalming/preservation technique for surgical skills training, Hayashi et al. (2014) compared formalin-fixed, Thiel-preserved, and SSS methods based on bacterial/fungal cultures and range of motion measurements (Hayashi et al., 2014). Results from the study indicated that the

Table 1. Advantages and disadvantages of soft-preservation techniques.

Soft Preservation Techniques			
Techniques	**Advantages**	**Disadvantages**	**Investigated Specialty**
Thiel	- Long term preservation - Thoroughly investigated	- Expensive - Immersion needed - low levels of formaldehyde	Pediatrics [21], TEVAR [22], Endoscopy [23], Brain Surgery [24], Temporal Bone [28], Oral Surgery [30], Liver surgery [35], Bariatric surgery [37]
Saturated Salt	- Long term preservation	- Expensive - Immersion needed - Corrosive material - Formaldehyde & phenol present	Orthopedics [40], Oral Procedures [41], Trauma Surgery [44]
ICL- SP	- Inexpensive - No immersion needed	- Short term preservation - Understudied - Formaldehyde & phenol present	Surgical Skills [11], Gynecology [44]
N-Vinyl-2-Pyrrolidone	- Inexpensive - No immersion needed - Long term preservation - No formaldehyde & phenol	- Understudied	Laparoscopic Training [45]
Modified Larssen	- Inexpensive - No immersion needed	- Formaldehyde present - Short term preservation	Surgical Training [46]

SSS method sufficiently neutralized infectious agents, produced bodies with flexible joints and high-quality tissue for surgical skills training that remained in good condition for a long period of time as outlined in Table 1. This method also produced tissues acceptable for ultrasound imaging, central venous catheterization, and incision with cauterization and auto suture stapling (Odobescu et al, 2019).

In the context of orthopedics specifically, Burns et al. (2018) sought to further evaluate SSS in the improvement of surgical skills training. Comparing SSS-preserved human body donors to those embalmed with formaldehyde or alcohol-glycol solution, the SSS bodies were regarded as superior to the bodies embalmed in other methods, producing joints with suitable motion, stiffness, visual and tactile tissue fidelity, and odor suitable for high-fidelity surgical skills training.

In the training of oral surgical skills, Watanabe et al. (2019) determined that, after completion of six procedures associated with intra- and extra-oral bone harvesting with SSS-preserved bodies, self-assessed confidence levels showed statistically significant increases. Additionally, in examining the anatomical features of the SSS-preserved human body donors, the oral mucosa and skin were regarded as similar to living tissues with bone tissue hardness and realism being maintained, and all procedures offering sufficient realism at lower preparation and storage cost, with minimal odor (Watanabe et al., 2019).

Evaluating SSS-preserved human body donors for the surgical simulation of trauma surgeries, Homma et al. (2019) concluded that SSS-preserved bodies are useful for surgical skills training, especially surgical repairs. Results specifically indicated that SSS bodies were more suitable than formalin-fixed bodies for surgical skills training and that participants in the study showed increased self-assessed confidence after completion of the trauma surgery seminar after half a year, with the exception of external fixation for pelvic fracture (Homma et al., 2019).

In a study by Nam et al. (2020), authors evaluated SSS-preserved, Thiel-preserved and formalin-fixed tissues. Tissues preserved by SSS were more expensive than formalin-fixation and less expensive than Thiel-preservation, but, like the Thiel-preserved tissues, the SSS-tissues facilitated superior joint and muscle movement in comparison to formalin-fixed tissues, preserving life-like muscle and internal organ color and texture, with no offensive smell, and being preferred by students for identification of anatomical structures (Nam et al., 2020).

Soft-preservatives have also expanded into phenol-based solutions including the Imperial College of London – Soft-Preservation (ICL-SP) technique.

Imperial College of London – Soft-Preservation in ME

A limited number of studies have investigated the ICL-SP technique compared to the Thiel and SSS embalming techniques. A study by Venne et al. (2020) compared Thiel-preservation to phenol-based preservatives such as the ICL-SP technique. This study concluded that donors embalmed using a phenol-based technique had similar features to that of Thiel embalmed donors. Results of the study indicated that all participants rated the phenol-based tissues consistently better or equivalent to the Thiel-preserved tissues for surgical skills training, there was no statistically significant difference in tensile elasticity between ICL-SP tissue and fresh tissue, and the phenol-based technique better preserved skin histologically (Venne et al., 2020).

In a study directly investigating the utility ICL-SP donors in the training of gynecological oncologists, Barton et al. (2009) concluded that soft-preserved bodies should be used over formalin-fixed in surgical training. It was noted that while the trainees' anatomical knowledge was initially weak, as the surgical skills lab progressed through surgical dissection of the abdomen and pelvis, subspecialty participant knowledge improved markedly, represented by pre- and post-skills lab evaluations (Barton et al., 2009).

Another soft-preservation technique developed in order to circumvent the health hazards and overhardening associated with formalin-based solutions is N-vinyl-2-pyrrolidone.

N-Vinyl-2-Pyrrolidone in ME

In a study performed by Nagase et al. (2022), it was determined that donors preserved using N-vinyl-2-pyrrolidone had soft and pliable tissue that lasted up to thirty-seven months without any change in the quality of tissue. In the review, they also introduced the preservation technique in surgical and medical procedural training, including endotracheal intubation, motion physiology of the vocal folds, laparoscopic and endoscopic procedures, and the development of medical devices (Nagase et al., 2022).

An embalming technique that also sought to mitigate the disturbing smell, mucosal irritation, discoloration, and rigidity associated with formalin-fixation was the modified Larssen solution.

Modified Larssen Solution in ME

In seeking to identify an appropriate and affordable embalming technique that preserved tissue color, texture, pliability, and flexibility for numerous repeated surgical trainings, Bilge and Celik (2017) concluded that Modified Larssen Solution (MLS) effectively served as a sustainable and cost-effective embalming method for surgical training. Results indicated that skin color did not change after MLS perfusion, and that the color of muscles, fasciae, fatty tissue, nerves, and vessels were determined to be life-like for both open and laparoscopic procedures. Additionally, MSL-preserved bodies had no irritating odor, exemplified elbow flexion comparable to fresh-frozen human body donors, and the tissue properties mimicked life-like tissues for several weeks without changing (Bilge and Celik, 2017).

Finally, a study performed by Balta et al. (2018) sought to compare the effects of embalming fluids on the structures and properties of tissues in human body donors. The quality of tissue did not change in an ICL-SP embalmed donor for 4-6 months. When comparing formalin, genelyn, Thiel and ICL-SP techniques, the results showed that formalin and genelyn solutions decreased joint mobility and Thiel technique increased mobility. Genelyn is a commercially available solution that does contain formaldehyde (Balta et al. 2015). ICL-SP joints demonstrated similar range of motion to their unembalmed measurements, indicating that ICL-SP faithfully mimics the joints of unembalmed bodies and would be ideal for the simulation of orthopedic and rheumatologic training. The study also sought to evaluate the effect of embalming solutions on internal organs and vessels. Results indicated that formalin-based solutions better maintained the shape of the organs and vessels investigated than did Thiel-preserved. It was noted that formalin is necessary in order to retain the size and shape of organs and vessels under study owing to the formaldehyde's fixing abilities, while solutions without strong fixing agents result in collapsing tissues (Balta et el., 2018).

CURRENT UTILITY AND FUTURE OF SOFT-PRESERVATION IN MEDICAL EDUCATION

Within the context of reduced work hours and an increased scrutiny of patient safety, there is an unmet need for more realistic and cost-effective training tools in ME. These modern constraints have led to an increased reliance on simulation to provide opportunities for simple and complex skill acquisition outside of clinical practice. Simulation in ME decreases stress, increases confidence, and allows for a mitigation of the learning curve for the medical trainee, particularly for procedural-based skills. While formaldehyde-fixed human body donors allow for accurate identification of relevant anatomy, soft-preserved models provide an invaluable experience for learners as cost-effective realistic simulation.

As evidenced in the studies previously cited, soft-preserved human body donors provide a more realistic model that has been proven effective in ME and training across specialties. As the models can be utilized for several months, a single donor can be efficiently utilized for numerous different procedure-specific or anatomic-based labs. Future studies should focus on comparative effective analyses of soft-preserved models compared to other high-fidelity models and the integration of additional techniques to better simulate a real patient experience (i.e., perfused models). It would be also important to perform an in-depth critical analysis of the benefits of human

body donor simulation through an assessment of students' skill development (objective measures of skill development/acquisition) and how these may potentially translate to improved patient outcomes.

CONCLUSION

Increasingly in the 21st century, there is a myriad of different simulation methods, embalming techniques, and innovations in technology that have benefit in ME. While many of them show immense promise and future potential, most have distinct drawbacks and are still in the infancy of their implementation, and/or are lacking in some capacity, being unable to wholly simulate and represent the immense variability of the live human. In seeking to emulate the unembalmed human body as accurately as possible, embalming and preservation techniques have evolved in order to circumvent and overcome the distinct drawback of traditional formalin-embalming techniques.

The purpose of this review was to provide an overview of the diversity of soft-preservation techniques presently available. Only once more research is performed on less readily known preservation techniques such as SSS, ICL-SP, N-Vinyl-2-pyrrolidone, and MLS, and direct comparison is performed against Thiel-preservation and fresh-frozen human body donors, can an optimal embalming solution be identified for future ME practices. However, as of now it is vital that users assess each embalming method and identify which techniques are optimal given their unique educational needs.

REFERENCES

AAMC (2022) How Medical Education is Changing. Available at: https://www.aamc.org/system/files/c/2/472906-howmedicaleducationischanging.pdf. (Accessed: 19 December 2022).

ACCME (2022) Policies. Available at: https://www.accme.org/accreditation-rules/policies/cme-content-definition-and-examples. (Accessed: 19 December 2022).

ALBERTY J, FILLER TJ, SCHMÄL F, PEUKER ET (2002) Nach Thiel fixierte Leichenohren ein neues verfahren für die aus- und Weiterbildung in der Mittelohrchirurgie (Thiel method fixed cadaver ears. A new procedure for graduate and continuing education in middle ear surgery). *HNO*, 50(8): 739-742.

AL-ELQ AH (2010) Simulation-based medical teaching and learning. *J Fam Community Med*, 17(1): 35-40.

BAILEY JR, TAPSCOTT DC, OTSUKA NY, BODEN KT, BECKER RM, KWASIGROCH TE, JOHNSTON BD (2021) Bringing physical exam skills back from the dead. *J Surg Orthop Adv*, 30(2): 112-115.

BALTA JY, CRONIN M, CRYAN JF, O'MAHONY SM (2015) Human preservation techniques in anatomy: A 21st century medical education perspective. *Clin Anat*, 28(6): 725-734.

BALTA JY, TWOMEY M, MOLONEY F, DUGGAN O, MURPHY KP, O'CONNOR OJ, CRONIN M, CRYAN JF, MAHER MM, O'MAHONY SM (2018) A comparison of embalming fluids on the structures and properties of tissue in human cadavers. *Anatomia, Histologia, Embryologia*, 48(1): 64-73.

BALTA JY, VENNE G, NOËL GPJC (2022) 10 tips on working with human body donors in medical training and research. *Anat Sci Int*, 97(3): 307-312.

BARTON DP, DAVIES DC, MAHADEVAN V, DENNIS L, ADIB T, MUDAN S, SOHAIB A, ELLIS H (2009) Dissection of soft-preserved cadavers in the training of gynaecological oncologists: Report of the first UK workshop. *Gynecol Oncol*, 113(3): 352-356.

BELE U, KELC R (2016) Upper and lower urinary tract endoscopy training on Thiel-embalmed cadavers. *Urology*, 15(93): 27-32.

BENKHADRA M, LENFANT F, NEMETZ W, ANDERHUBER F, FEIGL G, FASEL J (2008) A comparison of two emergency cricothyroidotomy kits in human cadavers. *Anesth Analg*, 106(1): 182-185.

BENKHADRA M, FAUST A, LADOIRE S, TROST O, TROUILLOUD PG, GIRARD C, ANDERHUBER F, FEIGL G (2009) Comparison of fresh and Thiel's embalmed cadavers according to the suitability for ultrasound-guided regional anesthesia of the cervical region. *Surg Radiol Anat*, 31: 531-535.

BERGMEISTER KD, AMAN M, KRAMER A, SCHENCK TL, RIEDL O, DAESCHLER SC, ASZMANN OC, BERGMEISTER H, GOLRIZ M, MEHRABI A, HUNDESHAGEN G (2020) Simulating surgical skills in animals: systematic review, costs & acceptance analyses. *Front Vet Sci*, 30(7): 570852.

BERNARDO A (2017) Virtual reality and simulation in neurosurgical training. *World Neurosurg*, 106: 1015-1029.

BILGE O, CELIK S (2017) Cadaver embalming fluid for surgical training courses: Modified Larssen solution. *Surg Radiol Anat*, 39(11): 1263-1272.

BURNS DM, BELL I, KATCHKY R, DWYER T, TOOR J, WHYNE CM, SAFIR O (2018) Saturated salt solution cadaver-embalming method improves orthopaedic surgical skills training. *J Bone Joint Surg Am*, 100(15): e104.

CAREY JN, ROMMER E, SHECKTER C, MINNETI M, TALVING P, WONG AK, GARNER W, URATA MM (2014) Simulation of plastic surgery and microvascular procedures using perfused fresh human cadavers. *J Plast Reconstr Aesthet Surg*, 67(2): e42-48.

EISMA R, MAHENDRAN S, MAJUMDAR S, SMITH D, SOAMES RW (2011) A comparison of Thiel and formalin embalmed cadavers for thyroid surgery training. *Surgeon*, 9(3): 142-146.

FEIGL GC, ROSMARIN W, STELZL A, WENINGER B, LIKAR R (2007) Comparison of Different injectate volumes for stellate ganglion block: an anatomic and radiologic study. *Reg Anesth Pain Med*, 32: 203-208.

GATT A, SCHEMBRI-WISMAYER P, CHOCKALINGAM N, FORMOSA C (2019) Kinematic and kinetic comparison of fresh frozen and Thiel-embalmed human feet for suitability for biomechanical educational and research settings. *J Am Podiatr Med Assoc*, 109(2): 113-121.

GOULD S, KNOWLING E, SMOLA R, TITER K, MARTIN K (2020) Efficacy of a cadaver-based procedural skills lab for Internal Medicine residents. *Cogent Med*, 7(1): 1780065.

GRECHENIG W, FELLINGER M, FANKHAUSER F, WEIGLEIN AH (1999) The Graz learning and training model for arthroscopic surgery. *Surg Radiol Anat*, 21(5): 347-350.

HAYASHI S, HOMMA H, NAITO M, ODA J, NISHIYAMA T, KAWAMOTO A, KAWATA S, SATO N, FUKUHARA T, TAGUCHI H, MASHIKO K, AZUHATA T, ITO M, KAWAI K, SUZUKI T, NISHIZAWA Y, ARAKI J, MATSUNO N, SHIRAI T, QU N, HATAYAMA N, HIRAI S, FUKUI H, OHSETO K, YUKIOKA T, ITOH M (2014) Saturated salt solution method: a useful cadaver embalming for surgical skills training. *Medicine*, 93(27): e196.

HAYASHI S, NAITO M, KAWATA S, QU N, HATAYAMA N, HIRAI S, ITOH M (2015) History and future of human cadaver preservation for surgical training: From formalin to saturated salt solution method. *Anat Sci Int*, 91(1): 1-7.

HEYMANS F, FEIGL G, GRABER S, COURVOISIER DS, WEBER KM, DULGUEROV P (2016) Emergency cricothyrotomy performed by surgical airway-naive medical personnel: a randomized crossover study in cadavers comparing three commonly used techniques. *Anesthesiology*, 125(2): 295-303.

HOMMA H, ODA J, SANO H, KAWAI K, KOIZUMI N, URAMOTO H, SATO N, MASHIKO K, YASUMATSU H, ITO M, FUKUHARA T, WATANABE Y, KIM S, HAYASHI S, KAWATA S, MIYAWAKI M, MIYASO H, ITOH M (2019) Advanced cadaver-based educational seminar for trauma surgery using saturated salt solution-embalmed cadavers. *Acute Med Surg*, 6(2): 123-130.

HUMBERT M, MICAULT E, MOREAU S, PATRON V, BOIS J, HITIER M (2022) The advantages of modified Thiel technique in head and neck surgical anatomy teaching. *Surg Radiol Anat*, 44(3): 345-352.

KONSCHAKE M, BRENNER E (2014) "Mors auxilium vitae"--causes of death of body donors in an Austrian anatomical department. *Ann Anat*, 196(6): 387-393.

MACCHI V, MUNARI PF, BRIZZI E, PARENTI A, DE CARO R (2003) Workshop in clinical anatomy for residents in gynecology and obstetrics. *Clin Anat*, 16(5): 440-447.

MCLEOD H, COX BF, ROBERTSON J, DUNCAN R, MATTHEW S, BHAT R, BARCLAY A, ANWAR J, WILKINSON T, MELZER A, HOUSTON JG (2017) Human Thiel-embalmed cadaveric aortic model with perfusion for endovascular intervention training and medical device evaluation. *Cardiovasc Intervent Radiol*, 40(9): 1454-1460.

MIYAKE S, SUENAGA J, MIYAZAKI R, SASAME J, AKIMOTO T, TANAKA T, OHTAKE M, TAKASE H, TATEISHI K, SHIMIZU N, MURATA H, FUNAKOSHI K, YAMAMOTO T (2020) Thiel's embalming method with additional intra-cerebral ventricular formalin injection (TEIF) for cadaver training of head and brain surgery. *Anat Sci Int*, 95(4): 564-570.

NAGASE M, NAGASE T, TOKUMINE J, SAITO K, SUNAMI E, SHIOKAWA Y, MATSUMURA G (2022) Formalin-free soft embalming of human cadavers using N-vinyl-2-pyrrolidone: Perspectives for cadaver surgical training and medical device development. *Anat Sci Int*, 97(3): 273-282.

NAM SM, MOON J-S, YOON H-Y, CHANG B-J, NAHM S-S (2020) Comparative evaluation of canine cadaver embalming methods for veterinary anatomy education. *Anat Sci Int*, 95(4): 498-507.

ODOBESCU A, DAWSON D, GOODWIN I, HARRIS PG, BOUMERHI J, DANINO MA (2019) High-fidelity microsurgical simulation: The Thiel cadaveric nerve model and evaluation instrument. *Plast Surg*, 27(4): 289-296.

PORZIONATO A, POLESE L, LEZOCHE E, MACCHI V, LEZOCHE G, DA DALT G, STECCO C, NORBERTO L, MERIGLIANO S, DE CARO R (2014) On the suitability of Thiel cadavers for natural orifice transluminal endoscopic surgery (NOTES): Surgical Training, feasibility studies, and Anatomical Education. *Surg Endosc*, 29(3): 737-746.

RASHIDIAN N, WILLAERT W, GIGLIO MC, SCUDERI V, TOZZI F, VANLANDER A, D'HERDE K, ALSEIDI A, TROISI RI (2019) Laparoscopic liver surgery training course on Thiel-embalmed human cadavers: Program evaluation, trainer's long-term feedback and steps forward. *World J Surg*, 43(11): 2902-2908.

REDDY R, IYER S, PILLAY M, THANKAPPAN K, RAMU J (2017) Soft embalming of cadavers for training purposes: Optimising for long-term use in tropical weather. *Indian J Plast Surg*, 50(01): 29-34.

RUIZ-TOVAR J, PRIETO-NIETO I, GARCÍA-OLMO D, CLASCÁ F, ENRIQUEZ P, VILALLONGA R, ZUBIAGA L (2019) Training courses in laparoscopic bariatric surgery on cadaver Thiel: Results of a satisfaction survey on students and professors. *Obes Surg*, 29(11): 3465-3470.

SCHWARZ G, FEIGL G, KLEINERT R, DORN C., LITSCHER G, SANDNER-KIESLING A, BOCK N (2002) Pneumatic pulse simulation for teaching peripheral plexus blocks in cadavers. *Anesth Analg*, 95(6): 1822-1823.

THIEL W (1992a) Die Konservierung ganzer Leichen in natürlichen Farben [The preservation of the whole corpse with natural color]. *Ann Anat*, 174: 185-195.

THIEL W (1992b) Eine Arterienmasse zur Nachinjektion bei der Konservierung ganzer Leichen [An arterial substance for subsequent injection during the preservation of the whole corpse]. *Ann Anat*, 174: 197-200.

VENNE G, ZEC ML, WELTE L, NOEL GP (2020) Qualitative and quantitative comparison of Thiel and phenol-based soft-embalmed cadavers for surgery training. *Anat Histol Embryol*, 49(3): 372-381.

UNIVERSITY OF BUFFALO, Continuing Medical Education (2018) CME Activity Guidelines. Available at: https://medicine.buffalo.edu/cme/planning_cme/policies/cme-activity-guidelines.html. (Accessed: 19 December 2022).

WATANABE M, YONEYAMA Y, HAMADA H, KOHNO M, HASEGAWA O, TAKAHASHI H, KAWASE-KOGA Y, MATSUO A, CHIKAZU D, KAWATA S, ITOH M (2019) The usefulness of saturated salt solution embalming method for Oral Surgical Skills training: A new cadaveric training model for bone harvesting. *Anat Sci Educ*, 13(5): 628-635.

YIASEMIDOU M, ROBERTS D, GLASSMAN D, TOMLINSON J, BIYANI S, MISKOVIC D (2017) A multispecialty evaluation of Thiel Cadavers for surgical training. *World J Surg*, 41(5): 1201-1207.

ZEVIN B, AGGARWAL R, GRANTCHAROV TP (2012) Simulation-based training and learning curves in laparoscopic Roux-en-Y gastric bypass. *Br J Surg*, 99(7): 887-895.

European Journal of Anatomy